The Dissertation Committee for Byoung Hooi Cho
certifies that this is the approved version of the following dissertation:

EFFECTS OF SUPPORT SYSTEM
ON BEHAVIOR AND PERFORMANCE
OF CONTINUOUSLY REINFORCED CONCRETE PAVEMENT

Committee:

David W. Fowler, Supervisor

Moon C. Won, Co-Supervisor

Zhanmin Zhang

Jorge G. Zornberg

Harovel G. Wheat

EFFECTS OF SUPPORT SYSTEM
ON BEHAVIOR AND PERFORMANCE
OF CONTINUOUSLY REINFORCED CONCRETE PAVEMENT

by

Byoung Hooi Cho, B.E., M.E.

Dissertation

Presented to the Faculty of the Graduate School of

The University of Texas at Austin

in Partial Fulfillment

of the Requirements

for the Degree of

Doctor of Philosophy

The University of Texas at Austin

December 2010

Dedication

To my wife, Eun-Gyeong Lee and lovely son, Daniel Minhyung Cho. You are my all.

To my parents for their endless love.

To my GOD for his never ending and steadfast love.

Acknowledgements

I am grateful to all people who supported me completing my graduate life. It would have been impossible to finish my Ph.D. work without their support and collaborations.

First, I would like to thank my advisor, Professor David W. Fowler, for his supporting and advising to finish my dissertation work. Also, I want to express my special appreciation to my co-advisor, Dr. Moon Won, for guiding and training me as a research scholar. I go on to thank my dissertation committee, Professor Zhanmin Zhang, Professor Jorge G. Zornberg, and Professor Harovel G. Wheat, who gave valuable comments for my dissertation.

I want to thank to CTR family, Dr. Soojun Ha and Jung Heum Yeon for their collaborations and friendship throughout my graduate year. Special thanks go to Professor Seong Cheol Choi for his advice, training, and friendship. I also extend my deep appreciation to Professor Seong-Min Kim who have always gave me generous advice and help, and Professor Sung Woo Shin who have been best senior, mentor, and friend to me.

Also, I give many thanks to AKPC PSALM and 14 Section members who shared Christian faith to encourage me to have a peaceful mind. I never forget their pray for me.

I specially thank my father, mother, grandmother, and brother for their devoted love and endless support. Also, I would like to expend my special thanks to my wife, Eun-Gyeong Lee, for her sincere love and limitless help.

Finally, please God all the glory. He has guided and reserved me to the best way.

Byoung Hooi Cho

The University of Texas at Austin
December 2010

v

EFFECTS OF SUPPORT SYSTEM

ON BEHAVIOR AND PERFORMANCE
OF CONTINUOUSLY REINFORCED CONCRETE PAVEMENT

Publication No._____

Byoung Hooi Cho, Ph.D.

The University of Texas at Austin, 2010

Supervisor: David W. Fowler

Support systems including base and subgrade layers play a pivotal role in manifesting and maintaining acceptable behavior and performance of continuously reinforced concrete pavement (CRCP). In Texas, especially, use of non-erodible stabilized base layers have been recommended to prevent failures of the CRCP related with pumping and erosion of the support materials. The non-erodible base materials, however, have given high initial construction cost of the rigid pavements. For this reason, it has been desired to decrease the construction cost with acceptable long-term performance of the pavement system.

The primary objective of this study is to determine acceptable combination of support properties and concrete slab thickness satisfying not only adequate structural ability but also construction expense. For this purpose, field support conditions were investigated using Falling Weight Deflectometer (FWD), Dynamic Cone Penetrometer (DCP), and static plate load test in phase one. Previously developed support analysis models for rigid pavement design were examined using finite element analysis method,

which model could more accurately express field support behavior. Also, effects of each support properties including base thickness, elastic modulus of base material, and subgrade k-value were mechanistically identified on composite k-value, and a method selecting optimum combinations of the support properties completing desired composite k-value was developed in phase two. Also, CRCP behavior were examined under not only diverse structural and material conditions of the support system but also the CRCP slab thickness and transverse crack spacing due to temperature and vehicle wheel loading conditions in phase three. In phase four, maximum critical stress induced in the CRCP slab was evaluated under various combinations of support conditions and slab thickness. Effects of the support properties and the slab thickness on the critical stress in the CRCP slab were mechanistically identified, and the factor with the greatest effect was verified. Moreover, regression equations were developed to estimate the maximum critical stresses for various support properties and the CRCP slab thickness under temperature and wheel loadings. In phase five, a guideline determining optimum combination of support properties and slab thickness were proposed as aspect of initial construction cost of the CRCP.

TABLE OF CONTENTS

LIST OF TABLES

LIST OF FIGURES

xvii

CHAPTER 1: INTRODUCTION

1.1. BACKGROUND

1.1.1. Continuously Reinforced Concrete Pavement (CRCP)

Continuously reinforced concrete pavement (CRCP) is one type of portland cement concrete (PCC) pavement. CRCP contains continuous steel reinforcement in the longitudinal direction. The steel controls the transverse cracks. In jointed plain concrete pavement (JPCP), another type of rigid pavement system, artificial transverse joints control the volume change of concrete slabs due to temperature and moisture variations. CRCP, which has no artificial transverse joints, however, allows irregular transverse crack generation because longitudinal steel holds the cracks tightly. CRCP has shown excellent performance for heavy vehicle loads state wide. It has become generally known that CRCP has a few distresses such as faulting that are developed at joints because there are no artificial transverse joints, and the efficiency of load transfer in CRCP at transverse cracks is excellent because of the longitudinal steel bars. Well designed CRCP can be expected to provide adequate performance with minimal maintenance for over 40 years [Rasmussen et al., 2009].

The first construction of CRCP was for experimental use in Columbia Pike near Washington, D.C. in 1921. Afterwards, several states including Texas, Virginia, Louisiana, Georgia, North and South Dakota, Oklahoma, Indiana, Illinois, California, and New Jersey constructed CRCP. In particular, Texas has done more CRCP construction projects than any other state. In Texas, it has been by state policy that newly-established concrete highways must be CRCP if there are no specific reasons to do otherwise [TxDOT, 2008]. Approximately 80 percent of current rigid pavement projects conducted in Texas are CRCP.

1.1.2.   Support System of CRCP

Analysis data from Long-Term Pavement Performance (LTPP) of Federal Highway Administration (FHWA) show that a support system of concrete pavement structures is one of the most critical design factors for adequate rigid pavement performance [ACPA, 2007]. The lowest part of support system is generally called subgrade, which is the native soil layer. A strong subgrade can provide a solid foundation to support the pavement structure, whereas a weak subgrade results in settlement which can cause damage to the pavement [CRSI, 2004]. Also, previous experiences in the state of Virginia have shown that poor subgrade calls for thicker CRCP slabs [CRSI, 2005]. Illinois have reported that well prepared subgrade for CRCP is one of the most crucial factors which provides a smooth, low-maintenance ride for many years of heavy traffic [CRSI, 2001].

Generally, to prevent negative impact, base layers have been placed on the compacted subgrade layer, and the concrete slab is placed on this base layer. For example, North and South Dakota have very expansive soil. This highly expansive subgrade is especially vulnerable to freeze and thaw heave. Full-depth asphalt pavements in South Dakota have experienced thermal cracks 1-in or wider crack width during the winter as a result of heave [CRSI, 2002]. Accordingly, the base layer underlying the concrete pavement slab, CRCP slab in this study, could play a pivotal role in providing desirable performance of the portland cement concrete pavement system. An adequate base layer, especially non-erodible stabilized base, can not only provide a stable construction platform and uniform slab support condition but also leading to prevent support erosion of the rigid pavement system. Erosion of base material, loss of support along pavement shoulder and longitudinal joint, has been revealed as a critical factor in developing punchouts which are a major type of distress in CRCP [Zollinger and Barenberg, 1990].

Another focus of base research is drainage. Research was done to determine the optimum base characteristics for a rigid pavement system for the most adequate

permeable support system [White et al., 2004]. However, the effects of the base characteristics on the behavior of concrete pavement slab itself have not been addressed.

A recently developed pavement design guide, Mechanistic Empirical Pavement Design Guide (MEPDG) [NCHRP, 2004], shows the analysis results that stiffer bases lead to more distresses in CRCP than less stiff bases do. On the other hand, extensive field investigations reveal that stiff bases which are normally cement or asphalt treated and non-erodible have provided better performance of CRCP than untreated cement or asphalt bases.

1.2.   PROBLEM STATEMENT

As increasing awareness of the importance of support function on behavior and performance of rigid pavement systems, stabilized non-erodible base materials have been used such as asphalt-stabilized base (ASB), cement-treated base (CTB), and lean concrete base (LCB). These non-erodible base materials, however, have resulted in high initial cost for the construction of the rigid pavements. For this reason, it is desirable to decrease construction cost with acceptable long-term performance of the pavement system.

1.3. OBJECTIVES

The main purposes of this study are identifying effects of each characteristic composing CRCP structure on behavior and performance of the CRCP, and finding optimum support compositions and thicknesses of the CRCP slab.

The objectives of this study are as follows:

(1) To examine field support conditions by field tests;

(2) To evaluate currently used support analysis models for rigid pavement design;

(3) To develop a method for finding the optimum combination of the support system to yield the desired support stiffness;

(4) To develop a modified CRCP finite element (FE) model for analysis of the CRCP behavior;

(5) To verify effects of the various support characteristics on CRCP behavior under diverse loading conditions;

(6) To examine CRCP behavior under diverse structural and material conditions of the CRCP support system;

(7) To compare composite k-values for different support analysis model for the pavement design;

(8) To verify effects of variables composing CRCP structure on behavior of CRCP slab under various loading conditions; and

(9) To develop guidelines to determine the optimum combination of components constituting the CRCP structure.

1.4.   SCOPES

To achieve the objectives of this study, general information about CRCP systems and support structures of the rigid pavement are introduced in chapter 1. Also, objectives of this study and the scope of this study are described.

In Chapter 2, the composition of support system of concrete pavement is reviewed. Moreover, a significance of the support system on CRCP performance is discussed, and European and USA practices for CRCP are reviewed and compared. CRCP distress types are also addressed in this chapter.

In Chapter 3, field support conditions are investigated by field tests. Falling Weight Deflectometer (FWD) tests, Dynamic Cone Penetrometer (DCP) tests, and non-repetitive static plate load tests are performed to identify the support conditions and characteristics.

In Chapter 4, existing support analysis models for pavement design are reviewed. Moreover, to verify appropriate support model for analysis, the plate load tests were simulated using finite element method. Also, effects of support layer properties on the k-value of the whole support system (composite k-value) are identified. A method estimating optimum combination of the support layer properties satisfying desired support stiffness is suggested.

In Chapter 5, basic behavior of the concrete slab placed on elastic foundation and traditional analysis theories due to temperature, wheel loading, and friction are reviewed. Also, numerical analyses of the concrete slab behavior are performed to compare the traditional theories, and appropriate finite element models for the concrete slab and loading conditions were selected.

In Chapter 6, to evaluate CRCP behavior, previous CRCP finite element models are reviewed and a modified CRCP finite element model with selected support model from chapter 4 is developed using ABAQUS 6.7 program. Effects of the support layer properties, thickness of base layer, elastic modulus of the base material, and subgrade k-value, on CRCP behavior were examined under temperature and vehicle wheel loading

conditions. Also, the behavior of CRCP on diverse support conditions such as non-uniform conditions and identical support stiffness conditions having different combinations of the support layer properties are evaluated.

In Chapter 7, composite *k*-values for two different support analysis models are compared under temperature and vehicle wheel loadings. One of the models is an elastic layer and *k*-value composite support model, and another one is a simplified support model using a single *k*-value. For differences of the two support models, effects of the support layer components are identified.

In Chapter 8, criteria examining behavior of the CRCP structure are reviewed. Also, effects of the components of the CRCP structure on the CRCP behavior are mechanistically identified under various loading conditions. Moreover, guidelines to determine optimum combination of the components constituting CRCP structure are developed.

Finally, a summary, conclusions, limitations, and recommendations are included in Chapter 9. In this chapter, performed researches for this study are summarized, and the results are addressed. Also, limitations of this study and recommendations for further studies are suggested.

CHAPTER 2: SUPPORT SYSTEM OF CONCRETE PAVEMENT

2.1.   COMPOSITION OF SUPPORT SYSTEM

The support system of rigid pavement structures including both of plain jointed concrete pavement (JCP) and continuously reinforced concrete pavement (CRCP) is generally composed of base, subbase, and subgrade layers [Rasmussen et al., 2009]. This study is focused on CRCP, and Figure 1 illustrates a typical CRCP cross section. However, to reduce the initial construction cost, an aggregate subbase is not utilized. Instead, a stabilized base layer is placed directly on compacted and/or stabilized subgrade. For the base layer, a chemically stabilized base layer has been used and directly placed on a compacted subgrade. Thus, it could be considered in this study that the support system of concrete pavement mainly consists of subgrade and base layers. Normally, the top 6 to 12 inches of subgrade layer are stabilized with cement or lime, depending on the plasticity of soil. The base layer is the layer placed on top surface of subgrade layer and under the concrete slab.
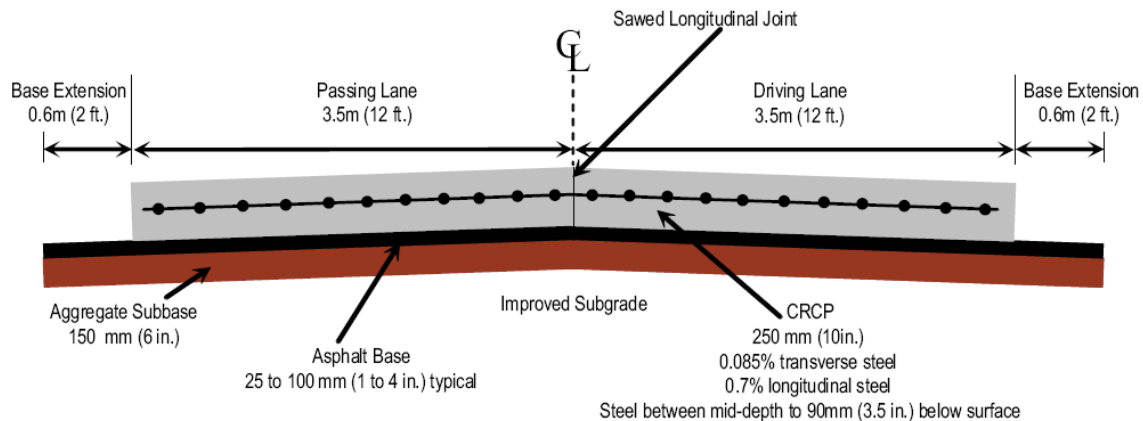
Figure 1. Typical CRCP cross section

2.1.1. Subgrade Layer

Existing native soils on which the concrete pavements are built for paving preparation are called subgrade. Generally, the subgrade is the lowest part of the rigid pavement structure. Performance of concrete pavements could be significantly affected by conditions of the subgrade layer. In other words, failures of the concrete pavement systems such as cracks, slab settlement, and other structural distresses are often initiated by problems of the subgrade layer, not by the deficiency of the concrete slab thickness or the concrete mix design. The drainage condition in the subgrade layer is also important. The moisture of the subgrade layer could change the volume of the soil and load bearing capacity, and these changes could give disadvantages to the pavement performances. In other words, k-value of subgrade soil could be determined from the soil classification and the degree of saturation in the upper 1 to 5 ft of soil [Darter, 1977; Darter and Barenberg, 1977]. Therefore, to prevent those effects and maintain uniform support condition, at least the upper part of the subgrade layer which is closest to the concrete slab, should not be affected by moisture variation because it can change the volume of the soil by shrinking or swelling. For this reason, the performance of the subgrade depends on two characteristics: load bearing capacity and volume changes. The load bearing capacity is affected by the degree of compaction, moisture content, and soil type, while volume changes of soil are affected by moisture freezing conditions, moisture contents of the soil, and the amount of fine soil particles. Accordingly, the support system of rigid pavement structures should satisfy sufficient strength, stiffness, and resistance to moisture. For these reasons, treating subgrade soil with diverse additives such as lime, hydraulic cement or fly ash has been suggested to reduce shrinkage or swelling of expansive soils or existing materials and increase strength to provide long-term support for the pavement structures [TxDOT, 2005]. Selection of the additives is based on soil classification [Tex-142-E, 1999], sieve analysis [Tex-110-E, 1999], Atterberg limit [Tex-104-E, 1999; Tex-105-E, 1999; Tex-106-E, 1999; Tex-107-E, 1999], and sulfate content [Tex-145-E, 2005; Tex-146-E, 2005]. In general, if the subgrade has high plasticity index (PI), the soil is

normally treated with lime, whereas cement is used to treat soil with low PI. Table 1 shows the additive selections for treating subgrade soils by Texas standards.

Table 1. Additive selection for treating subgrade soils

Subgrade	Plasticity Index (PI)	Additive selection
≥ 25% Passing No. 200 Sieve	PI < 15	Cement Asphalt Lime-Fly Ash
	15 ≤ PI <35	Lime Lime-Cement Lime-Fly Ash Fly Ash Cement
	PI ≥ 35	Lime Lime-Cement Lime-Fly Ash

The quality of the prepared subgrade layers has been typically specified by stiffness or strength of the materials for the rigid pavement design. In the U.S., three basic concepts of subgrade stiffness or strength characterizations have been commonly used: California bearing ratio (CBR), resistance value (R-value), and resilient modulus (M_R). Table 2 shows typical values of CBR, R-value, and resilient modulus for various materials [WAPA].

Table 2. Typical values of *CBR*, *R*-value, and resilient modulus for various materials

Material	CBR	R-value	Resilient modulus [psi]
Crushed stone (GW, GP, GM)	20 ~ 100	30 ~ 50	20,000 ~ 40,000
Sandy soils (SW, SP, SM, SC)	5 ~ 40	7 ~ 40	7,000 ~ 30,000
Silty soils (ML, MH)	3 ~ 15	5 ~ 25	5,000 ~ 20,000
Clay soils (CL, CH)	3 ~ 10	5 ~ 20	5,000 ~ 15,000
Organic soils (OH, OL, PT)	1 ~ 5	< 7	< 5,000

2.1.2. Base Layer

A base is a relatively thin layer generally located between the subgrade and the concrete slab. Although the base layer could reduce critical stress in the concrete slab, it is uneconomical to build the base layer for the purpose of reducing the concrete stress [Huang, 1993]. Recently, however, the base layer has usually been constructed with non-erodible stabilized materials such as asphalt concrete, lean concrete or cement-stabilized materials to resist erosion of the support materials which could produce failures in the rigid pavement systems. The main purposes for the use of base layer are not only to prevent erosion of support materials caused by repetitive pumping action, but also to provide a stable construction platform and uniform slab support condition. Also, the non-erodible base layer can effectively control frost action, shrinkage, and swelling of the subgrade layer due to moisture changes [Yoder and Witczak, 1975]. Several types of base have been constructed including asphalt-stabilized base, cement-stabilized base, lean concrete base, dense-graded granular base, and open-graded permeable base. An untreated base material gives lower frictional resistance with concrete slab than treated base materials. Therefore, the use of a treated base could lead to decreased crack spacing and crack width of concrete slab. Previous reports have shown that high restraint at the interface between base and concrete slab has produced undesirable early-age cracking and poor performance of CRCP on cement-treated permeable base [Yu et al., 1999; Heckel, 1997]. To prevent these problems, some States in the U.S. have recommended the use of 1 in of asphalt concrete layer between the cement-stabilized base and concrete slab. Another benefit of using 1 in of asphalt layer on the cement-stabilized base is providing contractors with better capability of estimating yield of concrete used in the project. The Texas Department of Transportation (TxDOT) has required one of the following base layer combinations for a concrete pavement support system: 1) 4 in of asphalt-stabilized base or 2) a minimum 1-in asphalt concrete bond breaker over 6 in of a cement-stabilized base [TxDOT, 2008]. Figure 2 shows an asphalt-stabilized base ready for the steel and concrete placement.

Figure 2. Asphalt-stabilized base (photo courtesy of Zachry Construction)

2.2. SIGNIFICANCE OF SUPPORT SYSTEM

2.2.1. Erodibility

Applications of heavy vehicles on concrete pavement could cause excessive slab deflections, especially when the support condition is not sufficient. In this case, the base materials under the concrete slab could be loosed by the repetitive heavy vehicle wheel loadings, and pumping actions could occur through slab joints or cracks. This pumping action washes the particle of base material away if the base materials are not well stabilized, and further applications of heavy vehicles will exacerbate the pumping. These pumping actions could cause severe erosion in the non-stabilized or under the stabilized base layer. Figure 3 shows the result of this pumping action at the slab edge through the longitudinal joint between outside lane and asphalt shoulder of CRCP.

Support loss due to the repetitive pumping actions and resulting erosion play a pivotal role in increasing deflection and tensile stress of the concrete slab. Finally, these repetitive excessive slab deflections and rebounding actions could lead to distresses in the CRCP due to excessive critical tensile distresses and damages in the concrete pavement structure. High tensile stresses and resulting damages in concrete slab could cause a serious structural damage in CRCP called punchout. Figure 4 presents an example of a punchout distress in CRCP due to excessive slab deflections.

The 1993 AASHTO Pavement Design Guide considers erodibility of base materials as a design input and the erodibility is expressed by loss of support index (LS) which ranges from 0 to 3. The LS factors, 0, 1, 2 and 3, are defined by a void area under the concrete slab [AASHTO, 1986]. This theoretical analysis concept is a result from SLAB-49 program [Panak and Matlock, 1972]. Table 3 shows typical range of LS factors for various types of base materials [AASHTO, 1993].

Figure 3. Pumping and erosion at longitudinal joint of CRCP (photo courtesy of M. Won)

Figure 4. CRCP distress due to excessive slab deflections (photo courtesy of M. Won)

Table 3. Typical ranges of loss of support factors for various types of materials

Type of Material	Loss of Support (LS)
Cement Treated Granular Base (E=1,000,000 to 2,000,000 psi)	0.0 to 1.0
Cement Aggregate Mixtures (E=500,000 to 1,000,000 psi)	0.0 to 1.0
Asphalt Treated Base (E=350,000 to 1,000,000 psi)	0.0 to 1.0
Bituminous Stabilized Mixtures (E=40,000 to 300,000 psi)	0.0 to 1.0
Lime Stabilized (E=20,000 to 70,000 psi)	1.0 to 3.0
Unbound Granular Materials (E=15,000 to 45,000 psi)	1.0 to 3.0
Fine Grained or Natural Subgrade Materials (E=3,000 to 40,000 psi)	2.0 to 3.0

Also, Mechanistic-Empirical Pavement Design Guide (MEPDG) developed under National Cooperative Highway Research Program (NCHRP) 1-37A has classified the erodibility of support materials into five levels. Table 4 presents material descriptions for each erodibility class, and the five classes of design inputs are as follows [NCHRP, 2004]:

Class 1: Extremely erosion resistant materials

Class 2: Very erosion resistant materials

Class 3: Erosion resistant materials

Class 4: Fairly erodible materials

Class 5: Very erodible materials

To prevent loss of support, use of non-erodible or stabilized base layer has been highly recommended for rigid pavement constructions. Recently constructed rigid pavement structures with stabilized materials for base layer such as cement stabilized base or asphalt stabilized base have rarely experienced pumping and erosion problems.

Table 4. MEPDG recommendations for assessing erosion potential of base material

Erodibility Class	Material Description and Testing
1	(a) Lean concrete with approximately 8 percent cement; or with long-term compressive strength > 2500 psi (>2000 psi at 28 days) and a granular subbase layer or a stabilized soil layer, or a geotextile fabric is placed between the treated base and subgrade, otherwise Class 2. (b) Hot-mixed asphalt concrete with 6 percent asphalt cement that passes appropriate stripping tests and aggregate tests and a granular subbase layer or a stabilized soil layer (otherwise Class 2). (c) Permeable drainage layer (asphalt treated aggregate or cement treated aggregate and with an appropriate granular or geotextile separation layer placed between the treated permeable base and subgrade.
2	(a) Cement-treated granular material with 5 percent cement manufactured in plant, or long-term compressive strength 2000 to 2500 psi (1500 to 2000 psi at 28 days) and a granular subbase layer or a stabilized soil layer, or a geotextile fabric is placed between the treated base and subgrade, otherwise Class 3. (b) Asphalt-treated granular material with 4 percent asphalt cement that passes appropriate stripping test and a granular subbase layer or a treated soil layer or a geotextile fabric is placed between the treated base and subgrade, otherwise Class 3.
3	(a) Cement-treated granular material with 3.5 percent cement manufactured in plant, or with long-term compressive strength 1000 to 2000 psi (750 to 1500 psi at 28 days). (b) Asphalt-treated granular material with 3 percent asphalt cement that passes appropriate stripping test.
4	Unbound crushed granular material having dense gradation and high quality aggregates.
5	Untreated soils (PCC slab placed on prepared/compacted subgrade)

2.2.2. Distresses of CRCP

2.2.2.1. Punchout

A punchout is the only structural distress in CRCP and accordingly most widely used as a structural indicator for the long term performance of CRCP structures. MEPDG has defined the mechanism of the punchout as:

1) Slab segment with narrow transverse crack spacing (2-ft or less) exists.
2) Large transverse crack widths and repeated heavy loads degrade load transfer efficiency (LTE) across transverse cracks.
3) Loss of support takes place along the pavement edge due to base erosion.
4) Negative temperature gradients through the slab depth and top of the slab drying shrinkage further magnify bending stress in the transverse direction at 4-ft away from the pavement edge.
5) Passages of heavy axles causing repetitive cycles of excessive tensile bending stresses lead to top-down longitudinal fatigue cracking that defines punchout.

Figure 5 shows the typical full-depth punchout of CRCP structure. According to MEPDG punchout mechanism, many factors including transverse crack spacing, crack width, heavy loading, base erosion, and stresses in concrete slab contribute to the punchout development. Thus, to improve CRCP performance by minimizing the punchout development, various measures should be considered. Steel reinforcement should be determined so that crack spacing and widths can be maintained within the acceptable limits. Adequate slab thickness should be provided to minimize slab deflections due to wheel loading applications and reduce stress in concrete. Base should be structurally sound and durable so that it will provide slab support needed to limit deflections and stresses in concrete to an acceptable level and to minimize erosion of the base materials. However, CRCP Design and Construction Guidelines define that the most

important factor in preventing the punchout is the use of a non-erodible base material to minimize loss of support [Rasmussen et al., 2009].

Figure 5. A typical full-depth punchout of CRCP

2.2.2.2. Other types of distresses

For a long time, punchouts have been accepted as the only structural distress for the performance evaluation of CRCP. There are several punchout distress mechanisms proposed and the one described in the previous section by MEPDG is one of them. However, many field evidences have shown the existence of other types of distresses that have a quite similar appearance to those of a typical full-depth punchout, but with different failure mechanisms. Figure 6 shows example of the distress. This failure meets the definition of a typical punchout; however, in this case, the transverse cracks reached to the middle depth of the concrete slab, where the steel is located. Horizontal cracking also exist at steel depth. The concrete below the steel is maintained in good conditions without any transverse crack propagation. Thus, this type of distress has a completely different failure mechanism although initially it seems like a full-depth punchout.

Figure 6. Partial-depth punchout of CRCP (photo courtesy of M. Won)

Figure 7 presents another type of failure in CRCP structure. This type of failure is also similar to a full-depth punchout. However, this type of distress has a totally different failure mechanism. This distress is produced at the transverse construction joint. Generally, contractors finish paving with this transverse construction joint at the end of a day, and the contractors start paving again from this construction joint. So, the adjacent two slabs should have different concrete material properties at the early ages, which include tensile strength and modulus of elasticity. For this reason, the left-side slab which has a higher tensile strength could pull the right-side slab which has a lower tensile strength when ambient temperature drops. In this area, the paving direction was from left to right. At the same time, the modulus of elasticity of concrete at the right side of the construction joint is lower than that of the previously placed concrete at the left side. As a result, transverse cracks could occur near the transverse construction joint at the right-side slab. Thus, this failure mechanism is totally different from the full-depth punchout, and this distress should not be included in the development of transfer function and the calibration of any MEPDG models.

Figure 7. Distress at transverse construction joint (photo courtesy of M. Won)

2.2.3. European and USA Practices

Many European countries used the concrete pavement system quite extensively. Jointed plain concrete pavements (JPCP) are more widely used in Europe, with CRCP being adapted in several countries, most commonly Belgium. The design lives are typically 30 to 40 years [US TECH, 1992]. Table 5 shows typical designs for a freeway in several European countries and the State of Texas in the USA. In this table, LCB stands for lean concrete base, AC is asphalt concrete, and CTB represents cement-treated base. Generally, European countries use stronger base layers than Texas. Also, it could be realized that European countries usually use thinner slabs than Texas, although they have used higher single axle loads than USA for pavement design. These typical European designs emphasize the contributions from all components of the pavement structures, not just the thickness of the concrete slab.

Table 5. European and USA practices

Country	Slab	Base	Single Axle [lbs]
France	CRCP (6.7 ~10 in)	LCB	28,660
	JPCP (8.7 ~ 11 in)	LCB	
Austria	JPCP (7 ~ 10 in)	2-in AC CTB	22,046
Germany	JPCP (7.9 ~ 11.8 in)	CTB / LCB (bonded)	25,353
Netherlands	JPCP (10.2 ~ 11 in)	LCB	25,353
Belgium	CRCP (7.9 in)	LCB	28,660
	JPCP (9 in)	LCB	
USA (Texas)	CRCP (6 ~15 in)	4-in AC 1-in AC + 6-in CTB	18,000

2.3. MODULUS OF SUBGRADE REACTION (*K*-VALUE)

The modulus of subgrade reaction, *k*-value, could be directly found by a static plate load test [ASTM, 2004]. This method measures the magnitude of applied pressure load and the corresponding static deflection of a steel load bearing plate. The static modulus of subgrade reaction is calculated by the following relationship.

$$k = \frac{p}{\Delta} \tag{2.4}$$

where, *p* is a pressure which has a unit of pound per square in [psi], and the calculated *k*-value has a unit of pound per cubic in [psi/in]. Even though this method measures *k*-value directly, it is time and cost consuming procedure. Accordingly, this static plate load test is rarely performed for pavement design and performance evaluation in the U.S.

Another method to estimate *k*-value is the *AREA* back-calculation method. Using deflection profile corresponding to the applied load, *AREA* is calculated. FWD would be one of the most widely used devices for this method. The concept of *AREA* was proposed by a previously conducted study as follow [Hoffman and Thompson, 1981]:

$$AREA = 6\left[1 + 2\left(\frac{d_{12}}{d_0} + \frac{d_{24}}{d_0}\right) + \frac{d_{36}}{d_0}\right] \tag{2.5}$$

where, d_i represent deflection at *i* in. from the loading center. *AREA* presents the characteristic of deflected basin of the support layer. To determine *k*-value for concrete pavement system using FWD data, a back-calculation method was developed as shown in the following equation [Hall, 1991].

$$k = \left(\frac{P}{8d_0 l^2}\right)\left[1 + \left(\frac{1}{2\pi}\right)\left(\ln\left(\frac{a}{2l}\right) + \gamma - 1.25\right)\left(\frac{a}{l}\right)^2\right] \tag{2.6}$$

26

where, *P* is applied load in pounds, *a* is the radius of the loading plate [in], and *γ* represents the Euler-Mascheroni constant. *l* is a radius of relative stiffness, which has a relationship with *AREA* as follow:

$$l = \left[\frac{\ln\left(\dfrac{36 - AREA}{1812.279}\right)}{-2.559} \right]^{4.387} \tag{2.7}$$

According to the basic concept of modulus of subgrade reaction, the *k*-value would be determined by magnitude of applied load and amount of deflection. Thus, the *k*-value seems to be a unique property for characterizing the subgrade layers. However, previous studies identified that *k*-value is affected by several factors. A study by Teller *et al* found that *k*-value estimated from a static plate load test is affected by the loading plate size [Teller and Sutherland, 1943]. Accordingly, ASTM (American Society for Testing and Materials) requires the use of 30-in diameter loading plate for the static plate load test [ASTM, 2004]. Vesic showed that the *k*-value of a foundation under beams is a function of the beam properties such as elastic modulus and dimensions [Vesic, 1961]. Field data from the AASHO Road Test have supported this assertion that the *k*-value decreases as PCC slab thickness increases [Vesic and Saxena, 1970]. Additionally, *k*-values for a finite slab on the Winkler foundation have shown different values depending on the locations of loading, i.e., under the slab center, edge, or corner [Daloglu and Vallabhan, 2000]. Consequently, other previous studies have suggested that the *k*-value of subgrade could be affected by the size, shape and structural stiffness of the structure placed on the subgrade [Biot, 1932]. In 1961, Vesic showed a formula estimating the *k*-value with a good approximation of bending moments and deflection of a beam resting on soil [Vesic, 1961].

$$kB = K = 0.65_{12}\sqrt{\frac{E_s B^4}{E_b I}} \frac{E_s}{1-v_s^2} \qquad (2.8)$$

where, B is width of the beam, $E_b I$ is structural stiffness of the beam, and E_s and v_s are elastic modulus and Poisson's ratio of soil, respectively, and the quantity $kB=K$ is the modulus of subgrade reaction.

Consequently, it can be stated that modulus of subgrade reaction, k-value, is a relationship between applied total loads and deflection characteristics such as quantity or shape. In other words, k-value could be expressed by total applied load [lbs] and volume of the deflected basin [in^3]. The volume of deflection bowl of support layer in rigid pavement system could be affected not only by the magnitude of the total load but also the loading types (temperature or wheel loading), size of the concrete slab, and thickness of the PCC slab. Thus, different k-values could be calculated due to loading types or structural characteristics of the concrete slab. For these reasons, the effect of finite size of the concrete slab on subgrade k-value was studied for concrete pavement systems [Crovetti, 1994]. Also, back-calculated k-value at edges and corners from the measuring deflections were studied. Some of these findings, however, have not been incorporated in the current rigid pavement design algorithms because of the very complex nature of the analysis the pavement system.

2.4.   SUMMARY

Support system of rigid pavement structure, especially CRCP, consists of compacted subgrade and stabilized base layers. Subgrade commonly consists of existing native soil. The subgrade should not be disturbed or deformed to provide adequate and uniform slab support. Thus, the native soil is compacted or treated using additives to improve poor soil conditions. The base layer which is located between subgrade and concrete slab plays a crucial role in preventing support erosion.

A support system having an adequate structural capacity and durability is essential for the pavement system to have satisfactory performance. Support system that is prone to erosion could easily lead to severe pavement distresses. Therefore, most of the current pavement design procedures adopted erodibility as a design criterion.

A punchout is the only structural distress in CRCP; however, its definition is still quite vague and there is confusion among pavement engineers regarding a precise definition of the punchout. There are other distress types that resemble punchouts, which include partial-depth punchouts due to horizontal cracking and distresses at transverse construction joints. Even though these distresses are very similar to typical full-depth punchouts, they have totally different mechanisms.

Not only in the U.S. but also many European countries use portland cement concrete pavement, especially for highways with a high volume of heavy truck traffic. These European countries have adopted a relatively stronger support structures than in the U.S.

Finally, the modulus of subgrade reaction, k-value, is one of the most important values for the rigid pavement design. This k-value could be defined by applied load and deflection characteristics corresponding to the load. Although currently developed pavement design guides deal with the k-value with a unique support characteristic, the k-value could be changed not only by the size of the loading area, but also the thickness and modulus of concrete slab. However, these characteristics of k-value have not been incorporated into most of the current design algorithms.

CHAPTER 3: FIELD SUPPORT CONDITIONS

To investigate field support conditions, three types of field tests including Falling Weight Deflectometer (FWD) test, Dynamic Cone Penetrometer (DCP) test, and non-repetitive static plate load test were performed at a Whitetopping test section located at the J. J. Pickle Research Campus at the University of Texas at Austin.

3.1. TESTING SITE

A full scale concrete slab, 18 ft. × 18 ft. × 6 in., was constructed and tested during the summer of 2007 at J. J. Pickle Research Campus at the University of Texas at Austin. The support foundation layer of this site under a 6-in concrete slab consisted of three different layers; 2-in asphalt concrete (AC) stabilized layer, 8-in aggregate layer, and a subgrade layer of compacted soil, as shown in the Figure 8. The field tests for this study were conducted on the top surface of asphalt layer and aggregate layer.
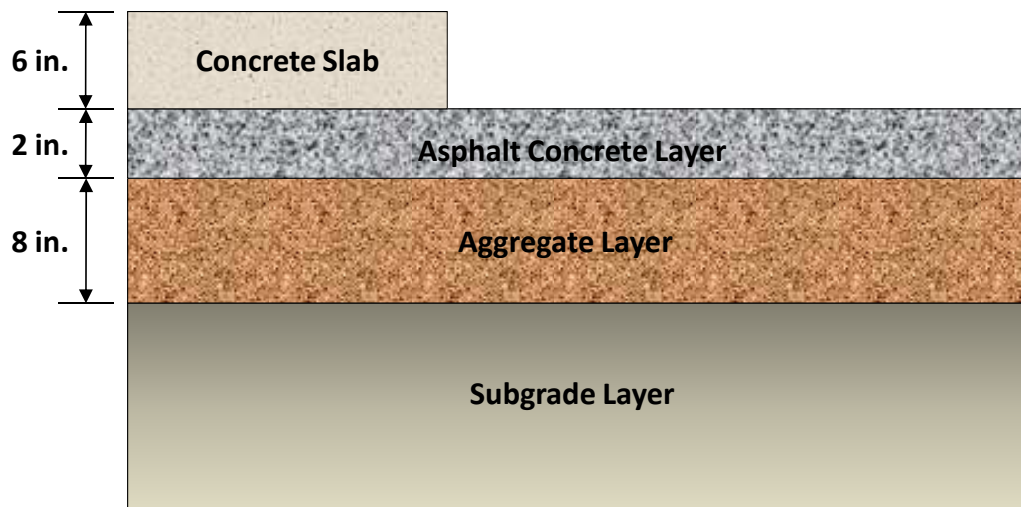
Figure 8. Composition of support foundation at test site

3.2. FALLING WEIGHT DEFLECTOMETER (FWD) TEST

FWD is one of the most widely used non-destructive testing devices for evaluating physical properties and performance conditions of pavements. FWD measures surface deflection due to dropping a load of heavy weight. The objectives for the FWD tests were to 1) check the uniformity of the supporting condition at the testing site and 2) obtain the elastic modulus of each layer.

3.2.1. Test Procedure

The FWD test was conducted prior to the placement of concrete slab to check ground uniformity of the test site and to obtain the elastic modulus of each layer. Here, the modulus of the 2-in asphalt concrete (AC) base layer could not be back-calculated from this test due to the deficiency of the thickness, but it should be assumed or directly tested in the lab. So, the elastic modulus of the AC stabilized base layer was assumed to be constant by a typical value. The FWD tests were performed at every crossing point on a three feet grid on the asphalt surface. Figure 9 shows the FWD field test. A load plate with a diameter of 12-in was used, and a load ranging from 6,000 to 15,000 lbs was applied. Deflection of the asphalt surface was measured by 7 sensors which are 1-ft apart.

Figure 9. FWD test

3.2.2. Results

Figure 10 shows the FWD deflection contour at sensor No. 1 that is located at the center of the loading plate. The deflections in the contour are normalized for 1,000 lbs loading. The distance of each grid is 3-ft. in both x and y coordinates. As illustrated in Figure 10, the support showed irregular and non-uniform conditions. Based on this result, three locations were selected for the DCP and static plate load tests: K8, K2 and I3, representing areas of high, medium and low support stiffness conditions. The average back-calculated elastic moduli of each layer from the FWD testing results are shown in Table 6.
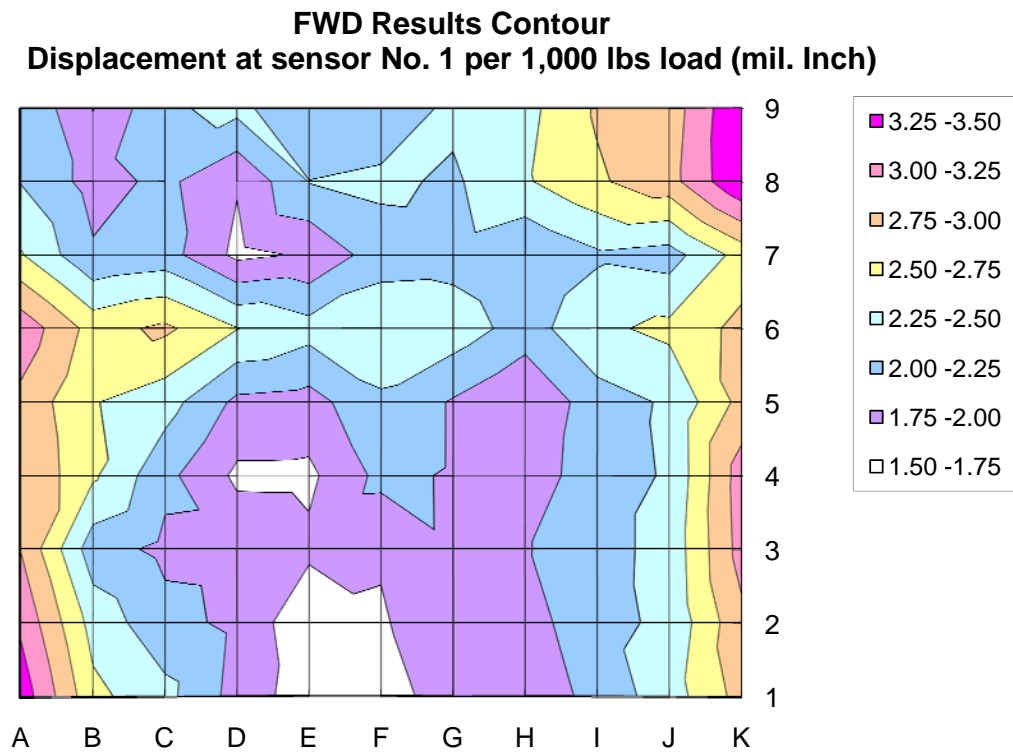
Figure 10. FWD deflection contour

Table 6. Average back-calculated elastic modulus from FWD testing

Layer	Average Elastic Modulus [psi]	Standard Deviation [psi]	Coefficient of Variance [%]
Asphalt Base	485,000	0	0.0
Aggregate Subbase	38,400	9,500	24.6
Subgrade	27,100	2,900	10.7

3.3. DYNAMIC CONE PENETROMETER (DCP) TEST

DCP is a device which can measure in-situ strength of subgrade. DCP test was developed in Australia by Scala in 1956 [Scala, 1956], and the current model was developed by the Transvaal Roads Department in South Africa [Luo et al., 1998]. As discussed in the previous section, adequate subgrade stiffness beneath the concrete slab is required to facilitate roadway construction. Also, for the analysis and design of rigid pavement using elastic theory, two subgrade material properties – resilient modulus and Poisson's ratio – are required. However, estimating the resilient modulus in a laboratory is time-consuming, and requires significant effort. On the other hand, the DCP test has many advantages including simplicity and economy. A number of previous researchers have developed a relationship between DCP results and material properties. The DCP test result is expressed by the number of hammer drops and penetration depth in inches per blow.

3.3.1. Test Procedure

DCP device consists of upper and lower shafts. The upper shaft has 17.6 lbs of drop hammer with a 22.6-in drop height and is attached to the lower shaft through the anvil. The lower shaft contains an anvil and a cone attached to the end of the shaft. The cone is replaceable and has a 60 degree of cone angle. Figure 11 illustrates the structure of the DCP device. Three operators were required to run the DCP test. One person held the upper shaft; the second person dropped the hammer and the third recorded measurements. The DCP test procedure is as follows;

1) Upper shaft and lower shaft containing cone tip is assembled.
2) The cone tip assembled with the shafts is put on the testing surface.
3) The equipment is stabilized due to the disturbed loose state of the ground surface and the self-weight of the device.

4) The value of the initial reading is counted as initial penetration corresponding to blow zero.

5) Hammer blows are repeated and the penetration depth is measured for each hammer drop or other drops as deemed appropriate by the operator.

6) This process is continued until a desired penetration depth is reached.

The DCP tests were performed at the location of K8, K2, and I3 that represent weak, medium, and strong support conditions based on the FWD testing results respectively to investigate support characteristics under the asphalt stabilized base layer. Because the DCP device could not penetrate the asphalt stabilized layer, holes were drilled at the three locations and the DCP tests were conducted. Figure 12 presents the DCP test procedures.
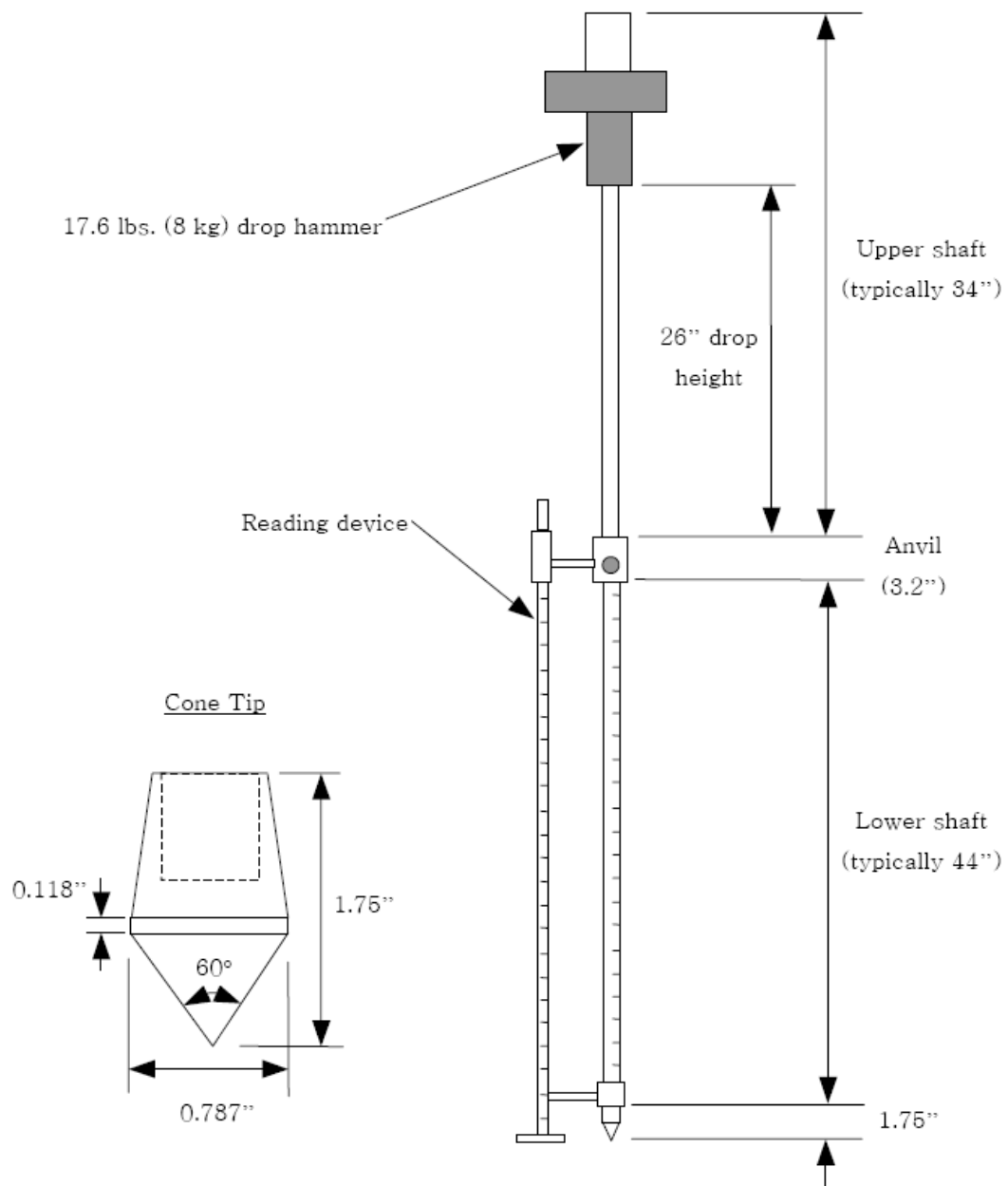
Figure 11. Structure of Dynamic Cone Penetrometer

Figure 12. DCP testing

3.3.2. Results

Resilient modulus (M_r) of subgrade is a very important factor for design and evaluation of a rigid pavement system. In this study, field resilient modulus of the site was back-calculated from DCP data.

The results of the DCP test could be expressed as DCP index (*DCPI*) described by penetration depth per blow [mm/blow]. A number of researchers identified relationships between *DCPI* and *CBR* (California Bearing Ratio) [Kleyn, 1975; Harison, 1987; Livneh et al., 1994; Ese et al., 1994; Coonse, 1999; Gabr et al., 2000]. The U.S Army Corps of Engineers developed correlations as follows, and Table 7 presents the various other suggested correlations [Salgado and Yoon, 2003].

$$CBR = \frac{292}{DCPI^{1.12}} \qquad (\text{if } CBR > 10) \qquad (3.1)$$

$$CBR = \frac{1}{[0.017019(DCPI)]^2} \qquad (\text{if } CBR < 10) \qquad (3.2)$$

Table 7. Correlations between *DCPI* and *CBR*

Author	Correlation	Material testes
Kleyn (1975)	log (*CBR*) = 2.62-1.27 log(*DCPI*)	Unknown
Harison (1987)	log (*CBR*) = 2.56-1.16 log(*DCPI*)	Cohesive
Harison (1987)	log (*CBR*) = 3.03-1.51 log(*DCPI*)	Granular
Livneh et al. (1994)	log (*CBR*) = 2.46-1.12 log(*DCPI*)	Granular and cohesive
Ese et al. (1994)	log (*CBR*) = 2.44-1.07 log(*DCPI*)	Aggregate subbase course
NCDOT	log (*CBR*) = 2.60-1.07 log(*DCPI*)	Aggregate subbase course
Coonse (1999)	log (*CBR*) = 2.53-1.14 log(*DCPI*)	Piedmont residual soil
Gabr (2000)	log (*CBR*) = 1.40-0.55 log(*DCPI*)	Aggregate subbase course

Many correlation equations between *CBR*, *R*-value, and resilient modulus have been proposed. Heukelom and Klomp suggested following equation 3.3. However, this relationship is limited to fine-grained non-expansive soils with a soaked *CBR* of 10 or less [Heukelom and Klomp, 1962].

$$M_r\,(psi) = 1,500(CBR) \tag{3.3}$$

Additionally, various other correlations are suggested by the U.S. Army Corps of Engineers (equation 3.4) and South African Council on Scientific and Industrial Research (equation 3.5).

$$M_r\,(psi) = 5,409(CBR)^{0.71} \tag{3.4}$$

$$M_r\,(psi) = 3,000(CBR)^{0.65} \tag{3.5}$$

Also, the MEPDG proposed following equation 3.6 with a limitation of a fair conversion over a wide range of values.

$$M_r\,(psi) = 2,555(CBR)^{0.64} \tag{3.6}$$

The DCP tests were performed to verify characteristics of support layers at locations K8, K2, and I3 that represent weak, medium, and strong support conditions based on the FWD testing results respectively. Figure 13 presents the results of the DCP tests. Because the support system of this test section is composed of two layers which are the aggregate subbase layer and subgrade layer, the DCP test results clearly presents a changing trend at the layer of the boundary which is located at a depth of 8 in. at all three test locations. Averaged *DCPI* were calculated separately from aggregate subbase layer and subgrade at the three locations. The lowest *DCPI* value of the aggregate layer is 1.649, and the maximum value is 3.84, whereas subgrade layer lowest value is 11.94 and 14.48 for the maximum value. A low *DCPI* value represents a strong support condition.

On the other hand, a large value means weak condition. As shown in Figure 13, aggregate subbase layer is stronger than subgrade. Also, the soil subgrade layer shows more uniform condition than the aggregate subbase layer. The aggregate layer shows larger difference of the *DCPI* values than subgrade.
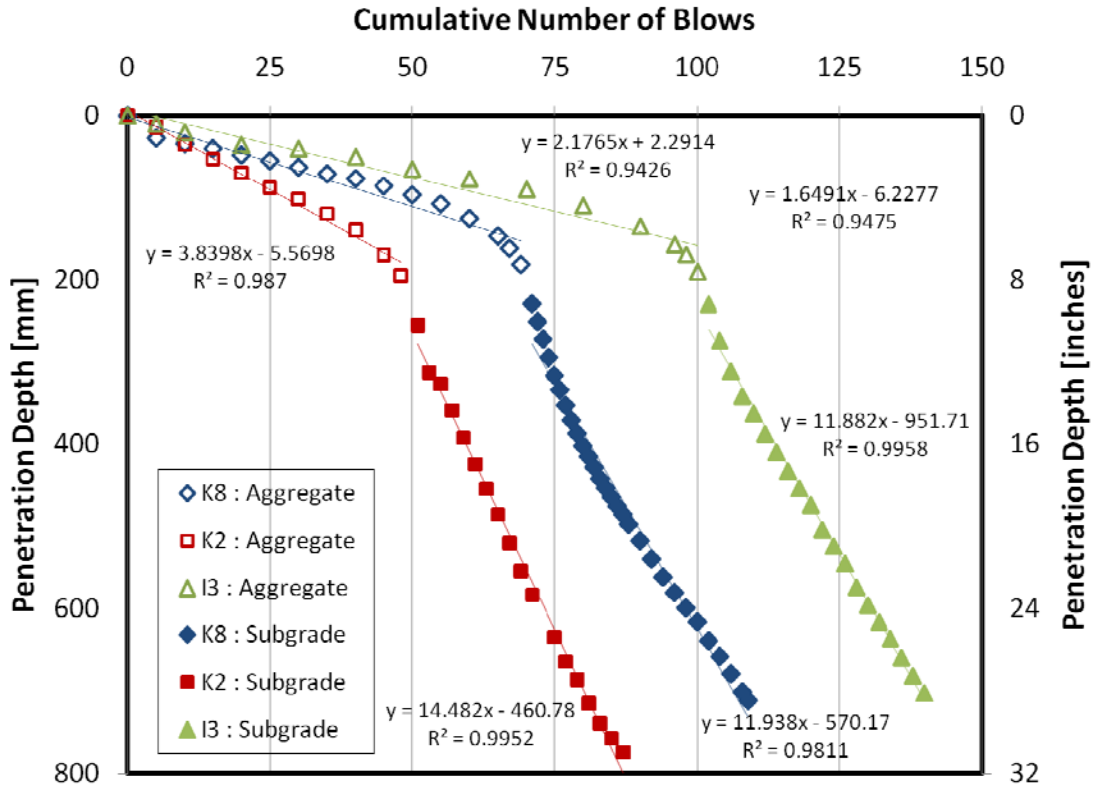
Figure 13. DCP test results

CBR value and resilient modulus of each layer were back-calculated from the *DCPIs* as shown in Table 8. The maximum back-calculated resilient modulus of aggregate layer is 67,536 psi from location I3, and the minimum value is 36,846 psi from location K2 where is the medium FWD spot. Also, from the subgrade layer, 16,399 psi of the maximum resilient modulus is back-calculated and 14,230 psi of the minimum value. The DCP tests have given different results from those of FWD testing at the location of K8 and K2. However, in this study, the back-calculated elastic moduli of each layer from

FWD testing results were used because the FWD data represented a wider range of test locations than DCP data.

Table 8. Back-calculated properties of support layers by DCP results

Location	Layer	DCPI [mm/blow]	CBR	M_r [psi]	Remark of FWD results
K8	Aggregate	2.18	122.0	55,288	Weak
	Subgrade	11.94	18.2	16,340	
K2	Aggregate	3.84	64.7	36,846	Medium
	Subgrade	14.48	14.6	14,230	
I3	Aggregate	1.649	166.8	67,536	Strong
	Subgrade	11.88	18.3	16,399	

3.4. STATIC PLATE LOAD TEST

The static plate load test is an in-place test method that can directly measure modulus of subgrade reaction value for evaluation and design of pavement structures. This test has been performed on soils and unbound base and subbase materials to determine the modulus of subgrade reaction, k-value, or a measure of the shear strength of pavement components. In this study, the non-repetitive static plate load tests were conducted to determine the k-values at selected locations.

3.4.1. Test Procedure

The static plate load tests were conducted at locations K8, K2, and I3 corresponding to weak, medium, and strong support locations respectively, for verifying the composite modulus of subgrade reaction. The k-value from this test provides a design k-value with higher accuracy compared to other back-calculation methods [Suh et al., 2008]. Standard test methods recommend the use of a load bearing plate which has 30-in diameter or more [ASTM, 2004]. In this field test, however, a steel loading bearing plate with a 12-in diameter was used because a 30-in plate not only requires significantly heavy rebound loading but also is difficult to handle.

Figure 14 and Figure 15 show schematic diagrams of front view and ground view of plate load test equipment setting respectively. First, sand was put on the test surface to level the test location (Figure 16) and sit the steel bearing plate. The steel bearing plate which has 12-in diameter and 1-in thickness was placed on the sand. On the 12-in steel bearing plate, 9-in and 6-in steel plates were stacked carefully centered in a pyramid shape for uniform dispersion of the load (Figure 17). These steel plates also have 1-in thickness. A load cell was settled to measure a total load on the surface of the top steel plate. A hydraulic jack was assembled to apply the load. A fully loaded dump truck was used as reaction equipment. The gross weight of the reaction equipment was 48,000 lbs (Figure 18).

To measure vertical displacement of the ground two linear variable differential transformers (LVDTs) and one dial gauge were used. For installation of these apparatus, reference frame was used. The reference frame must have a sufficient length so that when load is applied, supports of the reference frame are not moved downward. In this field test, a 9-ft long frame was used (Figure 19). Two LVDTs and one dial gauge were assembled to measure the vertical displacement. The gauges were settled on the top surface of the 12-in steel bearing plate, 120 degrees apart from each other (Figure 20).
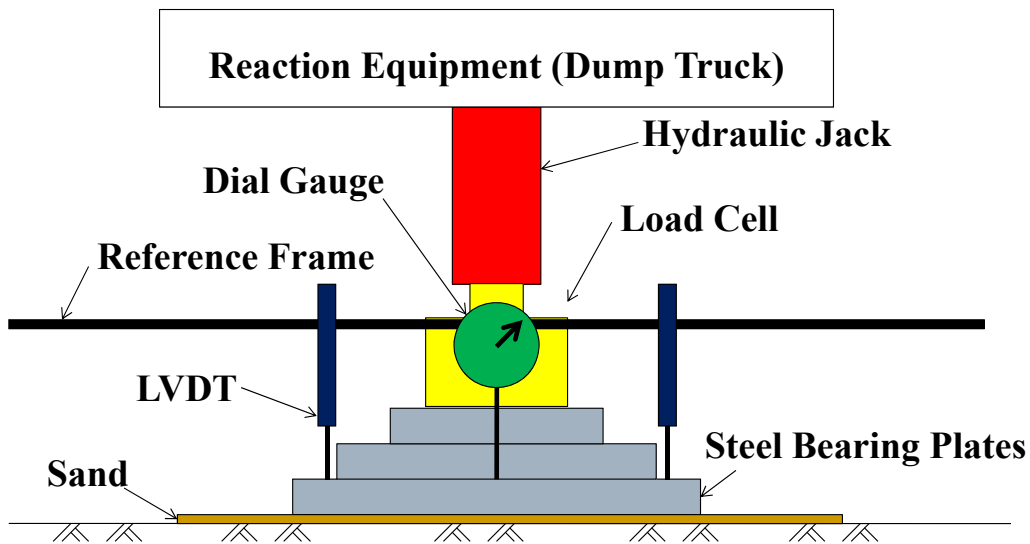
Figure 14. Plate load test setting (front view)
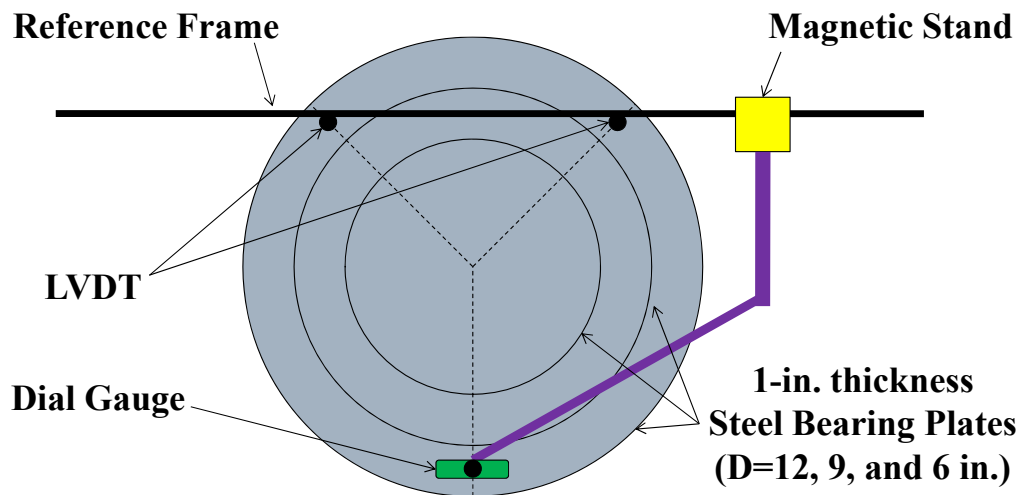
Figure 15. Plate load test setting (ground view)

Figure 16. Sand for leveling

Figure 17. Placing steel plates

Figure 18. Fully loaded dump truck for reaction

Figure 19. Reference bar installation

Figure 20. LVDTs and dial gauge installation

After all equipments have been properly assembled and arranged, the initial load was applied for sitting all equipments. Then, the preload was released until it was stabilized as indicated by the LVDTs. After stabilizing, load was applied again at a moderately rapid rate in uniform increments. In this field test, 0.005-in increment was applied. After each increment of load was applied, researchers waited until a rate of deflection was no more than 0.001-in per minute. Load and deflection readings were recorded for each load increment. This process was continued until the total deflection was more than 0.05 in. For all cases, more than 6 load-deflection points were obtained. The modulus of subgrade reaction was calculated at 0.05-in deflection point because many tests indicated that the deflection value of 0.05-in corresponded to k-value which agreed with the k-values obtained from deflection testing on full-size slabs [Phillippe, 1947; Middlebrooks and Bertram, 1942]. Additionally, to verify the effects of asphalt concrete stabilized layer for composite k-value, the plate load test was performed on the top surface of aggregate subbase layer at location K2 after removal of the 2-in asphalt concrete layer. Figure 21 illustrate the schema of the plate load field test.

Figure 21. Static plate load test

3.4.2. Results

Figure 22 shows the results of the *k*-value test. According to the standard test method and the Texas Department of Transportation [Tex-125-E, 1999], the *k*-value could be calculated at 50-mil deflection point with a corresponding pressure load. Measured *k*-values from static plate load test are affected by the size of the loading plate, diameter of the steel bearing plate. According to previous studies, a 12-in diameter loading plate produced twice the greater *k*-value than the use of a 30-in diameter plate. Also, the *k*-value was stabilized on the use of the 30-in diameter or bigger size loading plate.
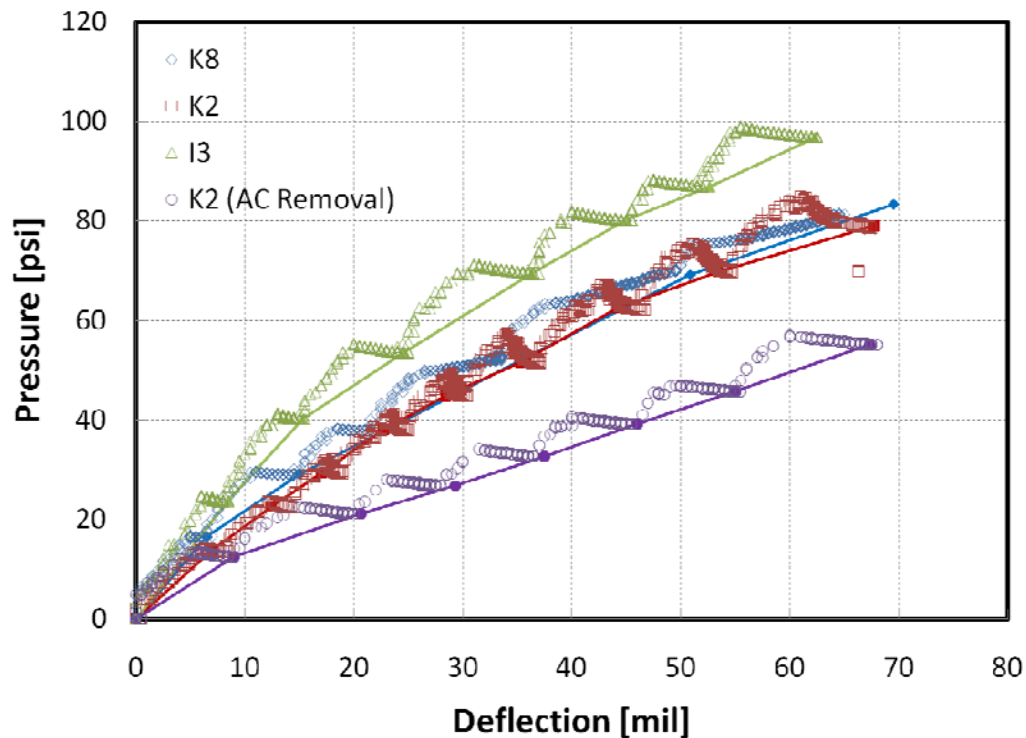
Figure 22. Static plate load test results

Figure 23 presents the correlation between *k*-value and size of the bearing plate [Teller and Sutherland, 1943]. For this reason, the obtained *k*-value from the test should be corrected. Table 9 presents both of *k*-values from raw data and the corrected *k*-value.

50

The measured *k*-values in this study are composite *k*-values including the effects of all layers under the loading plate. As shown in the results, the field testing site has composite *k*-values ranging from 670 to 920 psi/in, and locations K8 and K2 show almost identical support stiffness values. Also, in this field condition, the non-erodible asphalt concrete stabilized layer is apt to increase the composite *k*-value dramatically. The composite *k*-value increased from 420 to 670 psi/in due to the 2-in asphalt concrete stabilized base layer.
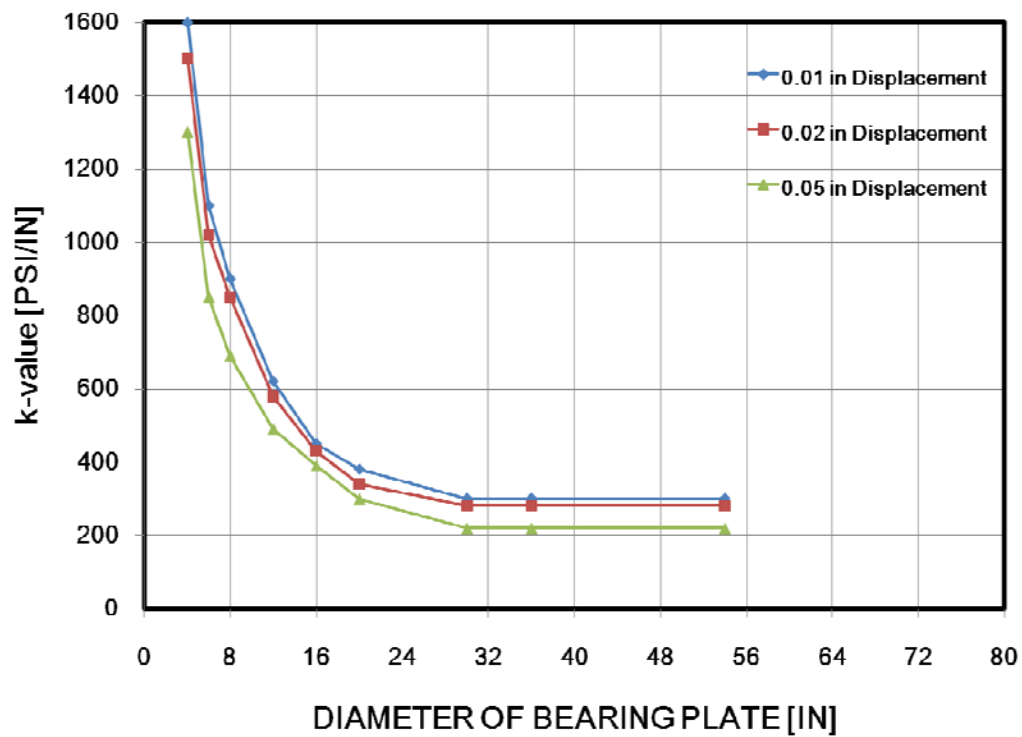
Figure 23. Relationship between *k*-value and bearing plate size

Table 9. Corrected *k*-value from static plate load test

Location	*k*-value from static plate load test [psi/in]	Corrected *k*-value [psi/in]	FWD Comparison
K8	1,360	680	Weak
K2	1,340	670	Medium
I3	1,840	920	Strong
K2 (AC Removal)	840	420	

3.5.   COMPARISON OF TEST RESULTS

Table 10 shows the results of FWD, DCP and plate load test. The result of FWD is represented by displacement at sensor No.1 when 9,000 lbs of load is applied. The result of DCP is represented by *DCPI*. The DCP index is the amount of penetrated distance per one blow. The result of static plate load test is represented by corrected *k*-value [psi/in] by 30-in diameter of bearing plate. As shown in the Table 10, the DCP index and the corrected *k*-values show a similar trend especially at the aggregate subbase. The location which has the largest corrected *k*-value, location I3, has the smallest DCP index at the aggregate subbase. The location which has the smallest corrected *k*-value, location K2, has the largest DCP index at the aggregate subbase also. Although DCP index follows the result of plate load test at the aggregate subbase, there is no relationship between the *DCPIs* of subgrade and the *k*-values. Therefore, it could be assumed that the impact on the composite *k*-value is governed by aggregate subbase property rather than subgrade property in this testing site.

Table 10. Comparison among FWD, DCP and *k*-value tests

Location	9-kip FWD displacement. at sensor no.1 [mils]	*DCPI* [mm/blow]		Corrected *k*-value [psi/in]
		Aggregate subbase	Subgrade	
K8	31.4	2.18	11.94	680
K2	26.5	3.84	14.48	670
I3	19.5	1.65	11.88	920
K2 (AC removal)	-	-	-	420

53

3.6.   SUMMARY

Three types of field tests, FWD, DCP, and plate load test, were performed to investigate field support conditions. The testing site consisted of 2-in asphalt concrete layer, 8-in aggregate layer, and subgrade layer. First, FWD tests were conducted on the top surface of asphalt concrete base layer to check support uniformity condition and obtain elastic modulus of each layer. The test results showed non-uniform support conditions. Also, three locations representing strong, medium, and weak spot were selected for DCP and the plate load test. Secondly, DCP tests were performed at the selected locations to investigate support characteristics under the asphalt stabilized base layer. The DCP results clearly presented characteristics of aggregate layer and subgrade. From these DCP results, *DCPI*, *CBR* and M_r were back-calculated using previously suggested relationships. Finally, static plate load tests were performed at the selected locations which are based on the FWD results to directly estimate modulus of subgrade reaction, *k*-value, of the testing site. Tests were conducted based on standard testing procedure, and *k*-values at the locations were directly estimated. Also, the estimated *k*-values were corrected since a 12-in diameter steel loading plate was used in this test. The corrected composite *k*-values of the testing site has 680-920 psi/in. On the other hand, the *k*-value on the top of aggregate layer was estimated as 420 psi/in. It could be identified that the asphalt stabilized base layer increased the composite *k*-value significantly in this field test. However, an obvious relationship between results of FWD, DCP and plate load test could not be verified.

CHAPTER 4: EVALUATION OF SUPPORT MODELS

For an accurate analysis of the behavior and performance of portland cement concrete (PCC) pavement systems, proper characterizations of support conditions provided by the layers below the PCC slabs is important. Modulus of subgrade reaction (*k*-value), by itself or in combination with other properties, has been historically used to characterize support conditions provided by the layers which are comprised of base and subgrade below the PCC slab. Also, the *k*-value has been an essential element in characterizing the support layers. However, determining an appropriate *k*-value that accurately represents the support layer conditions has been a challenge.

Considering an appropriate support model for the rigid pavement structures is one of the most important factors evaluating and estimating behavior and performance of the rigid pavement systems. However, because real behavior of the foundation layer that consists of fine-grained soil and aggregates is very complex, simplified support models have been developed and are used. As for the modeling of the support layers, two different models, elastic-isotropic solid model [Burmister et al., 1943; Hogg, 1938; Pickett and Ray, 1951] and the Winkler model [Westergaard, 1925; Westergaard, 1927a; Losberg, 1961], have been used. The Winkler model has been more widely used in modern rigid pavement design algorithms such as the '93 AASHTO Guide or MEPDG because of its simplicity. Currently, two different approaches based on Winkler foundation model are in use for rigid pavement design. These two pavement design algorithms have been and will be the most widely used. It is therefore important to identify the effects of these two methods in characterizing the support conditions on the analysis of the behavior and performance of rigid pavement structures. This will help in the selection process of the best pavement design.

4.1. SUPPORT MODELS FOR RIGID PAVEMENT ANALYSIS

4.1.1. Composite *k*-value Model

The '93 AASHTO Guide uses composite *k*-value support model for estimating pavement behavior and performance. Composite *k* contains the effects of all layers including stabilized base and subgrade under the concrete slab [AASHTO, 1986]. In this approach, the support condition of all the support layers could be characterized by a single *k* value. Here, the value of *k* is called composite *k*-value. The composite *k* can be viewed as a spring constant of a combined one layer that is "equivalent" to the same support characteristics as multiple layers. Figure 24 illustrates the composite *k*-value support model. Because this is the simplest model, historically, it has been most widely used to estimate structural behavior of rigid pavements. The first complete theory of structural behavior of rigid pavements was developed by Westergaard in the1920's [Westergaard, 1926; Westergaard, 1927b], and has been widely accepted as a tool to estimate stresses and deflections of the rigid pavement slabs. However, this composite *k*-value support model could not express detailed responses of subgrade such as shear behavior of the support structures, because a set of spring could only behave according to vertical loading, not horizontal or torsional loadings.
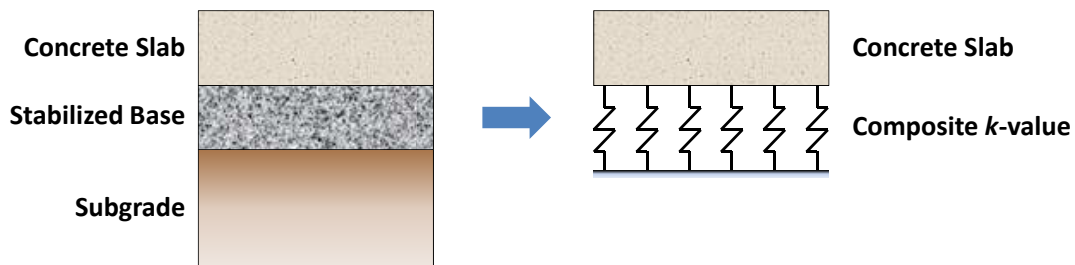
Figure 24. Composite *k*-value support model

4.1.2. Elastic-Isotropic Solid Layered Model

To express more realistic support behavior, elastic-isotropic solid layered support models were suggested. This approach is based on the assumption that the subgrade and base behave as an elastic-isotropic solid. Each layer beneath the concrete slab could be characterized by elastic modulus, E_{sb} and E_{sg}, and Poisson's ratio, v_{sb} and v_{sg}, of the layers which compose the support system. Figure 25 illustrate the elastic-isotropic solid layered support model. However, this multiple layered model gives complicated solutions to estimate behavior of concrete slab; finding or determining material properties of subbase and subgrade layer such as elastic modulus and Poisson's ratio of soil is also quite difficult. For this reason, this model for support system is rarely used.
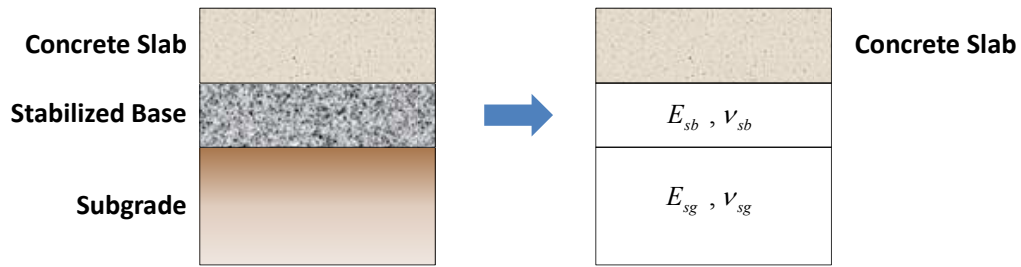
Figure 25. Elastic-Isotropic solid layered support model

4.1.3. Elastic Layer and *k*-value Composite Model

MEPDG uses the concept of effective *k* to characterize the support condition, especially subgrade condition. To determine an effective *k,* the support condition of all the layers beneath a stabilized base is characterized by *k*-value and that of a stabilized base is analyzed by the elastic-isotropic solid model [NCHRP, 2004]. Figure 26 shows the illustration of elastic layer and *k*-value composite support model. Material properties of stabilized base layer including elastic modulus and Poisson's ratio could be more easily measured than those of unbound soil properties. Subgrade *k*-value could be also estimated from previously developed methods such as FWD, DCP, or static plate load test. Using this support model for the analysis of concrete pavement behavior is more complicated than the use of a simple composite *k*-value; however, recently developed computer based analysis programs make it possible to solve the complicated problems more conveniently.
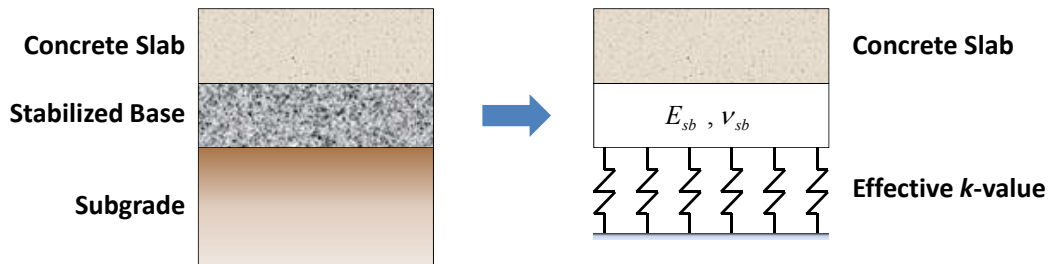
Figure 26. Elastic layer and *k*-value composite support model

4.2.   SIMULATION OF NON-REPETITIVE STATIC PLATE LOAD TEST USING FINITE ELEMENT METHOD

To evaluate an appropriate support model, numerical analyses were conducted using the ABAQUS 6.7, general purpose Finite Element (FE) analysis computer program. Using the FE program, non-repetitive static plate load tests were simulated, and k-values for selected support models were estimated. Also, to evaluate support models, the obtained k-values were compared with k-values from field tests.

4.2.1.   3-Dimensional Finite Element Models for Support System

Three different support models were considered. Case 1 is the composite k-value model which could be identified by a set of spring having coefficient k only. This model is the simplest model used in the current AASHTO Design Guide. Case 2 is the elastic-isotropic solid layered model which is composed of layered system defined by elastic modulus and Poisson's ratio for all layers including subgrade and base. Case 3 is the elastic layer and effective k-value composite model. In this model, a stabilized base layer is characterized by elastic solid elements and the subgrade is modeled by a set of springs which have coefficient k (termed 'effective k-value' in MEPDG). For the FE analysis, corrected k-values and elastic modulus from FWD field tests at location K2, which has medium stiffness condition, were used as input values.

Figure 27 illustrates the 3-dimentional finite element models for support system. For the elastic-isotropic solid layered model, 2-in stabilized base layer, 8-in aggregate subbase layer, and infinite subgrade layer were modeled by elastic solid element. For the elastic solid layer and k-value composite model, a 2-in stabilized base was developed by elastic solid element, and aggregate and subgrade layers identified by a set of spring which has a spring coefficient of 420 lb/in. Because the Case 1 model should be modeled by a set of vertical spring only having spring coefficient of 670 lb/in., modeling and k-value back-founding from the Case1 model is not meaningful. The back-founding k-value

must be 670 lb/in. Thus, Case1 support model was not considered in this study. The Case2 and Case 3 have been modeled quarter-symmetrically. Also, two different sizes of load bearing plates, 12 and 30-in diameter, were applied on top surface of base with a 2-in thickness, and 100 psi pressure loading was applied on the top surface of the plates for all analysis cases. Figure 28 shows the analysis results, vertical deflection contours of the support models.
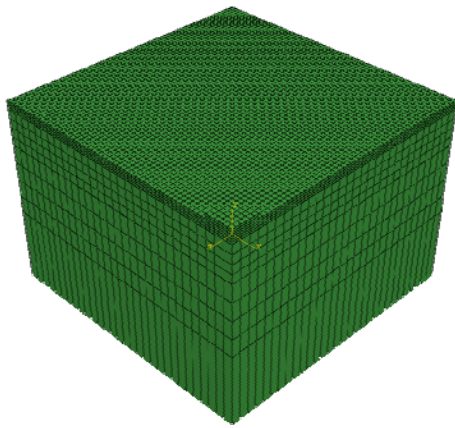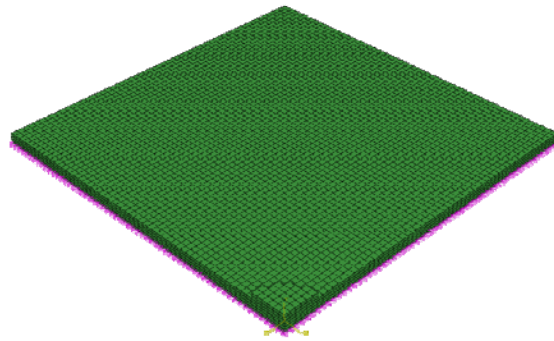
(a) Elastic solid layered model   **(b) Elastic layer and k-value composite model**

Figure 27. Finite element models for support system
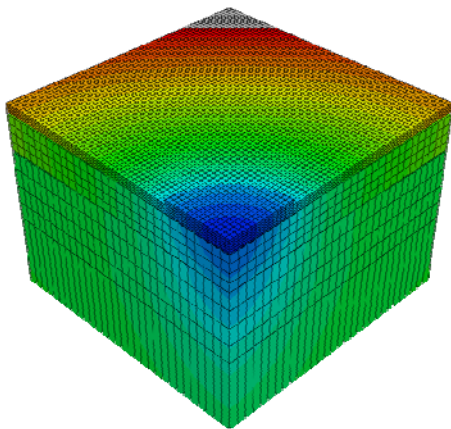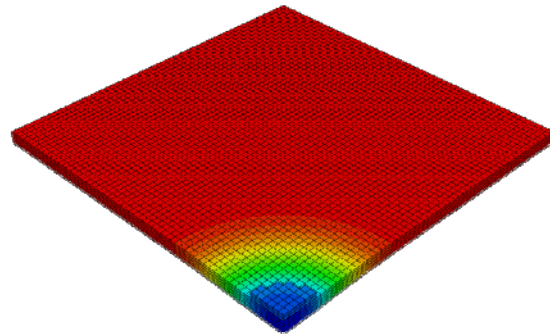
(a) Elastic solid layered model   **(b) Elastic layer and k-value composite model**

Figure 28. Deflection contours of support models

4.2.2.   Results and Comparison

Figure 29 illustrates the procedure of k-value computation for Case 3 support model. The k-values were calculated from average deflections obtained between center and edge of the loading areas which have 12 and 30-in diameter, and the applied pressure load was 100 psi. For Case 2 support model, an identical procedure was applied to estimate k-value. Table 11 presents the computed k-value for the three cases of support models and comparisons with field values. Field results show 1,340 psi/in for 12-in diameter loading area, and the corrected k-value is 670 psi/in corresponding to a 30-in diameter loading area. These values were set as criterion k-values which have been compared with computed k-values from the FE analysis of three of the cases. According to the results, the Case 3 support model, elastic solid layer and k-value composite model, gave the most identical k-value with the field results, whereas, case 2 support model, the elastic-isotropic solid layered model, produced relatively higher k-values. Case 1, the composite k-value support model, must give same computed k-value without any relationship with size of loading area.
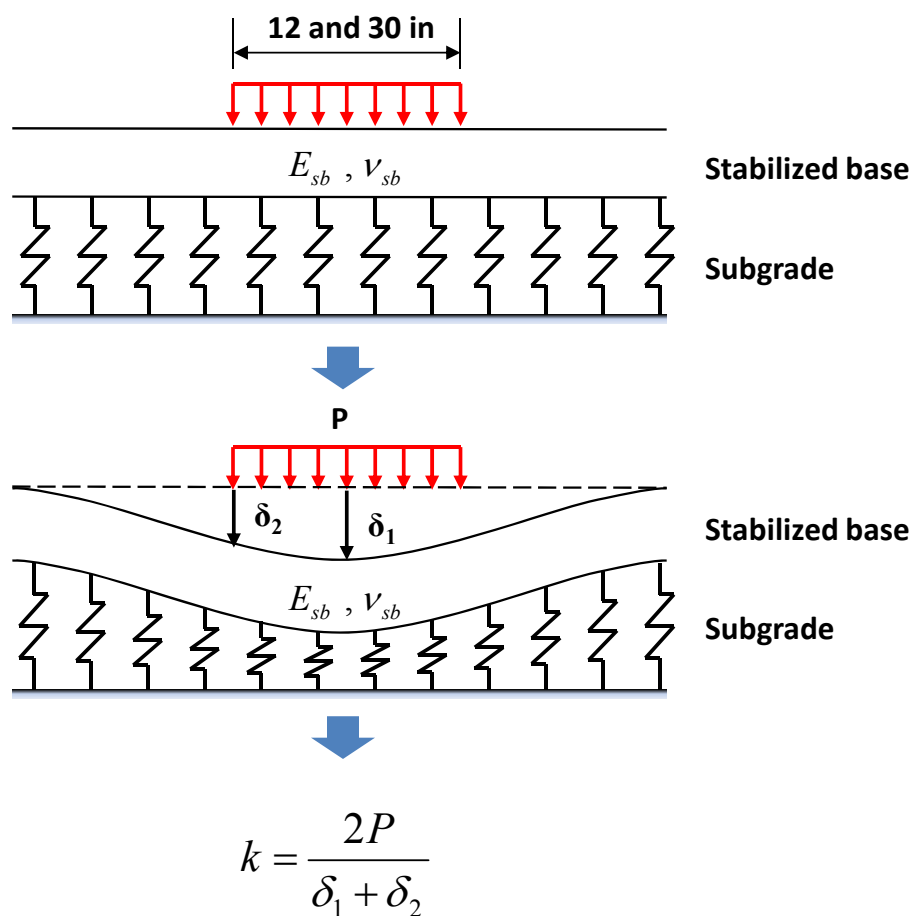
Figure 29. *k*-value computation procedure

$$k = \frac{2P}{\delta_1 + \delta_2}$$

Table 11. Computed *k*-value from FE analysis [psi/in]

Diameter of loading plate	12 in	30 in
Field case	1,340	670
Case 1	670	670
Case 2	3,091	975
Case 3	1,673	676

4.3.   EFFECTS OF LOADING PLATE SIZE

A previous study by Teller found that *k*-value estimated from a field static plate load test is affected by the loading plate size [Teller and Sutherland, 1943]. Thus, standard testing manuals have suggested the use of loading plate of 30-in diameter or more. To verify the effect of the size of the load bearing plate, the non-repetitive static plate load tests with varying size of the loading plate ranging from 6-in to 84-in diameter were simulated for the three different support models using the FE analysis method. Figure 30 shows the analysis results. The computed *k*-values was converged at more than 30-in diameter for Case 3 support model, and more than 60-in diameter for Case 2 support model. The Case 1 support model is not affected by size of the loading area. Thus, it could be assumed that Case 3 support model, elastic layer and *k*-value composite model, could express more reasonably field support conditions, and this Case 3 model is recommended for the design of rigid pavement system.
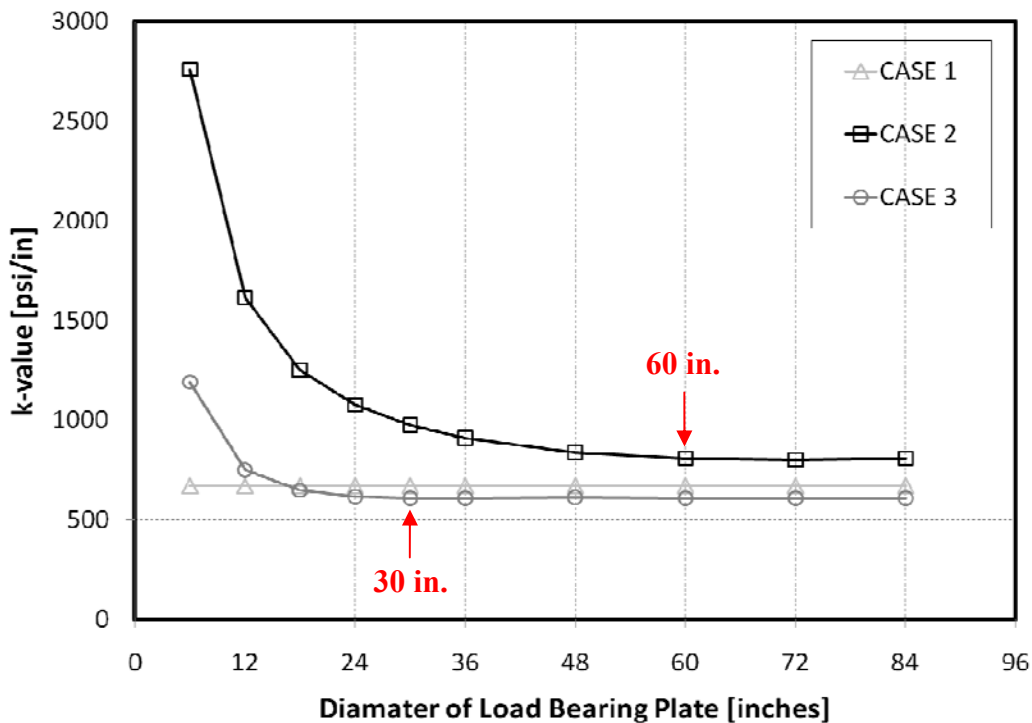
Figure 30. Effect of size of loading area for the three different support models

The amount of deflection could be determined by the magnitude of vertical resistance of base and subgrade layers and shear resistance along the circumference of the loading area. To identify the reasons the *k*-value could be affected by the size of the loading area, additional analysis were performed. The Case 3 support model was adapted for this study. First, to identify vertical resistance of the support system, vertical stress distributions in stabilized base layer were reviewed. Figure 31 presents the vertical stress distributions at the top, middle, and bottom of a stabilized base layer due to different size of loading area raging from 12 to 42-in diameter. The distribution is plotted along the distance from the center of the loading area. Vertical stress at the top surface of the base layer shows 100 pci, identical magnitude of pressure loading, for all cases of loading area. However, at the bottom of the base layer, the magnitudes of vertical stress for 12, 18, and 24-in diameter is decreased, but identical stress levels have been shown for cases larger than 30-in diameter. Secondly, vertical stress and deflection of subgrade layer modeled by a set of spring is also considered. Figure 32 shows the stress and deflection distributions of subgrade due to the different sizes of loading plate. The maximum vertical stress and displacement are increasing as diameter of loading area increases to 30-in, however, the maximum stress and displacement are identical for larger than 30 in of loading area. Finally, to identify shear resistance of the stabilized base layer, shear stress distributions were plotted. Figure 33 presents the shear stress distribution at the middle depth of base layer along distance from the center of the loading area. The maximum shear stress is induced at edge of the loading area, and the value is decreasing as the loading area increases to 30-in. For a larger diameter than 30-in, the value of maximum shear stress is the same as the case of vertical stress and displacement of subgrade. These phenomena present implications of the effect of loading area size on the variation of modulus of subgrade reaction, *k*-value. For this reason, the amount of deflection of the support layer might be determined by a composition of the magnitude of vertical and shear resistance of the support system. Accordingly, this deflection has directly affected the determination of *k*-value.
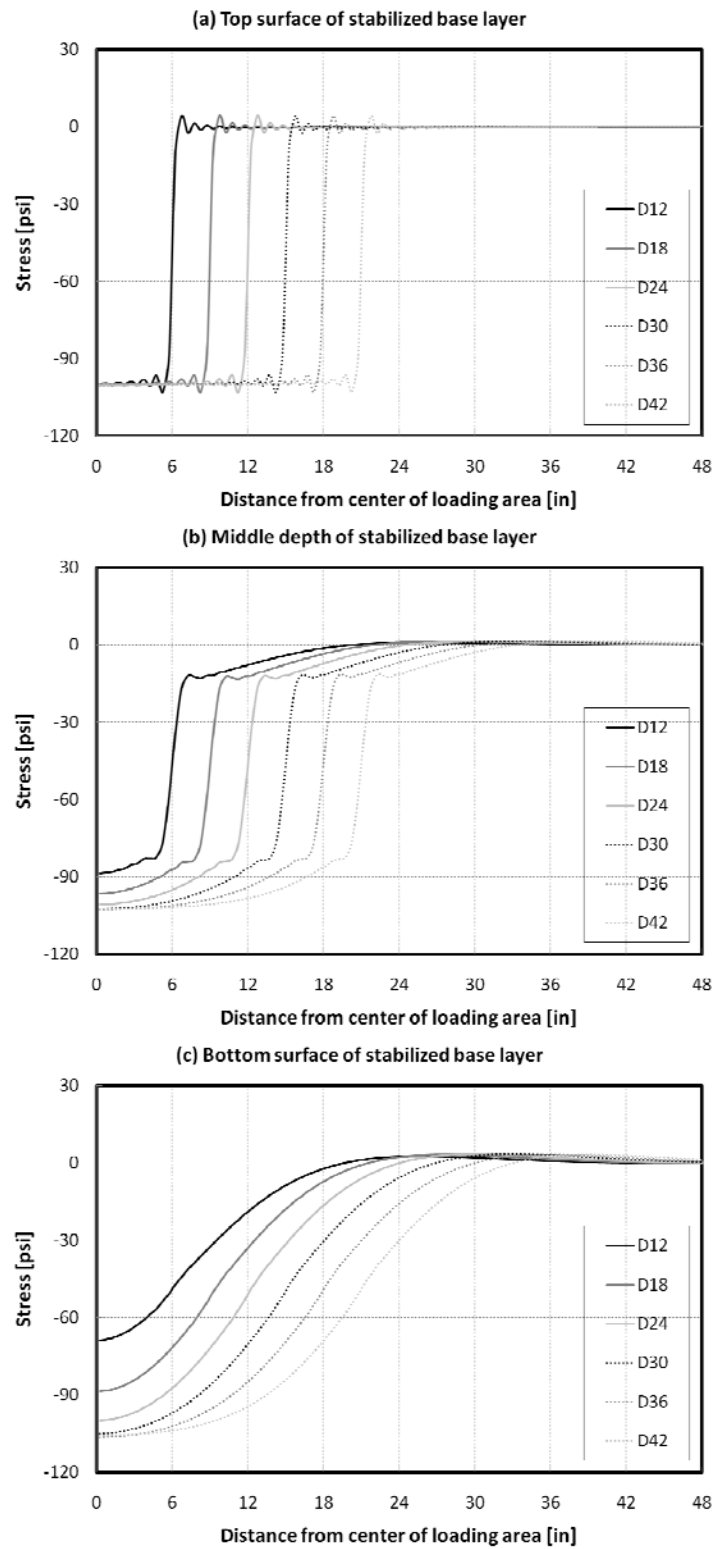
Figure 31. Vertical stress distribution due to diverse loading plate size
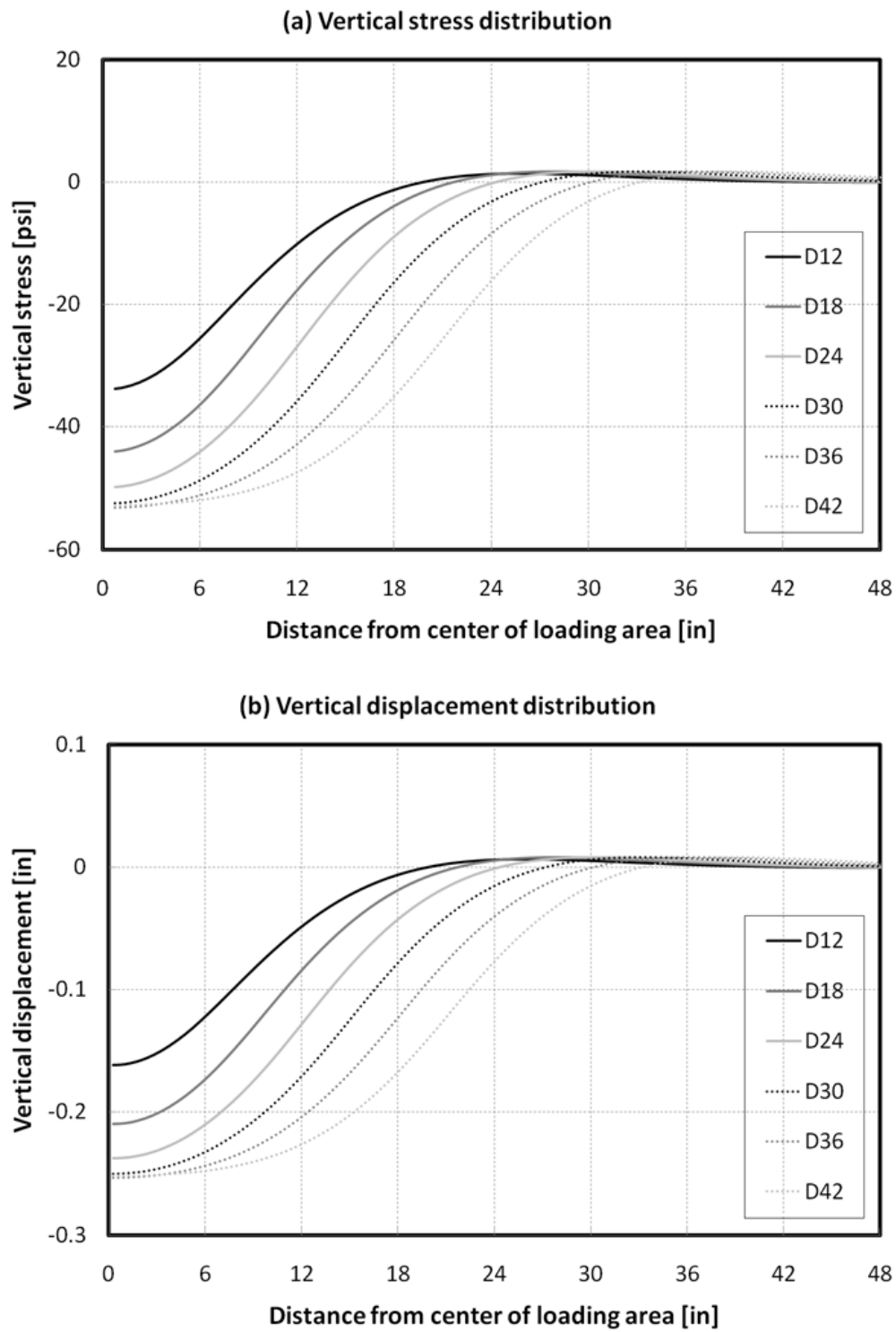
Figure 32. Stress and deflection of subgrade due to diverse sizes of loading plate
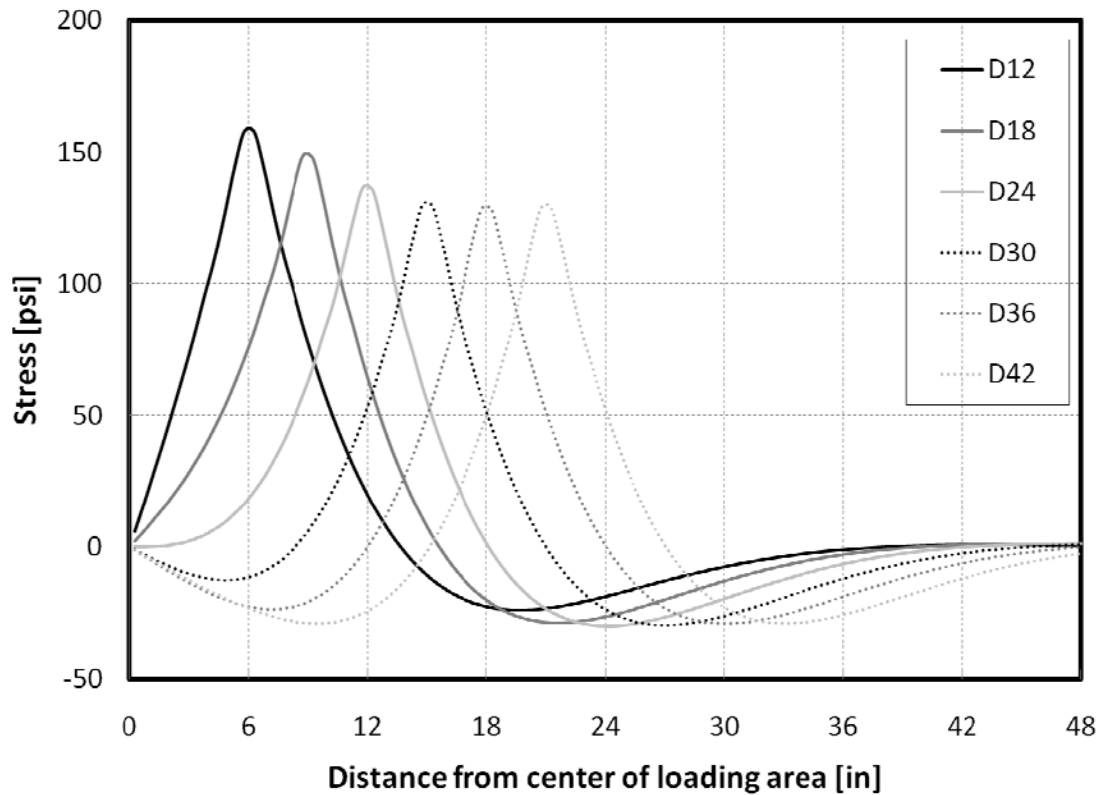
Figure 33. Shear stress distribution at middle depth of stabilized base layer

Field support conditions for both vertical and shear resistance depend on base and subgrade material characteristics. Model Case 1, composite k-value support model, which is composed with a set of spring, could reflect the vertical resistance, but the shear resistance could not be considered. On the other hand, the Case 2 model, elastic isotropic solid layered support model, which is modeled with a composition of elastic layers, could over-estimate the effect of shear resistance of the support, as well as, the k-value. However, the Case 3 support model, elastic solid layer and k-value composite model, has shown an appropriate level of combination of vertical and shear resistance.

4.4.   EFFECTS OF SUPPORT LAYER PROPERTIES ON COMPOSITE *K*-VALUE

To evaluate the effects of properties of support layers on composite *k*-value, non-repetitive static plate load tests were simulated and composite *k*-values were computed using ABAQUS FE analysis program for diverse combinations of support layer properties. In this study, an elastic solid layer and subgrade *k*-value composite support model was considered. As variables which could affect composite *k*-value, thickness of stabilized base, elastic modulus of the stabilized base, and subgrade *k*-value (effective *k*) were considered. The input variables and their ranges are shown in Table 12. The composite *k*-values were computed from average deflection at center and edge of loading area and 100 psi pressure loading which is applied on the top surface of the loading area having 30-in diameter.

Table 12. Input variables and values for computing composite *k*-values

Variables	Values
Thickness of stabilized base [in]	2, 3, 4, 5, 6
Elastic modulus of stabilized base [ksi]	50, 100, 300, 500, 1000, 2000
Subgrade *k*-value [psi/in]	50, 100, 150, 200, 250, 300

Table 13 presents the computed composite *k*-values due to various support properties. As shown in the table, the composite *k*-value increases as the values of variables are increasing. However, the increasing rates are different depending on the variables including thickness of stabilized base, elastic modulus of the base material, and subgrade *k*-value. Thus, the effects of the material and geometrical properties of support layers are discussed further, and the optimum combinations satisfying desired composite *k*-value are suggested in following chapters.

Table 13. Computed composite *k*-value due to various support properties

Thickness of base layer [in]	Elastic modulus of base material [ksi]	Subgrade *k*-value [psi/in]					
		50	100	150	200	250	300
2	50	69	128	189	251	314	378
	100	76	134	194	255	316	377
	300	92	156	217	278	339	399
	500	103	172	236	299	361	422
	1000	124	201	272	340	406	470
	2000	154	244	324	400	472	542
3	50	81	142	201	261	320	380
	100	93	158	221	282	342	402
	300	124	202	274	341	407	472
	500	145	233	311	384	455	523
	1000	184	289	380	464	544	620
	2000	239	367	476	576	669	758
4	50	95	161	223	284	343	402
	100	114	188	256	320	384	445
	300	161	255	338	415	489	560
	500	193	300	394	480	562	640
	1000	251	384	497	600	695	787
	2000	332	500	640	766	883	993
5	50	114	186	252	316	377	437
	100	141	226	301	372	440	507
	300	207	321	419	509	593	674
	500	250	382	494	596	691	781
	1000	330	498	637	762	878	986
	2000	441	660	837	994	1138	1273
6	50	133	214	286	353	418	480
	100	169	265	349	426	500	570
	300	255	389	502	604	695	790
	500	311	470	602	720	830	933
	1000	416	621	789	938	1074	1202
	2000	557	830	1049	1241	1415	1577

4.4.1.   Thickness of Base Layer

First, effects of thickness of the stabilized base layer on composite k-value of the support system are discussed. Figure 34 illustrates the thickness effects. Here, x-axis is the thickness of stabilized base layer, and y-axis is composite k-value of the whole support system. Computed composite k-value increased as subgrade k-value and elastic modulus of the base material increased. The plotted data also shows the different increment rates of composite k-value due to the base thickness changing under diverse values of subgrade k-value and elastic modulus of the base material. Table 14 presents the increment rates of composite k-value as changing base thickness. A support condition having low subgrade k-value but high elastic modulus of base material has more significant effect on composite k-value than a condition that subgrade k-value is high and elastic modulus of base layer is low.

Graphs for all cases are appended, which show the effect of stabilized base thickness on composite k-value in APPENDIX A. The results have given identical relationships as presented in the Table 14.

Table 14. Increment rates of composite k-value as thickness of base increases

Subgrade k-value	Elastic modulus of base material	Increment rate of composite k-value
Low	Low	**Low**
Low	High	**Medium**
High	Low	**Low**
High	High	**High**
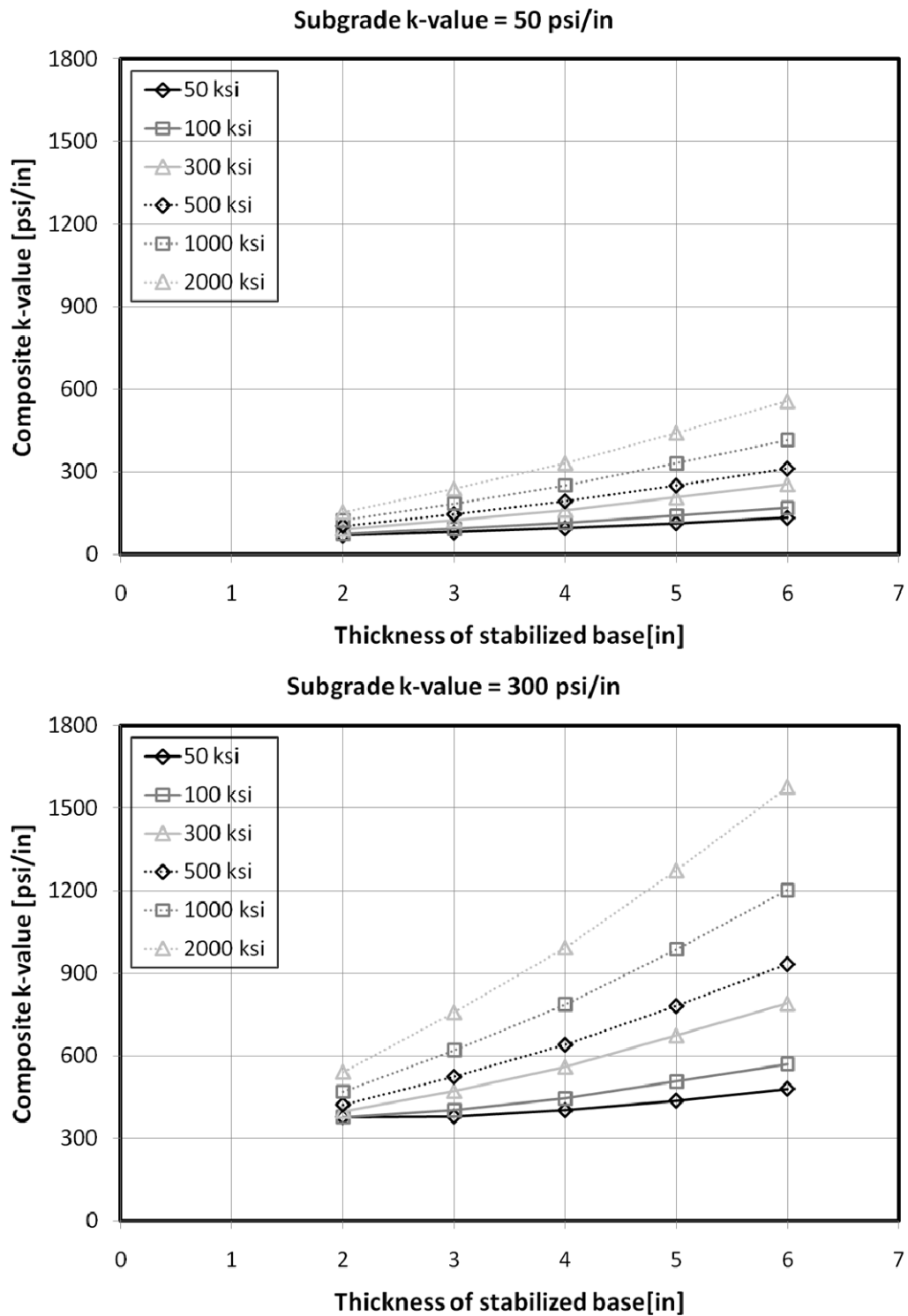
Figure 34. Effect of thickness of stabilized base on composite *k*-value

4.4.2.   Modulus of Elasticity of Base Material

Secondly, the effects of modulus of elasticity of stabilized base layer on composite k-value of the support system are discussed. Figure 35 illustrates the effects of the elastic modulus of the stabilized base material. Here, x-axis is the modulus of elasticity of the base layer, and y-axis is the composite k-value of the whole support system. As with the previous case, computed composite k-value increased as subgrade k-value and thickness of the stabilized base layer increased. The plotted data also show that the increment rates of composite k-value is changing due to change of the elastic modulus of the base material under diverse conditions of subgrade k-value and thickness of the stabilized base layer. Table 15 presents the increment rates of composite k-value as changing elastic modulus of base material. A support condition having low subgrade k-value but high thickness value of base layer has given larger effect in the increase of composite k-value of the whole support system than a combination case that subgrade k-value is high and thickness of base layer is low.

Graphs for all cases are appended showing the effect of elastic modulus of the stabilized base material on composite k-value of the support system in APPENDIX A. These results have shown identical relationships as presented in the Table 15.

Table 15. Increment rates of composite k-value as elastic modulus of base material increases

Subgrade k-value	Thickness of stabilized base layer	Increment rate of composite k-value
Low	Low	**Low**
Low	High	**Medium**
High	Low	**Low**
High	High	**High**
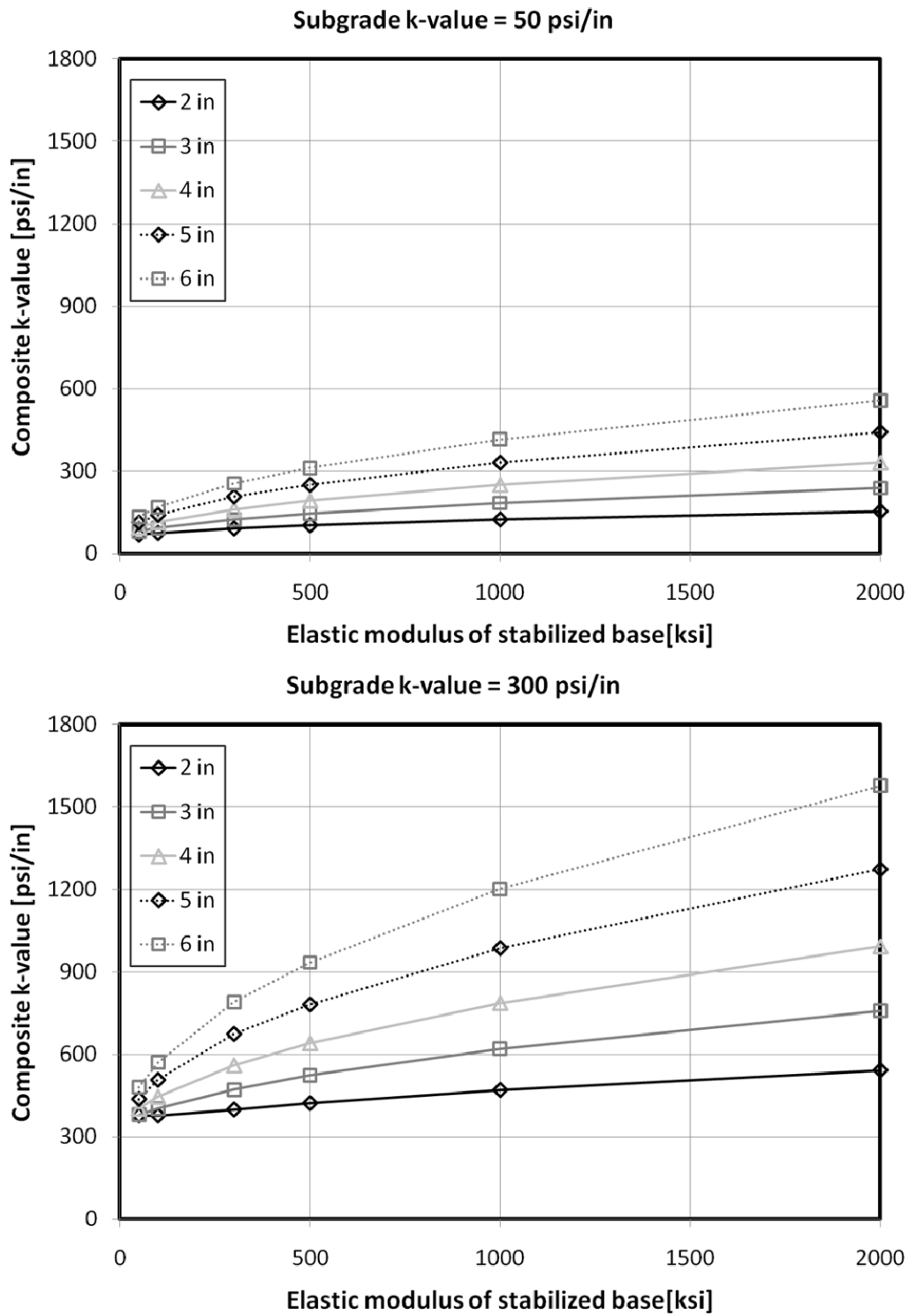
Figure 35. Effect of elastic modulus of stabilized base on composite *k*-value

4.4.3.   *k*-value of Subgrade Layer

Finally, the effects of subgrade *k*-value and effective *k*-value, on the composite *k*-value of the whole support system are discussed. Figure 36 shows the effects of subgrade *k*-value. Here, *x*-axis is the *k*-value of subgrade layer, and *y*-axis is the composite *k*-value of the whole support system. As with previous cases, the computed composite *k*-value of the support system increases as thickness and elastic modulus of the stabilized base increase. For this case, the plotted data have also revealed different increment rates of the composite *k*-value due to the change of the subgrade *k*-value under various ranges of base thickness and elastic modulus of the base material. Table 16 addresses the increment rates of composite *k*-value as increasing *k*-value of the subgrade layer. Unlike the former cases, a support condition which has low thickness of stabilized base layer but high elastic modulus of the base material shows similar effect, which is increasing composite *k*-value for a condition with high thickness of the base layer and elastic modulus of the stabilized base material is low.

Graphs for all cases are appended that present the effect of the subgrade *k*-value changing on composite *k*-value of the support system in APPENDIX A. These results have also addressed identical relationships as presented in Table 16.

Table 16. Increment rates of composite *k*-value as subgrade *k*-value increases

Thickness of stabilized base layer	Elastic modulus of base material	**Increment rate of composite *k*-value**
Low	Low	**Medium**
Low	High	**Medium**
High	Low	**Medium**
High	High	**High**
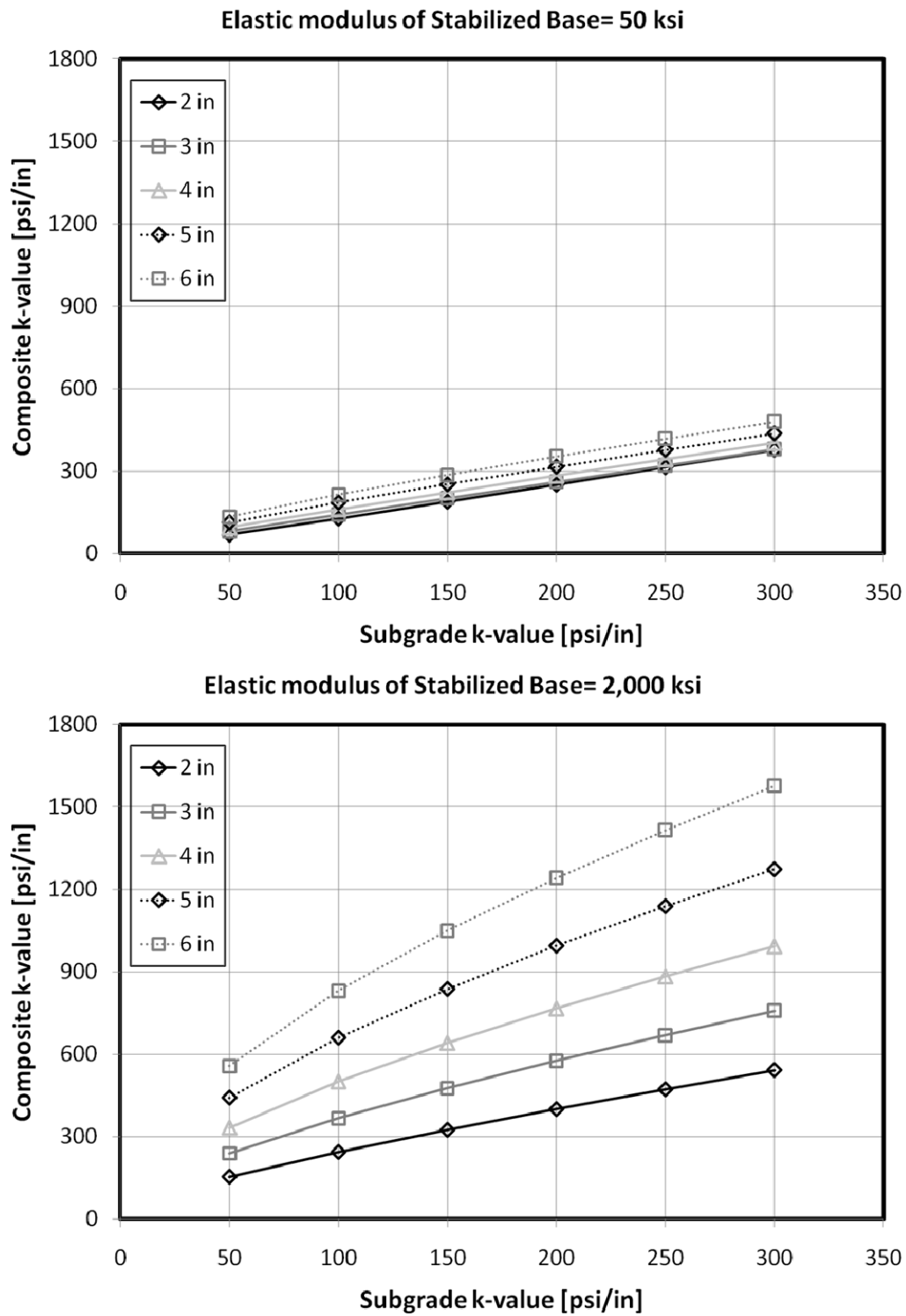
Figure 36. Effect of subgrade *k*-value on composite *k*-value

4.4.4. Results

Regression analysis is performed to verify the effects of the support layer properties on the composite k-value using SPSS computer program. In this analysis, the composite k-value is set as a dependent variable, and independent variables are thickness of base (T_b, in), elastic modulus of the base material (E_b, ksi), and subgrade k-value (k_{sg}, psi/in). Table 17 presents regression coefficients to estimate the composite k-value. Relative effects of the independent variables on the composite k-value could not be compared using un-standardized coefficients because the variables are measured in different units such as inches, ksi, and psi/in. Accordingly, standardized coefficients (β) are used, which are defined as follow:

$$\beta = Unstandardized\ coefficient \times \frac{S.D\ of\ Dependent\ variable}{S.D.\ of\ Independent\ variable} \qquad (4.1)$$

Table 17. Regression coefficients for composite k-value

Independent variables	Un-standardized coefficient	Standardized Coefficient
Constant	-395.669	-
Thickness of base	92.335	0.475
Elastic modulus of base material	0.223	0.550
Subgrade k-value	1.829	0.568

Consequently, subgrade k-value has the greatest effect on the composite k-value, then the elastic modulus of the base material is next, and the last is the thickness of the base layer. However, the differences among those are relatively very small. Therefore, it could be assumed that the effects of support layer properties defining composite k-value are almost identical. Also, the regression equation could be expressed by equation 4.2. This has 85.1% of R^2-*value*.

$$k_\infty = -395.7 + 92.3T_b + 0.223E_b + 1.829k_{sg} \tag{4.2}$$

4.4.5. Optimum combination of support layer properties for desired composite *k*-value

It is important to determine the optimum materials and structural design for rigid pavement support systems. A study conducted to determine optimum base material characteristics focused on pavement drainage such as the determination of base layer permeability [White et al., 2004]. However, one of the most important considerations for pavement construction has been initial construction cost. For example, Texas Department of Transportation (TxDOT) has become increasingly aware of the rising cost associated with the stabilized base layer below concrete slab for rigid pavement constructions [Jung et al., 2009].

Accordingly, in this chapter, an economic point of view is used to select optimum support characteristics. First, three types of support properties - subgrade *k*-value, elastic modulus of stabilized base material, and thickness of the base layer - were considered to determine an optimum combination of the characteristics. Secondly, composite *k*-value on the top surface of the stabilized base layer has been set as a criterion of the determination because the *k*-value has been directly or indirectly used on rigid pavement designs.

Based on results about the effects of the support properties on composite *k*-value, desired or target composite *k*-value was set first, and cases of combinations were found using graphs previously shown which satisfy the desired composite *k*-value. It would be difficult and unreasonable to adjust the subgrade *k*-value and elastic modulus of the stabilized base material in detail. The subgrade *k*-value might be set as a specific value after compacting existing soil at a construction field. Also, elastic modulus of the stabilized base material will be fixed by the type of the stabilized base such as cement stabilized base, asphalt concrete base, or lean concrete base. Thus, it would be more reasonable to adjust the thickness of the stabilized base layer. Figure 37 presents an example of a combination selection for desired composite *k*-value. In this case, the desired and targeted composite *k*-value is set at 300 psi/in. To achieve the condition of the subgrade *k*-value equaling 50 psi/in, three cases satisfy the target composite *k*-value, 300

psi/in. If a stabilized base material of 500 ksi of elastic modulus is used, 5.8 in of the base thickness is required for the target composite *k*-value, 300 psi/in. Also, material having 1000 ksi elastic modulus needs 4.6 in of the base thickness, and material having 2000 ksi requires 3.6-in thickness of the stabilized base.
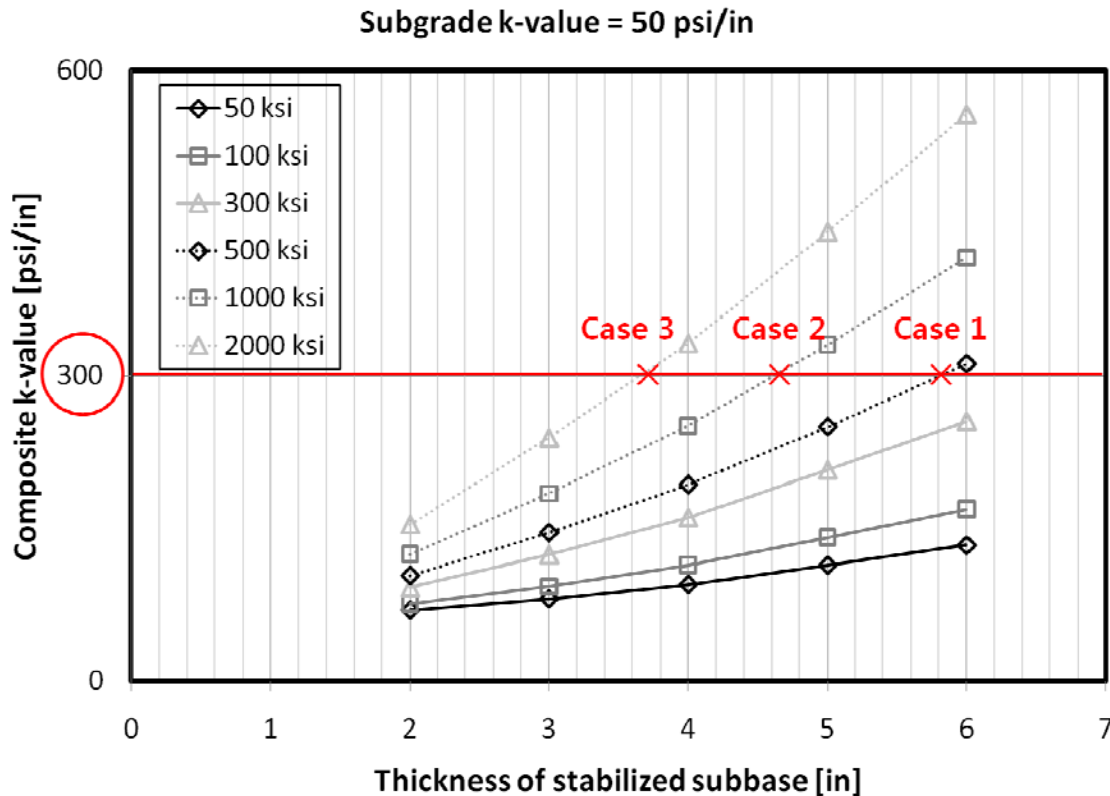
Figure 37. Example of combination selections for desired composite *k*-value

Table 18 shows the selected combinations for desired composite *k*-value, 300 psi/in. In this example, total of 14 cases are available according to subgrade *k*-value ranging from 50 to 200 psi/in. Based on this table, if the costs making subgrade having specific *k*-value (50, 100, 150, or 200 psi/in in this example) can be known, stabilized materials which have specified elastic modulus (50, 100, 300, 500, 1000, and 2000 ksi in this example), and constructing base layer with desired thickness, the most economical combination could be selected to complete a target composite *k*-value.

Table 18. Combinations for desired composite *k*-value 300 psi/in

No.	Subgrade *k*-value [psi/in]	Elastic modulus of base material [ksi]	Thickness of base layer [in.]
1		500	5.8
2	50	1,000	4.6
3		2,000	3.6
4		300	4.7
5	100	500	4
6		1,000	3.1
7		2,000	2.5
8		300	3.4
9	150	500	2.9
10		1,000	2.3
11		50	4.5
12	200	100	3.5
13		300	2.4
14		500	2

4.5.   SUMMARY

For an accurate analysis of behavior of rigid pavement systems, the selection of the most appropriate support model is critical. Different values of k which is an essential element in characterizing the support layer could be considered according to the different support models. Thus, determining appropriate k-value has been challenging.

Three types of support model have been introduced. The first one is composite k-value support model. The composite k-value support model could be expressed as a set of spring having coefficient k which includes all layers under the concrete slab. The second model is an elastic-isotropic solid layered support model. It is considered in this model that all layers beneath the concrete slab behave as an elastic-isotropic solid. However, this support model has not been widely used in modern design algorithms. The last one is an elastic layer and k-value composite support model. In this support model, stabilized base layer is considered as an elastic solid layer, and subgrade is analyzed by a set of spring having coefficient k.

Using an FE analysis computer program, static plate load tests were simulated on the three different support models to verify the most appropriate one. The computed k-values were compared with the k-values from the field tests. The analysis results showed that the elastic layered and k-value composite support model could predict the behavior of a support system more closely in aspects of the computed k-value and effects of loading plate size. Also, to verify the effect of size of the loading area, another analysis was performed. Vertical and shear resistance of the support system are obviously affected by size of loading area. Thus, the computed k-values are influenced by the loading plate size.

The effects of support layer properties on composite k-value were also identified. Here, the thickness of the stabilized base, elastic modulus of the stabilized base material, and subgrade k-value were set as the support layer properties. Based on the study results, a method is suggested to find optimum combination of support layer properties for satisfying the desired composite k-value.

CHAPTER 5: BEHAVIOR OF CONCRETE SLAB ON ELASTIC FOUNDATION

Behavior of concrete slab on elastic foundation could be affected by several factors such as temperature distributions in the concrete slab, external physical loading, and friction between the slab and foundation. Historically, before computers with sufficient arithmetic power were available, researchers relied on close-form solutions to investigate the behavior of concrete slab. With the improved computing capability available, the behavior of concrete slab has been modeled with various numerical methods. In this chapter, the basic causes of stress or deflections of concrete slab relying on elastic foundation are reviewed. Classical theories of estimating the behavior of the concrete slab are also compared to recently developed analysis solutions.

5.1. BASIC UNDERSTANDING OF CONCRETE SLAB BEHAVIOR

Traditional theories estimating concrete slab stresses and deflections have been based on Winkler foundation model. Thus, modulus of subgrade reaction, *k*-value, is one of the most important variables in predicting concrete slab stresses and deflections. Factors in concrete slab behavior could be categorized by temperature loading, vehicle wheel loading, and friction effect between the bottom surface of the concrete slab and the top surface of the support system.

5.1.1. Temperature Loading

Concrete slab curls up and down due to daytime and nighttime temperature variations. Ambient daytime temperature makes that the temperature on the top surface of the concrete slab, T_t, is higher than bottom of the slab, T_b. This temperature difference between top and bottom produces a curling down of the concrete slab. On the other hand,

nighttime ambient temperatures produce higher temperature at bottom of the slab than top surface, and cause the slab to curl up. Figure 38 illustrates curling down and up conditions of concrete slab due to daytime and nighttime temperature conditions respectively.

$$T_t > T_b \qquad\qquad\qquad T_t < T_b$$

Day-time Condition   **Night-time Condition**
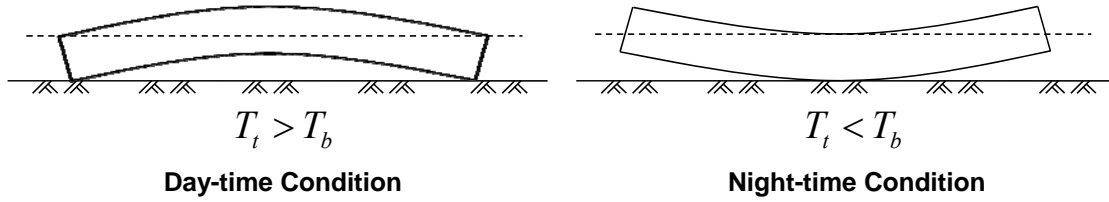
Figure 38. Slab curling due to temperature conditions

These curling up and down conditions induce tensile and compressive stresses in the concrete slab. Since portland cement concrete (PCC) has a much stronger compressive strength than tensile strength, concrete pavement design has been governed by the level of tensile stress under various loading cases. Previous studies report that because the maximum temperature difference and tensile stress is much larger during the daytime than nighttime, the daytime curling stress is the most critical [Teller and Sutherland, 1935].

The stresses induced by temperature difference in the top and bottom of the concrete slab are called warping stress, and Bradbury suggested following equation 5.1 and 5.2 to estimate the maximum tensile warping stresses induced at the edge and interior of the concrete slab center respectively [Bradbury, 1938].

$$Edge\, stress: \quad \sigma = \frac{CE\,\alpha\Delta T}{2} \tag{5.1}$$

$$Interior\, stress: \quad \sigma = \frac{E\alpha\Delta T}{2}\left[\frac{C_1 + \nu C_2}{1-\nu^2}\right] \tag{5.2}$$

In these equations, E is the modulus of elasticity of concrete material, α is the coefficient of thermal expansion (*CTE*), and v is the Poisson's ratio of the concrete. $\varDelta T$ is the temperature difference between the top and the bottom of the concrete slab and C means stress coefficient. Here, C_1 is the coefficient in the direction of calculated stress, and C_2 represents the coefficient in perpendicular direction to C_1. The stress coefficient, C, can be obtained from Figure 39 developed by Bradbury in 1938.
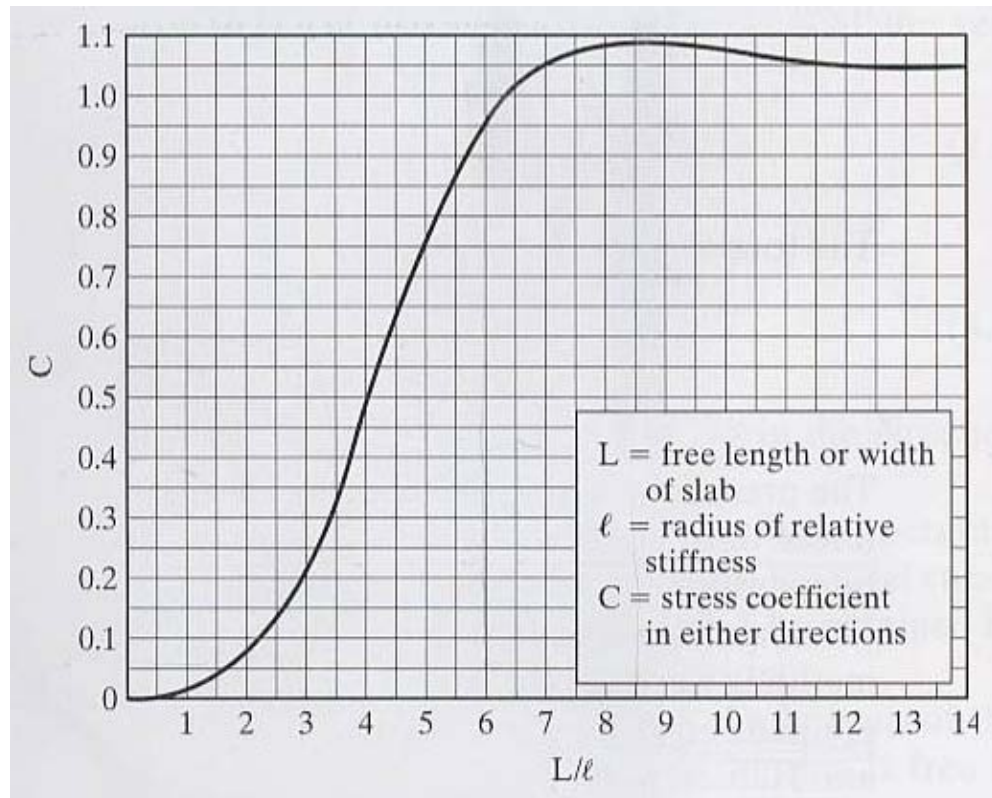
Figure 39. Stress coefficient chart by Bradbury in 1938

Here, l represents the radius of relative stiffness which is the relative stiffness of the PCC slab to the stiffness of the elastic foundation structure beneath the concrete slab. The radius of relative stiffness could be calculated by the following formula 5.3 which was developed by Westergaard in 1926 [Westergaard, 1926].

84

$$l = \sqrt[4]{\frac{Eh^3}{12(1-v^2)k}}$$

(5.3)

According to Bradbury's theoretical formulas, the modulus of subgrade reaction, k, has effects on the maximum tensile stresses induced in the concrete slab due to temperature differential between the top and bottom of the slab. A high k-value indicates a stiff support condition with the radius of relative stiffness, l, decreasing, and this increases the stress coefficient. Accordingly, the tensile stress induced in the PCC slab is increased. In other words, strong support conditions produce higher tensile stress, which is a disadvantage to the concrete slab in respect to stress development.

5.1.2. Wheel Loading

Concrete slab structures relying on elastic foundation, especially, rigid pavement system, support and endure heavy vehicle wheel loadings, which induce stresses. Historically, researchers have developed theories which could estimate stresses induced in the concrete slab due to wheel loading. In 1926, Westergaard developed closed form solutions to estimate critical stresses for three loading conditions, corner, interior, and edge loading conditions [Westergaard, 1926].

Corner loading condition is when the center of a load is placed on the top surface at the bisector of the corner angle that produces critical tensile stress at top surface of the concrete slab. The maximum stress can be obtained from equation 5.4, and the maximum deflection of the concrete slab is calculated by equation 5.5.

$$\sigma_c = \frac{3P}{h^2}\left[1-\left(\frac{a\sqrt{2}}{l}\right)^{0.6}\right]$$

(5.4)

$$\delta_c = \frac{P}{kl^2}\left[1.1-0.88\left(\frac{a\sqrt{2}}{l}\right)\right]$$

(5.5)

85

Interior loading condition is when a load is applied to the top surface of the interior of a concrete slab. This loading condition induces critical tensile stress at the bottom surface of the concrete slab. The critical stress due to interior wheel loading can be calculated by equation 5.6, and the maximum deflection can be computed from equation 5.7.

$$\sigma_i = \frac{0.316P}{h^2}\left[4\log\left(\frac{l}{b}\right)+1.069\right] \tag{5.6}$$

$$\delta_i = \frac{P}{8kl^2}\left[1+\frac{1}{2\pi}\left\{\ln\left(\frac{a}{2l}\right)-0.673\right\}\left(\frac{a}{l}\right)^2\right] \tag{5.7}$$

$$b = a \qquad\qquad when,\ a \geq 1.724h$$
$$b = \sqrt{1.6a^2 + h^2} - 0.675h \qquad when,\ a < 1.724h$$

Edge loading condition is when a load is applied on the top surface at the edge of the concrete slab; critical tensile stress occurs at the bottom surface of the concrete slab. The tensile stress due to edge wheel loading can be expressed by equation 5.8, and the maximum deflection can be estimated from equation 5.9.

$$\sigma_e = \frac{0.803P}{h^2}\left[4\log\left(\frac{l}{a}\right)+0.666\left(\frac{a}{l}\right)-0.034\right] \tag{5.8}$$

$$\delta_e = \frac{0.431P}{kl^2}\left[1-0.82\left(\frac{a}{l}\right)\right] \tag{5.9}$$

For these Westergaard closed form solutions, P represents vehicle wheel load [lbs], h is thickness of the concrete slab [in], a is radius of wheel contact area [in], and l is radius of relative stiffness [in]

As another method which estimates wheel load stress, influence charts methods were developed by Pickett and Ray in 1951 [Pickett and Ray, 1951]. Figure 40 shows a sample of the influence chart. The influence charts were developed using the Westergaard theory with Poisson's ratio of 0.15 for concrete slab to find stresses and deflections at the interior and edge wheel loading conditions.

According to these classical theories, it could be identified that the modulus of subgrade reaction affects stresses and deflections of the concrete slab due to vehicle wheel loading. With increasing k-value, the maximum tensile stresses in concrete slab may decrease. In other words, a stiff support system could have beneficial effects on the concrete slab behavior, which is the reverse effect compared to the concrete slab performances due to temperature loading.

Recently, to estimate the concrete slab behavior including stresses and deflections due to diverse wheel loading conditions, finite element (FE) analysis method has been extensively utilized with the advancement in computing technologies. Many numerical analysis programs for design of rigid pavement systems have been developed including FEDFAA, EVERFE, and ISLAB2000 etc. [SAR International, 2007; Davids et al., 1998; Khazanovich et al., 2000]. Also, general purpose FE programs such as ABAQUS and ANSYS have been widely used to evaluate behavior and performance of not only rigid pavement structures but also flexible pavement systems. These FE analysis programs can consider and handle not only complex loading conditions but also the intricate geometry of the rigid pavement structures.
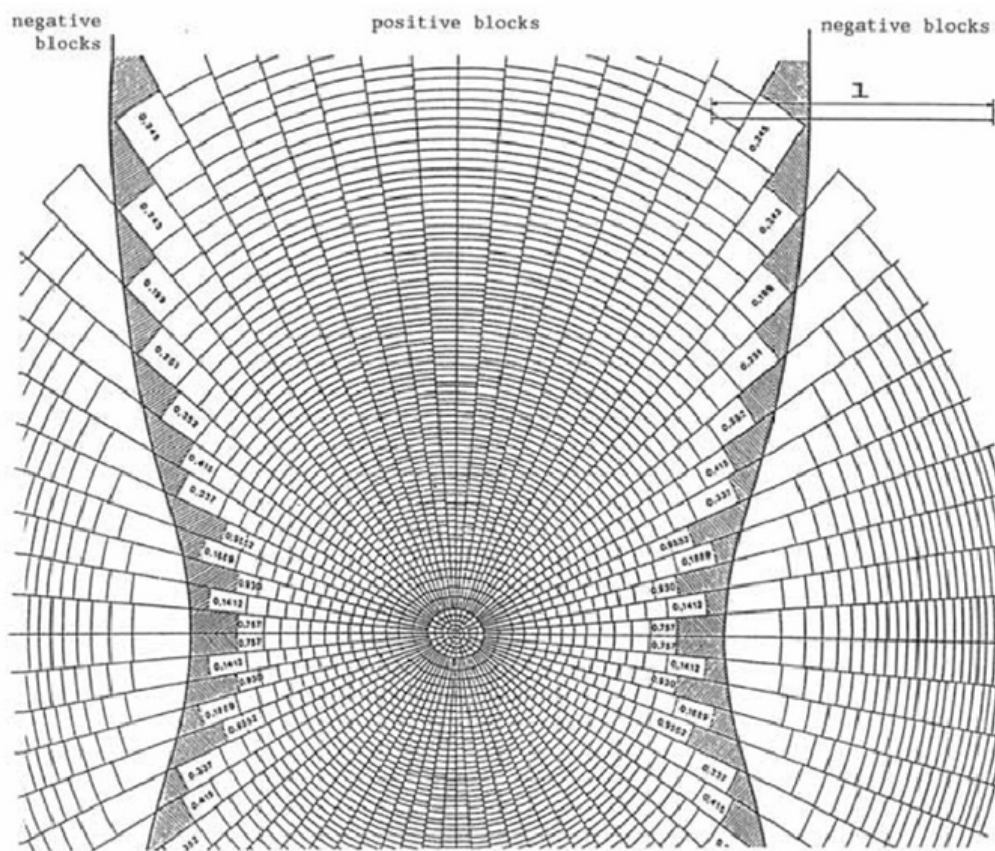
Figure 40. Sample of influence chart by Picket and Ray in 1951

5.1.3. Base Friction

Another factor which produces stress in concrete slabs of rigid pavement structures is friction between the concrete slab and stabilized base layer. The maximum tensile stresses might be induced at the middle of the concrete slab with decrement of the slab volume due to shrinkage or temperature drop in the concrete slab. The maximum tensile stress due to friction between the concrete slab and the base layer can be determined by Equation 5.10.

$$\sigma_f = \frac{\gamma_c L f_c}{2} \tag{5.10}$$

where, γ_c is the unit weight of concrete, L is slab length, and f_c is frictional coefficient.

The first experimental friction study was conducted in 1924 by the U.S. Bureau of Public Road. This study measured frictional resistance of various materials including loam, clay, old macadam, gravel, and sand, which were used as base material for rigid pavement system [Goldbeck, 1924]. After that, several friction tests on the unbound and un-stabilized bases were performed [Stott, 1961; Timms, 1963; Friberg, 1934]. Recently, however, to prevent pumping action of the unbound base layer, base layer using stabilized materials such as cement and lime materials have been widely used. According to studies conducted in 1987, it has been realized that these stabilized bases bring higher friction resistance than un-stabilized materials [Wesevich et al., 1987], and the effects of thickness and textures of the stabilized bases on frictional characteristics were investigated [Wimsatt et al., 1987]. Accordingly, a recently developed CRCP analysis computer program, CRCP10, has used frictional resistance expressed in psi/in as shown in Table 19 [Kim et al., 2001]. However, generally, tensile stresses induced by friction between concrete slab and the stabilized bases have shown a relatively very low stress level [Wesevich et al., 1987]. Thus, frictional stresses might not be a critical factor for rigid pavement design.

Table 19. Frictional resistance of base materials

Base type	Frictional resistance (psi/in)
Flexible	145.5
Asphalt-stabilized	55.9
Cement-stabilized	15400
Lime-treated clay	154.5
Untreated clay	22

5.2. NUMERICAL ANALSYSIS OF CONCRETE SLAB BEHAVIOR

Recently, finite element (FE) analysis has been one of the most widely used analysis methods to estimate behavior and performances of rigid pavement structures. Accordingly, to complete the objectives of this study, the FE method was adopted to verify behavior of concrete slab placed on elastic foundation. Especially, ABAQUS 6.7, a general purpose finite element analysis computer package, was employed in this research. Although the ABAQUS FE program has been widely used, usefulness and accuracy of the program were compared with Westergaard's solutions and Bradbury's equations. Also, basic behavior of the concrete slab placed on elastic foundation was reviewed by this FE computer program.

5.2.1. Finite Element Analysis VS Classical Theories

The FE methods were compared with Westergaard's closed form solutions and Bradbury's equations. Table 20 presents input variables and control values which were used in the comparison between FE methods and the classical theories. Identical concrete material properties and support conditions were considered for both cases of wheel loading and temperature loading conditions.

Table 20. Input variables and control values for analysis comparisons

Input Variable	Value
Elastic Modulus of Concrete	5,000,000 psi
Coefficient of Thermal Expansion of Concrete	$6.0 \times 10^{-6}/°F$
Poisson's ratio of Concrete	0.15
Modulus of Subgrade Reaction (k-value)	300 psi/in
Thickness of Concrete Slab	10 in

5.2.1.1. Wheel Loading

Maximum tensile stress and maximum deflection due to wheel loading were computed and compared. Three different loading positions, interior, edge, and corner loading condition, were considered by Westergaard's closed form solutions. For FE analysis, models were developed using 4-nodes shell elements. A sufficiently large size of slab was modeled to avoid the effect of finite size. Thus, 50 ft × 50 ft size of the concrete slab was modeled with quarter-symmetric geometry. The selection of this size model is expected to minimize the edge and/or corner effects for the analysis of stresses and deflections in the interior condition. Magnitude of total load was 10,000 lbs, and the circular loading area with a radius of 6-in was applied on the top surface of the slab interior, edge, and corner.

Figure 41 illustrates the contours of the maximum principal stresses under interior, edge, and corner wheel loading conditions. For the interior and edge loading conditions, the maximum tensile stresses are induced on the bottom surface of the slab under the loading positions, whereas corner loading condition produces the maximum tensile stress at the top surface of the concrete slab at the bisector of the corner angle. Table 21 presents the result comparisons between Westergaard's closed form solutions and FE analysis for three different wheel loading positions. For interior and edge loading conditions, the two methods, FE and classical theories, have brought almost identical magnitudes of maximum tensile stress and maximum deflection of the concrete slab. On the other hand, relatively large differences have been shown for the corner loading condition.
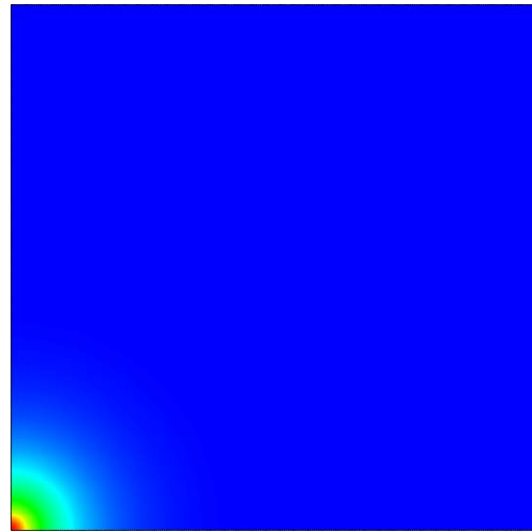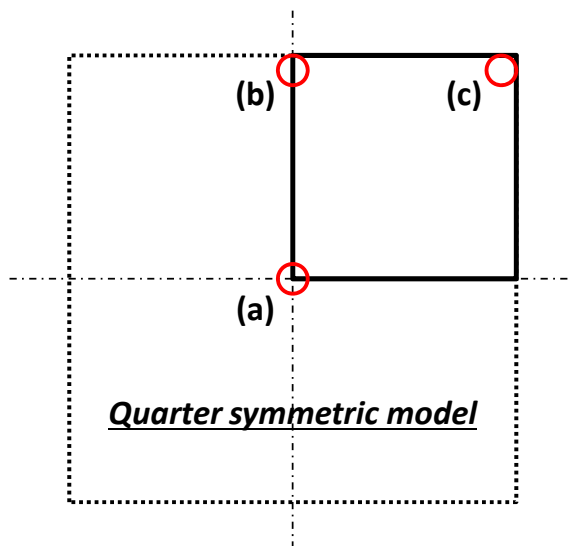
(a) Interior loading condition
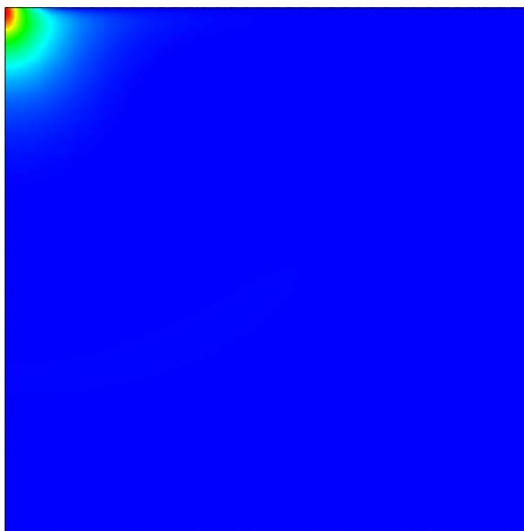
(b) Edge loading condition
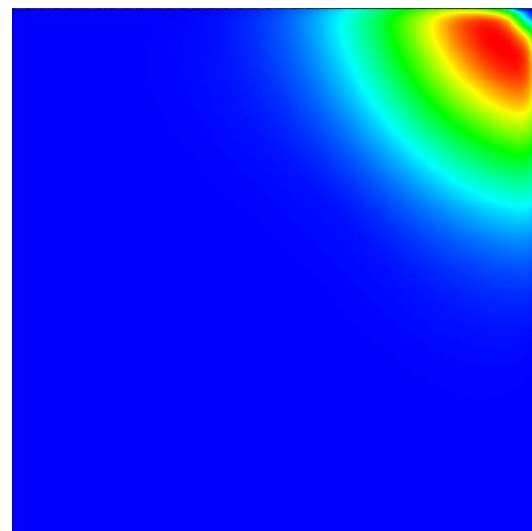
(c) Corner loading condition

Figure 41. Contours of maximum principal stress due to wheel loading conditions

Table 21. Westergaard's solutions and FE analysis under wheel load conditions

Loading Position	Maximum Tensile Stress [psi] Maximum Deflection [in]	Westergaard's Solution	Finite Element Analysis	Difference [%]
Interior	σ_{max}	131.7	129.4	1.7
	δ_{max}	0.00344	0.00363	5.2
Edge	σ_{max}	250.7	232.7	7.2
	δ_{max}	0.01034	0.01086	4.8
Corner	σ_{max}	170.7	187.5	9.0
	δ_{max}	0.0247	0.0286	13.6

5.2.1.2. Temperature Loading

Secondly, the maximum tensile stress and maximum deflection due to temperature difference between top and bottom of concrete slab were computed and compared using FE methods and Bradbury's equations. The temperature difference was set by 20 ˚F, and size of the concrete slab was 24 ft × 12 ft. As with the wheel loading analysis, FE models were developed using 4-nodes shell elements, and the concrete slab was quarter-symmetrically modeled. First, relative stiffness was calculated as 34.5 by equation 5.3. Also, since the concrete slab has finite size, stress correction factors, C, were determined using Figure 39 as C_x is 1.09 and C_y is 0.5.

Figure 42 illustrates stress contour induced in the concrete slab due to linear nighttime temperature condition having difference of 20 ˚F between the top and bottom surface of the slab. The maximum tensile stress is induced on the top surface of the slab center. Table 22 presents the comparison results between Bradbury's equations and FE analysis due to the temperature loading at the center of the interior and edge of the concrete slab. The maximum tensile stresses at the center of the slab interior and edge have shown similar values of the two different analysis methods.

The Bradbury theories are based on the assumption that the temperature distribution through the concrete slab depth is linear. However, actual measurements in the field show nonlinear temperature distribution though the concrete slab depth [Thompson et al., 1987; Nam, 2005]. So, the numerical method which could consider nonlinear temperature distribution was introduced [Harik et al., 1994]. Also, closed form solutions were developed for calculating curling stress due to nonlinear temperature gradients [Mohamed and Hansen, 1997].
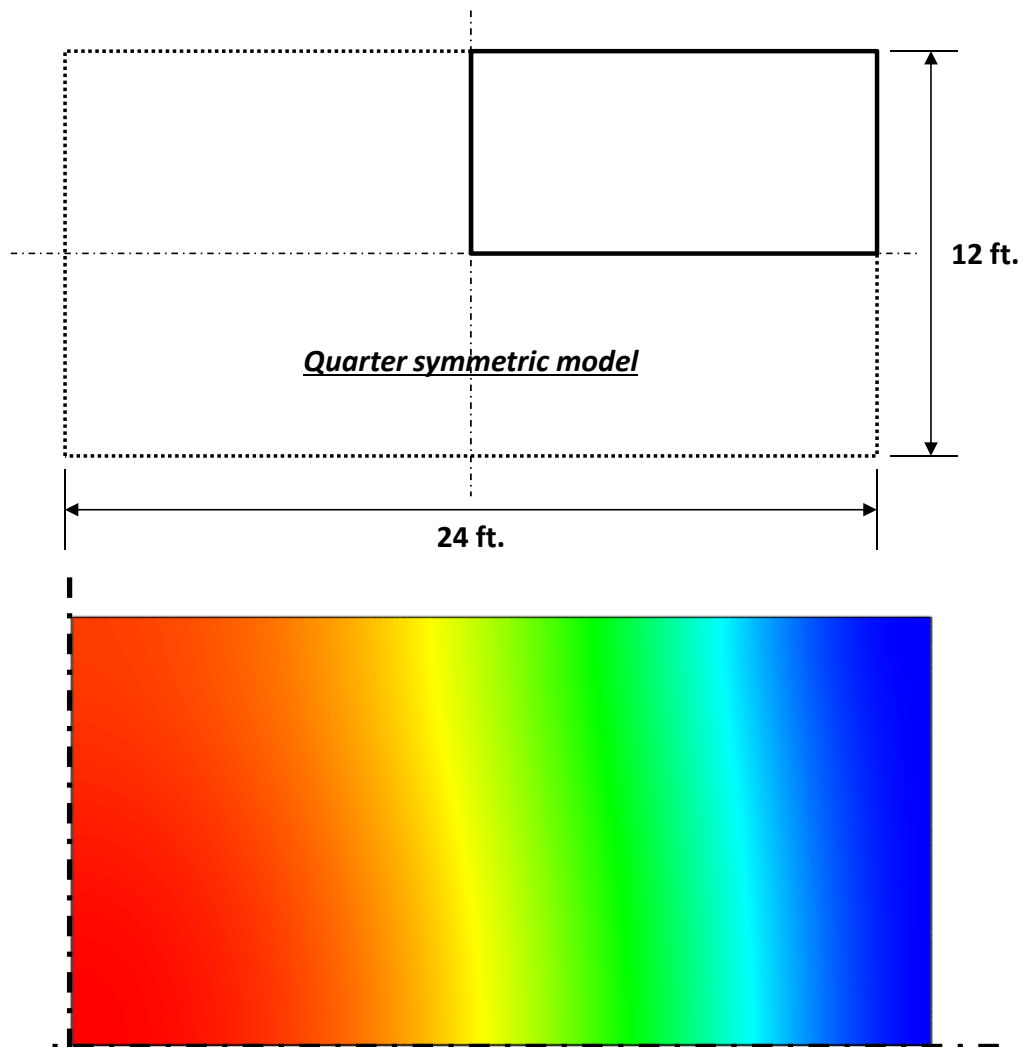
Figure 42. Stress contour due to temperature loading

Table 22. Bradbury's equations and FE analysis for temperature loading

Location	Tensile Stress at Slab Center [psi]		
	Bradbury's Equation	**Finite Element Analysis**	**Difference [%]**
Interior	306.9	328.3	6.5
Edge	357.5	349.8	2.2

5.2.2. Selection of FE Model for Concrete Slab and Loading Conditions

According to comparison results between FE methods and classical theories, it has been shown that FE methods would be reasonable to estimate the behavior of concrete slab on elastic foundation. Here, one of the most considerable problems for use of the FE method is selection of element type, i.e. how to make the model simple and easy to develop. For instance, a 3-dimensional solid element model may give the most accurate response. However, the task will take unreasonable amount of time. For this reason, it is necessary to find an appropriate element type and simple model which could explain the slab behavior properly. A previous study identified that responses of concrete slab placed on elastic foundation are almost identical for both the FE model using 3-dimensional solid elements and shell elements [Ha and Won, 2009]. In this chapter, simple model using 2-dimensional plane strain elements was considered, and the maximum tensile stress and the maximum deflection were compared under vehicle wheel loading and temperature loading conditions using the 4-nodes shell elements model and the 2-dimensional plane strain elements.

5.2.2.1. Vehicle Wheel Loading Condition

To simulate actual vehicle load, a heavy dump truck used in typical highway construction projects was considered. Figure 43 illustrates dimensions of typical dump truck. This type of dump truck has dual tire and tandem axles. Generally, vehicle load has been applied with the axle load on the top surface of concrete slab for rigid pavement structures. Also, most pavement design programs convert vehicle wheel loads of various magnitudes and repetitions to an equivalent number of standard axle loads. This standard axle load is called equivalent single axle load (ESAL). Thus, using axle load rather than circular load which have been adopted by Westergaard's solutions, might be more reasonable and practical to predict behavior of concrete slab resting on elastic foundation.

97
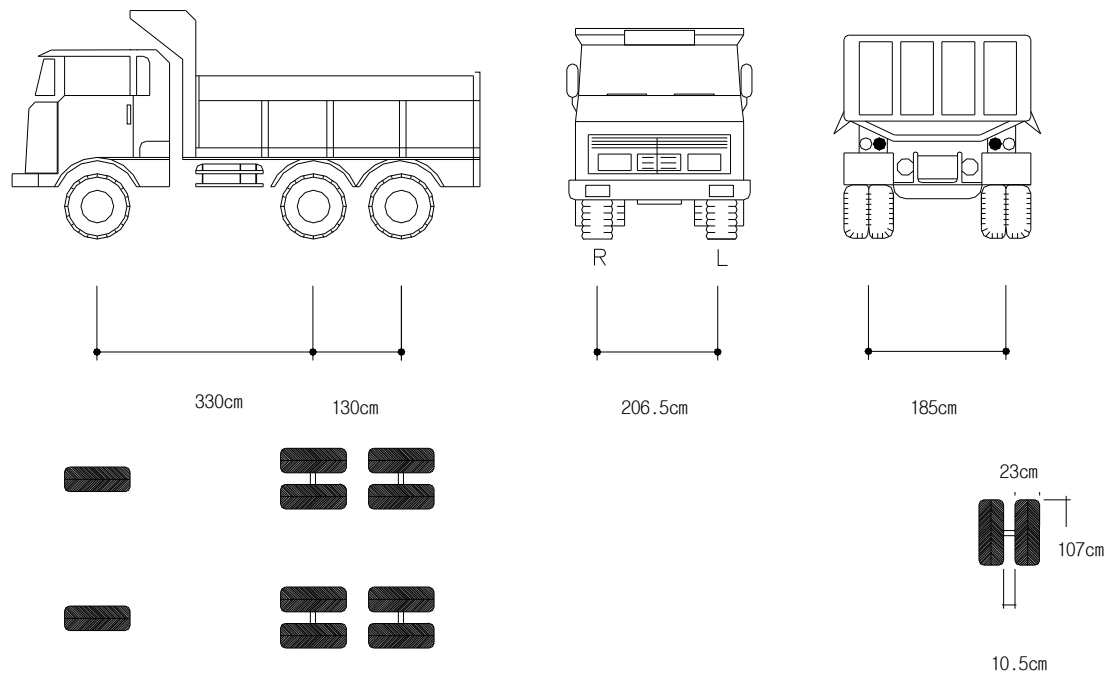
Figure 43. Dimensions of typical dump truck

Analysis models were developed using shell elements and 2D solid plain strain elements. Figure 44 illustrates overview of the analysis models. Dimension of concrete slab is 12 ft. × 24 ft., and thickness is 10-in. The single axle load having dual tires is placed on the center of the concrete slab developed by shell elements, and it is quarter-symmetrically modeled as shown in Figure 44(a). A contact area of a single tire is 6 in. × 10 in. For comparison with this shell element model, another type analysis model was considered, which was developed by 2-dimentional solid plain strain elements. This is modeled through longitudinal cross section of the concrete slab. So, this model has a longitudinal length of 24-ft, and is 10-in thick. However, it is impossible to accurately apply dual tire single axle load to the model. The load applied to the center of the model is assumed to be line load along the transverse direction. Thus, it could be expected that a relatively large magnitude of total load will be applied on the structure and the response will be larger than the case of the shell element model.
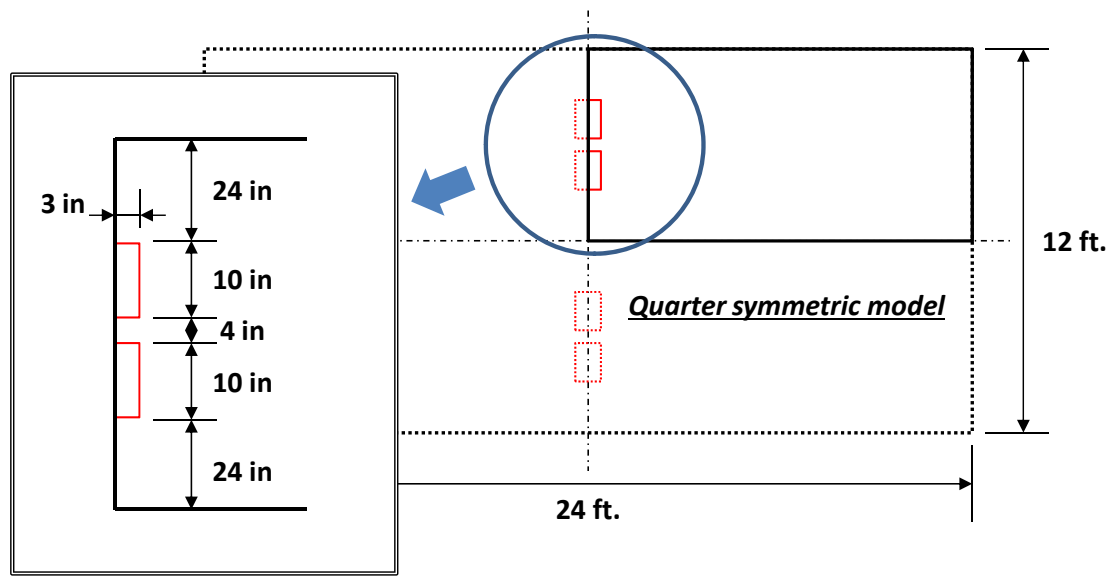
(a) Model using shell element (Plane view)
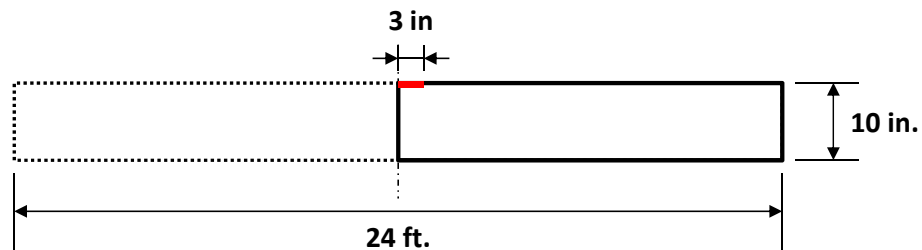
(b) Model using plane strain element (Side view)

Figure 44. Analysis overview for loading dimensions

Table 23 presents the weight of each wheel of a typically used heavy dump truck [Cho, 2007]. Since the middle and rear axle have dual tires, the magnitude of total axle loads are 17,990 lbs and 17,548 lbs for the middle axle and real axle respectively. These axle loads are almost identical to AASHTO standard which regulates the equivalent single axle load as 18,000 lbs. Because the load must be applied to the FE model as pressure load, the axle load, 18,000 lbs, is divided by total contact area of the four tires. Thus, 80 psi of pressure was applied on the top surface of the concrete slab model.

Table 23. Weight of each wheel of dump truck

Wheel Position	Load (lbs)
Front Wheel (Driver's Seat)	5,467
Front Wheel (Assistant's Seat)	5,952
Middle Wheel (Driver's Seat)	4,409
Middle Wheel (Assistant's Seat)	4,586
Rear Wheel (Driver's Seat)	4,365
Rear Wheel (Assistant's Seat)	4,409

Figure 45 shows the contours of stress in the longitudinal direction and slab deflection for the analysis models developed by shell elements and 2D plane strain elements. The maximum tensile stress due to wheel loading is induced in the bottom of the concrete slab. So, for the model by shell elements, the contour is plotted from bottom surface of the slab.

Shell element : Stress at bottom   Shell element : Deflection

Plane strain element : Stress   Plane strain element : Deflection

Figure 45. Contours of stress and deflection due to single axle loading

Table 24 presents maximum tensile stress and maximum deflection developed in the concrete slab under the wheel loads corresponding to different analysis models using shell elements and plane strain elements. As shown in the results, the applied pressure loading of 80 psi produced 126.2 psi of the maximum tensile stress and 5 mil of the maximum deflection of the slab for the shell element model, whereas, for the plane strain element model, 293.1 psi of stress and 17 mil of the deflection were induced in the slab due to 80 psi of pressure line load. It is because the wheel loads is applied as a line load along transverse direction on the plane strain element model whereas the load is applied as circular loads on the shell element model. Accordingly, the total load is exaggerated on the plane strain element model.

Table 24. Stresses and deflections under different element types due to wheel loading

Element Type	Pressure Loading [psi]	Maximum Tensile Stress [psi]	Maximum Deflection [in]
Shell element	80.00	126.2	0.00497
Plane strain element	80.00	293.1	0.01694
	34.45	126.2	0.00729

When determining and evaluating performance of rigid pavement systems, stress level has been used in modern pavement design guide. For example, a punchout which is one of the most important types of distress to evaluate CRCP performance is a function of accumulated fatigue damage associated with the formation of longitudinal cracks [Zollinger, 1989; Zollinger and Barenberg, 1990; LaCourseiere et al., 1978]. Also, crack occurrences have been directly related with the level of maximum tensile stresses. Thus, the modeling comparisons are focused on the maximum tensile stress level rather than deflections in this study. For the plane strain analysis model, the applied pressure load was adjusted to produce identical maximum tensile stress, 126.2 psi, which is induced

stress from the shell element model. Consequently, the adjusted pressure magnitude acting on the plane strain model was computed as 34.45 psi which could match the maximum tensile stress from the shell element model. However, the adjusted pressure load could not bring the identical maximum deflection from the shell element model.

5.2.2.2. Temperature Loading Condition

Previously developed classical theories estimating behavior of concrete slab due to temperature loadings assumed that the temperature gradient through the slab depth is linearly distributed. However, numerous researchers have observed that the temperature gradient profiles on the concrete slabs generally show nonlinear gradients [Nam, 2005; Mirambell, 1990; Choubane and Tia, 1992; Choubane and Tia, 1995; Lee and Darter, 1993; Masad et al., 1996; Ioannides and Khazanovich, 1998; Ioannides and Salsilli-Murua, 1999]. Also, these nonlinear temperature gradients could significantly affect the magnitude of the maximum tensile stress and critical location on the concrete slabs [Hiller and Roesler, 2010]. Figure 46 shows examples of linear and nonlinear temperature gradients through depth of the concrete slab for nighttime temperature condition. Also, the temperature distributions of the concrete slab have always changed due to variation of ambient temperature conditions. In other words, daytime and nighttime ambient temperatures have given different temperature distribution of the slab.

Therefore, to find the most critical temperature condition that produces the highest level of maximum tensile stress in the concrete slab, the maximum tensile stresses were computed under various temperature distributions including not only nighttime and daytime temperature conditions but also, linear and nonlinear temperature gradient. Here, temperature differences between the top and bottom of the concrete slab are considered raging from 5 ˚F to 30 ˚F.

102
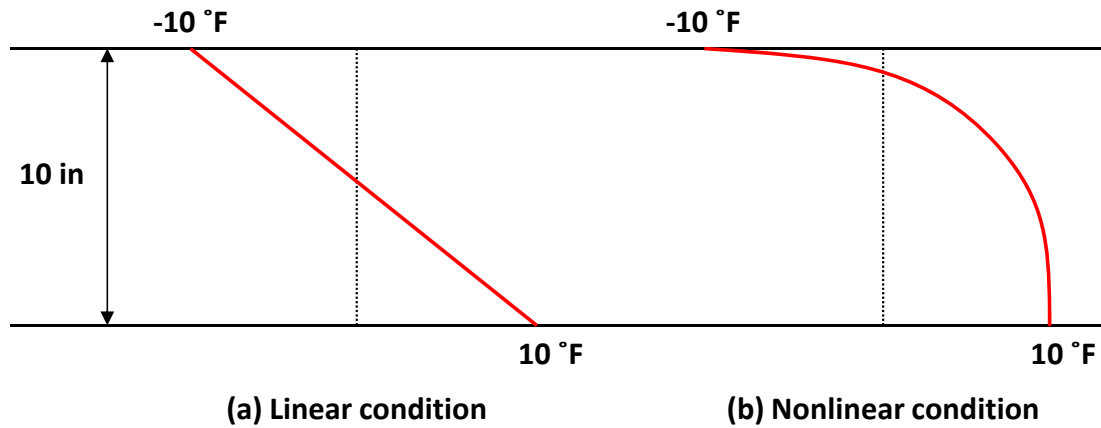
Figure 46. Linear and nonlinear temperature gradients for nighttime condition

Table 25 presents the maximum tensile stresses under the various temperature distributions. The maximum tensile stresses were induced on the top surface of the slab for nighttime temperature condition, whereas the stresses were produced on the bottom of the slab for daytime condition. Also, nonlinear temperature gradient produces a higher level of tensile stress for nighttime temperature condition. On the other hand, the maximum tensile stresses were decreased by nonlinear temperature gradient for daytime conditions. Consequently, the nighttime nonlinear temperature gradient gives the highest level of maximum tensile stress for the range of temperature differences between the top and bottom of the concrete slab.

Table 25. Maximum tensile stresses under various temperature conditions

Condition	ΔT (˚F)	Maximum Tensile Stress [psi]	
		Linear Temperature Gradient	Nonlinear Temperature Gradient
Nighttime	5	86.5	107.6
	10	172.3	214.5
	15	258.0	321.4
	20	343.8	428.3
	25	429.6	535.2
	30	515.4	642.1
Daytime	5	85.1	63.98
	10	170.9	128.7
	15	256.7	193.4
	20	342.6	258.1
	25	428.4	322.8
	30	514.2	387.6

Figure 47 shows the contours of stresses of longitudinal direction and slab vertical deflections under nighttime linear temperature condition for the analysis models developed by shell elements and 2D plane strain elements. The critical tensile stress due to the nighttime wheel loading is induced in the top surface of the concrete slab. So, for the model by shell elements, the stress contour of the top surface of the slab is plotted.
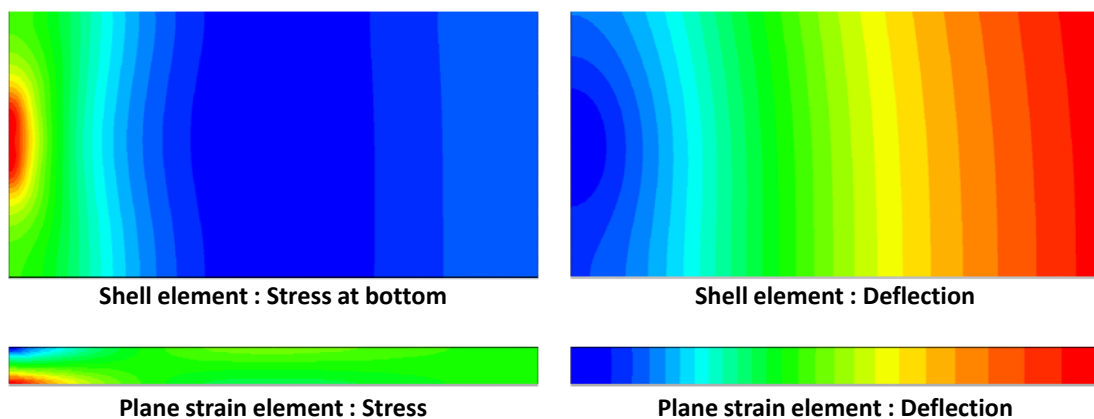
Table 26 presents the maximum tensile stress and maximum deflection induced in the concrete slab under the nighttime temperature condition corresponding to the

different analysis models using shell elements and plane strain elements. Almost identical maximum tensile stresses were developed in the concrete slab for the two different models by both of linear and nonlinear temperature gradients. However, magnitudes of maximum deflection show different values in accordance with the model types since the maximum deflection from the shell element model came from the corner of the slab, whereas the deflection of plane strain element model represents vertical displacement at the edge of the slab.

Shell element : Stress at top	Shell element : Deflection

Plane strain element : Stress	Plane strain element : Deflection
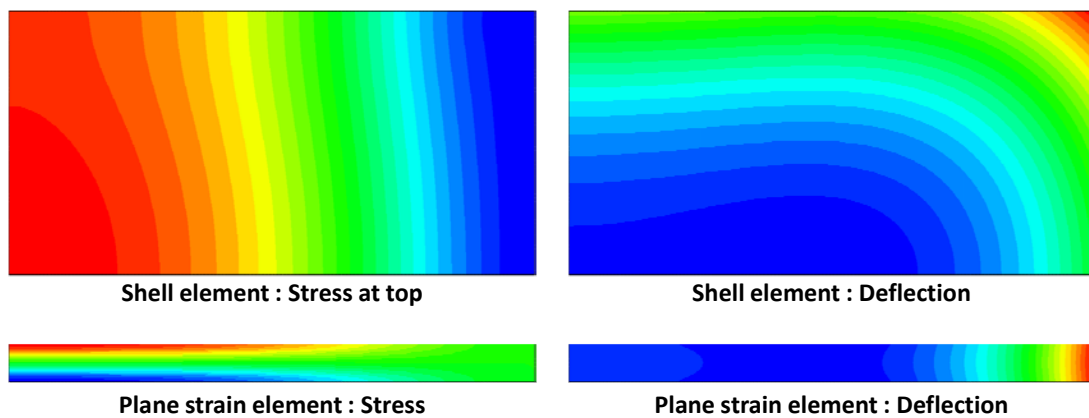
Figure 47. Contours of stress and deflection due to linear temperature loading

Table 26. Stresses and deflections under different element types due to temperature

Element Type	Temperature Difference [$\varDelta$T]	Maximum Tensile Stress [psi]	Maximum Deflection [in]
Shell element	Linear : 20 ˚F	349.8	0.00970
	Nonlinear : 20 ˚F	444.7	0.00728
Plane strain element	Linear : 20 ˚F	343.1	0.00326
	Nonlinear : 20 ˚F	454.6	0.00294

5.3.   SUMMARY

Behavior of concrete slab on elastic foundation can be affected by temperature variations, external physical loading, and friction between the slab and the base layer. Bradbury introduced equations estimating stresses induced in the concrete slab due to linear temperature gradient through the slab depth. Westergaard developed closed form solutions to compute maximum tensile stresses and maximum deflections of the concrete slab due to wheel loadings applied on the top surface of the interior, edge, and corner of the concrete slab. Additionally, the tensile stress could be developed in the concrete slab due to friction between the bottom surface of the concrete slab and top surface of the base layer when volume of the slab is changing, and the frictional stress could be statically computed. Other than the classical solutions, FE analysis method has become widely used to estimate the behavior of the concrete slab structures like rigid pavement systems.

First, the ABAQUS 6.7 FE program was selected for this study, and to evaluate the accuracy of the ABAQUS 6.7, analysis results from the program were compared with Westergaard's closed form solutions and Bradbury's equations. For cases of wheel loading conditions, interior and edge loading condition have shown almost identical results in stresses and deflections. For corner loading condition, however, FE analysis has given relatively large values in the stress and deflection compared to Westergaard's solutions. For the temperature loading, Bradbury's equations and FE methods have shown a similar level of maximum tensile stress in both of interior and edge of the slab. Thus, the FE method might be a reasonable solution to examine the behavior of concrete slab relying on elastic foundation.

To select the element type for the body of the slab and loading conditions, additional evaluations were conducted. For the selection of element type, 4-nodes shell element and 2-dimentional solid plane strain element were considered for the analysis of the concrete slab. Also, single axle load was adopted rather than circular wheel load. The model using plane strain elements has given a higher level of maximum tensile stress than the shell element model. So, for use of the plane strain FE model, the applied

pressure load has been adjusted, which produced identical maximum tensile stress to the shell element model. For temperature loading, nighttime nonlinear temperature gradient produced the maximum tensile stress. Also, the models developed by shell elements and plane strain elements have shown similar maximum tensile stress.

CHAPTER 6: EFFECTS OF VARIOUS SUPPORT CONDITONS ON CRCP BEHAVIOR

To verify the effects of various support conditions on CRCP responses under temperature and vehicle wheel loadings, FE analysis were conducted. The effects of support layer properties including thickness of stabilized base layer, elastic modulus of the base material, and subgrade vertical stiffness, subgrade k-value, were discussed. Also, critical stresses of the CRCP slab placed on support systems having identical composite k-value composed with various combinations of the support layer properties are estimated under the temperature and wheel loadings. Moreover, the effects of non-uniformity subgrade vertical stiffness are examined under both of the temperature and vehicle wheel loading conditions.

6.1. OUTLINE OF FINITE ELEMENT ANALYSIS

To evaluate the effects of support conditions on CRCP behavior, finite element (FE) analysis was used. Using ABAQUS 6.7, general purpose finite element analysis computer program, the CRCP structure is embodied, and the temperature and vehicle wheel loadings are applied on the CRCP slab.

6.1.1. Geometry and Input Variables

2-dimensional and 3-dimensional finite element models for CRCP structures have been developed in previous studies [Kim et al., 1997; 1998; 2000a; 2000b; 2003]. Based on the previous CRCP FE models, modified 2-dimensional CRCP FE model was developed using 4-nodes plane strain elements. Here, longitudinal steel rebar is modeled using 2-nodes beam elements. To consider the effects of the stabilized base layer, the base

layer underlying CRCP slab is separately modeled from the subgrade by the 2-dimensional 4-nodes elastic solid plane strain elements. Even though crack spacing of CRCP structure depends on the steel ratio, generally, CRCP has crack spacing raging from 3 to 8 ft [The Transtec Group, 2004], and average crack spacing has been shown less than 6-ft after 3 year of service opening [Cho, 2007]. In fact, the mean crack spacing decreases as the steel ratio increases. Accordingly, in this study, 6-ft long CRCP slab was considered, which means that the length between two adjacent transverse cracks is 6-ft. Figure 48 illustrates the outline of the modified 2-dimensional CRCP FE model. A half length of the CRCP slab is considered to develop the numerical model because the CRCP behavior could be assumed to be symmetric with respect to the center of the slab. The boundary conditions of the finite element model should be correctly defined to obtain reasonable results. So, at the center of the CRCP slab, a vertical degree of freedom is allowed, but longitudinal and rotational displacements of the slab are restrained. For the longitudinal steel rebar, longitudinal and rotational displacements are not allowed at the ends of the steel bar. Finally, for the base layer, longitudinal and rotational displacements are prohibited at both end of the base layer although vertical degree of freedom is allowed. Also, a previous study for the finite element modeling of CRCP has shown that good convergence in the analysis results is achieved with an element size smaller than 1.5 in [Kim et al., 1997]. Thus, 0.5 in of the element size is adopted in this study. The stresses evaluating CRCP slab responses are calculated at four integration points of one element, and average values are used for each element in this study.
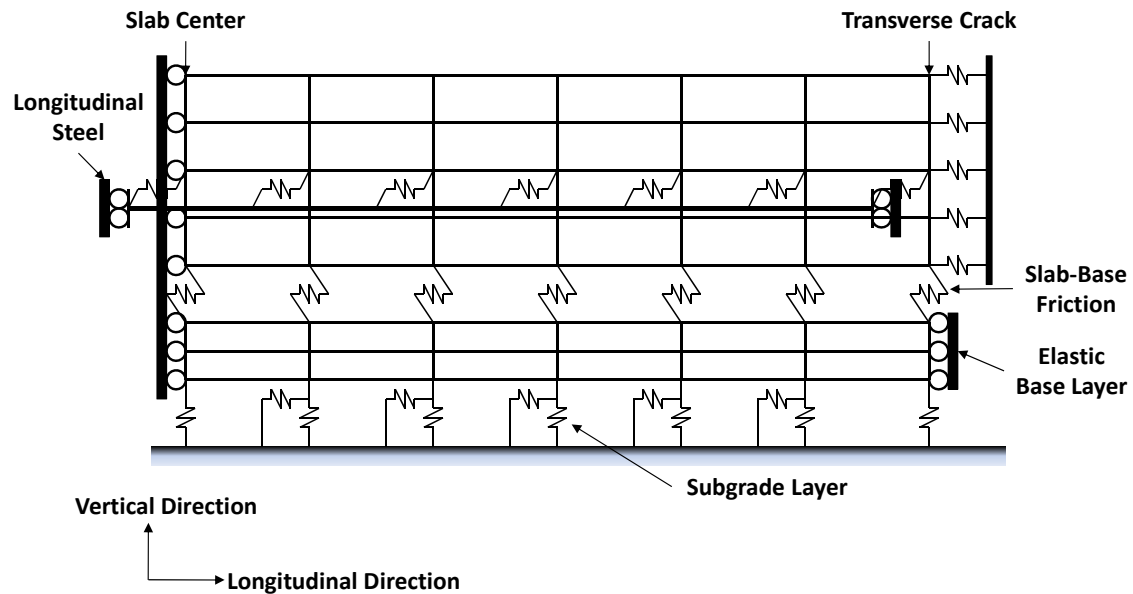
Figure 48. CRCP FE model

Compatibility between the concrete slab and longitudinal steel rebar is modeled using horizontal and vertical spring elements. Nonlinear bond slip relationship between concrete and the longitudinal steel bar are considered in the horizontal direction as shown in Figure 49 [Kim et al., 1997; 2000a]. Perfect bonding condition has been assumed in vertical direction because relative vertical displacement between the concrete slab and the steel is not possible. Friction behavior between concrete slab and base layer and also the interface of the base layer and underlying subgrade are also modeled using a horizontal spring element having stress-displacement correlation as shown in Figure 50. For horizontal friction resistance between concrete slab and base layer, 145.5 psi/in is used, and 22 psi/in is adopted for the horizontal friction value of subgrade layer and the base layer.

Subgrade soil layer could resist vertical downward pressure loading according to the vertical stiffness of subgrade layer. However, the subgrade layer could not withstand against the vertical upward loading, for example, at slab edge or corner of upward curled concrete slab. Thus, the underlying subgrade layer was modeled using vertically tensionless spring elements to properly consider the upward curling effects. The spring

elements react against compressive pressure with spring coefficient k, but it does not respond to tensile pressure, as shown in Figure 51.
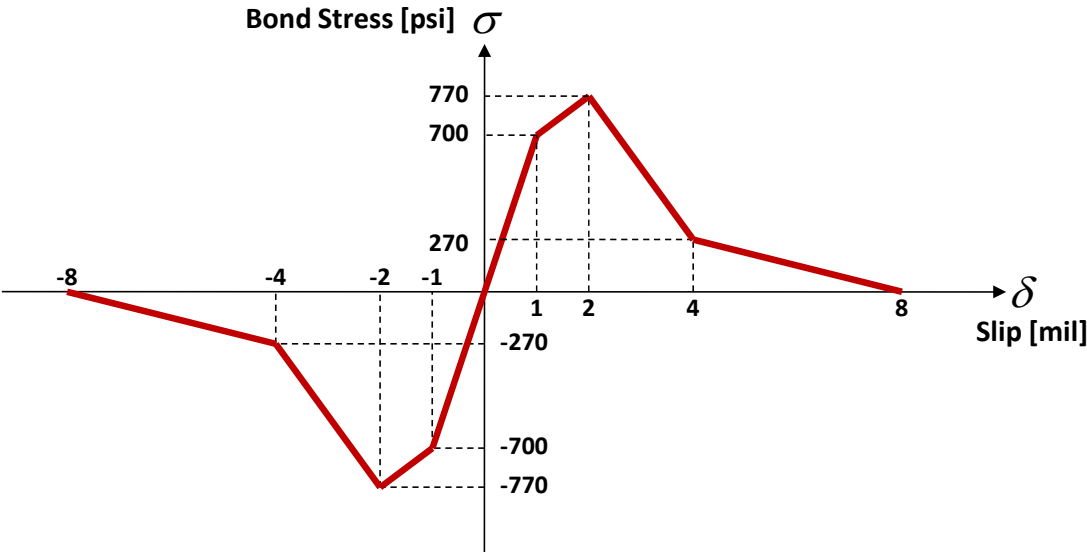
Figure 49. Bond slip behavior
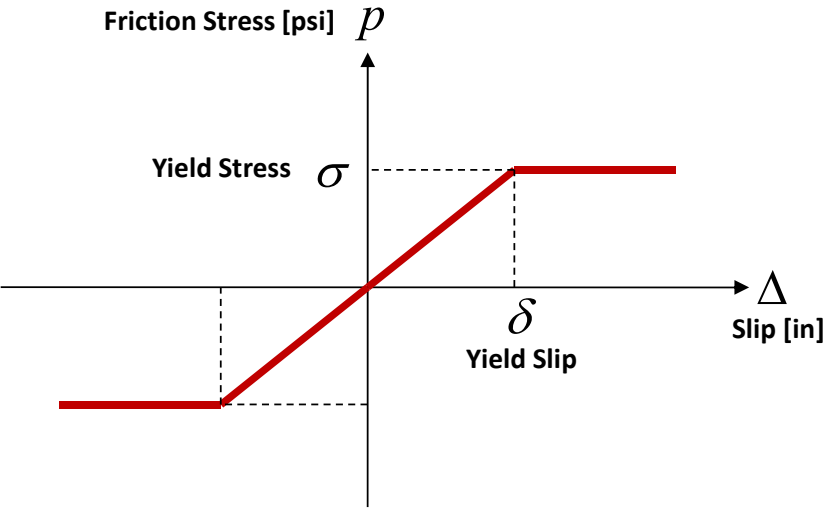
Figure 50. Friction behavior
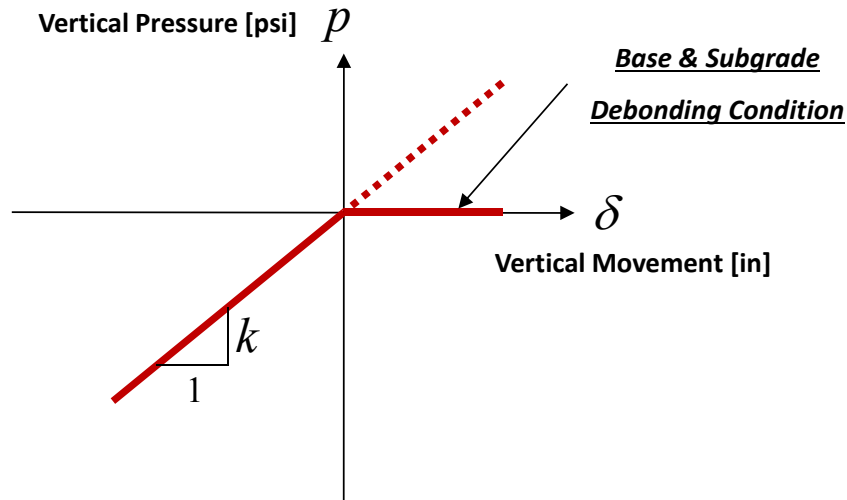
Figure 51. Subgrade behavior

To consider the behavior of concrete slab at transverse cracks, spring element is used in the horizontal direction. It could be assumed that the vertical shear and moment transfer to the adjacent concrete slab at transverse cracks could be ignored. Vertical shear and moment transfer should be present when effective aggregate interlock exists at transverse cracks. In that case, the damages to the concrete due to wheel loading applications could be minimal and not much different from other locations in the slab. On the other hand, once transverse cracks are deteriorated to the point where maximum damages occur to the concrete, aggregate interlock might not exist and the damages should be included for the analysis of damages and performance of CRCP. Horizontal movement at transverse cracks is allowed within the crack width due to expansion of the concrete slab. In other words, concrete at the crack could be freely moved by volume change in the CRCP slab until contact to the adjacent concrete slab. After the contact, the horizontal movement at the transverse crack is totally restrained. Figure 52 illustrates the behavior of transverse crack. According to previous studies, there is no significant correlation between crack spacing and crack width in CRCP structures [Nam, 2005; Suh et al., 1992]. So, based on Figure 53, 0.01-in crack width, average value, is used in this study. Table 27 shows the input variables and control values used in this analysis of

CRCP responses due to variations of support layer properties under temperature and vehicle wheel loading conditions.
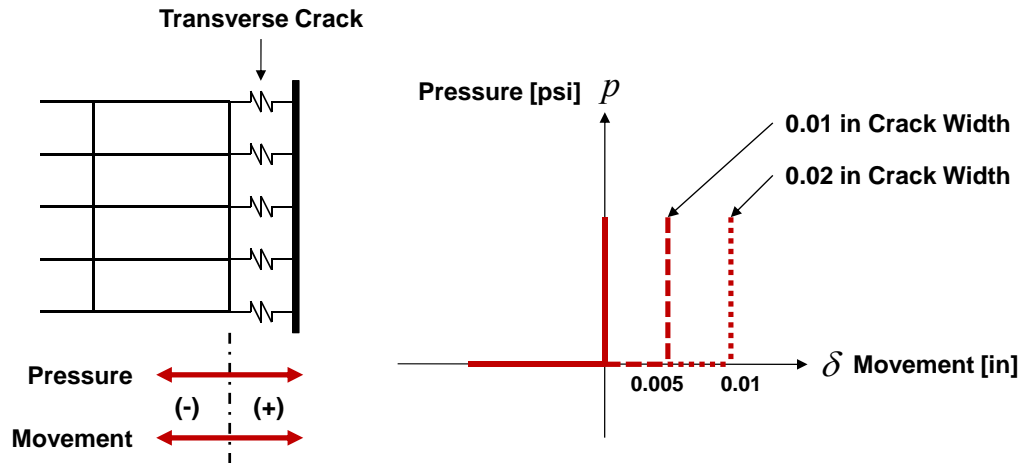
Figure 52. Transverse crack behavior
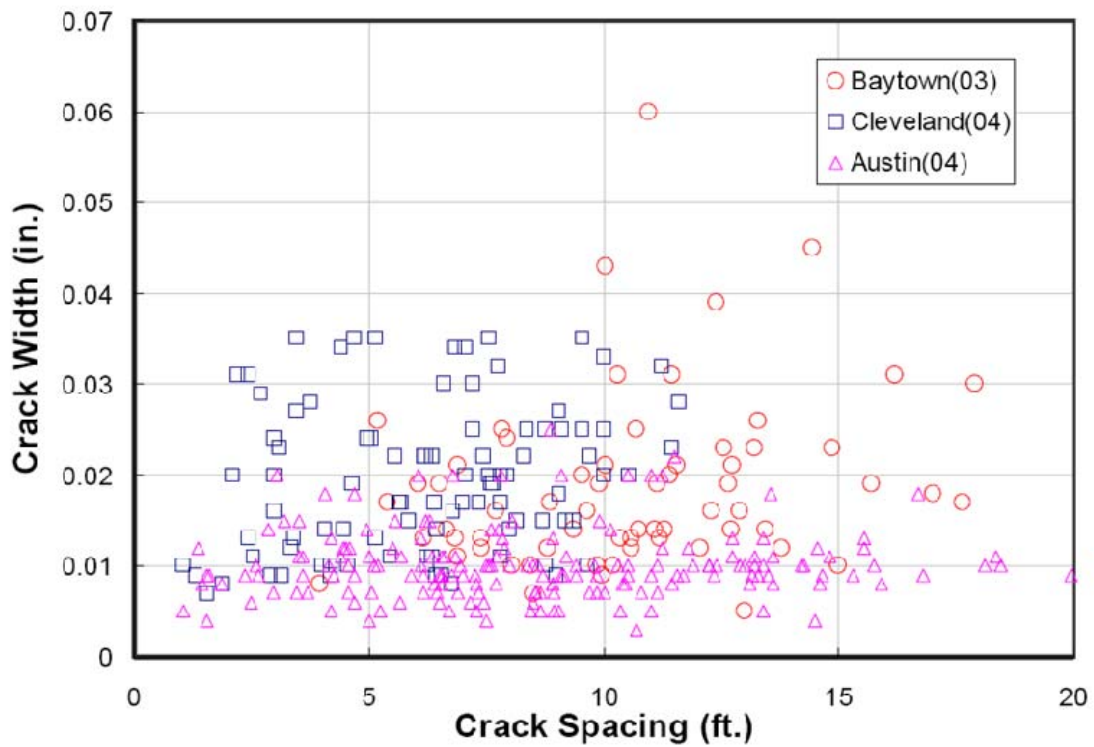
Figure 53. Correlation between crack spacing and crack width [Nam, 2005]

Table 27. Input variables and control values for CRCP analysis

Input Variables	Control Values
Crack spacing	6 ft
Crack width	0.01 in
Longitudinal steel spacing	6 in
Concrete slab thickness	10 in
Depth of steel location	5 in
Base thickness	4 in
Concrete Young's modulus	3.0×10^6 psi
Concrete Poisson's ratio	0.15
Concrete unit weight	150 pcf
Concrete CTE	6.0×10^{-6} /ºF
Modulus of subgrade reaction	150 pci
Base material Young's modulus	3.0×10^5 psi
Base material Poisson's ratio	0.35
Base material unit weight	150 pcf
Base material CTE	1.2×10^{-5} /ºF
Steel Young's modulus	2.9×10^7 psi
Steel Poisson's ratio	0.29
Steel unit weight	480 pcf
Steel CTE	5.0×10^{-6} /ºF
Diameter of steel	0.75 in
Reference Temperature	95.0 ºF

6.1.2. Loading Conditions

Temperature gradients through slab depth could generate stresses in the CRCP slab. Temperature on the top surface is higher than the bottom at daytime, while the opposite is the cast for nighttime. In this study, simplified field measured daytime and nighttime temperature gradients were used. Field measured temperature distributions through the CRCP slab depth have shown nonlinear gradient conditions for both daytime and nighttime. Also, the temperature daily variation at the top surface of the slab is larger than bottom. The daily maximum temperature variations at top and bottom are about 22.5 and 4.5 ºF measured at field test section in Cleveland, Texas in 2004, respectively [Nam, 2005]. Figure 54 shows the simplified temperature gradients at daytime and nighttime temperature conditions.

Also, a typical dual tire single axle was adopted to estimate vehicle wheel load stresses in this study. As described in the previous chapter, the comparison study between the plane strain CRCP FE model and the shell element model shows the need for the adjustment of tire pressure from 80 psi to 34.5 psi for 2-dimensional 4-nodes plane strain FE model. For the vehicle wheel loading cases, two different loading conditions were considered: center loading condition with the tire located between two adjacent transverse cracks, and edge loading condition, with the tire placed on a transverse crack.
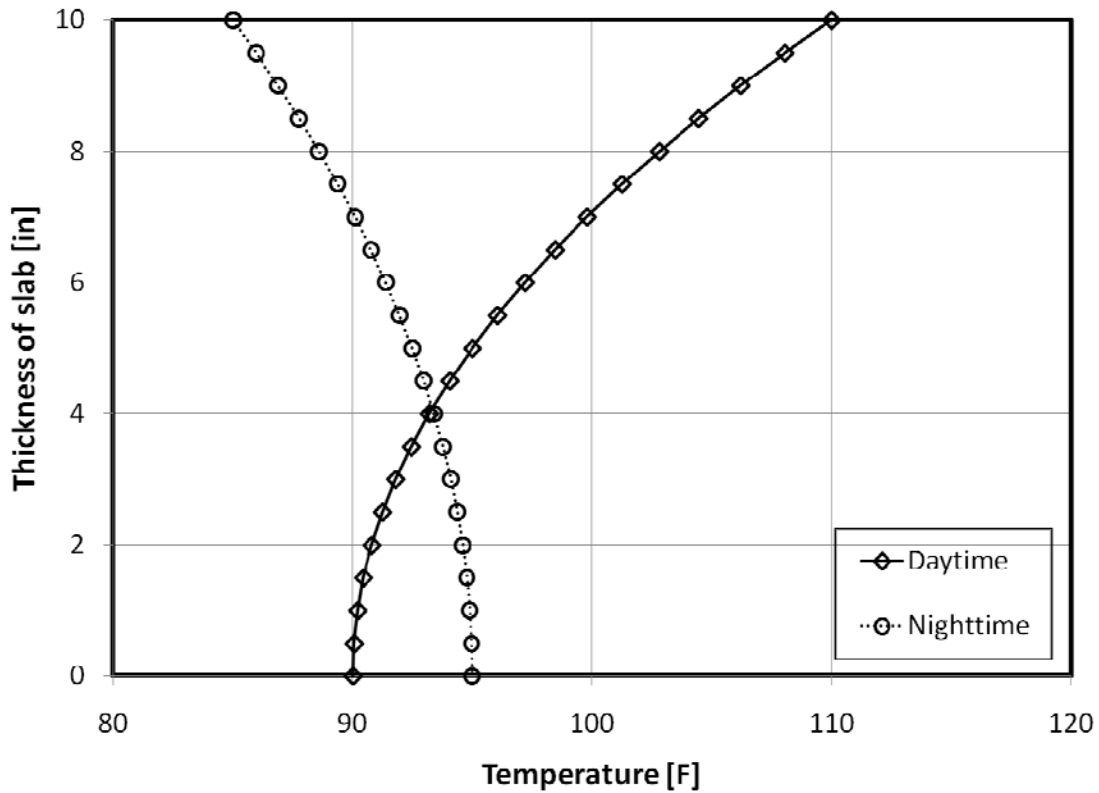
Figure 54. Temperature gradients at daytime and nighttime

For the temperature and wheel loading conditions, longitudinal stresses in the concrete slab are calculated and plotted at the slab center, between two adjacent transverse cracks, through the CRCP slab depth. Figure 55 presents the stress distributions at slab center due to the temperature and wheel loading conditions. As shown in the figure, the maximum longitudinal tensile stress is induced at the middle depth of the slab due to daytime temperature condition whereas the maximum stress is produced on top surface for nighttime temperature gradient. For the temperature loadings, the critical stress is generated by the nighttime temperature gradient. For the vehicle wheel loading conditions, both of center loading and edge loading conditions produced almost identical maximum longitudinal tensile stresses at the bottom and top of the CRCP slab, respectively.

In these temperature and wheel loading cases, the maximum longitudinal tensile stress was induced by wheel loading. The critical loading case producing critical stress could depend on different concrete slab dimensions, support layer properties, or loading magnitudes. Moreover, it is necessary to estimate ranges of the critical stresses within implemental ranges of the variables. Thus, the maximum critical stresses of the CRCP slab due to temperature and wheel loadings are estimated in accordance with actual ranges of support layer properties which have been widely adopted and used in pavement construction fields.
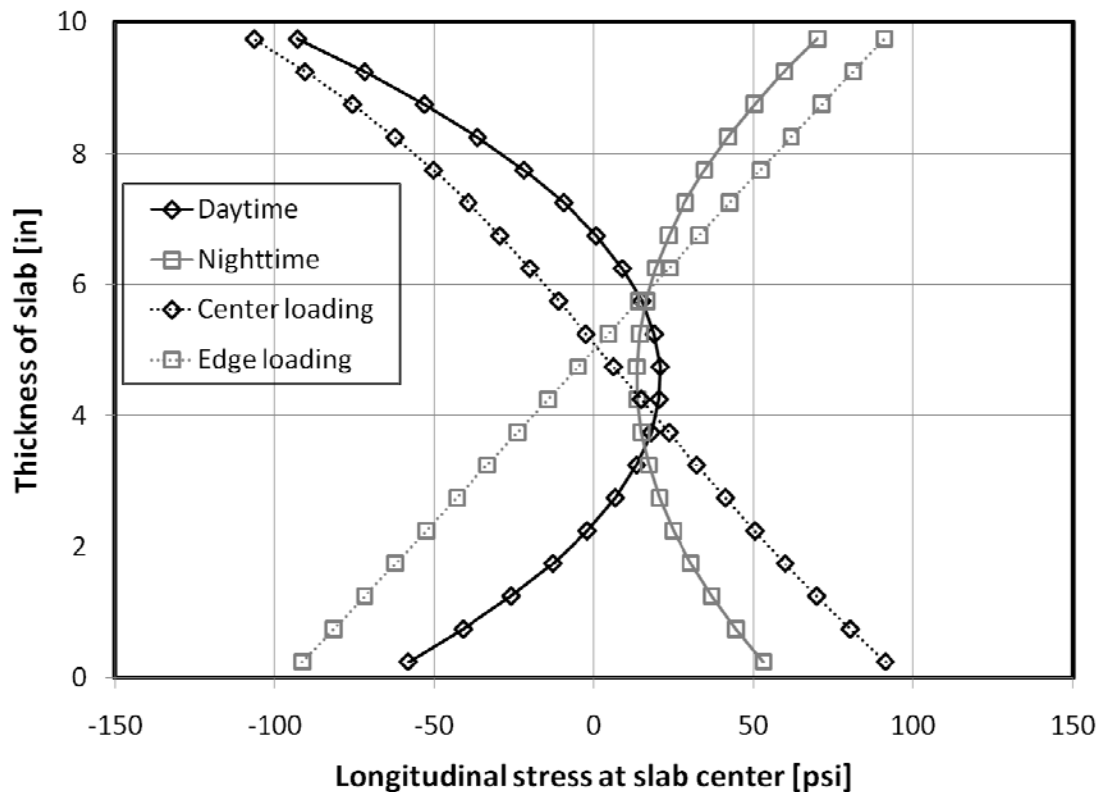
Figure 55. Stress distributions at slab center due to temperature and wheel loadings

117

6.2.   EFFECTS OF SUPPORT LAYER PROPERTIES ON CRCP BEHAVIOR

To verify the effects of support layer properties on CRCP behavior, the maximum longitudinal tensile stresses are calculated at the center of the CRCP slab, i.e. between two adjacent transverse cracks, under both nighttime temperature gradient and center wheel loading condition. Critical tensile stress is produced at the nighttime temperature condition, not at the daytime temperature gradient, whereas the center and edge loading cases bring almost similar magnitude of the maximum critical stress level. Also, the calculated maximum longitudinal tensile stresses are compared in accordance with various combinations of support layer properties including thickness of the stabilized base layer, elastic modulus of the base material, and vertical stiffness of subgrade layer, i.e., subgrade k-value.

6.2.1. Temperature Loading

The maximum longitudinal stresses at slab center are estimated under nighttime temperature condition due to change of the support layer properties. Here, thickness of stabilized base layer ranges from 2 to 6 in, elastic modulus of the base material is between 50 to 2000 ksi, and subgrade k-value is from 50 to 300 psi/in. These values represent the most realistic limits in materials used in rigid pavement construction.

Table 28 presents the estimated maximum longitudinal tensile stresses due to nighttime temperature gradient under the various conditions of support layer properties. As shown in the table, the critical stresses increase as the values of variables increase. These are reasonable responses considering the typical behavior of concrete slab placed on elastic foundation. However, the rate of increase in stress depends on the variables included in the analysis - thickness of stabilized base, elastic modulus of the base material, and subgrade k-value. Thus, the effects of the material and geometrical properties of the support layers are discussed in more depth.

Table 28. Maximum tensile stresses due to nighttime nonlinear temperature gradient

Thickness of stabilized base [in]	Elastic modulus of base material [ksi]	Subgrade *k*-value [psi/in]					
		50	100	150	200	250	300
2	50	66.2	67.4	68.7	69.9	71.1	72.2
	100	66.5	67.8	69.0	70.2	71.4	72.6
	300	67.6	68.9	70.1	71.3	72.5	73.6
	500	68.6	69.9	71.1	72.2	73.4	74.5
	1000	70.9	72.0	73.2	74.3	75.4	76.5
	2000	74.5	75.6	76.7	77.8	78.8	79.9
3	50	66.7	68.0	69.2	70.4	71.5	72.6
	100	67.4	68.7	69.9	71.1	72.2	73.3
	300	69.9	71.1	72.3	73.4	74.5	75.6
	500	72.1	73.3	74.4	75.5	76.6	77.7
	1000	76.9	77.9	79.0	80.0	81.0	82.0
	2000	84.2	85.1	86.0	86.9	87.7	88.6
4	50	67.4	68.6	69.8	71.0	72.1	73.2
	100	68.6	69.8	71.0	72.2	73.3	74.4
	300	72.9	74.1	75.2	76.3	77.3	78.4
	500	76.7	77.7	78.8	79.8	80.8	81.7
	1000	84.3	85.2	86.1	87.0	87.8	88.7
	2000	95.0	95.7	96.4	97.1	97.7	98.4
5	50	68.3	69.4	70.6	71.7	72.8	73.9
	100	70.1	71.3	72.4	73.6	74.6	75.7
	300	76.6	77.6	78.7	79.7	80.7	81.6
	500	82.0	82.9	83.8	84.7	85.6	86.5
	1000	92.3	93.0	93.8	94.5	95.2	95.9
	2000	105.4	106.0	106.5	107.0	107.5	108.0
6	50	69.2	70.4	71.5	72.6	73.7	74.7
	100	71.9	73.0	74.1	75.2	76.2	77.2
	300	80.7	81.7	82.6	83.5	84.4	85.3
	500	87.7	88.5	89.3	90.1	90.9	91.7
	1000	100.2	100.9	101.5	102.0	102.6	103.2
	2000	114.9	115.3	115.7	116.0	116.4	116.8

6.2.1.1. Effects of Thickness of Stabilized Base Layer

First, the effects of stabilized base layer thickness on the maximum stress in longitudinal direction are discussed under the nighttime nonlinear temperature gradient. Figure 56 illustrates the effects of base thickness. Here, *x*-axis is the thickness of the stabilized base layer, and *y*-axis is the maximum critical stress at slab center. The estimated maximum critical tensile stress increases with the stiffness of the support system. However, the plotted stresses show different increment rates of the maximum longitudinal tensile stress, which depends on the base thickness under diverse values of subgrade *k*-value and elastic modulus of the base material. Table 29 presents the increment rates of the maximum longitudinal tensile stress at various stabilized base layer thicknesses. A support condition with low subgrade *k*-value but high elastic modulus of base material gives a more significant effect on the increase in the maximum tensile stresses. Also, both higher subgrade *k*-value and elastic modulus of the base brings a more sensitive effect to the critical stress increments. For this case, increase in the values of the stabilized base layer thickness and the elastic modulus of base material seems to be more sensitive to the slab response than subgrade *k*-value.

All cases showing effects of the stabilized base thickness on the maximum longitudinal tensile stress are shown in APPENDIX B. The results give identical relationships as presented in Table 29.

Table 29. Increment rates of maximum tensile stress as thickness of base increases

Subgrade *k*-value	Elastic modulus of base material	Increment rate of maximum tensile stress
Low	Low	**Low**
Low	High	**High**
High	Low	**Low**
High	High	**High**
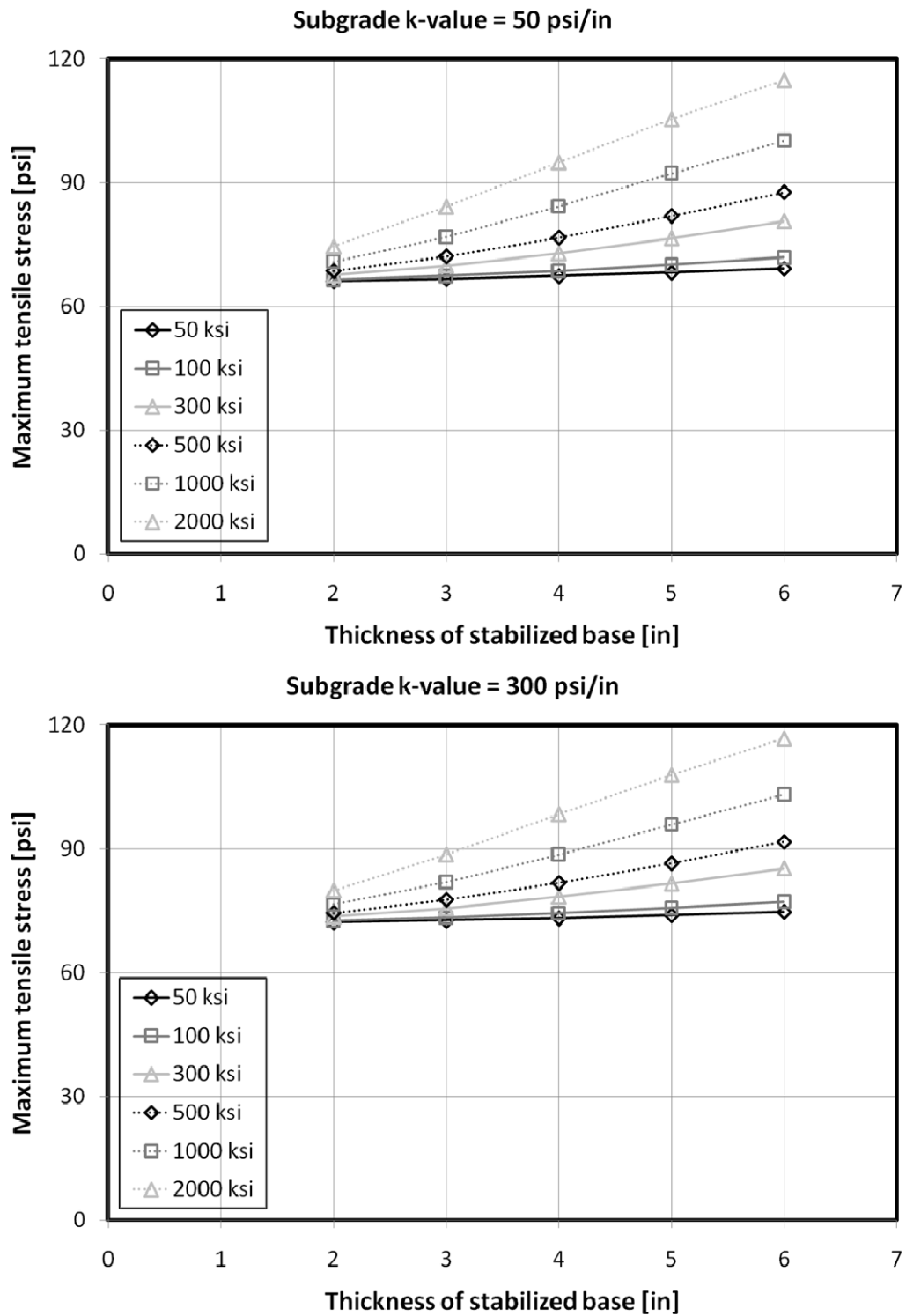
Figure 56. Effects of thickness of stabilized base under temperature loading

6.2.1.2. Effects of Modulus of Elasticity of Base Material

The effects of elastic modulus of base material on the maximum tensile stresses in longitudinal direction are also discussed under the nighttime nonlinear temperature gradient. Figure 57 shows the effects of elastic modulus of the base material. Here, the x-axis is the elastic modulus of the base material, and y-axis is the maximum critical stress at slab center. As with the effects of base thickness, the critical tensile stress increased as the elastic modulus of base material increases. However, the results show different increment rates of the maximum longitudinal tensile stress when the base elastic modulus changes under diverse combinations between different subgrade k-value and base thickness. Table 30 addresses the increment rates of the maximum critical stress as changing elastic modulus of the base material. Increasing elastic modulus of the base layer, the thickness of the stabilized base layer seems to give more significant effect to the variations of the maximum longitudinal tensile stress in the CRCP slab than subgrade k-value does.

For all cases of effects of elastic modulus of the base material under nighttime temperature condition, the plotted maximum longitudinal tensile stresses are included in APPENDIX B. The results also show identical correlations as presented in Table 30.

Table 30. Increment rates of maximum tensile stress as elastic modulus of base material increases

Subgrade k-value	Thickness of stabilized base	Increment rate of maximum tensile stress
Low	Low	**Low**
Low	High	**High**
High	Low	**Low**
High	High	**High**
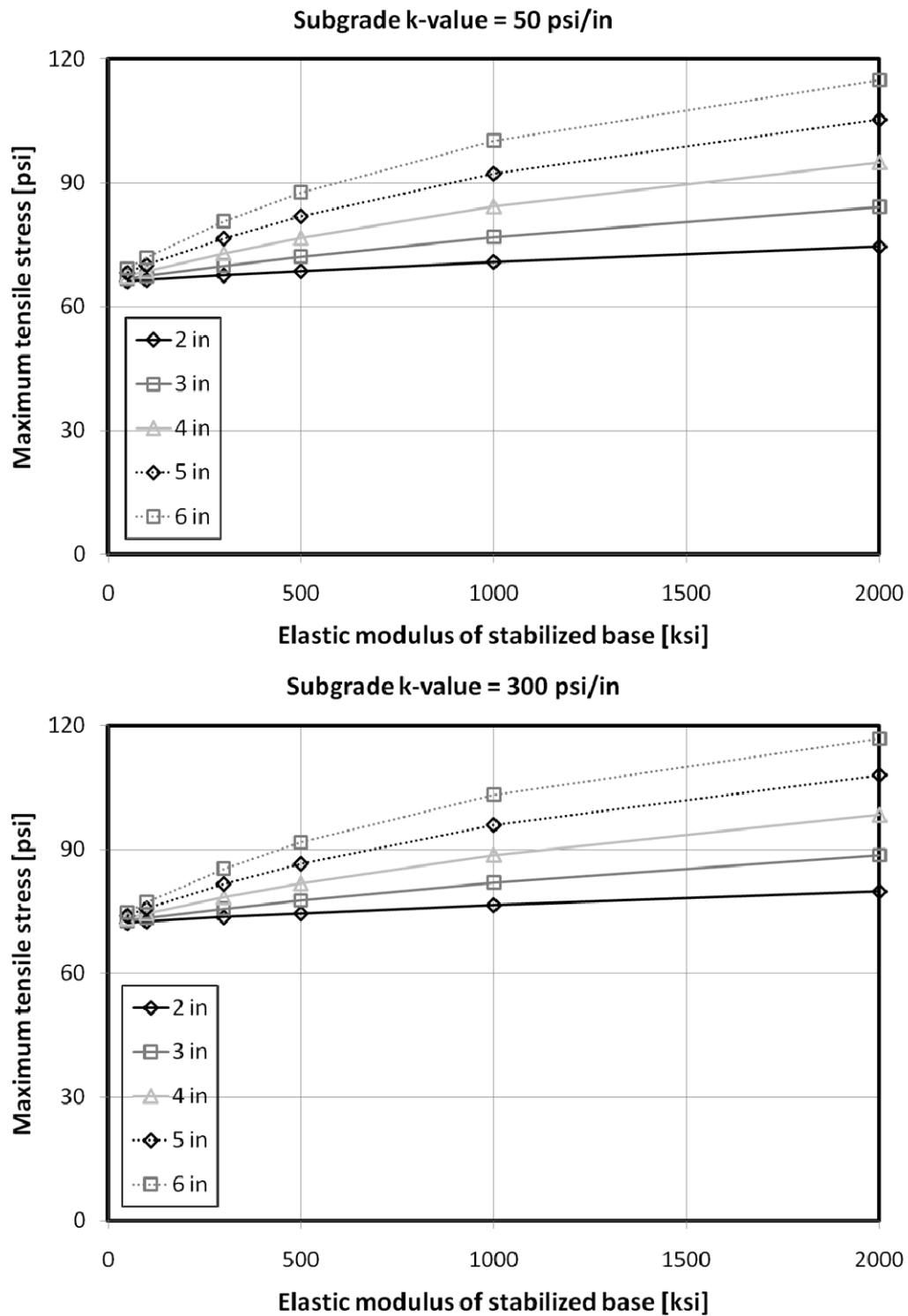
Figure 57. Effects of elastic modulus of base material under temperature loading

6.2.1.3. Effects of *k*-value of Subgrade Layer

Additionally, effects of subgrade *k*-value on the maximum longitudinal tensile stresses are also reviewed under the nighttime nonlinear temperature gradient. Figure 58 presents the effects of subgrade *k*-value on the maximum critical stresses due to nighttime temperature gradient. Here, *x*-axis is the subgrade *k*-value, and *y*-axis is the maximum critical stress at the center of the CRCP slab, between two adjacent transverse cracks. Unlike the effects of base thickness and elastic modulus of the base material, the maximum longitudinal tensile stress rarely changed as the subgrade *k*-value increases. Table 31 addresses the increment rates of the maximum critical stress as increasing subgrade *k*-value under nighttime temperature condition. For all combinations of base thicknesses and elastic modulus of the base materials, the change ratios of the critical stresses in the CRCP slab have been very small. In other words, it appears that the variations of subgrade *k*-value do not significantly affect the responses of CRCP slab due to nighttime temperature gradient.

For all cases of effects of subgrade *k*-value under nighttime temperature condition, the estimated critical stresses and the variations are included in APPENDIX B. The results also show similar relationships as presented in Table 31.

Table 31. Increment rates of maximum tensile stress as subgrade *k*-value increases

Thickness of base layer	Elastic modulus of base material	Increment rate of maximum tensile stress
Low	Low	**Low**
Low	High	**Low**
High	Low	**Low**
High	High	**Very low**

Figure 58. Effects of subgrade *k*-value under temperature loading

6.2.1.4. Results

The maximum longitudinal tensile stress has increased as the support system stiffens. For the computed maximum critical stresses, regression analysis is conducted using SPSS computer package. Table 32 shows the estimated regression coefficients. According to the standardized coefficients which ignore unit effects of the independent variables, it could be identified that the elastic modulus of base material gives the largest effect to the critical stress, and thickness of the base layer is the next, whereas, subgrade k-value has little affected on the maximum critical stress (i.e. Elastic modulus of base material > Thickness of base layer > Subgrade k-value).

Table 32. Regression coefficients for critical stress under temperature loading

Independent variables	Unstandardized coefficient	Standardized Coefficient
Constant	50.569	-
Thickness of base	4.407	0.518
Elastic modulus of base material	0.013	0.743
Subgrade k-value	0.02	0.141

The maximum critical stress at slab center (σ_{cr}) could be estimated by the regression equation 6.1. Here, a linear regression relationship is assumed between the dependent and independent variables. Units of the variables are inches, ksi, and psi/in for thickness of base layer, elastic modulus of the base material, and subgrade k-value, respectively. This relationship among the support properties and the critical stress has 84.0% of R^2-value.

$$\sigma_{cr} = 50.6 + 4.41T_b + 0.013E_b + 0.02k_{sg} \qquad (6.1)$$

126

6.2.2. Vehicle Wheel Loading

As with the case of temperature loading condition, the maximum longitudinal tensile stresses at the slab center are estimated under vehicle wheel condition applied on the center of the CRCP slab, between two adjacent transverse cracks, due to change of the support layer properties. Here, all support layer properties are exactly identical with the analysis by temperature loading. Thickness of stabilized base layer ranges from 2 to 6 in, elastic modulus of the base material is between 50 to 2000 ksi, and subgrade k-value is from 50 to 300 psi/in. These values represent the practical limits of the material properties used in rigid pavement construction.

Table 33 presents the computed maximum longitudinal tensile stresses under the various conditions of support layer properties due to center vehicle wheel loading. As shown in the table, the maximum critical stresses decreases as the values of variables increase, which means the support system is stiffening. This is the opposite responses compared with cases of temperature loading conditions. These are also reasonable response considering the basic behavior of concrete slab placed on elastic foundation due to wheel loading condition. However, the decreasing rates depend differently on alterations of the variables which are thickness of stabilized base, elastic modulus of the base material, and subgrade k-value. Thus, the effects of the material and geometrical properties of the support layers are more detailed reviewed under the vehicle wheel loading condition.

Table 33. Maximum tensile stresses due to vehicle wheel loading

Thickness of Base layer [in]	Elastic modulus of base material [ksi]	Subgrade *k*-value [psi/in]					
		50	100	150	200	250	300
2	50	93.5	92.7	92.0	91.3	90.6	89.9
	100	93.3	92.5	91.8	91.1	90.4	89.7
	300	92.8	92.0	91.3	90.6	89.8	89.2
	500	92.3	91.5	90.8	90.1	89.4	88.7
	1000	91.2	90.5	89.8	89.1	88.4	87.8
	2000	89.5	88.8	88.1	87.5	86.8	86.2
3	50	93.2	92.4	91.7	91.0	90.3	89.6
	100	92.8	92.1	91.3	90.6	89.9	89.2
	300	91.6	90.9	90.2	89.5	88.8	88.1
	500	90.5	89.8	89.1	88.4	87.8	87.1
	1000	88.2	87.5	86.9	86.2	85.6	85.0
	2000	84.4	83.8	83.2	82.7	82.1	81.6
4	50	92.8	92.0	91.3	90.6	89.9	89.3
	100	92.1	91.4	90.7	90.0	89.3	88.6
	300	90.0	89.3	88.6	87.9	87.3	86.7
	500	88.1	87.4	86.8	86.2	85.5	84.9
	1000	84.1	83.5	82.9	82.4	81.8	81.3
	2000	78.1	77.6	77.1	76.7	76.2	75.8
5	50	92.3	91.5	90.8	90.2	89.5	88.9
	100	91.3	90.6	89.9	89.2	88.6	87.9
	300	87.9	87.3	86.7	86.0	85.4	84.8
	500	85.1	84.5	83.9	83.3	82.8	82.2
	1000	79.3	78.8	78.3	77.9	77.4	76.9
	2000	71.2	70.8	70.4	70.0	69.7	69.3
6	50	91.7	91.0	90.3	89.6	89.0	88.4
	100	90.3	89.6	88.9	88.3	87.7	87.0
	300	85.6	85.0	84.4	83.8	83.2	82.7
	500	81.7	81.1	80.6	80.1	79.6	79.1
	1000	74.1	73.7	73.3	72.9	72.5	72.1
	2000	64.1	63.8	63.5	63.2	63.0	62.7

6.2.2.1. Effects of Thickness of Stabilized Base Layer

The effects of thickness of stabilized base layer on the maximum critical stress in longitudinal direction are discussed under wheel loading condition applied at the center of the CRCP slab. Figure 59 illustrates the effects of the base thickness on the critical stress due to vehicle wheel loading. Here, x-axis is the thickness of stabilized base layer, and y-axis is the critical longitudinal stress at slab center. The critical tensile stress decreases as stiffness of the support system increases. However, the decrements of the stress show different rates due to increment of the base thickness under diverse subgrade k-values and elastic modulus of the base material. Table 34 presents the decrement rates of the maximum critical stress as changing thickness of the stabilized base layer. A support condition which has a low subgrade k-value but high elastic modulus of base material gives a larger effect to decrease the maximum tensile stress. Also, higher subgrade k-value and elastic modulus of the base show more sensitive effect to the critical stress decrement. Accordingly, as thickness of the stabilized base layer increases, the elastic modulus of the base material seems to be more susceptible to the slab response than subgrade k-value. However, these are less sensitive than the case of temperature loading condition. More detailed graphs for all cases are included in APPENDIX B.

Table 34. Decrement rates of maximum tensile stress as thickness of base increases

Subgrade k-value	Elastic modulus of base material	Decrement rate of maximum tensile stress
Low	Low	**Very low**
Low	High	**Medium**
High	Low	**Very low**
High	High	**Medium**
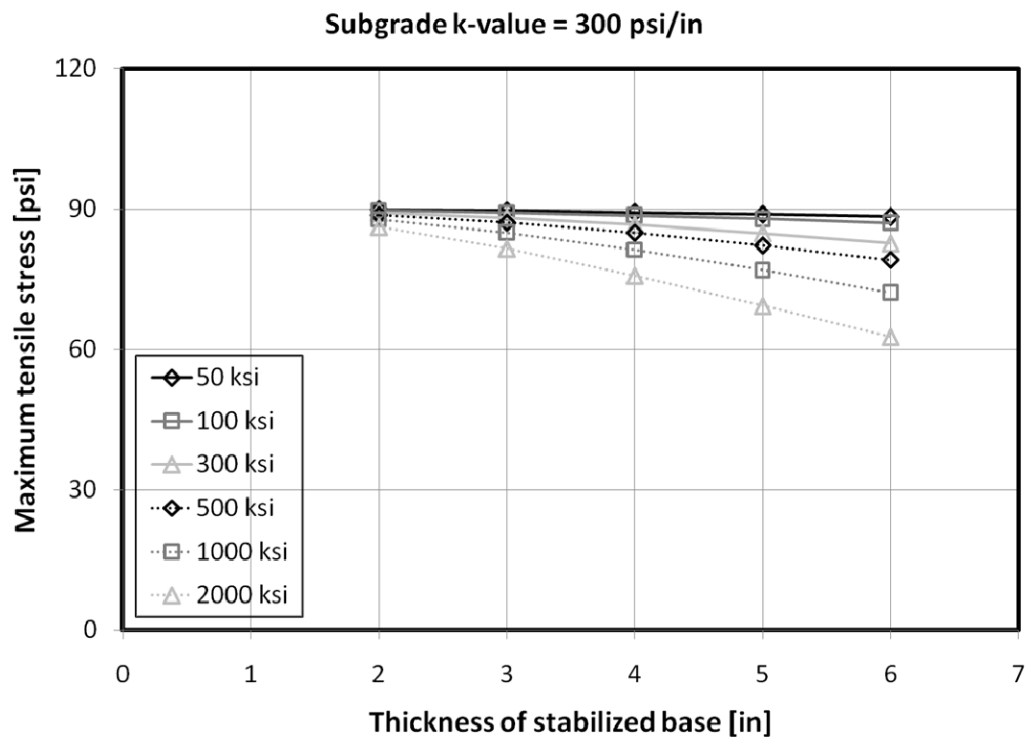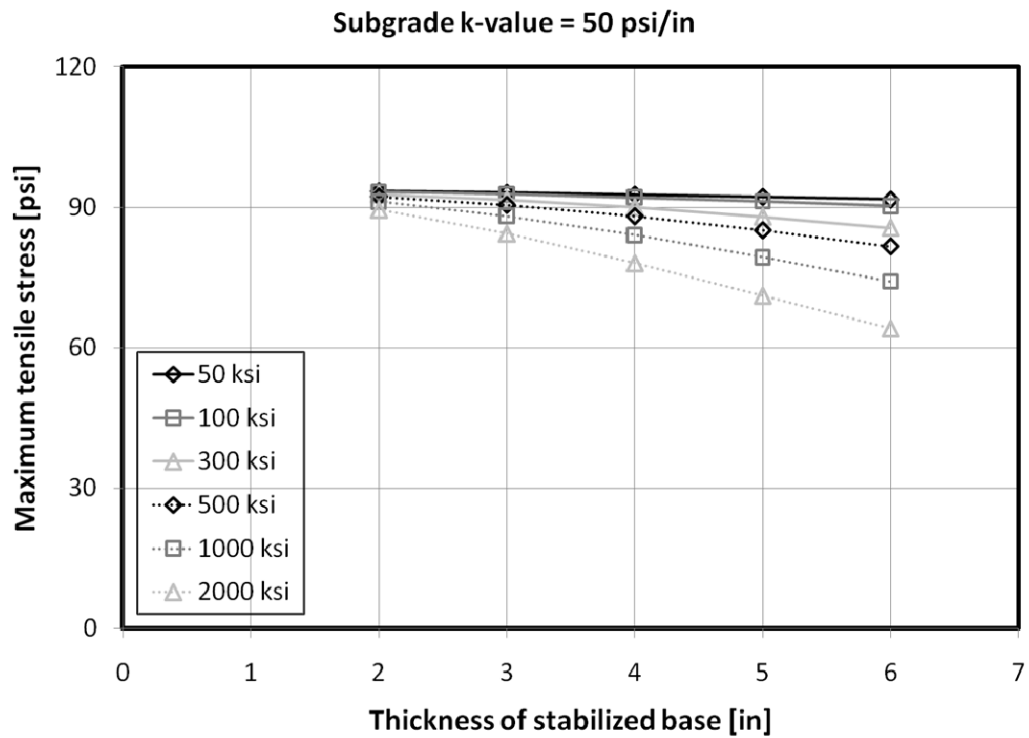
Figure 59. Effects of thickness of stabilized base under vehicle wheel loading

6.2.2.2. Effects of Modulus of Elasticity of Base Material

Secondly, the effects of elastic modulus of the base material on the maximum longitudinal critical stress are also reviewed under wheel loading condition applied at center between two adjacent transverse cracks of the CRCP slab. Figure 60 presents the effects of elastic modulus of base layer on the maximum longitudinal tensile stress due to center loaded vehicle wheel loading. Here, x-axis is the elastic modulus of the base material, and y-axis is the critical longitudinal stress at the slab center. The maximum critical tensile stresses decrease as the stiffness of support system increases due to wheel loading. However, the decrements of the stress have also shown different rates due to the increment of the base thickness. Table 35 addresses the decrement rates of the maximum critical stress as increasing elastic modulus of the base layer. As with the previous cases, the support condition which has a low subgrade k-value but a thick base decreases the maximum tensile stress. Also, higher subgrade k-value and base thickness has shown a more sensitive effect to the critical stress decrement. Therefore, with increasing elastic modulus of base material, it seems that the base thickness could affect the CRCP slab response more than subgrade k-value could. However, these cases are less sensitive than the case of temperature loading condition as well. More detailed results for these cases are also included in APPENDIX B.

Table 35. Decrement rates of maximum tensile stress as elastic modulus of base material increases

Subgrade k-value	Thickness of base layer	Decrement rate of maximum tensile stress
Low	Low	**Low**
Low	High	**Medium**
High	Low	**Low**
High	High	**Medium**
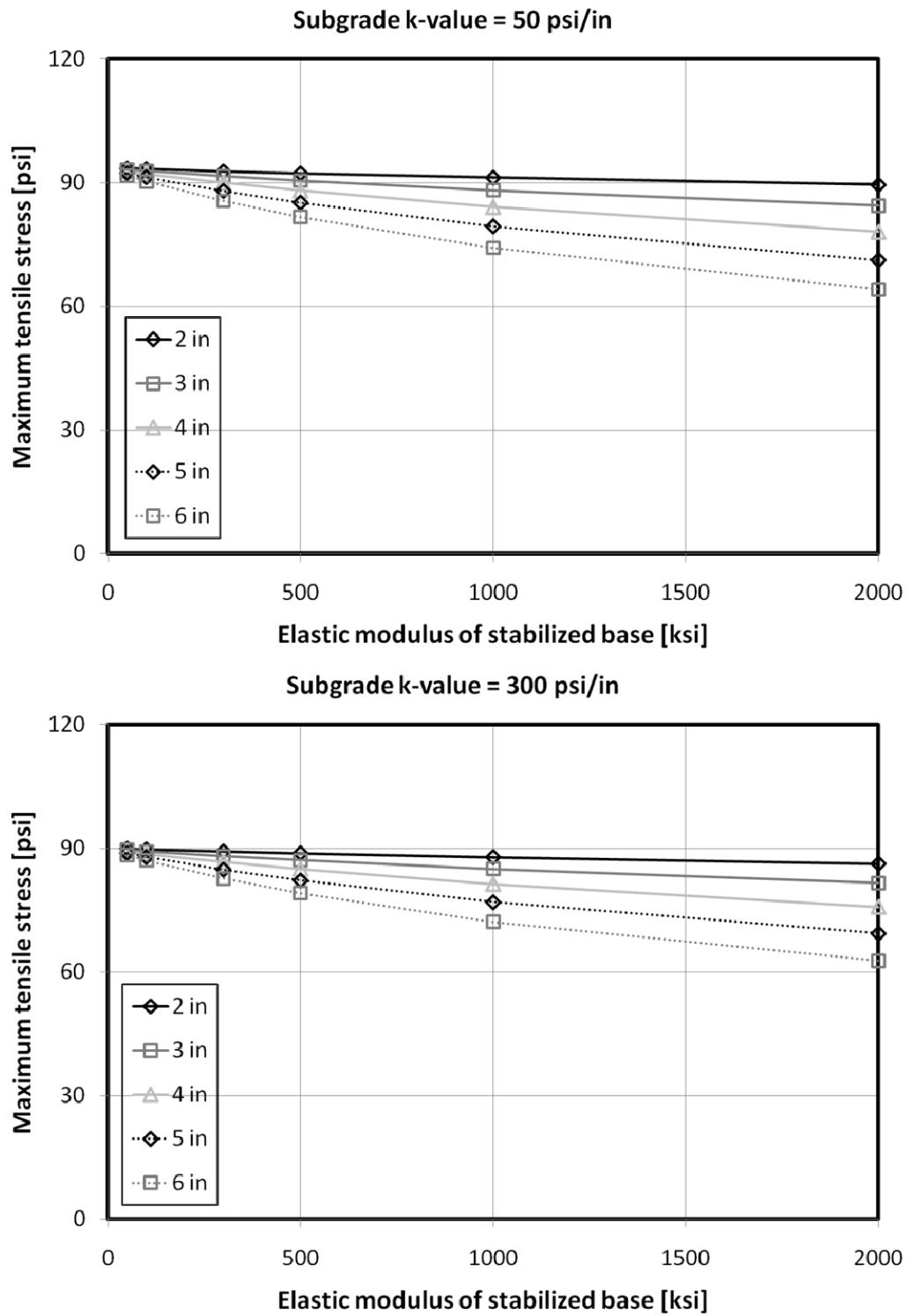
Figure 60. Effects of elastic modulus of base material under vehicle wheel loading

6.2.2.3. Effects of *k*-value of Subgrade Layer

      Finally, the effects of subgrade *k*-value on the maximum longitudinal tensile stress in the CRCP slab are reviewed under center-placed vehicle wheel loading conditions. Figure 61 illustrates the effects of the subgrade *k*-value on the maximum longitudinal tensile stress due to vehicle wheel loading applied at the center of the CRCP slab. Here, *x*-axis is the subgrade *k*-value, and *y*-axis is the maximum critical stress between two adjacent transverse cracks. For the wheel loading condition, unlike the effects of base thickness and elastic modulus of the base material, the maximum longitudinal tensile stress rarely changed as the subgrade *k*-value increased. These are identical results compared with the cases of temperature loading condition. Table 36 shows the decrement rates of the maximum critical stress as increasing subgrade *k*-value under vehicle wheel loading condition. For all combinations of base thicknesses and elastic modulus of the base materials, the maximum critical stress in the CRCP slab rarely changed as subgrade *k*-value increased. In other words, the subgrade *k*-value does not largely affect to the behavior of CRCP slab as with the cases applying the nighttime temperature gradient.

      For all cases of effects of subgrade *k*-value under the vehicle wheel loading applied at center of the CRCP slab, the computed critical stresses and the variations are included in APPENDIX B.

Table 36. Decrement rates of maximum tensile stress as subgrade *k*-value increases

Thickness of base layer	Elastic modulus of base material	Decrement rate of maximum tensile stress
Low	Low	**Low**
Low	High	**Low**
High	Low	**Low**
High	High	**Very low**

Figure 61. Effects of subgrade *k*-value under vehicle wheel loading

6.2.2.4. Results

The regression analysis is also performed for the vehicle wheel loading condition. Opposite from the cases of temperature loading, the maximum longitudinal tensile stress decreased as the stiffness of support system increased. Table 37 addresses the estimated regression coefficients using the computed maximum critical stresses. The estimated standardized coefficients have revealed that the elastic modulus of base material gives the greatest influence to the critical stress negatively, and the thickness of the base layer is the next. The subgrade k-value gives little effect to the change of the maximum critical stress, as well as temperature loading. In other words, Elastic modulus of base material > Thickness of base layer > Subgrade k-value, negatively.

Table 37. Regression coefficients for critical stress under wheel loading

Independent variables	Unstandardized coefficient	Standardized Coefficient
Constant	103.0	-
Thickness of base	-2.607	-0.528
Elastic modulus of base material	-0.007	-0.720
Subgrade k-value	-0.012	-0.150

The maximum critical stress at the slab center (σ_{cr}) due to vehicle wheel loading could be estimated by the regression equation 6.2. Here, a linear regression relationship is assumed between the dependent and independent variables. Units of the variables are inches, ksi, and psi/in for the thickness of base layer, elastic modulus of the base material, and subgrade k-value, respectively. This relationship among the support properties and the critical stress has 82.0% of R^2-value.

$$\sigma_{cr} = 103.0 - 2.61 T_b - 0.007 E_b - 0.012 k_{sg} \tag{6.2}$$

6.3. CRCP BEHAVIOR ON SUPPORT SYSTEMS HAVING IDENTICAL
COMPOSITE *K*-VALUES

It has been discussed that the maximum critical stresses induced in the CRCP slab due to temperature and vehicle wheel loadings have been affected by the support layer properties. The property characterizing the total support system which consists of various layers is called composite *k*-value. This composite *k*-value has been widely and commonly used for modern rigid pavement design. Chapter 4 of this report identified the combinations of support layer properties, which have identical composite *k*-values. Accordingly, the behavior of CRCP slab placed on these support combinations having identical composite *k*-values but different combinations of the support layer properties are discussed.

6.3.1. Effects of Support Properties Combinations

In Chapter 4, a total 14 of combination cases of support layer properties having identical composite *k*-value of 300 psi/in were selected by simulations of static plate load test. For the 14 cases, CRCP slabs which have 6-ft crack spacing have been placed, and the maximum longitudinal tensile stresses at the slab center are estimated under nighttime temperature and center wheel loading conditions.

Table 38 presents the maximum critical stress under the various combinations of support properties having identical composite *k*-value of 300 psi/in. The maximum stress due to temperature loading ranges from 71.3 to 90.7 psi, whereas the values between 80.7 and 90.4 psi were estimated for the wheel loading condition. With increasing subgrade *k*-value, elastic modulus of base material, and thickness of the base layer, the maximum longitudinal stresses decreased under temperature loading, but increased under vehicle wheel loading although all cases have the same composite *k*-value.

Case No.11 gives the minimum value of the maximum critical stress for the nighttime temperature gradient, and Case No.3 shows the minimum stress level for the

center loaded wheel loading condition. On the other hands, Case No.7 produces the minimum stress level for both temperature and wheel loadings. Thus, for this example, combination Case No.7, subgrade *k*-value is 100 psi/in, elastic modulus of base material is 2000 ksi, and the base thickness is 2.5 in, might be the optimum composition of the support system having composite *k*-value, 300 psi/in as an aspect of the maximum critical stress. However, for the selection of optimum composition of the support system, the economical aspect is significant as well. Also, in this study, the thickness of CRCP slab is fixed as 10 in, but the thickness of CRCP slab should be included as a variable to verify optimum composition of CRCP structure as an aspect of the critical stress. Therefore, the variables defining optimum composition of the CRCP structure could be categorized by CRCP slab thickness, thickness of base layer, elastic modulus of the base material, and *k*-value of subgrade. A method to determine the optimum combination of the variables will be introduced and discussed more in Chapter 8.

Table 38 Maximum longitudinal tensile stresses under various support properties combinations having identical composite *k*-value of 300 psi/in

No.	Subgrade *k*-value [psi/in]	Elastic modulus of base material [ksi]	Thickness of base layer [in]	Maximum tensile stress [psi]	
				due to temperature	due to wheel loading
1		500	5.8	86.5	82.4
2	50	1,000	4.6	89.1	81.3
3		2,000	3.6	**90.7**	**80.7**
4		300	4.7	76.5	87.9
5		500	4	77.7	87.4
6	100	1,000	3.1	78.6	87.1
7		2,000	2.5	**80.2**	**86.5**
8		300	3.4	73.4	89.6
9	150	500	2.9	74.0	89.3
10		1,000	2.3	74.7	89.1
11		50	4.5	**71.3**	**90.4**
12		100	3.5	71.6	90.3
13	200	300	2.4	72.1	90.2
14		500	2	72.2	90.1

6.3.2. Effects of Slab Thickness

To verify the effects of slab thickness, CRCP slabs having thicknesses ranging from 6 to 14 in are considered. These support layer properties were selected as control values; 150 psi/in for subgrade k-value, 4 in of base thickness, and 300 ksi for elastic modulus of the base material. This composition gives 338 psi/in of composite k-value. For these CRCP models, nighttime temperature and center wheel loadings are applied. Figure 62 shows the maximum longitudinal tensile stress under the temperature and wheel loading conditions due to change of the CRCP slab thickness. As shown in the figure, the critical stresses decreased as the slab thickness increased. Also, the decrement rate by the wheel loading is greater than the rate of temperature loading. Thus, it seems that the critical stress could be more sensitively affected by vehicle wheel loads when the CRCP slab thickness is changing.
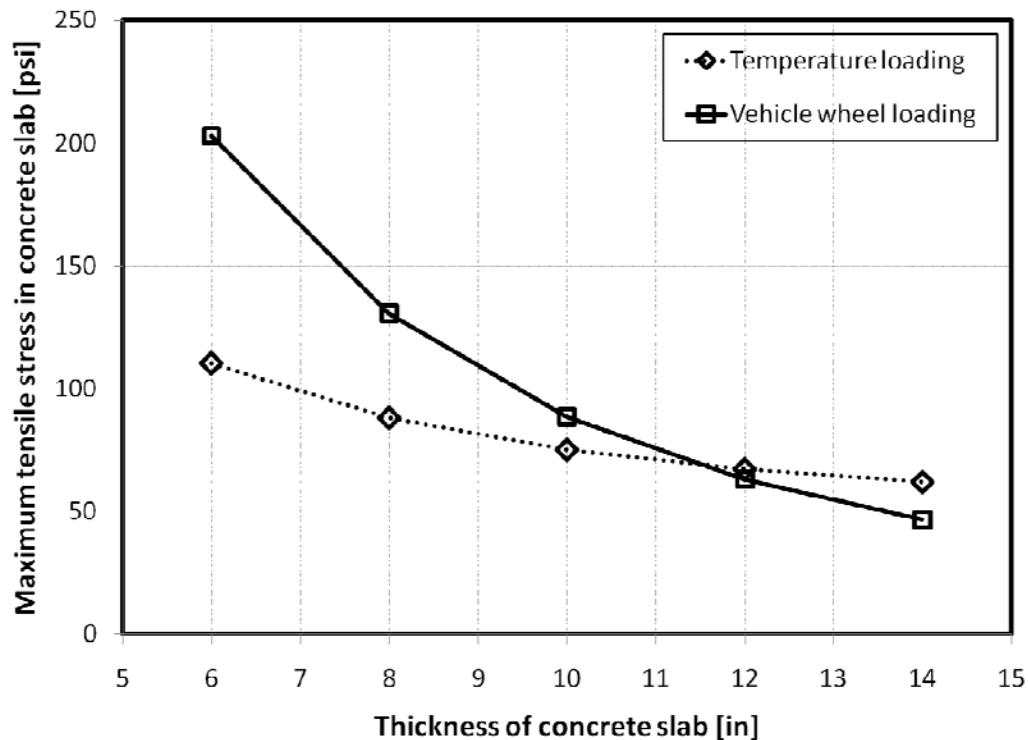
Figure 62. Effects of slab thickness on maximum tensile stresses

6.3.3. Effects of Crack Spacing

A CRCP structure has shown diverse crack spacing raging from 0.25 to 10 ft [Seleznava et al., 2003]. CRCP slabs with crack spacing from 2 to 10 ft were considered to verify the effects of the crack spacing. Support layer properties were selected as control values which give 338 psi/in of the composite k-value. For these CRCP models, nighttime temperature and center wheel loadings were applied. Figure 63 shows the maximum longitudinal tensile stress under the temperature and wheel loading conditions due to a change of the CRCP crack spacing. As shown in the figure, the maximum critical stresses increased as the slab thickness increased. Also, the increment rate by the wheel loading is larger than the temperature loading condition. Therefore, it is likely that the critical longitudinal stresses could be more susceptible to the vehicle wheel loads than temperature gradient when the CRCP crack spacing changes.
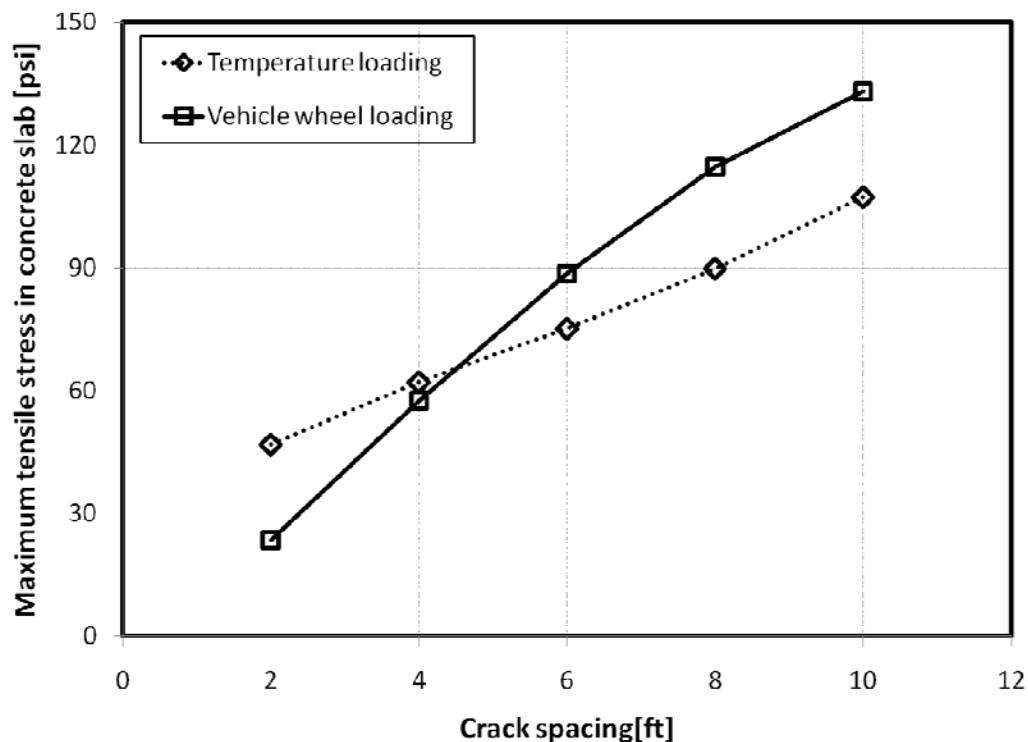
Figure 63. Effects of crack spacing on maximum tensile stress

6.4. EFFECTS OF NON-UNIFORMITY SUPPORT CONDITIONS ON CRCP BEHAVIOR

Support systems of rigid pavement structures usually provide non-uniform support to the pavement slabs because soil parameters vary from point to point, even in normally homogeneous layers [White et al., 2005]. In other words, the distribution of vertical stiffness of the foundation supporting pavement slabs has shown non-uniform conditions as identified in Chapter 3 using FWD test. Accordingly, the effects of the non-uniform support conditions on the responses of the CRCP slab are discussed in this study.

6.4.1. Non-Uniform Support Cases

To verify the effects of non-uniform support conditions of CRCP structures, 4 cases of the non-uniform conditions were considered. Figure 64 illustrates the non-uniform support conditions of CRCP. The non-uniform area was considered as 2-ft long at the subgrade layer because base layer has been generally uniformly stabilized. Case 1 means that the non-uniform spot is located under the slab center which is between two adjacent transverse cracks. Also, Case 2 represents the non-uniform area just under the transverse crack of the CRCP slab. For both Case 1 and Case 2, locally weak and locally strong conditions were considered. Locally weak condition means that the non-uniform spot has 50 psi/in of subgrade k-value, and locally strong condition has 300 psi/in of subgrade k-value at the non-uniform spot. Basically, it has been assumed that the CRCP slab is placed on 150 psi/in of subgrade k-value. For these 4 cases of non-uniform conditions, daytime and nighttime temperature gradients and vehicle wheel loadings at the slab center and crack are applied on the CRCP slab. Table 39 presents the cases of the non-uniform support conditions and their naming for this study.
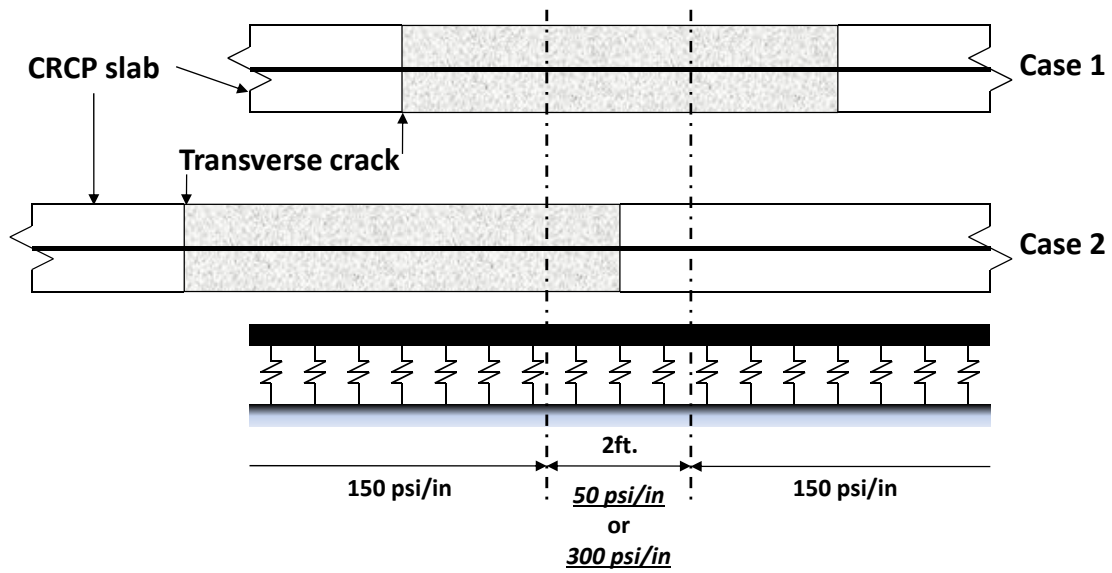
Figure 64. Non-uniformity support conditions of CRCP structure

Table 39. Cases of non-uniform support conditions and naming

Location of non-uniform spot	Subgrade *k*-value at non-uniform spot [psi]	Naming
Under slab center	50	Center weak
	300	Center strong
Under transverse crack	50	Crack weak
	300	Crack strong

6.4.2. Stress Analysis of CRCP Slabs on Non-Uniform Support Conditions

For the 4 cases of non-uniformity support conditions and 4 cases of loading conditions, stresses at the center of the CRCP slab were plotted through the slab depth. The stresses for uniform support condition were also plotted and compared with the non-uniform cases. Figure 65 shows the stress distributions at the center of the CRCP slab due to temperature and wheel loading conditions under the non-uniform support conditions. For this case study, the center weak condition and crack strong condition produce almost identical responses on the CRCP behavior for all loading cases although the absolute subgrade k-values are different. Also, crack weak condition and center strong condition behaved similarly by the loadings even though the absolute k-values of subgrade are also totally different. The maximum tensile stresses induced in the CRCP slab are almost twice as large for the non-uniform support conditions as for the uniform condition. Consequently, it could be recommended that, to improve CRCP performance, efforts should be made to provide a more uniform support condition of the subgrade soil.
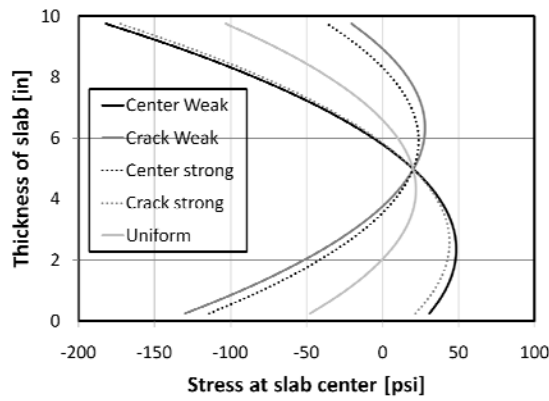
(a) Daytime temperature loading
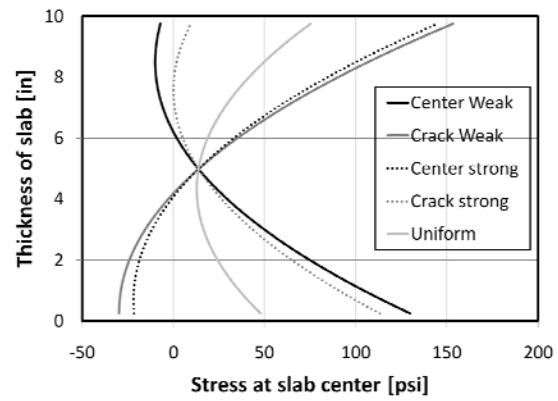
(b) Nighttime temperature loading
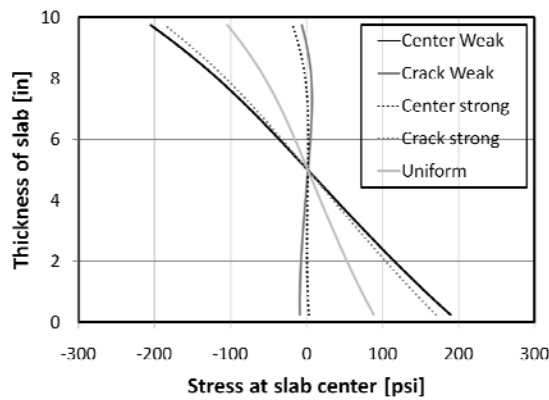
(c) Wheel loading at slab center
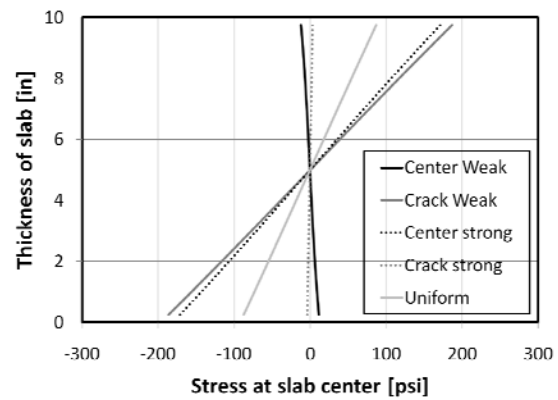
(d) Wheel loading at slab crack

Figure 65. Stresses at center of CRCP slab for non-uniform support conditions

144

6.5.   SUMMARY

The effects of various support conditions on CRCP behavior have been estimated using FE analysis under the temperature gradient and wheel loading condition. A 2-dimensional CRCP FE model was developed using 4-nodes plane strain elements. The stabilized base layer was independently modeled as elastic solid layer, and behavior of transverse crack is also considered. Nonlinear temperature gradients through the slab depth and the typical dual tire single axle loads have been adopted to estimate the critical stresses in the CRCP slab. Especially, the nonlinear nighttime temperature condition and vehicle wheel loading placed at the center of the CRCP slab were applied.

To verify the effects of support layer properties on CRCP behavior, the maximum longitudinal tensile stresses were estimated at the center of the CRCP slab, between two adjacent transverse cracks, under nighttime nonlinear temperature gradient and center loaded wheel loading conditions. The considered properties of the support system were thickness of the stabilized base layer, elastic modulus of the base material, and k-value of subgrade. For both the temperature and wheel loading conditions, the stabilized base layer properties such as thickness and elastic modulus have larger effects on the maximum longitudinal tensile stresses than subgrade vertical stiffness, k-value. However, the variation rates have been relatively greater for the temperature loading condition than for the vehicle wheel loading case.

Additionally, the maximum longitudinal tensile stresses are computed and compared for diverse combinations of the support layer properties accomplishing identical composite k-value, 300 psi/in. Although a support system has identical composite k-value, the maximum critical stresses depend on the compositions of the properties. Temperature loading gives more sensitive effects to the variation of the maximum critical stresses than vehicle wheel loading. However, for the change of CRCP slab thickness and transverse crack spacing, vehicle wheel loading more significantly affects the responses of the CRCP slab than temperature loading.

The effects of non-uniformity support conditions on CRCP behavior were also

examined. 4 cases of non-uniformity support conditions have been considered, locally weak and locally strong conditions under the CRCP slab center and transverse crack. Center weak condition and crack strong condition have shown similar maximum critical stresses although they have different absolute k-values, on the other hand, center strong and crack weak conditions gives almost identical stress distributions in the CRCP slab. Also, the maximum longitudinal tensile stresses induced in the CRCP slab are almost twice as greater for the non-uniform support conditions than for uniform support condition. Consequently, the uniformity of support system could be more emphasized for responses of the CRCP slab rather than the absolute level of the subgrade k-value.

CHAPTER 7: COMPOSITE *K*-VALUE COMPARISONS BASED ON STRESS ASPECT

Composite *k*-value was directly estimated on the top surface of stabilized base layer under various compositions of support layer properties by FE simulation of static plate load test (*k*-value test) using elastic *k*-value composite support model in chapter 4. Also, concrete slabs (CRCP slabs in this study) have been placed on these support combinations, and the maximum longitudinal tensile stresses were estimated under temperature and vehicle wheel loading conditions using the elastic *k*-value composite support model in chapter 6. However, many design guides for rigid pavement systems have not been considered separately according to the base and subgrade layer, but a single value of *k* that is a spring coefficient representing all layers under the concrete slabs including base, base and subgrade layers. Here, it may be assumed that the elastic *k*-value composite support model and the computed composite *k*-value from simulation of the static plate load test could more realistically express actual field support conditions. On the other hand, the currently used design guides have simplified the support system as a single value of *k* using the simple support model. However, if the simplified current support model could predict and evaluate the slab responses reasonably, i.e. the simplified model shows identical results with the elastic and *k*-value composite support model, the use of the simple support model would be the best. Thus, it has been needed to verify whether the two different support models could estimate identical responses on the CRCP slab on the same support conditions, identical composite *k*-value, or not. Accordingly, as an aspect of the maximum longitudinal tensile stresses in the CRCP slab under both of temperature and wheel loadings, the directly computed composite *k*-value by the simulation of the static plate load tests and back-found a single value of *k* (this name is also composite *k*-value) from the simplified model are compared.

7.1. COMPOSITE *K*-VALUES CORRESPONDING MAXIMUM TENSILE STRESS

To compare composite *k*-values from elastic and *k*-value composite support model, corresponding composite *k*-values of the single *k*-value support model, simple support model, are back-found by matching the identical maximum longitudinal tensile stresses due to temperature and vehicle wheel loadings. Figure 66 illustrates the algorithm to find the composite *k*-value of the simple support model, which is corresponding to the maximum critical stresses from the CRCP slab placed on the elastic and *k*-value composite support model. Firstly, the maximum longitudinal tensile stresses in the CRCP slab were estimated from elastic and *k*-value composite support model. Then, using the single *k*-value support model, spring coefficient is back-found, which could induce the identical maximum critical stress in the CRCP slab on the composite support model. In other words, σ_1 is calculated in advance, and σ_2 same as σ_1 is found with changing the spring coefficient, *k*, and the *k* is composite *k*-value of the simple support model. Using this manner, the composite *k*-values were estimated, which is corresponding to the maximum longitudinal tensile stresses due to both of the nighttime nonlinear temperature gradient and center applied vehicle wheel loadings.

(a) Wheel loading

(b) Temperature loading
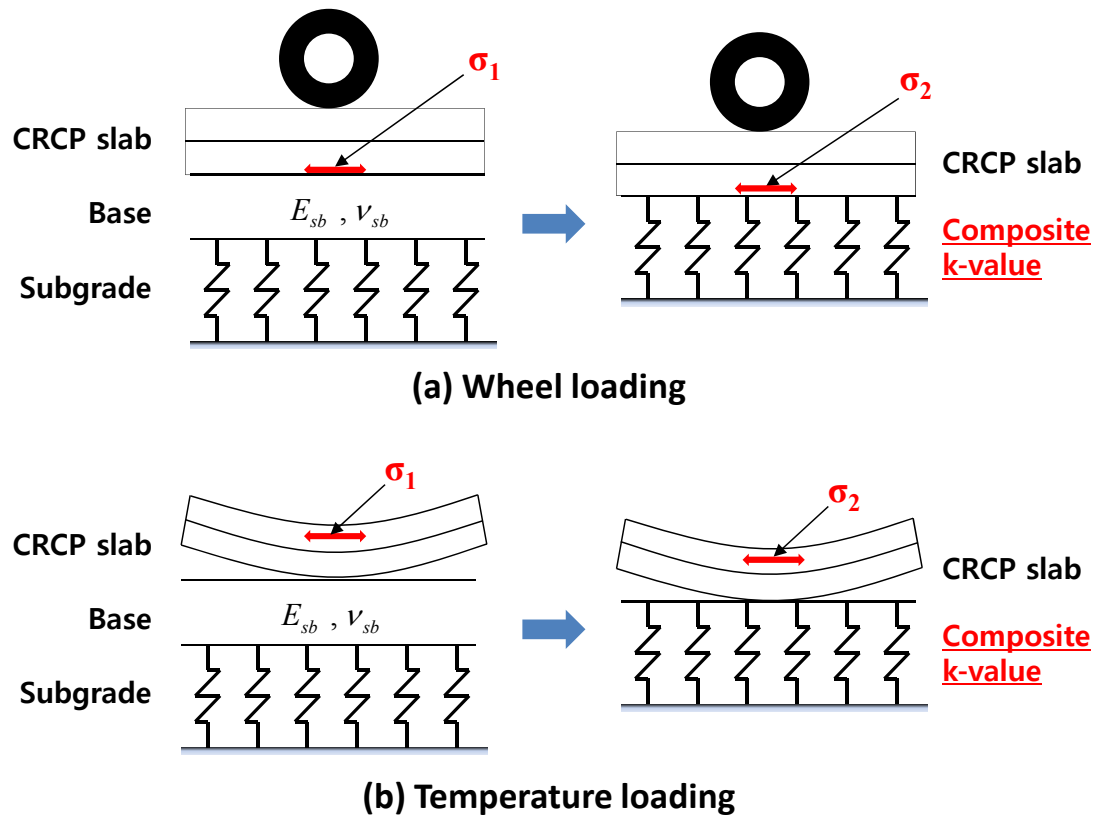
$$\sigma_1 = \sigma_2 \implies \text{Composite k-value}$$

Figure 66. Algorithm to find composite *k*-values corresponding to maximum critical stresses due to wheel and temperature loading conditions

7.1.1. Temperature Loading

Composite *k*-values corresponding to the maximum longitudinal tensile stresses at slab center are estimated on the simple support model using a single value of *k* under nighttime nonlinear temperature condition under changing of the support layer properties. Here, the same variables and ranges have been used with the *k*-value test simulations in chapter 4. The thickness of the stabilized base layer has ranging from 2 to 6 in, elastic modulus of the base material is between 50 to 2000 ksi, and subgrade *k*-value is from 50 to 300 psi/in.

Table 40 presents the back-found composite *k*-values corresponding to the maximum longitudinal tensile stresses due to the temperature gradient under the various support layer properties. As shown in the table, surely, the back-found composite *k*-values corresponding to the critical stresses are increasing as the values of the variables are increasing. It is a reasonable response compared with the directly computed composite *k*-values from simulation of static plate load test using elastic and *k*-value composite support model. However, the variations of the back-found composite *k*-values are relatively larger than those of the directly obtained composite *k*-values. Also, the variations of the differences are apparently depended on the kinds of the support properties which are thickness of stabilized base, elastic modulus of the base material, and subgrade *k*-value.

Table 40. Composite *k*-values corresponding maximum tensile stresses due to temperature loading under various support conditions

Base thickness [in]	Elastic modulus of base material [ksi]	Subgrade *k*-value [psi/in]					
		50	100	150	200	250	300
2	50	65	115	168	218	270	315
	100	80	130	180	230	280	335
	300	123	175	225	275	330	380
	500	165	218	270	315	370	410
	1000	260	305	360	400	450	500
	2000	410	460	510	560	610	660
3	50	85	140	190	240	285	335
	100	115	168	218	270	315	365
	300	218	270	320	370	410	460
	500	310	365	405	455	505	555
	1000	520	565	615	665	715	765
	2000	893	940	993	1045	1090	1145
4	50	115	165	215	265	310	360
	100	165	215	265	315	365	405
	300	345	398	440	490	535	590
	500	510	555	610	655	705	750
	1000	900	945	1000	1050	1095	1150
	2000	1518	1565	1618	1670	1715	1773
5	50	150	195	245	295	343	390
	100	225	275	325	380	415	465
	300	505	550	605	650	700	745
	500	765	820	870	920	970	1020
	1000	1340	1385	1435	1483	1530	1580
	2000	2315	2365	2410	2450	2500	2540
6	50	190	240	285	335	383	420
	100	303	350	398	440	485	533
	300	700	750	795	855	905	955
	500	1090	1140	1185	1215	1260	1305
	1000	1920	1970	2015	2050	2095	2140
	2000	3250	3300	3350	3380	3430	3480

7.1.2. Wheel Loading

The composite *k*-values corresponding to the maximum critical tensile stresses at slab center are also back-found on the simple support model which uses a single value of *k* under vehicle wheel loading condition that is applied slab center, between two adjacent transverse cracks, on the variations of the support layer properties, thickness of stabilized base layer, elastic modulus of the base material, and subgrade *k*-value. Here, the same ranges for the variables are also adopted as the *k*-value test simulations in chapter 4.

Table 41 addresses the back-found composite *k*-values corresponding to the maximum longitudinal tensile stresses at center of the CRCP slab under the center applied vehicle wheel loading condition in accordance with the various support layer properties. As shown in the table, the back-found composite *k*-values from simple support model are increasing as the values of the variables are increasing, i.e. the support system is getting stiff. The back-found composite *k*-values for the wheel loading condition have been shown almost identical with the *k*-values for the temperature loading condition. In the same manner with the case of temperature loading, the variations of the values are relatively larger than the cases of directly obtained composite *k*-values using elastic and *k*-value composite support model. Also, the variations of the differences are apparently depended on the kinds of the support layer properties including thickness of stabilized base, elastic modulus of the base material, and subgrade *k*-value.

Table 41. Composite *k*-values corresponding maximum tensile stresses due to wheel loading under various support conditions

Base thickness [in]	Elastic modulus of base material [ksi]	Subgrade *k*-value [psi/in]					
		50	100	150	200	250	300
2	50	65	115	160	210	260	315
	100	80	130	175	220	270	320
	300	110	160	210	260	310	355
	500	140	195	240	290	340	390
	1000	215	265	310	360	410	460
	2000	335	385	435	480	530	580
3	50	85	135	180	230	280	330
	100	110	155	210	260	305	355
	300	190	235	285	335	385	435
	500	265	310	360	410	460	510
	1000	430	480	525	580	630	680
	2000	730	780	830	870	930	970
4	50	110	160	210	260	305	350
	100	155	200	250	300	350	400
	300	300	350	400	450	495	540
	500	435	490	530	580	640	685
	1000	750	800	855	900	955	1000
	2000	1330	1380	1420	1460	1510	1550
5	50	140	195	240	285	335	380
	100	210	260	305	355	400	450
	300	450	495	540	600	645	690
	500	670	720	770	820	860	920
	1000	1200	1250	1305	1350	1395	1440
	2000	2120	2170	2220	2270	2310	2360
6	50	180	230	280	330	370	410
	100	280	330	380	420	465	520
	300	630	680	730	780	830	870
	500	960	1020	1070	1120	1170	1220
	1000	1745	1790	1845	1895	1950	2000
	2000	3200	3240	3300	3360	3400	3460

7.2. COMPARISONS OF COMPOSITE *K*-VALUES

For use of the simple support model for rigid pavement design, appropriate *k*-value should be adopted to examine behavior of concrete slab. However, the back-found composite-values from the simple support model have shown relatively large values than the directly obtained composite *k*-value. Accordingly, to verify the difference between the two different composite *k*-values, the back-found *k*-values are compared with the directly obtained composite *k*-values by simulation of the *k*-value test. The comparisons have been expressed by difference ratios as follow:

$$Difference\,ratio = \frac{k_B}{k_D} \tag{7.1}$$

Where, k_B is back-found composite *k*-value from the simple support model, and k_D is directly computed composite *k*-value of elastic and *k*-value composite support model from simulation of static plate load test, *k*-value test.

Thus, if the ratio is less than one the back-found composite *k*-value is smaller than the directly obtained composite *k*-value by the simulation, if the ratio is exactly one the *k*-values are exactly identical, and when the ratio is larger than 1, this means that the back-found *k*-value is greater than the composite *k*-value by the simulation of static plate load test. The composite *k*-value comparisons are conducted for both of the temperature and vehicle wheel loading conditions.

7.2.1. Temperature loading

By the nighttime nonlinear temperature gradient condition through the depth of CRCP slab, difference ratios between the composite k-values are computed. Table 42 presents the difference ratios of the composite k-values under the nighttime nonlinear temperature loading condition. Generally, the two different types of k-values, directly computed composite k-value from elastic and k-value support model and the back-found composite k-value corresponding to the maximum longitudinal tensile stress using the simple support model, have been shown to be almost identical when the stabilized base has low structural stiffness, thin thickness of the stabilized base layer and low modulus of elasticity of the base material. However, the difference rates have been increasing as thickness of the stabilized base layer is increasing, elastic modulus of the base material is increasing, but subgrade k-value is decreasing.

Table 42. Difference ratios of composite *k*-values under temperature loading

Thickness of base layer [in]	Elastic modulus of base material [ksi]	Subgrade *k*-value [psi/in]					
		50	100	150	200	250	300
2	50	0.9	0.9	0.9	0.9	0.9	0.8
	100	1.1	1.0	0.9	0.9	0.9	0.9
	300	1.3	1.1	1.0	1.0	1.0	1.0
	500	1.6	1.3	1.1	1.1	1.0	1.0
	1000	2.1	1.5	1.3	1.2	1.1	1.1
	2000	2.7	1.9	1.6	1.4	1.3	1.2
3	50	1.1	1.0	0.9	0.9	0.9	0.9
	100	1.2	1.1	1.0	1.0	0.9	0.9
	300	1.8	1.3	1.2	1.1	1.0	1.0
	500	2.1	1.6	1.3	1.2	1.1	1.1
	1000	2.8	2.0	1.6	1.4	1.3	1.2
	2000	3.7	2.6	2.1	1.8	1.6	1.5
4	50	1.2	1.0	1.0	0.9	0.9	0.9
	100	1.4	1.1	1.0	1.0	1.0	0.9
	300	2.1	1.6	1.3	1.2	1.1	1.1
	500	2.6	1.8	1.5	1.4	1.3	1.2
	1000	3.6	2.5	2.0	1.8	1.6	1.5
	2000	4.6	3.1	2.5	2.2	1.9	1.8
5	50	1.3	1.0	1.0	0.9	0.9	0.9
	100	1.6	1.2	1.1	1.0	0.9	0.9
	300	2.4	1.7	1.4	1.3	1.2	1.1
	500	3.1	2.1	1.8	1.5	1.4	1.3
	1000	4.1	2.8	2.3	1.9	1.7	1.6
	2000	5.2	3.6	2.9	2.5	2.2	2.0
6	50	1.4	1.1	1.0	0.9	0.9	0.9
	100	1.8	1.3	1.1	1.0	1.0	0.9
	300	2.7	1.9	1.6	1.4	1.3	1.2
	500	3.5	2.4	2.0	1.7	1.5	1.4
	1000	4.6	3.2	2.6	2.2	2.0	1.8
	2000	5.8	4.0	3.2	2.7	2.4	2.2

7.2.1.1. Effects of Thickness of Stabilized Base Layer

Effects of base thickness on difference ratio between the two different composite k-values, directly computed composite k-value from simulation of static plate load test and back-found composite k-value corresponding to the maximum critical stress using the simple support model characterized by a single k-value, are discussed under temperature loading condition. Figure 67 shows the effects of base thickness about difference ratio of the composite k-values. x-axis is the thickness of the stabilized base layer, and y-axis is the difference ratio of the two composite k-values. The discrepancy ratios are increased as the thickness of stabilized base layer is increasing. Table 43 addresses the increment rate of the composite k-value discrepancies. The difference ratios are significantly increasing when the subgrade k-value is low and elastic modulus of the base material is high. On the other hands, at a condition having high subgrade k-value and low elastic modulus of base material, the difference rates are rarely increased when the base thickness is increasing. It seems that the change of the discrepancies of the two composite k-values is mainly affected by elastic modulus of the base material rather than subgrade k-value when the thickness of the stabilized base layer increases.

Table 43. Difference rates of composite k-values as thickness of base increases

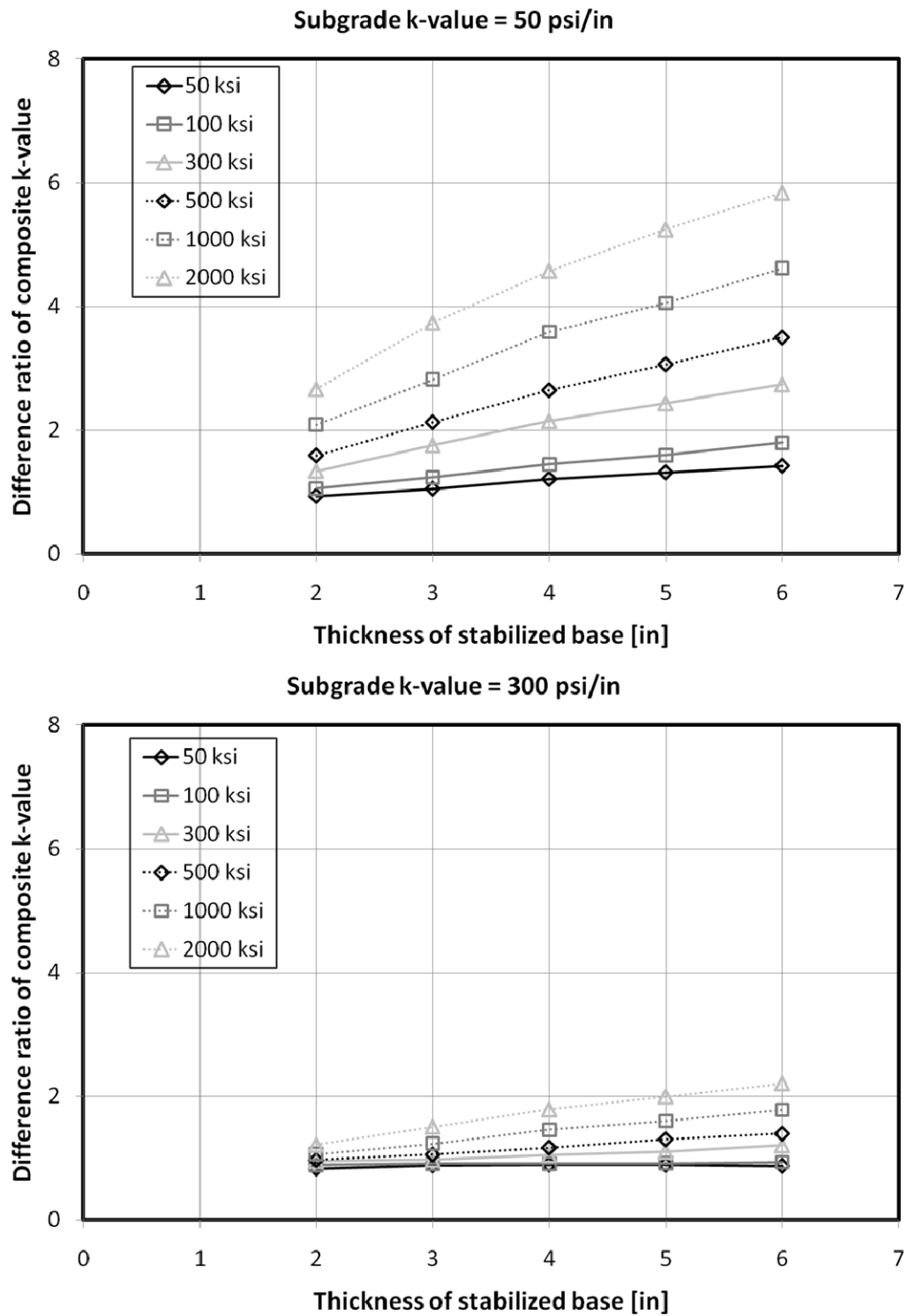| Subgrade k-value	Elastic modulus of base material	Increment rate of the discrepancy
Low	Low	**Medium**
Low	High	**Very high**
High	Low	**Very low**
High	High	**High**

Figure 67. Effects of thickness of base layer under temperature loading

7.2.1.2. Effects of Elastic Modulus of Base Material

The effects of elastic modulus of the base material on the discrepancy ratios of the two different composite k-values, directly computed composite k-value from simulation of static plate load test and back-found composite k-value corresponding to the maximum critical stress using the simple support model characterized by a single k-value, are analyzed under the nighttime nonlinear temperature loading condition. Figure 68 presents the effects of base modulus for the difference ratios of the composite k-values. Here, x-axis presents the modulus of elasticity of the base material, and y-axis shows the discrepancy ratios of the two different composite k-values. The difference ratios are increased as the elastic modulus of the stabilized base material is increasing. Table 44 addresses the increment rate of the composite k-value discrepancies under various states of subgrade k-values and base thicknesses. The difference ratios are significantly increased when the subgrade k-value is low and the base thickness is thick. On the other hands, at a condition having high subgrade k-value and thin base thickness, the difference rates are not increased as much relatively, when the elastic modulus of the stabilized base material is increasing.

Table 44. Difference rates of composite k-values as elastic modulus of base increases

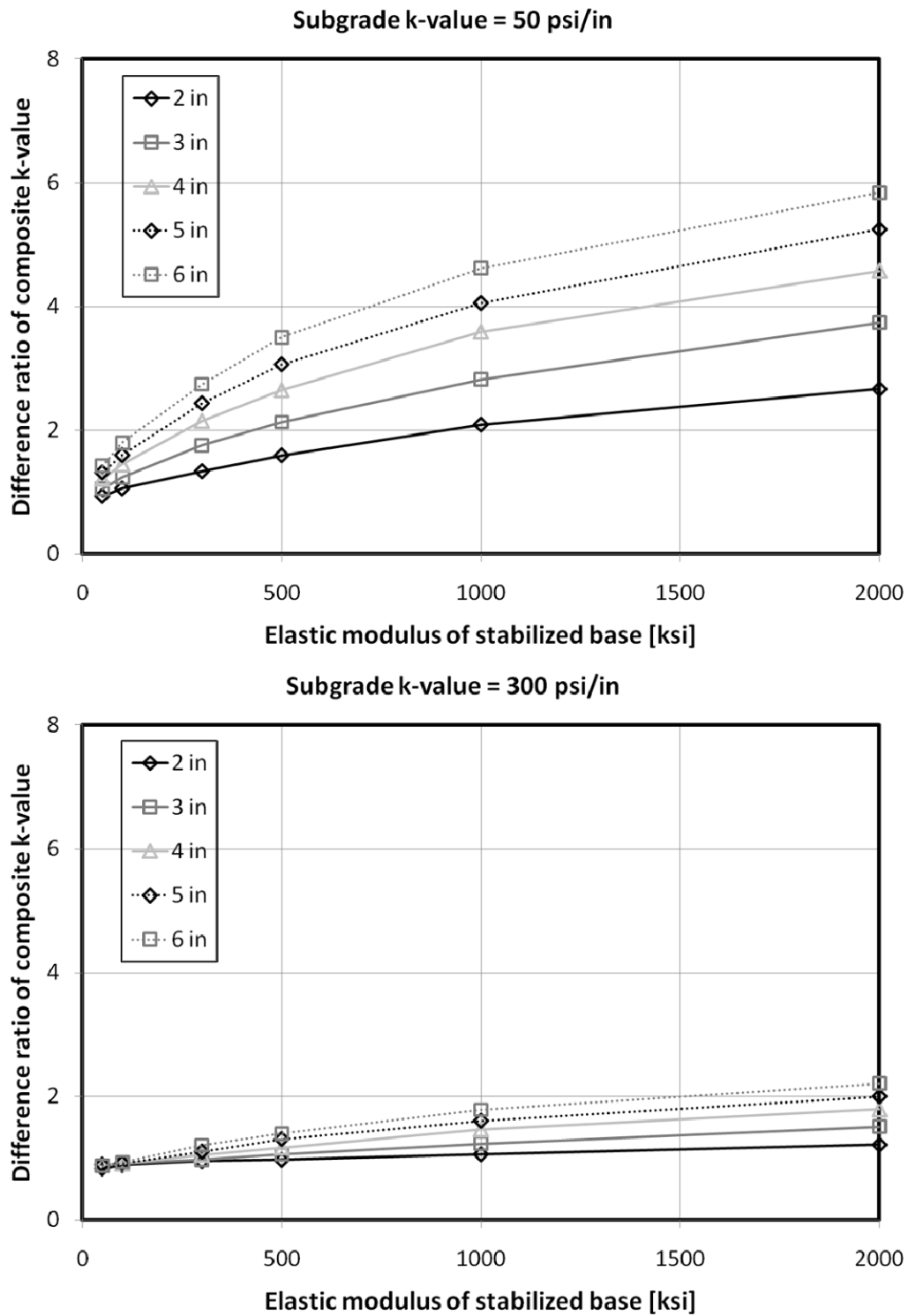| Subgrade k-value	Thickness of base layer	Increment rate of the discrepancy
Low	Low	**High**
Low	High	**Very high**
High	Low	**Medium**
High	High	**High**

159

Figure 68. Effects of elastic modulus of base material under temperature loading

7.2.1.3. Effects of *k*-value of Subgrade Layer

Effects of subgrade *k*-value on the difference ratios between the two different composite *k*-values, which are the directly computed composite *k*-value from simulation of static plate load test and the back-found composite *k*-value corresponding to the maximum longitudinal tensile stress using the simple support model characterized by a single *k*-value, are reviewed for nighttime nonlinear temperature gradient condition. Figure 69 illustrates the effects of subgrade *k*-value about difference ratios of the composite *k*-values. Here, *x*-axis means the subgrade *k*-value, and *y*-axis shows the difference ratios of the two different composite *k*-values. For this analysis, the difference rates are decreased as the subgrade *k*-value is increasing unlike the previous two cases, which are the effects of base thickness and elastic modulus. Table 45 presents the decrement rate of the composite *k*-value discrepancies. The difference ratios are significantly decreased at the conditions of high subgrade *k*-value and high elastic modulus of the base material. On the other hand, for a condition having low values of the subgrade *k*-value and the elastic modulus of the base material, the discrepancy rates are barely decreased when the subgrade *k*-value increases. Consequently, to adjust identical composite *k*-values from both of the elastic and *k*-value composite support model and the simple support model, the support condition might be composed of low levels of elastic modulus of base material and the base thickness might be used, but the values of subgrade *k*-value does not matter.

Table 45. Difference rates of composite *k*-values as subgrade *k*-value increases

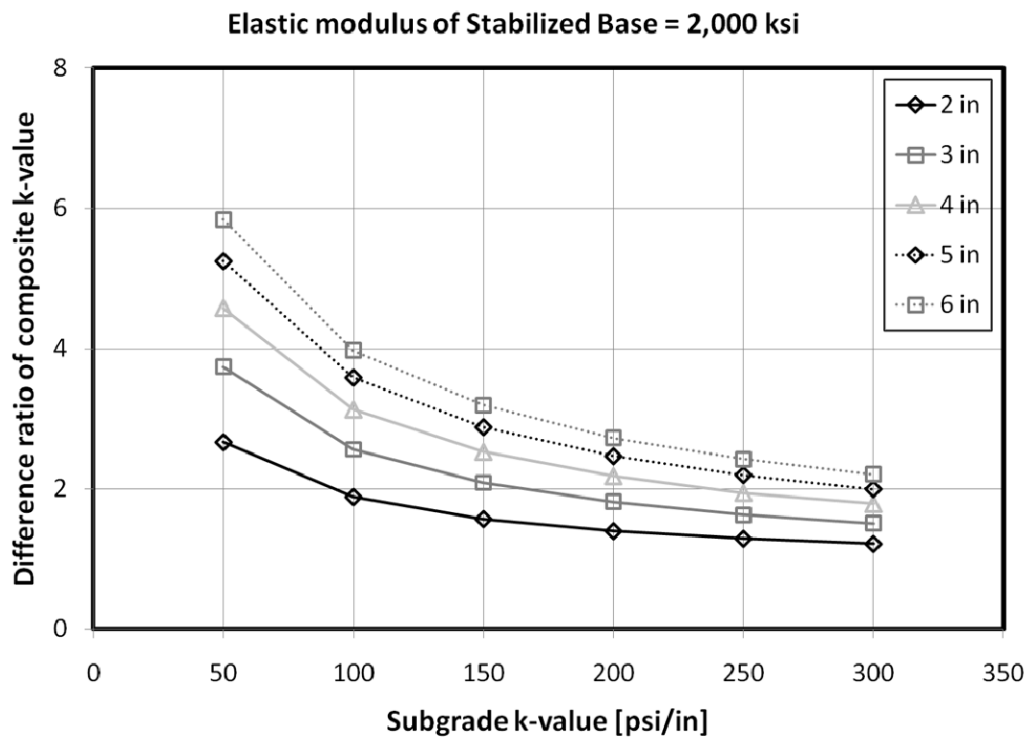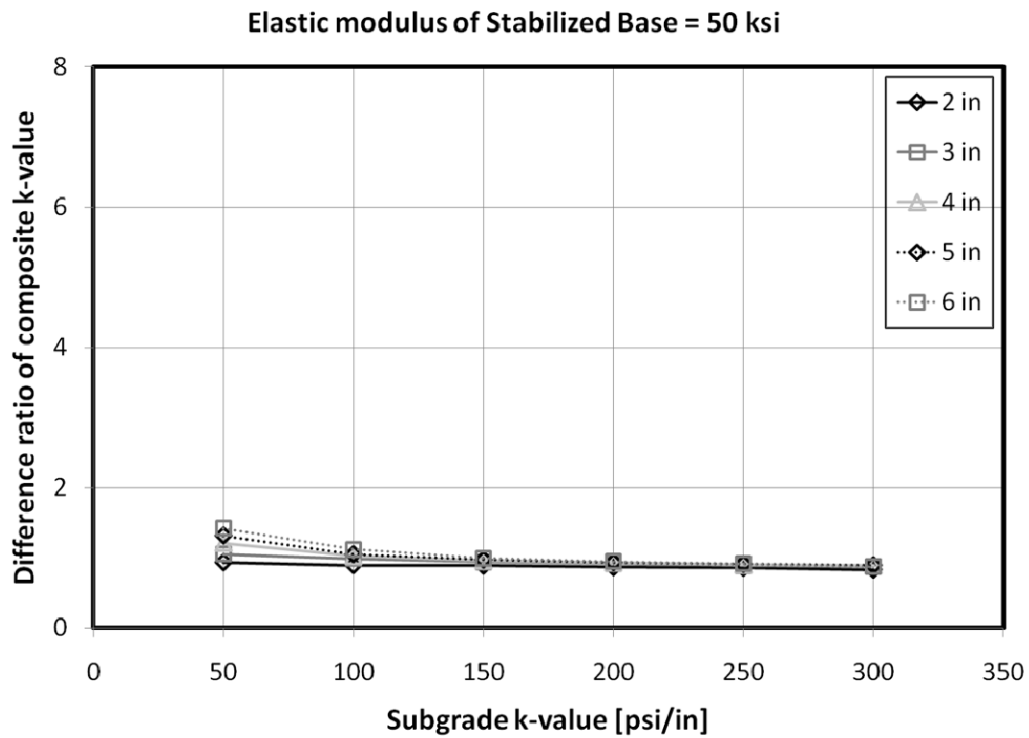| Thickness of base layer	Elastic modulus of stabilized base	Decrement rate of the discrepancy
Low	Low	**Low**
Low	High	**Medium**
High	Low	**High**
High	High	**Very high**

Figure 69. Effects of subgrade *k*-value under temperature loading

7.2.2. Wheel loading

For the vehicle wheel loading condition which is applied center of the CRCP slab, difference ratios of the composite *k*-values are also computed. Table 46 shows the difference ratios of the composite *k*-values under center loaded vehicle wheel loading condition. As same with the cases of temperature conditions, almost identical difference rates have been shown for the wheel loading condition, and the two different types of *k*-values, directly computed composite *k*-value from elastic *k*-value support model and back-found composite *k*-value corresponding maximum critical stress using the simple support model, have been generally shown almost identical when the stabilized base has low structural stiffness, thin thickness of the stabilized base layer and low elastic modulus of the base material. However, the difference ratios have been increasing as thickness of the stabilized base layer is increasing, the elastic modulus of the base material is increasing, but *k*-value of subgrade is decreasing. The effects of each support layer properties including thickness of stabilized base layer, elastic modulus of the base material, and subgrade *k*-value are discussed in depth under the center applied vehicle wheel loading.

Table 46. Difference ratios of composite *k*-values under wheel loading

Thickness of base layer [in]	Elastic modulus of base material [ksi]	Subgrade *k*-value [psi/in]					
		50	100	150	200	250	300
2	50	0.9	0.9	0.8	0.8	0.8	0.8
	100	1.1	1.0	0.9	0.9	0.9	0.8
	300	1.2	1.0	1.0	0.9	0.9	0.9
	500	1.4	1.1	1.0	1.0	0.9	0.9
	1000	1.7	1.3	1.1	1.1	1.0	1.0
	2000	2.2	1.6	1.3	1.2	1.1	1.1
3	50	1.1	1.0	0.9	0.9	0.9	0.9
	100	1.2	1.0	1.0	0.9	0.9	0.9
	300	1.5	1.2	1.0	1.0	0.9	0.9
	500	1.8	1.3	1.2	1.1	1.0	1.0
	1000	2.3	1.7	1.4	1.3	1.2	1.1
	2000	3.1	2.1	1.7	1.5	1.4	1.3
4	50	1.2	1.0	0.9	0.9	0.9	0.9
	100	1.4	1.1	1.0	0.9	0.9	0.9
	300	1.9	1.4	1.2	1.1	1.0	1.0
	500	2.3	1.6	1.3	1.2	1.1	1.1
	1000	3.0	2.1	1.7	1.5	1.4	1.3
	2000	4.0	2.8	2.2	1.9	1.7	1.6
5	50	1.2	1.0	1.0	0.9	0.9	0.9
	100	1.5	1.2	1.0	1.0	0.9	0.9
	300	2.2	1.5	1.3	1.2	1.1	1.0
	500	2.7	1.9	1.6	1.4	1.2	1.2
	1000	3.6	2.5	2.0	1.8	1.6	1.5
	2000	4.8	3.3	2.7	2.3	2.0	1.9
6	50	1.3	1.1	1.0	0.9	0.9	0.9
	100	1.7	1.2	1.1	1.0	0.9	0.9
	300	2.5	1.7	1.5	1.3	1.2	1.1
	500	3.1	2.2	1.8	1.6	1.4	1.3
	1000	4.2	2.9	2.3	2.0	1.8	1.7
	2000	5.7	3.9	3.1	2.7	2.4	2.2

7.2.2.1. Effects of Thickness of Stabilized Base Layer

For the vehicle wheel loading condition, the effects of base thickness on difference ratios between the two different composite *k*-values, directly computed composite *k*-value from simulation of static plate load test and back-found composite *k*-value corresponding to the maximum critical stress using the simple support model characterized by a single *k*-value, are discussed. Figure 70 presents the effects of thickness of the stabilized base layer on discrepancy ratios of the two different composite *k*-values. The discrepancy rates are increased as the thickness of stabilized base layer is increasing. This trend is very similar with the case for the nighttime nonlinear temperature loading condition. Table 47 addresses the increment rates of the difference of the two composite *k*-values. Same with the temperature loading case, the difference ratios are significantly increased as the subgrade *k*-value is low and elastic modulus of the base material is high. On the other hands, at a condition having high subgrade *k*-value and low elastic modulus of base material, the difference rates are rarely increased when the base thickness increases. These responses are almost identical with the results for the temperature loading condition.

Table 47. Difference rates of composite *k*-values as thickness of base increases

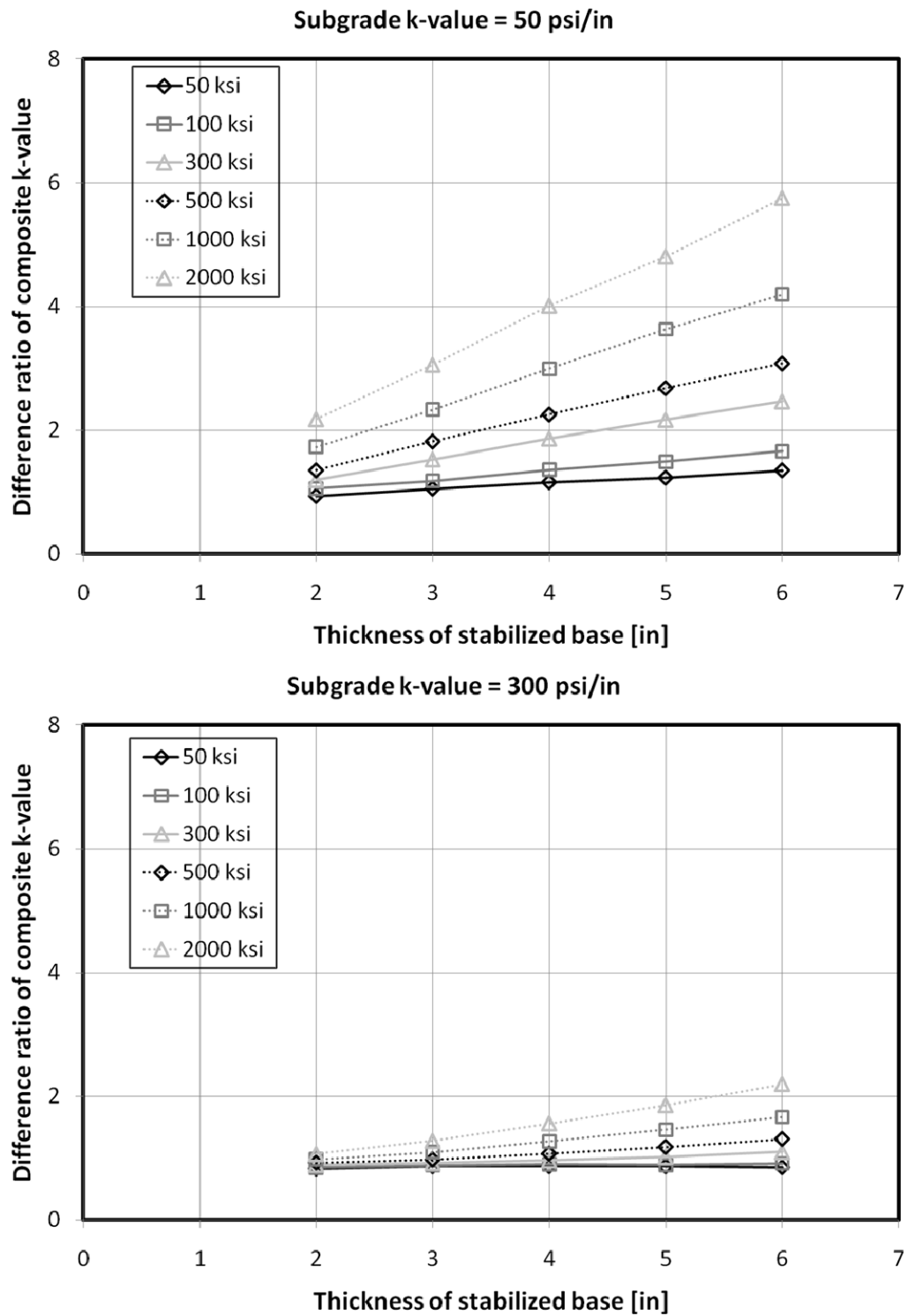| Subgrade *k*-value	Elastic modulus of base material	Increment rate of the discrepancy
Low	Low	**Medium**
Low	High	**Very high**
High	Low	**Very low**
High	High	**High**

Figure 70. Effects of thickness of base layer under wheel loading

7.2.2.2. Effects of Elastic Modulus of Base Material

Additionally, effects of elastic modulus of the base material on the discrepancy ratios of the two different composite k-values are also analyzed under the center loaded vehicle wheel loading condition. Figure 71 shows the effects of the base elastic modulus for the difference rates of the composite k-values. Here, x-axis is the modulus of elasticity of the base material, and y-axis is the difference ratios of the two composite k-values. For this analysis, the difference ratios are increased as the elastic modulus of the stabilized base material is increasing as same as the temperature loading condition. Table 48 presents the increment rate of the discrepancy of the two different composite k-values under diverse conditions of subgrade k-value and base thickness. The trends of difference ratio variations are almost identical with cases under the nighttime temperature gradient condition. For a support condition having low level of subgrade k-value and thick base thickness, increment rate of the composite k-value difference is very high as the elastic modulus of base material increases. On the other hands, the variation rates are relatively unchanged as the base modulus is increasing under high subgrade and thin base thickness support conditions.

Table 48. Difference rates of composite k-values as elastic modulus of base increases

Subgrade k-value	Thickness of base layer	Increment rate of the discrepancy
Low	Low	**High**
Low	High	**Very high**
High	Low	**Medium**
High	High	**High**

Figure 71. Effects of elastic modulus of base material under wheel loading
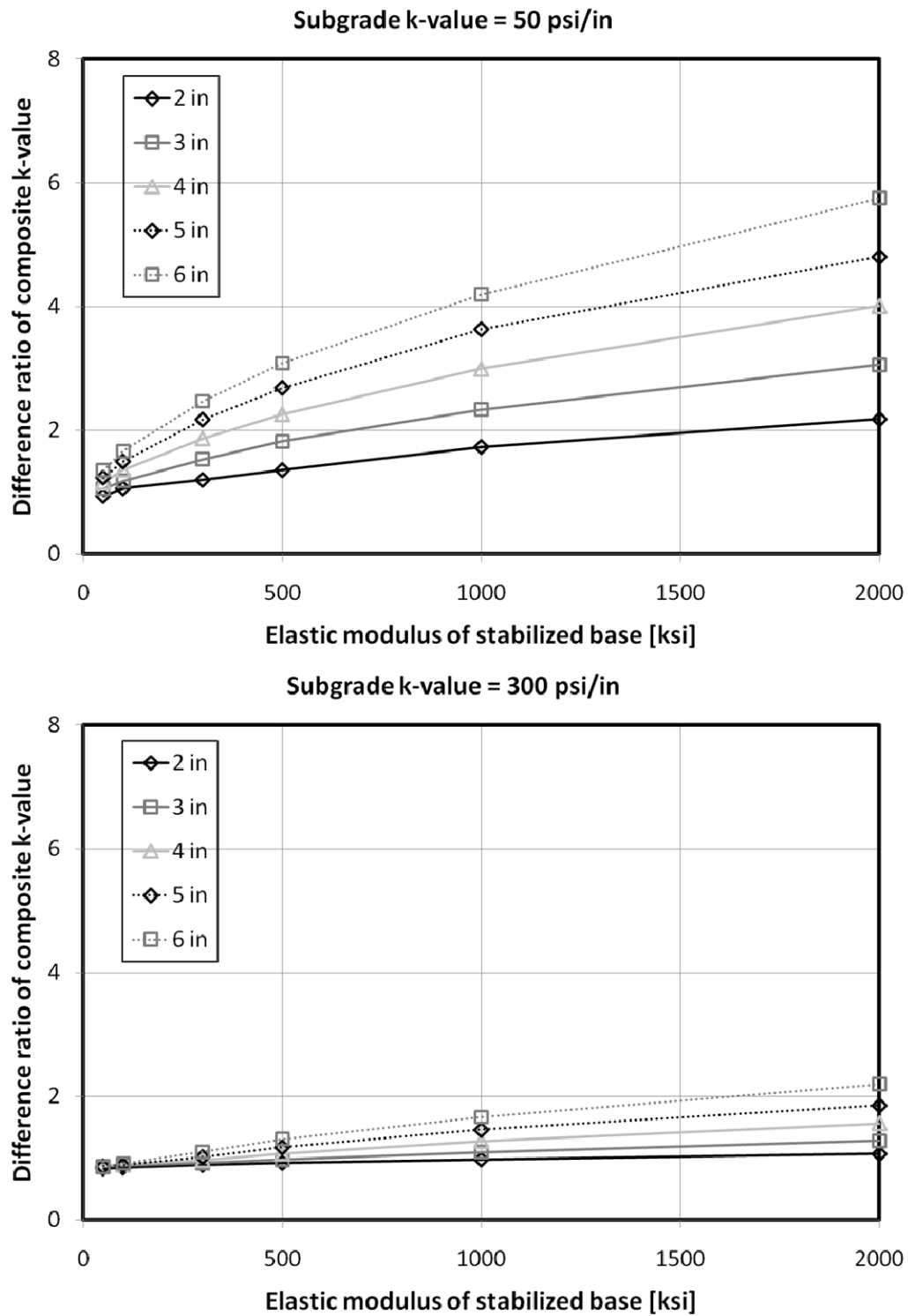
7.2.2.3. Effects of *k*-value of Subgrade Layer

For the effects of *k*-value of subgrade layer under vehicle wheel loading condition applied at the CRCP slab center, the differences between the directly computed and back-found composite *k*-values are decreased as the subgrade *k*-value increases as same as the temperature loading cases. Figure 72 presents the effects of subgrade *k*-value concerning the changing of differences between the two types of composite *k*-values. Here, *x*-axis is subgrade *k*-value and *y*-axis represents the difference ratio of the two composite *k*-values. Table 49 shows the summary of the decrement rates of the composite *k*-value discrepancies under various conditions of the base thickness and the base material elastic modulus. In the same manner with the temperature loading condition, higher structural rigidity of the base layer, thick base thickness and high elastic modulus of the base material makes the decrement rate highly, but lower rigidity of the stabilized base layer produces low decrement rate of the discrepancy of the two different composite *k*-values of directly computed from elastic *k*-value composite support model and stress corresponding *k*-value from simplified support model. These results are also identical with responses under temperature loading condition.

Table 49. Difference rates of composite *k*-values as subgrade *k*-value increases

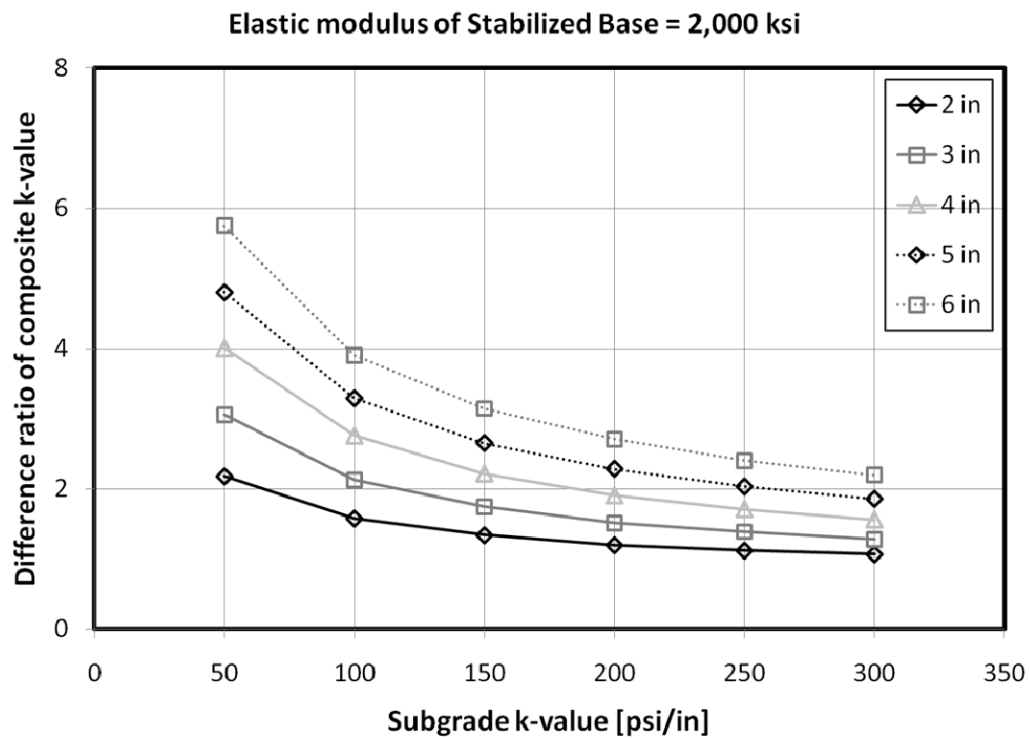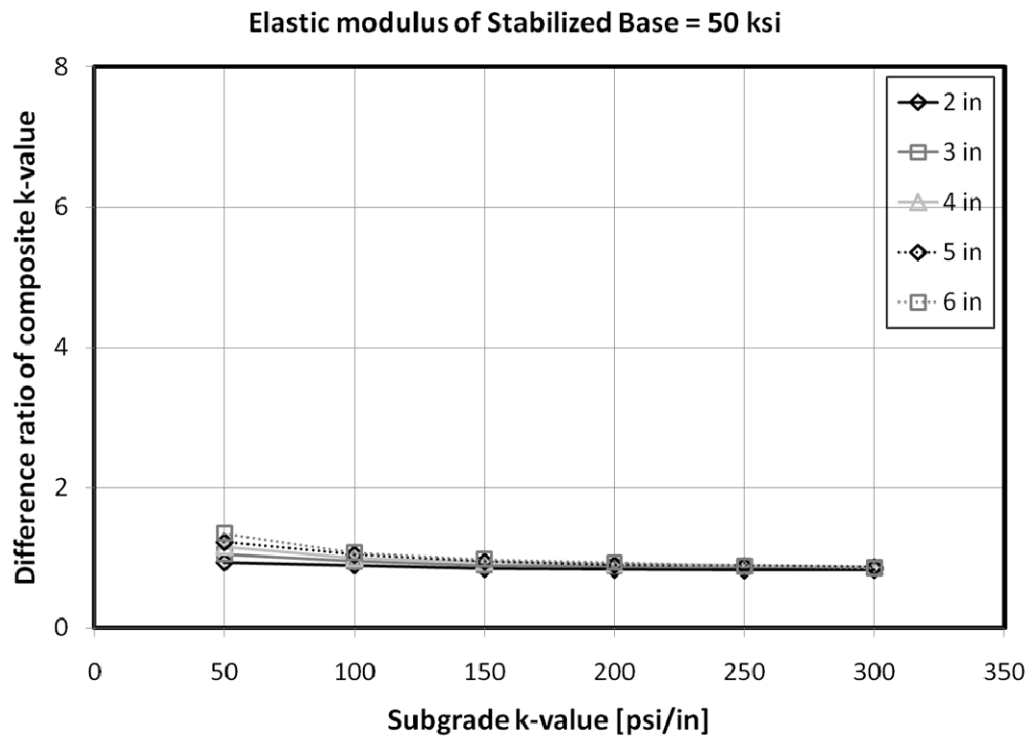| Thickness of base layer	Elastic modulus of base material	**Decrement rate of the discrepancy**
Low	Low	**Low**
Low	High	**Medium**
High	Low	**High**
High	High	**Very high**

Figure 72. Effects of subgrade *k*-value under wheel loading

7.3. SUMMARY

In chapter 4, composite *k*-values were directly computed using elastic and *k*-value composite support model. However, the simple support model has been widely adopted in currently used rigid pavement design guide, which have been identified by a single spring coefficient representing all support layers such as base and subgrade. Thus, it is needed to verify whether the two different support models could estimate identical responses on the CRCP slab on the same support conditions or not.

For this reason, composite *k*-values of the simplified support model are back-found as stress aspect. Using the elastic and *k*-value composite support model, the maximum longitudinal tensile stresses in the CRCP slab are calculated, and corresponding composite *k*-values which could induce the critical stress are back-found by adjusting the spring coefficient, *k*, using the simple support model under the both of temperature and vehicle wheel loadings.

For the temperature and vehicle wheel loadings, the back-found composite *k*-values corresponding to the maximum critical stresses are increased as the values of the support layer properties increase. The back-found composite *k*-values are relatively larger than the directly computed composite *k*-value.

Finally, the back-found *k*-values are compared with the directly obtained composite *k*-values by simulation of the *k*-value test. The comparisons have been expressed by difference ratios. For both of the temperature and wheel loading conditions, it has been shown the identical discrepancies between the two different composite *k*-value. Due to increase of base modulus and thickness, the difference ratios are increased. On the other hands, the difference rates are decreased as the base properties increases. Consequently, higher level of structural rigidity of stabilized base layer produces larger difference ratio between the two different composite *k*-values of directly computed from elastic and *k*-value composite support model and the stress corresponding composite *k*-value from simplified support model, but the subgrade *k*-value does not affect to the variations of the composite *k*-values as much.

CHAPTER 8: OPTIMUM COMBINATION OF CRCP STRUCTURES

CRCP structures have endured numerous repetitive loadings including passing vehicle loading and daily cyclic temperature loading, during its lifespan. Due to these loadings, stresses have been induced in the CRCP slab every time the loads are applied. Finally, the CRCP structures get failure because of these repetitive stresses. For this reason, controlling the stress level of the CRCP structure is significant for the pavement design. Accordingly, effects of the CRCP properties are evaluated on the maximum critical stress, and the method determining optimum combinations of CRCP structures is developed as aspect of stress level induced in the CRCP slab in this chapter.

8.1. EVALUATION OF CRCP BEHAVIOR AND PERFORMANCE

Performance of CRCP structures have been evaluated by total stress at critical point due to loadings and number of the load applications. For example, a punchout, which has been treated as a typical distress type of CRCP structure, could be estimated by the following mechanism [NCHRP, 2004]. A number of punchout per mile (PO) could be computed by equation 8.1. Here, $a, b,$ and c is calibration constants, and D is accumulated fatigue damage. The damage (D) is defined as equation 8.2. Here, n is the number of load applications, and N is number of allowable load applications. Also, N could be estimated by equation 8.3. Here, the number of allowable load applications (N) is function of PCC modulus of rupture (MR) and total bending stress at critical point (σ_{tot}).

$$PO = \sum \frac{a}{1+b \cdot D^c} \tag{8.1}$$

$$D = \sum \frac{n}{N} \tag{8.2}$$

172

$$Log\ N = 2.2 \times \left(\frac{MR}{\sigma_{tot}}\right)^{1.22} + a \qquad (8.3)$$

Accordingly, the total bending stress must be one of the most important factors for the rigid pavement design. For this reason, maximum tensile stress has been adopted as a criterion for selection of optimum compositions of CRCP structures in this study.

8.2. EFFECTS OF PROPERTIES COMPOSING CRCP STRUCTURE ON MAXIMUM STRESS IN THE CRCP SLAB

To find the optimum combination of CRCP structure, thickness of CRCP slab, thickness of base layer, elastic modulus of the base material, and subgrade k-value are selected as independent variables affecting the level of stress in the CRCP slab. Table 50 shows the properties of the CRCP structure and those values which are used in this study. All combinations of the variables bring 900 cases of CRCP composition. On these various CRCP compositions, nighttime temperature gradient condition and wheel loading condition applied at center of the CRCP slab are considered to estimate the maximum longitudinal tensile stresses in the CRCP slab as changing values of the CRCP structural and material properties.

Table 50. Independent variables and values for CRCP structures

Variables	Values
Thickness of CRCP slab [in]	6, 8, 10, 12, 14
Thickness of stabilized base [in]	2, 3, 4, 5, 6
Elastic modulus of stabilized base [ksi]	50, 100, 300, 500, 1000, 2000
Subgrade k-value [psi/in]	50, 100, 150, 200, 250, 300

In real condition, the temperature loading and vehicle wheel loading are simultaneously applied on the CRCP structures. So, the most critical loading condition, combining nighttime temperature gradient and wheel loading applied on transverse crack, are considered, which could induce the maximum longitudinal tensile stress at center of the CRCP slab. Figure 73 illustrates the combined loading condition.
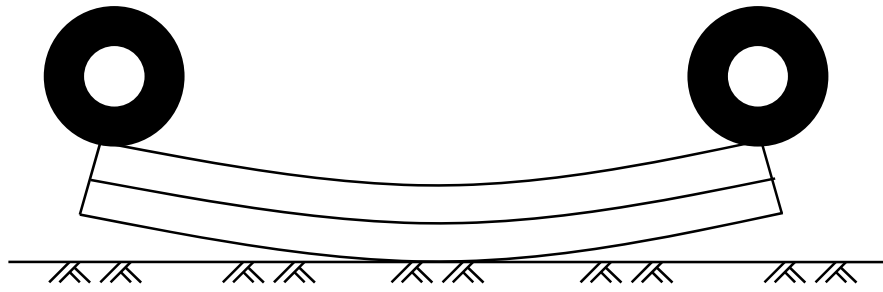
174

Figure 73. Combined loading condition inducing maximum critical stress

For the three loading cases, the effects of the properties composing CRCP structure are evaluated. Also, the optimum combinations of the properties are suggested when allowable stress is decided for the rigid pavement design.

8.2.1. Temperature Loading

Nighttime temperature gradient condition is applied through different CRCP slab depth, and the maximum critical stresses are computed using FE analysis. Table 51 to Table 55 shows the estimated maximum critical stress under various support conditions for the different slab thickness 6 to 14 in with 2-in increment, respectively.

For the 6 in of CRCP slab, range of the computed maximum critical stresses is from 85.2 psi to 153.5 psi under the various support combinations. The variation is 68.3 psi. For the 8 in of CRCP slab, the range of the stresses is from 73.0 to 136.1 psi. The variation is 63.1 psi. For the 10 in of CRCP slab, range of the maximum critical stresses is 66.2 to 116.8 psi and the variation is 50.6 psi. For the 12 in of CRCP slab, the range of the maximum stresses is 61.7 to 99.8 psi and the variation is 38.1 psi. Finally, for the 14 in of CRCP slab, the range of the estimated critical stresses is from 58.4 to 86.5 psi, and the variation is 28.1 psi.

Generally, the maximum critical stress is mainly decreased as the slab thickness increase although the stresses are increasing as the support system is strong under temperature loading. Also, the stress variation between on the weakest support and strongest support condition is reduced as the CRCP slab is thickened.

175

Table 51. Maximum critical stresses due to temperature loading [H = 6 in]

Thickness of base layer [in]	Elastic modulus of base material [ksi]	Subgrade *k*-value [psi/in]					
		50	100	150	200	250	300
2	50	85.2	89.6	93.7	97.4	100.8	104.0
	100	86.3	90.7	94.6	98.3	101.7	104.9
	300	90.1	94.1	97.9	101.3	104.5	107.5
	500	93.3	97.1	100.6	103.9	106.9	109.7
	1000	99.8	103.1	106.2	109.0	111.7	114.1
	2000	108.9	111.5	114.0	116.3	118.4	120.5
3	50	86.9	91.2	95.1	98.7	102.0	105.0
	100	89.3	93.4	97.1	100.6	103.8	106.8
	300	97.0	100.5	103.7	106.7	109.5	112.1
	500	103.0	106.0	108.8	111.5	113.9	116.2
	1000	113.6	115.9	118.0	120.1	122.0	123.8
	2000	125.7	127.3	128.8	130.1	131.5	132.7
4	50	89.2	93.2	96.9	100.3	103.4	106.3
	100	93.0	96.8	100.2	103.4	106.4	109.2
	300	104.8	107.7	110.4	112.9	115.2	117.4
	500	113.0	115.3	117.5	119.5	121.5	123.3
	1000	125.8	127.3	128.7	130.1	131.4	132.6
	2000	138.1	139.0	139.8	140.6	141.4	142.1
5	50	91.8	95.6	99.0	102.2	105.2	107.9
	100	97.3	100.7	103.8	106.8	109.5	112.0
	300	112.7	115.0	117.2	119.2	121.1	122.9
	500	122.3	124.0	125.6	127.1	128.5	129.9
	1000	135.4	136.4	137.3	138.2	139.1	139.9
	2000	146.5	147.0	147.5	147.9	148.4	148.8
6	50	94.7	98.2	101.5	104.4	107.2	109.8
	100	101.9	104.9	107.7	110.3	112.8	115.0
	300	120.2	122.0	123.7	125.3	126.8	128.3
	500	130.2	131.4	132.6	133.7	134.8	135.8
	1000	142.7	143.4	144.0	144.6	145.1	145.7
	2000	152.2	152.5	152.8	153.0	153.3	153.5

Table 52. Maximum critical stresses due to temperature loading [H = 8 in]

Thickness of base layer [in]	Elastic modulus of base material [ksi]	Subgrade *k*-value [psi/in]					
		50	100	150	200	250	300
2	50	73.0	75.3	77.5	79.6	81.6	83.5
	100	73.6	75.9	78.0	80.1	82.1	84.1
	300	75.6	77.8	79.9	81.9	83.9	85.8
	500	77.4	79.5	81.6	83.5	85.4	87.3
	1000	81.2	83.2	85.1	87.0	88.7	90.5
	2000	87.3	89.0	90.7	92.3	93.9	95.5
3	50	73.9	76.2	78.3	80.3	82.3	84.2
	100	75.2	77.4	79.5	81.5	83.5	85.3
	300	79.6	81.6	83.5	85.4	87.3	89.0
	500	83.3	85.2	87.0	88.8	90.5	92.1
	1000	90.8	92.5	94.0	95.5	97.0	98.4
	2000	101.2	102.5	103.8	105.0	106.1	107.3
4	50	75.2	77.3	79.4	81.4	83.3	85.1
	100	77.3	79.4	81.4	83.4	85.2	87.0
	300	84.6	86.4	88.2	89.9	91.5	93.1
	500	90.4	92.1	93.6	95.2	96.6	98.1
	1000	101.3	102.6	103.8	105.0	106.1	107.3
	2000	114.5	115.4	116.2	117.0	117.9	118.6
5	50	76.6	78.7	80.7	82.6	84.4	86.2
	100	79.8	81.8	83.7	85.6	87.3	89.0
	300	90.3	91.9	93.5	95.0	96.4	97.8
	500	98.1	99.5	100.8	102.0	103.3	104.5
	1000	111.3	112.3	113.2	114.1	115.0	115.8
	2000	125.6	126.1	126.7	127.3	127.8	128.3
6	50	78.3	80.3	82.2	84.1	85.8	87.5
	100	82.7	84.6	86.4	88.1	89.8	91.4
	300	96.3	97.7	99.0	100.3	101.6	102.8
	500	105.7	106.8	107.9	108.9	109.9	110.9
	1000	120.3	121.0	121.6	122.3	123.0	123.6
	2000	134.3	134.7	135.0	135.4	135.8	136.1

Table 53. Maximum critical stresses due to temperature loading [H = 10 in]

Thickness of base layer [in]	Elastic modulus of base material [ksi]	Subgrade *k*-value [psi/in]					
		50	100	150	200	250	300
2	50	66.2	67.4	68.7	69.9	71.1	72.2
	100	66.5	67.8	69.0	70.2	71.4	72.6
	300	67.6	68.9	70.1	71.3	72.5	73.6
	500	68.6	69.9	71.1	72.2	73.4	74.5
	1000	70.9	72.0	73.2	74.3	75.4	76.5
	2000	74.5	75.6	76.7	77.8	78.8	79.9
3	50	66.7	68.0	69.2	70.4	71.5	72.6
	100	67.4	68.7	69.9	71.1	72.2	73.3
	300	69.9	71.1	72.3	73.4	74.5	75.6
	500	72.1	73.3	74.4	75.5	76.6	77.7
	1000	76.9	77.9	79.0	80.0	81.0	82.0
	2000	84.2	85.1	86.0	86.9	87.7	88.6
4	50	67.4	68.6	69.8	71.0	72.1	73.2
	100	68.6	69.8	71.0	72.2	73.3	74.4
	300	72.9	74.1	75.2	76.3	77.3	78.4
	500	76.7	77.7	78.8	79.8	80.8	81.7
	1000	84.3	85.2	86.1	87.0	87.8	88.7
	2000	95.0	95.7	96.4	97.1	97.7	98.4
5	50	68.3	69.4	70.6	71.7	72.8	73.9
	100	70.1	71.3	72.4	73.6	74.6	75.7
	300	76.6	77.6	78.7	79.7	80.7	81.6
	500	82.0	82.9	83.8	84.7	85.6	86.5
	1000	92.3	93.0	93.8	94.5	95.2	95.9
	2000	105.4	106.0	106.5	107.0	107.5	108.0
6	50	69.2	70.4	71.5	72.6	73.7	74.7
	100	71.9	73.0	74.1	75.2	76.2	77.2
	300	80.7	81.7	82.6	83.5	84.4	85.3
	500	87.7	88.5	89.3	90.1	90.9	91.7
	1000	100.2	100.9	101.5	102.0	102.6	103.2
	2000	114.9	115.3	115.7	116.0	116.4	116.8

Table 54. Maximum critical stresses due to temperature loading [H = 12 in]

Thickness of base layer [in]	Elastic modulus of base material [ksi]	Subgrade *k*-value [psi/in]					
		50	100	150	200	250	300
2	50	61.7	62.4	63.2	63.9	64.7	65.4
	100	61.9	62.6	63.4	64.1	64.9	65.6
	300	62.5	63.3	64.1	64.8	65.5	66.2
	500	63.1	63.9	64.6	65.4	66.1	66.8
	1000	64.5	65.2	66.0	66.7	67.4	68.1
	2000	66.8	67.5	68.2	68.9	69.6	70.2
3	50	62.0	62.8	63.5	64.2	64.9	65.7
	100	62.4	63.2	63.9	64.7	65.4	66.1
	300	63.9	64.7	65.4	66.1	66.8	67.5
	500	65.3	66.0	66.7	67.4	68.1	68.8
	1000	68.3	69.0	69.7	70.4	71.0	71.7
	2000	73.2	73.8	74.5	75.1	75.7	76.3
4	50	62.4	63.2	63.9	64.6	65.3	66.0
	100	63.2	63.9	64.6	65.4	66.1	66.8
	300	65.8	66.5	67.2	67.9	68.6	69.3
	500	68.2	68.9	69.6	70.2	70.9	71.6
	1000	73.3	73.9	74.5	75.2	75.8	76.4
	2000	81.1	81.6	82.2	82.7	83.2	83.7
5	50	62.9	63.7	64.4	65.1	65.8	66.5
	100	64.1	64.8	65.5	66.2	66.9	67.6
	300	68.2	68.9	69.5	70.2	70.8	71.5
	500	71.7	72.4	73.0	73.6	74.3	74.9
	1000	79.1	79.6	80.2	80.7	81.3	81.8
	2000	89.6	90.0	90.5	90.9	91.3	91.7
6	50	63.6	64.3	65.0	65.7	66.3	67.0
	100	65.2	65.9	66.6	67.3	67.9	68.6
	300	70.9	71.6	72.2	72.8	73.4	74.0
	500	75.8	76.4	76.9	77.5	78.1	78.6
	1000	85.3	85.8	86.3	86.7	87.2	87.7
	2000	98.1	98.4	98.8	99.1	99.4	99.8

Table 55. Maximum critical stresses due to temperature loading [H = 14 in]

Thickness of base layer [in]	Elastic modulus of base material [ksi]	Subgrade *k*-value [psi/in]					
		50	100	150	200	250	300
2	50	58.4	58.9	59.4	59.9	60.4	60.8
	100	58.5	59.0	59.5	60.0	60.5	61.0
	300	59.0	59.5	60.0	60.4	60.9	61.4
	500	59.4	59.9	60.3	60.8	61.3	61.8
	1000	60.2	60.7	61.2	61.7	62.1	62.6
	2000	61.7	62.2	62.7	63.1	63.6	64.0
3	50	58.6	59.1	59.6	60.1	60.6	61.0
	100	58.9	59.4	59.9	60.4	60.8	61.3
	300	59.9	60.4	60.8	61.3	61.8	62.3
	500	60.8	61.2	61.7	62.2	62.7	63.1
	1000	62.7	63.2	63.7	64.1	64.6	65.0
	2000	66.0	66.5	66.9	67.3	67.8	68.2
4	50	58.9	59.4	59.9	60.3	60.8	61.3
	100	59.4	59.9	60.4	60.8	61.3	61.8
	300	61.1	61.6	62.1	62.5	63.0	63.4
	500	62.7	63.1	63.6	64.1	64.5	64.9
	1000	66.1	66.6	67.0	67.4	67.8	68.3
	2000	71.7	72.1	72.5	72.8	73.2	73.6
5	50	59.3	59.7	60.2	60.7	61.1	61.6
	100	60.0	60.5	60.9	61.4	61.9	62.3
	300	62.7	63.1	63.6	64.0	64.5	64.9
	500	65.1	65.5	66.0	66.4	66.8	67.2
	1000	70.2	70.6	71.0	71.4	71.8	72.2
	2000	78.2	78.5	78.8	79.2	79.5	79.8
6	50	59.7	60.1	60.6	61.0	61.5	61.9
	100	60.7	61.2	61.6	62.1	62.5	63.0
	300	64.5	65.0	65.4	65.8	66.3	66.7
	500	67.9	68.3	68.7	69.1	69.5	69.9
	1000	74.9	75.2	75.6	76.0	76.3	76.7
	2000	85.1	85.4	85.7	85.9	86.2	86.5

8.2.2. Vehicle Wheel Loading

Vehicle wheel loading is applied at the center of the CRCP slab, which means between two adjacent transverse cracks for the different CRCP slab thickness. The maximum critical stresses are also estimated using FE analysis. Table 56 to Table 60 presents the computed maximum critical stress under various support conditions for the different slab thickness 6 to 14 in with 2-in increment, respectively.

For the 6 in of CRCP slab, range of the computed maximum critical stresses is from 240.1 psi to 100.7 psi under the various support combinations. The variation is 139.4 psi. For the 8 in of CRCP slab, the range of the stresses is from 143.1 to 80.3 psi. The variation is 62.8 psi. For the 10 in of CRCP slab, range of the maximum critical stresses is 93.5 to 62.7 psi, and the variation is 30.8 psi. For the 12 in of CRCP slab, the range of the maximum stresses is 65.3 to 49.1 psi, and the variation is 16.2 psi. Finally, for the 14 in of CRCP slab, the range of the estimated critical stresses is from 47.8 to 38.8 psi, and the variation is 9.0 psi.

For the vehicle wheel loading condition, the maximum critical stress is significantly decreased as the slab thickness increase compared with the cases of temperature loading condition. As a matter of fact, the stresses are decreased as the support system stiffens under vehicle wheel loading. Also, the stress variation between the weakest support and strongest support condition is more largely reduced as the CRCP slab is thickened than for the temperature loading cases.

Table 56. Maximum critical stresses due to wheel loading [H = 6 in]

Thickness of base layer [in]	Elastic modulus of base material [ksi]	Subgrade *k*-value [psi/in]					
		50	100	150	200	250	300
2	50	240.1	232.8	226.1	219.9	214.1	208.8
	100	238.7	231.4	224.8	218.6	212.9	207.6
	300	234.1	227.2	220.9	215.0	209.5	204.4
	500	230.2	223.7	217.6	212.0	206.7	201.8
	1000	222.2	216.3	210.8	205.7	200.9	196.4
	2000	210.5	205.4	200.7	196.3	192.1	188.2
3	50	237.5	230.5	224.0	218.0	212.4	207.3
	100	234.5	227.7	221.3	215.4	210.0	204.9
	300	224.8	218.7	213.0	207.7	202.8	198.2
	500	216.9	211.4	206.3	201.4	196.9	192.7
	1000	202.1	197.6	193.4	189.4	185.6	182.0
	2000	182.6	179.2	175.9	172.9	169.9	167.1
4	50	234.2	227.5	221.2	215.5	210.2	205.2
	100	229.1	222.7	216.7	211.2	206.1	201.4
	300	213.1	207.8	202.9	198.3	194.0	190.0
	500	201.1	196.7	192.5	188.5	184.8	181.3
	1000	180.2	176.9	173.7	170.7	167.9	165.2
	2000	154.4	152.1	150.0	148.0	146.0	144.1
5	50	230.2	223.8	217.9	212.4	207.4	202.7
	100	222.5	216.6	211.2	206.1	201.3	196.9
	300	199.9	195.5	191.4	187.5	183.8	180.4
	500	184.2	180.7	177.4	174.2	171.2	168.4
	1000	158.2	155.8	153.6	151.4	149.3	147.4
	2000	127.9	126.5	125.1	123.8	122.6	121.4
6	50	225.5	219.5	214.0	208.9	204.1	199.7
	100	215.0	209.7	204.7	200.1	195.8	191.7
	300	186.0	182.4	179.0	175.8	172.7	169.8
	500	167.1	164.4	161.9	159.4	157.0	154.8
	1000	137.3	135.7	134.1	132.6	131.1	129.7
	2000	104.8	103.9	103.1	102.3	101.5	100.7

Table 57. Maximum critical stresses due to wheel loading [H = 8 in]

Thickness of base layer [in]	Elastic modulus of base material [ksi]	Subgrade *k*-value [psi/in]					
		50	100	150	200	250	300
2	50	143.1	141.0	139.0	137.0	135.2	133.4
	100	142.6	140.5	138.5	136.6	134.7	132.9
	300	141.2	139.1	137.2	135.3	133.5	131.7
	500	139.9	137.9	136.0	134.2	132.4	130.7
	1000	137.2	135.3	133.5	131.8	130.1	128.4
	2000	132.9	131.2	129.5	127.9	126.3	124.8
3	50	142.3	140.2	138.2	136.4	134.5	132.8
	100	141.3	139.3	137.3	135.4	133.6	131.9
	300	138.2	136.2	134.4	132.6	130.9	129.2
	500	135.4	133.6	131.8	130.1	128.5	126.9
	1000	129.7	128.1	126.6	125.0	123.6	122.2
	2000	121.3	120.0	118.7	117.4	116.2	115.0
4	50	141.2	139.2	137.3	135.5	133.7	132.0
	100	139.6	137.6	135.7	133.9	132.2	130.5
	300	134.1	132.3	130.6	129.0	127.4	125.8
	500	129.5	127.9	126.4	124.9	123.4	122.0
	1000	120.6	119.3	118.0	116.7	115.5	114.3
	2000	108.4	107.4	106.4	105.4	104.5	103.6
5	50	139.9	138.0	136.1	134.4	132.7	131.0
	100	137.4	135.6	133.8	132.0	130.4	128.8
	300	129.2	127.6	126.1	124.6	123.1	121.7
	500	122.7	121.3	119.9	118.6	117.4	116.1
	1000	110.6	109.6	108.5	107.6	106.6	105.6
	2000	95.2	94.5	93.8	93.1	92.5	91.8
6	50	138.4	136.6	134.8	133.1	131.4	129.9
	100	134.9	133.1	131.4	129.8	128.2	126.7
	300	123.7	122.3	120.9	119.6	118.3	117.0
	500	115.2	114.1	112.9	111.8	110.8	109.7
	1000	100.5	99.7	98.9	98.1	97.3	96.6
	2000	82.7	82.2	81.7	81.3	80.8	80.3

Table 58. Maximum critical stresses due to wheel loading [H = 10 in]

Thickness of base layer [in]	Elastic modulus of base material [ksi]	Subgrade *k*-value [psi/in]					
		50	100	150	200	250	300
2	50	93.5	92.7	92.0	91.3	90.6	89.9
	100	93.3	92.5	91.8	91.1	90.4	89.7
	300	92.8	92.0	91.3	90.6	89.8	89.2
	500	92.3	91.5	90.8	90.1	89.4	88.7
	1000	91.2	90.5	89.8	89.1	88.4	87.8
	2000	89.5	88.8	88.1	87.5	86.8	86.2
3	50	93.2	92.4	91.7	91.0	90.3	89.6
	100	92.8	92.1	91.3	90.6	89.9	89.2
	300	91.6	90.9	90.2	89.5	88.8	88.1
	500	90.5	89.8	89.1	88.4	87.8	87.1
	1000	88.2	87.5	86.9	86.2	85.6	85.0
	2000	84.4	83.8	83.2	82.7	82.1	81.6
4	50	92.8	92.0	91.3	90.6	89.9	89.3
	100	92.1	91.4	90.7	90.0	89.3	88.6
	300	90.0	89.3	88.6	87.9	87.3	86.7
	500	88.1	87.4	86.8	86.2	85.5	84.9
	1000	84.1	83.5	82.9	82.4	81.8	81.3
	2000	78.1	77.6	77.1	76.7	76.2	75.8
5	50	92.3	91.5	90.8	90.2	89.5	88.9
	100	91.3	90.6	89.9	89.2	88.6	87.9
	300	87.9	87.3	86.7	86.0	85.4	84.8
	500	85.1	84.5	83.9	83.3	82.8	82.2
	1000	79.3	78.8	78.3	77.9	77.4	76.9
	2000	71.2	70.8	70.4	70.0	69.7	69.3
6	50	91.7	91.0	90.3	89.6	89.0	88.4
	100	90.3	89.6	88.9	88.3	87.7	87.0
	300	85.6	85.0	84.4	83.8	83.2	82.7
	500	81.7	81.1	80.6	80.1	79.6	79.1
	1000	74.1	73.7	73.3	72.9	72.5	72.1
	2000	64.1	63.8	63.5	63.2	63.0	62.7

Table 59. Maximum critical stresses due to wheel loading [H = 12 in]

Thickness of base layer [in]	Elastic modulus of base material [ksi]	Subgrade *k*-value [psi/in]					
		50	100	150	200	250	300
2	50	65.3	64.9	64.6	64.3	64.0	63.7
	100	65.2	64.8	64.5	64.2	63.9	63.6
	300	64.9	64.6	64.3	64.0	63.6	63.3
	500	64.7	64.4	64.1	63.8	63.4	63.1
	1000	64.3	63.9	63.6	63.3	63.0	62.7
	2000	63.5	63.1	62.8	62.5	62.2	61.9
3	50	65.1	64.8	64.5	64.2	63.8	63.5
	100	64.9	64.6	64.3	64.0	63.7	63.4
	300	64.4	64.1	63.8	63.5	63.1	62.8
	500	63.9	63.6	63.3	63.0	62.7	62.4
	1000	62.8	62.5	62.2	61.9	61.6	61.4
	2000	61.0	60.7	60.5	60.2	59.9	59.6
4	50	64.9	64.6	64.3	64.0	63.7	63.4
	100	64.6	64.3	64.0	63.7	63.4	63.1
	300	63.7	63.4	63.0	62.7	62.4	62.2
	500	62.8	62.5	62.2	61.9	61.6	61.3
	1000	60.9	60.6	60.3	60.0	59.8	59.5
	2000	57.8	57.5	57.3	57.1	56.8	56.6
5	50	64.7	64.4	64.1	63.8	63.5	63.2
	100	64.3	63.9	63.6	63.3	63.0	62.7
	300	62.7	62.4	62.1	61.8	61.6	61.3
	500	61.4	61.1	60.8	60.5	60.3	60.0
	1000	58.5	58.2	58.0	57.7	57.5	57.2
	2000	54.0	53.8	53.6	53.4	53.2	53.0
6	50	64.4	64.1	63.8	63.5	63.2	63.0
	100	63.8	63.5	63.2	62.9	62.6	62.3
	300	61.6	61.3	61.0	60.8	60.5	60.2
	500	59.7	59.4	59.1	58.9	58.6	58.4
	1000	55.7	55.5	55.3	55.0	54.8	54.6
	2000	49.9	49.7	49.6	49.4	49.2	49.1

Table 60. Maximum critical stresses due to wheel loading [H = 14 in]

Thickness of base layer [in]	Elastic modulus of base material [ksi]	Subgrade *k*-value [psi/in]					
		50	100	150	200	250	300
2	50	47.8	47.6	47.5	47.3	47.2	47.0
	100	47.7	47.6	47.4	47.3	47.1	47.0
	300	47.6	47.5	47.3	47.1	47.0	46.8
	500	47.5	47.4	47.2	47.0	46.9	46.7
	1000	47.3	47.1	47.0	46.8	46.7	46.5
	2000	46.9	46.7	46.6	46.4	46.3	46.1
3	50	47.7	47.6	47.4	47.2	47.1	46.9
	100	47.6	47.5	47.3	47.2	47.0	46.8
	300	47.4	47.2	47.0	46.9	46.7	46.6
	500	47.1	47.0	46.8	46.6	46.5	46.3
	1000	46.6	46.4	46.3	46.1	46.0	45.8
	2000	45.6	45.5	45.3	45.2	45.0	44.9
4	50	47.6	47.5	47.3	47.2	47.0	46.9
	100	47.5	47.3	47.2	47.0	46.9	46.7
	300	47.0	46.8	46.7	46.5	46.4	46.2
	500	46.5	46.4	46.2	46.1	45.9	45.8
	1000	45.5	45.4	45.2	45.1	45.0	44.8
	2000	43.9	43.7	43.6	43.5	43.3	43.2
5	50	47.5	47.3	47.2	47.0	46.9	46.8
	100	47.3	47.1	47.0	46.8	46.7	46.5
	300	46.5	46.3	46.2	46.1	45.9	45.8
	500	45.8	45.6	45.5	45.4	45.2	45.1
	1000	44.2	44.1	44.0	43.8	43.7	43.6
	2000	41.7	41.6	41.5	41.4	41.2	41.1
6	50	47.4	47.2	47.1	46.9	46.8	46.6
	100	47.0	46.9	46.7	46.6	46.4	46.3
	300	45.9	45.8	45.6	45.5	45.3	45.2
	500	44.9	44.8	44.6	44.5	44.3	44.2
	1000	42.7	42.6	42.4	42.3	42.2	42.1
	2000	39.3	39.2	39.1	39.0	38.9	38.8

8.2.3. Combined Loading

For the combined loading condition, the temperature and vehicle wheel loading is simultaneously applied on the CRCP slab for the different CRCP slab thickness. Here, the temperature loading is nighttime condition, and the vehicle wheel loading is applied on transverse crack of the CRCP slab. The maximum critical stresses are also estimated using FE analysis. Table 61 to Table 65 presents the computed maximum longitudinal tensile stresses under the various support combinations for the different slab thickness 6 to 14 in with 2-in increment, respectively.

As the support system is stiffening, for the 6 in of CRCP slab, range of the computed maximum critical stresses is decreased from 314.2 to 217.3 psi, and the variation is 96.9 psi. For the 8 in of CRCP slab, the range of the stresses is also decreased from 214.4 to 196.5 psi. The variation is 17.9 psi. However, For the 10 in of CRCP slab, the range of the maximum critical stresses is increased from 160.6 to 170.2 psi, and the variation is 9.6 psi. For the 12 in of CRCP slab, the range of the maximum stresses is also increased from 128.8 to 145.4 psi. The variation is 16.6 psi. Finally, for the 14 in of CRCP slab, the range of the estimated critical stresses is increased from 108.5 to 124.9 psi, and the variation is 16.4 psi.

For the combined loading condition, the maximum critical stresses are decreased as the support stiffness increases for the cases of that CRCP slab thickness is 6 and 8 in. on the other hands, the stresses are increased as the support system is stronger when the CRCP slab thickness is 10, 12, and 14 in. These results reveal that the temperature loading has mainly governed for CRCP system having thick slab thickness, whereas, the wheel loading condition has significantly affected the behavior of CRCP system, which has a thin slab thickness.

Table 61. Maximum critical stresses due to combined loading [H = 6 in]

Thickness of base layer [in]	Elastic modulus of base material [ksi]	Subgrade *k*-value [psi/in]					
		50	100	150	200	250	300
2	50	314.2	308.0	302.3	297.1	292.3	287.9
	100	313.1	307.0	301.4	296.2	291.4	287.0
	300	309.6	303.8	298.5	293.5	288.9	284.7
	500	306.6	301.1	296.0	291.3	286.9	282.8
	1000	300.6	295.6	291.0	286.7	282.6	278.9
	2000	291.9	287.6	283.6	279.9	276.4	273.1
3	50	312.2	306.2	300.8	295.7	291.1	286.8
	100	309.9	304.1	298.8	293.9	289.3	285.0
	300	302.5	297.3	292.6	288.1	284.0	280.1
	500	296.6	291.9	287.6	283.5	279.8	276.2
	1000	285.7	281.9	278.3	274.9	271.8	268.8
	2000	271.8	269.0	266.2	263.7	261.2	258.9
4	50	309.6	303.9	298.7	293.9	289.4	285.3
	100	305.7	300.3	295.3	290.7	286.4	282.4
	300	293.6	289.2	285.0	281.2	277.6	274.2
	500	284.7	281.0	277.5	274.1	271.0	268.1
	1000	269.8	267.0	264.4	261.9	259.6	257.3
	2000	252.6	250.8	249.0	247.3	245.7	244.1
5	50	306.5	301.1	296.1	291.5	287.3	283.4
	100	300.6	295.6	291.0	286.8	282.8	279.1
	300	283.6	279.9	276.4	273.2	270.1	267.2
	500	272.2	269.3	266.5	263.9	261.4	259.0
	1000	254.4	252.5	250.6	248.8	247.1	245.5
	2000	235.3	234.2	233.1	232.0	230.9	229.9
6	50	302.8	297.7	293.1	288.8	284.8	281.1
	100	294.7	290.2	286.1	282.2	278.6	275.2
	300	273.1	270.1	267.3	264.6	262.1	259.6
	500	259.8	257.6	255.5	253.4	251.5	249.6
	1000	240.2	238.9	237.6	236.4	235.2	234.0
	2000	220.6	219.9	219.2	218.6	217.9	217.3

Table 62. Maximum critical stresses due to combined loading [H = 8 in]

Thickness of base layer [in]	Elastic modulus of base material [ksi]	Subgrade *k*-value [psi/in]					
		50	100	150	200	250	300
2	50	214.4	213.6	212.9	212.2	211.5	210.9
	100	214.3	213.5	212.8	212.1	211.4	210.8
	300	214.1	213.3	212.6	211.9	211.3	210.6
	500	213.9	213.2	212.5	211.8	211.1	210.5
	1000	213.5	212.8	212.1	211.5	210.8	210.2
	2000	212.9	212.2	211.6	211.0	210.3	209.8
3	50	214.2	213.4	212.7	212.0	211.4	210.8
	100	214.0	213.3	212.6	211.9	211.2	210.6
	300	213.5	212.8	212.1	211.4	210.8	210.2
	500	213.1	212.4	211.7	211.1	210.4	209.8
	1000	212.1	211.4	210.8	210.2	209.6	209.1
	2000	210.4	209.9	209.3	208.8	208.3	207.8
4	50	213.9	213.2	212.5	211.8	211.2	210.6
	100	213.6	212.9	212.2	211.5	210.9	210.3
	300	212.6	211.9	211.3	210.6	210.0	209.4
	500	211.7	211.1	210.4	209.9	209.3	208.7
	1000	209.8	209.2	208.7	208.2	207.7	207.2
	2000	206.8	206.4	205.7	205.5	205.1	204.7
5	50	213.5	212.8	212.2	211.5	210.9	210.3
	100	213.0	212.3	211.7	211.0	210.4	209.8
	300	211.3	210.7	210.1	209.5	208.9	208.4
	500	209.8	209.2	208.7	208.2	207.7	207.2
	1000	206.8	206.4	205.9	205.5	205.1	204.7
	2000	202.4	202.1	201.7	201.4	201.1	200.8
6	50	213.1	212.4	211.8	211.1	210.5	210.0
	100	212.3	211.6	211.0	210.4	209.8	209.2
	300	209.6	209.1	208.5	208.0	207.5	207.0
	500	207.5	207.0	206.5	206.1	205.6	205.2
	1000	203.3	203.0	202.6	202.3	201.9	201.6
	2000	197.6	197.4	197.1	196.9	196.7	196.5

Table 63. Maximum critical stresses due to combined loading [H = 10 in]

Thickness of base layer [in]	Elastic modulus of base material [ksi]	Subgrade *k*-value [psi/in]					
		50	100	150	200	250	300
2	50	160.6	160.7	160.9	161.1	161.3	161.4
	100	160.6	160.8	161.0	161.2	161.3	161.5
	300	160.9	161.1	161.3	161.5	161.6	161.8
	500	161.2	161.4	161.6	161.7	161.9	162.0
	1000	161.9	162.0	162.2	162.3	162.5	162.6
	2000	162.9	163.0	163.2	163.3	163.4	163.6
3	50	160.7	160.8	161.0	161.2	161.3	161.5
	100	160.8	161.0	161.2	161.3	161.5	161.7
	300	161.5	161.7	161.8	162.0	162.1	162.3
	500	162.1	162.3	162.4	162.6	162.7	162.9
	1000	163.4	163.5	163.7	163.8	163.9	164.0
	2000	165.3	165.4	165.5	165.6	165.7	165.8
4	50	160.8	161.0	161.1	161.3	161.5	161.6
	100	161.1	161.3	161.4	161.6	161.8	161.9
	300	162.2	162.4	162.5	162.7	162.8	162.9
	500	163.2	163.3	163.4	163.6	163.7	163.8
	1000	165.1	165.2	165.3	165.4	165.5	165.6
	2000	167.5	167.6	167.6	167.7	167.7	167.8
5	50	161.0	161.1	161.3	161.4	161.6	161.8
	100	161.4	161.6	161.7	161.9	162.0	162.2
	300	163.0	163.1	163.3	163.4	163.5	163.6
	500	164.3	164.4	164.5	164.6	164.7	164.8
	1000	166.6	166.7	166.7	166.8	166.9	167.0
	2000	169.2	169.2	169.2	169.3	169.3	169.3
6	50	161.1	161.3	161.5	161.6	161.8	161.9
	100	161.7	161.9	162.1	162.2	162.3	162.5
	300	163.8	163.9	164.0	164.1	164.2	164.4
	500	165.3	165.4	165.5	165.6	165.7	165.8
	1000	167.8	167.9	167.9	168.0	168.0	168.1
	2000	170.1	170.1	170.2	170.2	170.2	170.2

Table 64. Maximum critical stresses due to combined loading [H = 12 in]

Thickness of base layer [in]	Elastic modulus of base material [ksi]	Subgrade *k*-value [psi/in]					
		50	100	150	200	250	300
2	50	128.8	129.1	129.4	129.7	130.0	130.3
	100	128.9	129.2	129.5	129.8	130.1	130.4
	300	129.2	129.5	129.8	130.1	130.4	130.7
	500	129.5	129.8	130.1	130.4	130.7	131.0
	1000	130.2	130.5	130.8	131.0	131.3	131.6
	2000	131.3	131.6	131.9	132.1	132.4	132.7
3	50	128.9	129.2	129.5	129.8	130.1	130.4
	100	129.1	129.4	129.7	130.0	130.3	130.6
	300	129.9	130.1	130.4	130.7	131.0	131.3
	500	130.5	130.8	131.1	131.4	131.6	131.9
	1000	132.0	132.3	132.5	132.8	133.0	133.3
	2000	134.3	134.6	134.8	135.0	135.3	135.5
4	50	129.1	129.4	129.7	130.0	130.3	130.5
	100	129.5	129.8	130.0	130.3	130.6	130.9
	300	130.7	131.0	131.3	131.6	131.8	132.1
	500	131.9	132.1	132.4	132.7	132.9	133.2
	1000	134.3	134.5	134.7	135.0	135.2	135.4
	2000	137.9	138.1	138.3	138.4	138.6	138.6
5	50	129.3	129.6	129.9	130.2	130.5	130.7
	100	129.9	130.1	130.4	130.7	131.0	131.3
	300	131.8	132.0	132.3	132.6	132.8	133.1
	500	133.4	133.7	133.9	134.2	134.4	134.6
	1000	136.8	137.0	137.2	137.4	137.6	137.8
	2000	141.5	141.6	141.8	141.9	142.1	142.2
6	50	129.6	129.9	130.2	130.4	130.7	131.0
	100	130.3	130.6	130.9	131.2	131.4	131.7
	300	133.0	133.2	133.5	133.7	133.9	134.2
	500	135.2	135.4	135.6	135.8	136.0	136.3
	1000	139.4	139.6	139.8	139.9	140.1	140.3
	2000	144.8	144.9	145.1	145.2	145.3	145.4

Table 65. Maximum critical stresses due to combined loading [H = 14 in]

Thickness of base layer [in]	Elastic modulus of base material [ksi]	Subgrade *k*-value [psi/in]					
		50	100	150	200	250	300
2	50	108.5	108.8	109.1	109.3	109.6	109.9
	100	108.6	108.9	109.1	109.4	109.7	109.9
	300	108.9	109.1	109.4	109.7	109.9	110.2
	500	109.1	109.4	109.6	109.9	110.2	110.4
	1000	109.6	109.9	110.2	110.4	110.7	110.9
	2000	110.6	110.8	111.1	111.3	111.6	111.8
3	50	108.6	108.9	109.2	109.4	109.7	110.0
	100	108.8	109.1	109.3	109.6	109.9	110.1
	300	109.4	109.7	109.9	110.2	110.5	110.7
	500	109.9	110.2	110.5	110.7	111.0	111.2
	1000	111.2	111.4	111.7	111.9	112.2	112.4
	2000	113.2	113.4	113.6	113.9	114.1	114.3
4	50	108.8	109.1	109.3	109.6	109.8	110.1
	100	109.1	109.4	109.6	109.9	110.1	110.4
	300	110.1	110.4	110.6	110.9	111.2	111.4
	500	111.1	111.3	111.6	111.8	112.1	112.3
	1000	113.2	113.4	113.6	113.9	114.1	114.3
	2000	116.5	116.7	116.9	117.1	117.3	117.5
5	50	109.0	109.3	109.5	109.8	110.0	110.3
	100	109.4	109.7	110.0	110.2	110.5	110.7
	300	111.0	111.3	111.5	111.8	112.0	112.3
	500	112.5	112.7	113.0	113.2	113.4	113.7
	1000	115.6	115.8	116.0	116.2	116.4	116.6
	2000	120.2	120.4	120.6	120.8	120.9	121.1
6	50	109.2	109.5	109.7	110.0	110.2	110.5
	100	109.8	110.1	110.4	110.6	110.9	111.1
	300	112.1	112.4	112.6	112.8	113.1	113.3
	500	114.1	114.3	114.6	114.8	115.0	115.2
	1000	118.2	118.4	118.6	118.8	119.0	119.2
	2000	124.1	124.3	124.4	124.6	124.7	124.9

8.2.4. Results

To verify effects of the properties composing CRCP structure on the maximum critical stress generation in the CRCP slab, linear regression analysis are conducted under temperature, wheel, and combined loading conditions.

Table 66 shows the estimated regression coefficients. According to the obtained standardized coefficients, thickness of CRCP slab could negatively affect on determining the stress level, whereas, other properties have affected positively. However, absolute magnitudes of the influences are in order as follow: Thickness of CRCP slab > Elastic modulus of base material > Thickness of base layer > Subgrade k-value.

Table 66. Regression coefficients on maximum critical stress due to nighttime temperature loading condition

Independent variables	Unstandardized coefficient	Standardized Coefficient
Constant	117.504	-
Thickness of CRCP slab	-6.256	-0.798
Thickness of base	4.391	0.280
Elastic modulus of base material	0.013	0.401
Subgrade k-value	0.024	0.091

Also, regression equation is linearly assumed like equation 8.4 to estimate the maximum longitudinal tensile stress at center of the CRCP slab. Where, H is the thickness of CRCP slab, T_b is the thickness of base layer (in), E_b is the elastic modulus of the base material (ksi), and k_{sg} represents the subgrade k-value (psi/in). This has 88.3% of R^2-value.

$$\sigma_{cr} = 117.5 - 6.26H + 4.39T_b + 0.013E_b + 0.024k_{sg} \qquad (8.4)$$

Table 67 addresses the estimated regression coefficients under center loaded vehicle wheel loading condition. According to the obtained standardized coefficients, all properties composing CRCP structure affect negatively on the maximum critical stresses. Especially, thickness of CRCP slab has mainly influenced to determine the stress level. The effect of the slab thickness for this case is greater than temperature loading cases. The absolute magnitudes of the influences are as follow in order: Thickness of CRCP slab > Elastic modulus of base material > Thickness of base layer > Subgrade k-value.

Table 67. Regression coefficients on maximum critical stress due to center loaded vehicle wheel loading condition

Independent variables	Unstandardized coefficient	Standardized Coefficient
Constant	308.834	-
Thickness of CRCP slab	-17.614	-0.918
Thickness of base	-4.535	-0.118
Elastic modulus of base material	-0.013	-0.157
Subgrade k-value	-0.027	-0.043

Linear regression equation is also assumed as equation 8.5, which could estimate the maximum critical stresses at center of the CRCP slab under vehicle wheel loading condition applied at slab center. This has 88.3% of R^2-value.

$$\sigma_{cr} = 308.8 - 17.61H - 4.54T_b - 0.013E_b - 0.027k_{sg} \qquad (8.5)$$

Table 68 presents the estimated regression coefficients under combined loading condition including nighttime temperature gradient and vehicle wheel load applied at transverse crack. Standardized coefficients have shown that all properties composing CRCP structure affect negatively on the maximum critical stresses. In this case, especially,

the maximum critical stresses could almost be determined by the thickness of CRCP slab rather than other properties. The effect of the slab thickness for this case is greater than cases of temperature or wheel loading conditions only. The absolute magnitudes of the influences are as follow: Thickness of CRCP slab > Elastic modulus of base material > Thickness of base layer > Subgrade k-value.

Table 68. Regression coefficients on maximum critical stress due to combined loading condition

Independent variables	Unstandardized coefficient	Standardized Coefficient
Constant	391.301	-
Thickness of CRCP slab	-20.25	-0.960
Thickness of base	-1.337	-0.032
Elastic modulus of base material	-0.003	-0.035
Subgrade k-value	-0.014	-0.020

As stated previously, for the combined loading condition, the stresses are decreasing as the support stiffness increases for thin CRCP slab. On the other hands, the stresses are increasing as the support system is stronger in the thick slab condition. However, because the thickness of CRCP slab has governed the stress level for the most part, regression equation is linearly assumed as equation 8.6, which could approximately determine the maximum critical stresses at center of the CRCP slab under the combined loading condition. Here, the units of the independent variables are inches, ksi, and psi/in for thickness of base layer, elastic modulus of the base material, and subgrade k-value, respectively. This has 92.4% of R^2-*value*.

$$\sigma_{cr} = 391.3 - 20.25H - 1.337T_b - 0.003E_b - 0.014k_{sg} \qquad (8.6)$$

8.3. OPTIMUM COMBINATION OF CRCP STRUCTURE

To maintain uniformity of support system and prevent support erosion under concrete slabs, chemical treatment of the subgrade soils and construction of the stabilized base layer have been highly recommended for rigid pavement design. So, these achievements have required composite k-value of the support system. For this reason, combinations of support layer properties satisfying a desired composite k-value should be firstly considered to determine optimum compositions of the CRCP structure including slab thickness and the support properties. Afterwards, allowable critical stress is determined which could satisfy mixed traffic and environmental loading conditions during design life. For the all combinations of support properties, thickness of CRCP slab is determined which could produce a stress not exceeding the allowable critical stress. Finally, the most economical combination case is selected. Figure 74 illustrate the procedure to determine optimum combination of CRCP slab thickness and support properties.

STEP1 • Determine required composite k-value for rigid pavement design

STEP2 • Determine combinations of support peoperties satisfying the target composite k-value

STEP3 • Determine allowable critical stress corrresponding mixed loading conditions and design life

STEP4 • Determine thickness of CRCP slab for the all combinations of support properties

STEP5 • Select the most economical combination of the slab thickness and support properties

Figure 74. Procedure to determine optimum combination of CRCP slab thickness and support properties

For example study, 300 psi/in of composite *k*-value is selected based on Texas rigid pavement design guide [TxDOT, 2008], and the combination cases of the support layer properties such as thickness of base layer, elastic modulus of the base material, and subgrade *k*-value completing the composite *k*-value, 300 psi/in are used which developed in Table 18 in the chapter 4.

To determine allowable critical stress, number of load applications (*N*) should firstly be considered which represents traffic value for the pavement design. Most of damages have been come out as fatigue damage in rigid pavement system. The general expression for fatigue damage accumulation is as follows:

$$FD = \sum \frac{n}{N} \qquad (8.7)$$

Where, *FD* = total fatigue damage

n = applied number of load applications

N = allowable number of load applications

The applied number of load applications is the actual number of passed traffic load, and the allowable number of load applications is the number of load cycles at which fatigue failure is expected. The allowable number of load applications is determined using the following fatigue model [NCHRP, 2004];

$$\log(N) = C_1 \cdot \left(\frac{MR}{\sigma}\right)^{C_2} + 0.4371 \qquad (8.8)$$

Where, *N* = allowable number of load applications

MR = concrete modulus of rupture

σ = applied stress

C_1 = calibration constant = 2.0

C_2 = calibration constant = 1.22

Texas rigid pavement specification have regulated that *MR* of 620 psi at 28 days should be used for concrete pavement design [TxDOT, 2008]. For example study, three different values of number of load applications were considered. The allowable critical stresses (σ_{allow}) which corresponding the different values of number of load applications were calculated using the equation 8.8, and stress/strength ratio for the three cases were presented in Table 69.

To find acceptable thickness of CRCP slab, which could produce a stress less than the computed allowable stress for the three cases, longitudinal maximum tensile stresses were computed with changing of the slab thickness under combined loading condition of nighttime temperature and vehicle wheel load applied at transverse crack for the selected combinations of the support layer properties. Table 70 presents the combinations of CRCP structure which are not exceeding the allowable maximum critical stress for the combined loading conditions and the different values of the number of load applications.

Table 69. Maximum allowable tensile stresses corresponding number of load applications for case study

Case	Number of Load Applications	Maximum Allowable Tensile Stress [psi]	Stress/Strength Ratio
1	2,500,000	253.3	0.41
2	250,000	294.4	0.47
3	25,000	354.1	0.57

The optimum combination of the CRCP structure should satisfy financial aspect, low construction cost. Accordingly, the most economical combination which has the lowest initial construction cost among these 14 cases of combinations might be the

optimum combination of the CRCP structure for each different traffic value. Based on information of average low bed unit price from Texas Department of Transportation [TxDOT, 2010], initial construction costs of CRCP were theoretically calculated as shown in Figure 75, Figure 76, and Figure 77. In these Figures, the computed costs include CRCP slab thickness and base thickness of the selected base type. Table 71 shows the optimum combination of support properties and thickness of CRCP slab for the three different design traffic values and their initial construction costs. Because this exercise is theoretical, final combinations should be adjusted based on the practicality of the base thickness and availability of local materials so on. In other words, 2.4 in cement stabilized base cannot be built.

Table 70. Optimum combinations between slab thickness of CRCP and support layer properties for combined loading conditions

No.	Subgrade *k*-value [psi/in]	Elastic modulus of base material [ksi]	Thickness of base layer [in]	Thickness of CRCP slab [in.]		
				Case1	Case2	Case3
1		500	5.8	9	7	7
2	50	1,000	4.6	9	7	7
3		2,000	3.6	9	7	7
4		300	4.7	8	7	6
5		500	4	9	7	6
6	100	1,000	3.1	9	7	6
7		2,000	2.5	9	7	6
8		300	3.4	8	7	6
9	150	500	2.9	8	7	6
10		1,000	2.3	8	7	6
11		50	4.5	8	7	6
12		100	3.5	8	7	6
13	200	300	2.4	8	7	6
14		500	2	8	7	6
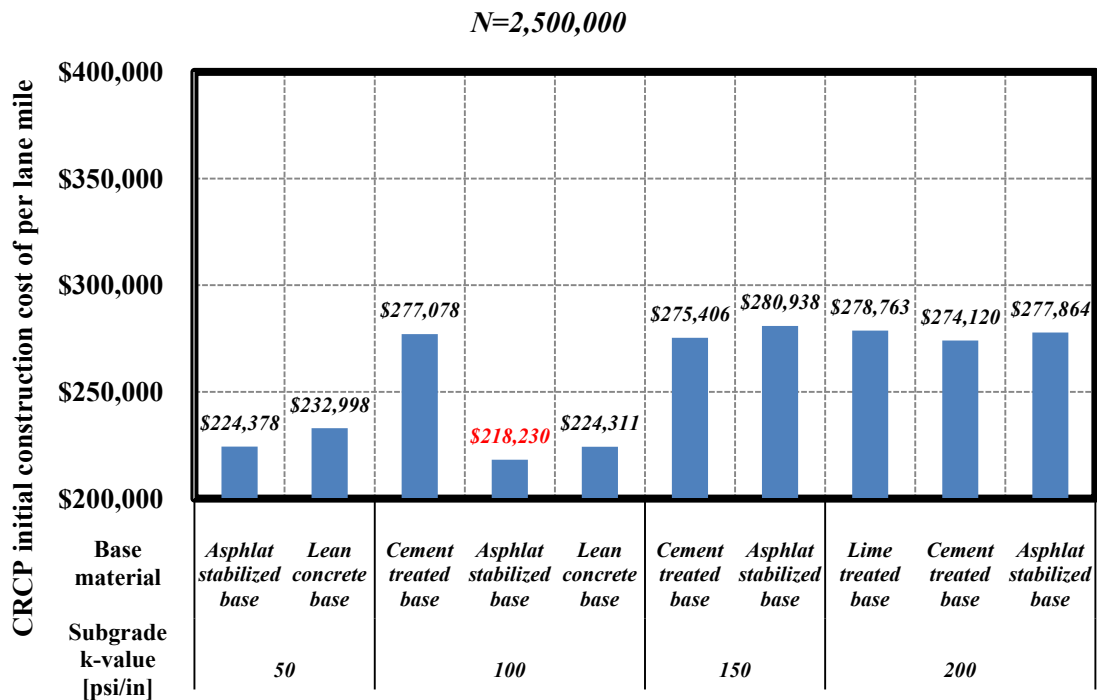
Figure 75. CRCP initial construction cost per lane mile [N=2,500,000]
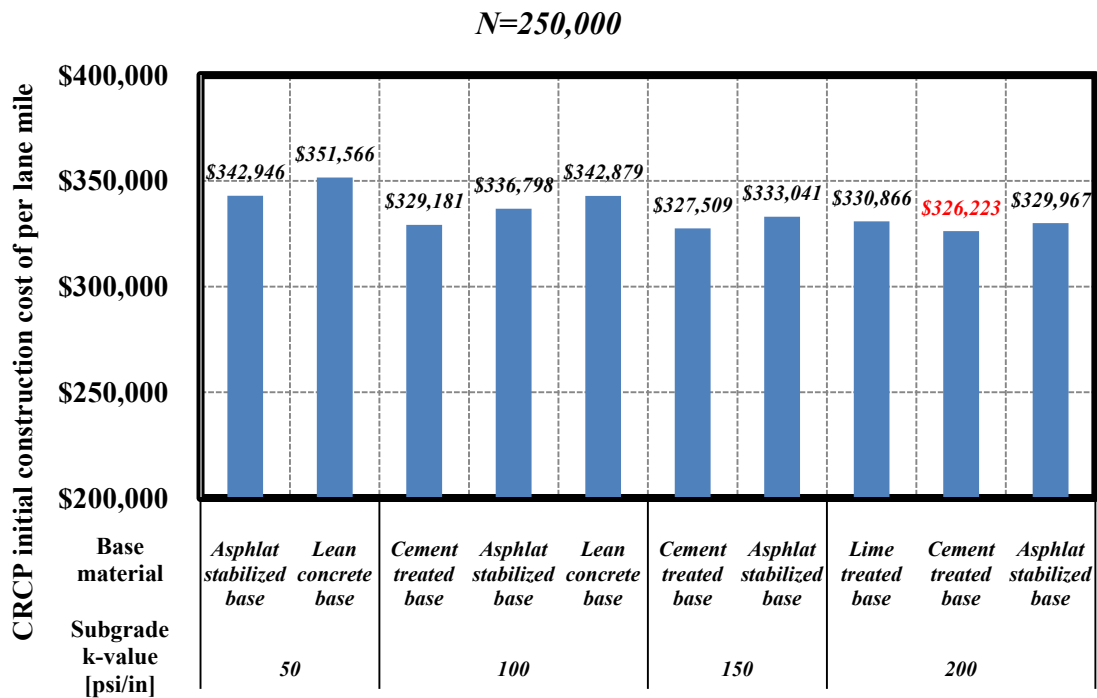
Figure 76. CRCP initial construction cost per lane mile [N=250,000]
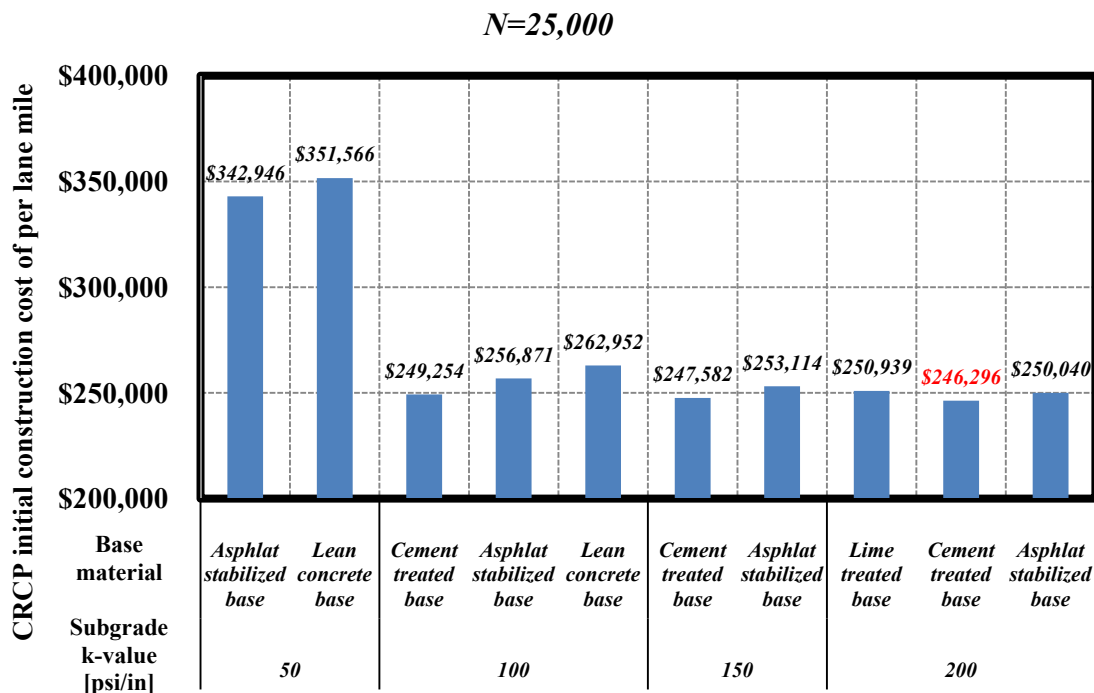
Figure 77. CRCP initial construction cost per lane mile [N=25,000]

Table 71. Optimum combinations and initial construction costs of CRCP

Case No.	1	2	3
Subgrade *k*-value [psi/in]	100	200	200
Base type	Asphalt stabilized base	Cement treated base	Cement treated base
Thickness of base layer [in]	4	2.4	2.4
Thickness of CRCP slab [in]	9	7	6
Initial construction cost [$]	**218,230**	**326,223**	**246,296**

8.4. SUMMARY

To find the optimum combination of CRCP structure, thickness of CRCP slab, thickness of base layer, elastic modulus of the base material, and subgrade k-value were selected as independent variables affecting level of the maximum critical stress in the CRCP slab, and these variables gave 900 different conditions of CRCP composition. Nighttime temperature gradient and center loaded vehicle wheel loading were considered. Also, the most critical loading condition, simultaneously combining nighttime temperature gradient and wheel loading applied on transverse crack, were considered.

The maximum longitudinal tensile stresses were estimated under diverse combinations of the CRCP properties due to temperature, wheel, and the combined loading conditions. For both of the temperature and vehicle wheel loadings, the maximum critical stress was significantly decreased as the slab thickness increases. However, the stress decrement was greater for the wheel loading condition than for the temperature loading cases. Additionally, for the combined loading condition, the analysis results have revealed that the temperature loading has mainly governed when the slab is thick, whereas, the wheel loading condition has significantly affected when the slab is thin. It had also been identified by regression analysis that the effects of the CRCP properties are as follow: Thickness of CRCP slab > Elastic modulus of base material > Thickness of base layer > Subgrade k-value for the all loading cases. Also, regression equations were developed for the loading conditions.

Based on the results identified from these studies, a procedure was suggested to determine optimum combination of CRCP structural and support layer properties. First of all, combinations of support layer properties are determined, completing desired composite k-value. Secondly, thickness of CRCP slab is back-calculated, which satisfying the computed allowable maximum critical stress based on design traffic value. Finally the optimum combination of CRCP structure is selected providing financial advantage among the combinations.

CHAPTER 9: SUMMARY, CONCLUSIONS AND RECOMMENDATIONS

9.1. SUMMARY

Continuously reinforced concrete pavement (CRCP) is the most widely used rigid pavement type in Texas. In CRCP structure, foundation system supporting portland cement concrete (PCC) slab plays a crucial role in fully playing sufficient ability of the CRCP system. Historically, concrete slab had been directly placed on native soil layer, subgrade, during the early age of constructions. However, it has been revealed that unstable support system could induce severe failure in the PCC slab. Therefore, modern pavement design guides have recommended the use of stabilized base layer between subgrade and PCC slab. However, the uses of stabilized base layers have resulted in high cost for the CRCP construction. For this reason, this study was started with considerations to decrease construction cost with acceptable long-term performance of the CRCP system.

To achieve the research goals, firstly, field support conditions were investigated by field tests such as FWD test, DCP test, and non-repetitive static plate load test. Through these field tests, field support conditions and characteristics were investigated. Not only the modulus of support layers were estimated, but also the modulus of subgrade reaction values were directly measured on the top surface of subgrade layer (subgrade *k*-value) and stabilized base layer (composite *k*-value).

Three kinds of analytical support models were previously developed by many researchers. Those are a single composite *k*-vale support model which is the simplest model, elastic isotropic solid layered support model, and elastic layer and *k*-value composite support model. To verify which model most effectively describe the field support conditions, three different support analysis models were examined simulating the static plate load test using finite element (FE) methods. Effects of structural and material properties composing support system, such as thickness of base layer, elastic modulus of

the base material, and subgrade k-value, on composite k-value of the support system were identified. Also, a method to find the optimum combinations of the support layer properties completing desired composite k-value was developed.

To evaluate CRCP behavior on diverse support conditions, CRCP FE model was developed using ABAQUS 6.7 FE program, which considers the effects of support layer properties on the CRCP behavior. Nighttime temperature gradient and vehicle wheel loading applied at center of the CRCP slab are considered as loading conditions. Also, behavior of CRCP slabs was evaluated, which are placed on identical composite k-value having different combinations of the support layer properties. Finally, effects of non-uniform support conditions on the CRCP behavior were examined.

A simple support model, composite k-value model, has been more widely used in pavement design than the elastic and k-value composite support model. Composite k-values from these two different support models were compared under temperature and wheel loading conditions, and effects of the support layer properties on the differences of the support models were identified.

Thickness of CRCP slab is one of the most critical factors increasing construction costs. Therefore, effects of the components of CRCP structure including not only the support layer properties, but also PCC slab thickness were mechanistically identified on the slab behavior. Moreover, guideline to determine the optimum combination of the components constituting CRCP structure was developed as an aspect of the lowest initial construction cost of the CRCP.

9.2. CONCLUSIONS

Verifications of field support conditions for rigid pavement structure

- FWD deflection test results show that the support vertical stiffness, i.e. vertical deflections, are non-uniformly distributed on top surface of asphalt stabilized base layer.

- DCP test results clearly show boundary between aggregate subbase layer and subgrade soil layer. Generally, aggregate subbase layer is stronger than subgrade. However, subgrade layer shows relatively uniform condition than aggregate subbase layer.

- Directly measured composite k-value on the asphalt-stabilized base ranges from 680 to 920 psi/in, which are corrected values by loading plate size, whereas, the measured k-value on top of aggregate subbase is 420 psi/in. The 2-in asphalt-stabilized base layer increased support stiffness about 1.5 times in this field test.

Evaluation of support analysis models

- Most identical composite k-value is computed from elastic layer and k-value composite support model compared with the composite k-value from field test, rather than elastic-isotropic solid layered support model or a single composite k-value support model.

- The elastic layer and k-value composite support model described effect of bearing plate size on determining composite k-value.

- Elastic-isotropic solid layered support model over-estimates the composite k-value. A simple composite k-value support model could not express the effect of loading plate size on the composite k-value of support system.

- For the different size of load bearing plates, vertical stresses and deflections at bottom of the stabilized base layer and top of the subgrade layer are converged

for 30 in or more of the loading plate size.

■ Maximum shear stresses at the stabilized base layer are induced at the edge of the loading plate, and also converged for 30-in or more diameters of the load bearing plate.

■ It could be concluded that composite k-value is determined by the magnitudes of vertical resistance and shear resistance, and the elastic layer and k-value composite support model can effectively express the vertical and shear resistances of support system.

Effects of support layer properties on composite k-value

■ Magnitude of composite k-value of support system could be affected by values of the support layer properties such as thickness of base layer, elastic modulus of the base material, and subgrade k-value.

■ Composite k-value is increased as the bases of support layer properties increase.

■ Effect of subgrade k-value is greatest to the composite k-value, and effect of elastic modulus of the base material is second. The effect of base thickness is last. However, the differences are relatively very small.

■ The regression equation is developed to estimate composite k-value.

$$k_\infty = -395.7 + 92.3T_b + 0.223E_b + 1.829k_{sg}$$

Here, T_b is the thickness of the base (in), E_b is the elastic modulus of the base material (ksi), and k_{sg} is the subgrade k-value (psi/in).

■ A method to determine the combination of the support layer properties completing desired composite k-value is developed. Because it is impossible to adjust subgrade k-value or elastic modulus of base material in decimal points, thickness of the stabilized base layer is determined for standard values of elastic modulus of the base material and subgrade k-value. The most economical case is selected among the determined combinations.

Numerical analysis of behavior of concrete slab on elastic foundation

- ABAQUS 6.7 FE program can estimate identical responses compared with traditional theories such as Westergaard's closed form solutions and Bradbury's equations.
- For the temperature loading conditions, nighttime nonlinear temperature gradient gives the most critical stress in concrete slab rather than linear or daytime temperature gradients.
- FE model of concrete slab on elastic foundation using 2-dimensional plane strain elements gives almost identical responses with 3-dimentionsal solid element or shell element models for temperature loading condition.
- For vehicle axle loading conditions, the magnitude of tire pressure should be decreased about 57% for use of 2-dimensional plane strain element model to match stresses in concrete slab with the use of 3-dimentional solid element or shell element models.

Effects of support layer properties on CRCP behavior

- For temperature loading, estimated maximum longitudinal tensile stress at the center of CRCP slab, between two adjacent transverse cracks, is increased as the values of the support layer properties increase.
- For the temperature loading condition, elastic modulus of base material is mainly affected to the magnitude of maximum critical stress at the center of CRCP slab, and effect of the base thickness is secondly large. The subgrade k-value scarcely affects to the maximum longitudinal tensile stress.
- The regression relationship is developed to estimate maximum critical stress at center of the CRCP slab under temperature loading condition.

$$\sigma_{cr} = 50.6 + 4.41T_b + 0.013E_b + 0.02k_{sg}$$

Here, T_b is the thickness of base (in), E_b is the elastic modulus of the base

material (ksi),   and k_{sg} is the subgrade k-value (psi/in).

- For vehicle wheel loading condition, estimated maximum critical stress at center of the CRCP slab is decreased as the values of support layer properties increase.

- For the vehicle wheel loading condition, elastic modulus of base material gives the greatest influence to the critical stress negatively, and thickness of the base layer is the next. The subgrade k-value gives little effect to the change of the maximum critical stress, which is same with the temperature loading.

- The regression relationship is developed to estimate the maximum critical stress at center of the CRCP slab under vehicle wheel loading condition.

$$\sigma_{cr} = 103.0 - 2.61T_b - 0.007E_b - 0.012k_{sg}$$

Effects of various support property combinations having identical composite k-value

- Although support systems have identical composite k-value, maximum critical stresses in the CRCP slab could be varied in accordance to the combinations of support layer properties due to temperature and wheel loadings.

- As thickness of CRCP slab is increased, the maximum critical stress is decreased. Here, the stresses due to vehicle wheel loading is more significantly decreased than due to temperature loading as the slab thickness increases.

- The maximum longitudinal tensile stress is increased as crack spacing of CRCP increases. The stresses under the vehicle wheel loading condition is also more considerably increased than under temperature loading condition as the crack spacing increases.

- Locally strong or locally weak non-uniform support conditions at the slab center and transverse crack have given almost twice as much maximum critical stresses than uniform support condition for not only both nighttime and daytime temperature loading conditions but also vehicle wheel loading conditions applied at the slab center and transverse crack.

Composite *k*-value comparisons for different support analysis models

■ Composite *k*-values for two different support analysis models, elastic layer and *k*-value composite support model and the simplified composite *k*-value support model are compared, which are inducing identical maximum longitudinal tensile stress at the slab center.

■ Back-found composite *k*-values of the simplified composite *k*-value support model show discrepancies with directly computed composite *k*-values from the elastic layer and *k*-value composite support model.

■ The discrepancy between two composite *k*-values from the two different support models is increased as 1) thickness of stabilized base layer increases, 2) elastic modulus of the base material increases, and 3) subgrade *k*-value decreases.

■ Use of the simplified support model has been acceptable for rigid pavement design when structural rigidity of the stabilized base layer is low but subgrade *k*-value is high for both the temperature and vehicle wheel loading conditions.

Effects of components of CRCP structure on the CRCP behavior

■ For temperature loading, the maximum critical stress at the slab center is dramatically decreased as the CRCP slab thickness increases although the larger the stress is, the stronger the support system. The regression relationship is developed to estimate the maximum critical stress at center of the CRCP slab under the nighttime temperature loading condition.

$$\sigma_{cr} = 117.5 - 6.26H + 4.39T_b + 0.013E_b + 0.024k_{sg}$$

Here, T_b is the thickness of base (in), E_b is the elastic modulus of the base material (ksi), and k_{sg} is the subgrade *k*-value (psi/in).

■ For the vehicle wheel loading condition, the maximum critical stress is also significantly decreased as the slab thickness increases rather than the case of temperature loading condition. The regression equation is also developed under

the center loaded vehicle wheel loading condition.

$$\sigma_{cr} = 308.8 - 17.61H - 4.54T_b - 0.013E_b - 0.027k_{sg}$$

- For the combined loading of nighttime temperature and wheel loading at transverse crack of CRCP, the maximum longitudinal tensile stress is decreased as thickness of CRCP slab increases. The decrement rate is much larger than in the case of temperature loading or vehicle wheel loading only. The regression relationship has also been developed under the combined loading condition.

$$\sigma_{cr} = 391.3 - 20.25H - 1.337T_b - 0.003E_b - 0.014k_{sg}$$

- For all loading cases, effect of the CRCP slab thickness is overwhelmingly large than other properties such as base thickness, elastic modulus of the base material, or subgrade k-value.

- Guideline to determine optimum values of structural and material components of CRCP structure has been suggested. First of all, a composite k-value must be set, which could provide uniform and non-erodible support conditions. Secondly, determine the allowable maximum critical stress in the CRCP slab, guaranteeing adequate long-term performance of the CRCP system. Lastly, find thickness of the CRCP slab, which is not exceeding the selected allowable critical stress.

9.3. LIMITATIONS AND RECOMMENDATIONS

- For the wheel loading cases, only static loading is considered in this study. However, actual wheel loading conditions in field are moving and are dynamic loads. The critical stress level and location could be altered by the moving dynamic wheel loading conditions. Thus, additional studies on these loads are required.

- For the critical stress to evaluate CRCP performance, longitudinal maximum tensile stress on surface of the slab was considered in this study. However, it have not been verified that which stress component have mainly governed the performance of the CRCP structures and occurrences of distresses. Therefore, additional studies about diverse stress components have been required.

- Only four components constituting CRCP structure have been considered in this study, thickness of CRCP slab, thickness of base layer, elastic modulus of the base material, and subgrade k-value. However, crack spacing and steel ratio are desired as variables which are included in regression equations to estimate the CRCP stresses.

- Number of loading applications is one of the critical factors evaluating long-term performance of the CRCP system. Although temperature loading is repeating with daily cycle, vehicle wheel loading is repeating thousands times in a day. Accordingly, the portions of the two different loadings might be considered differently to determine the critical stress for evaluation of the long-term performance.

- In this study, effects of the independent variables composing CRCP structure on the CRCP behavior are evaluated by mechanistic solutions. To support the conclusions, field evaluations have been required.

APPENDIX A

Effects of Support Layer Properties on Composite *k*-value

➤ *Effects of Thickness of Stabilized Base Layer on Composite k-value*

Figure A 1. Effects of thickness of stabilized base on composite *k*-value (1)

Figure A 2. Effects of thickness of stabilized base on composite *k*-value (2)
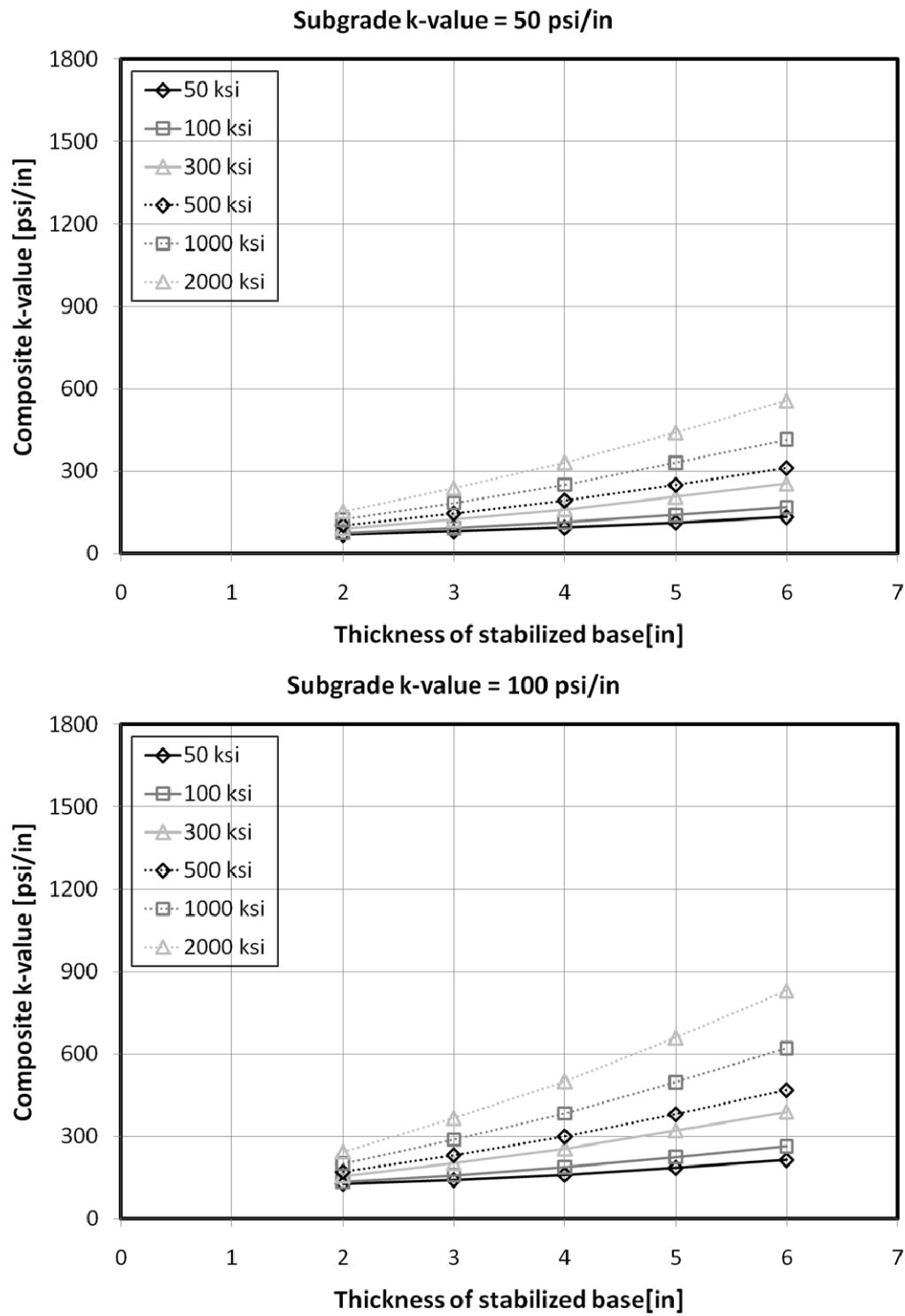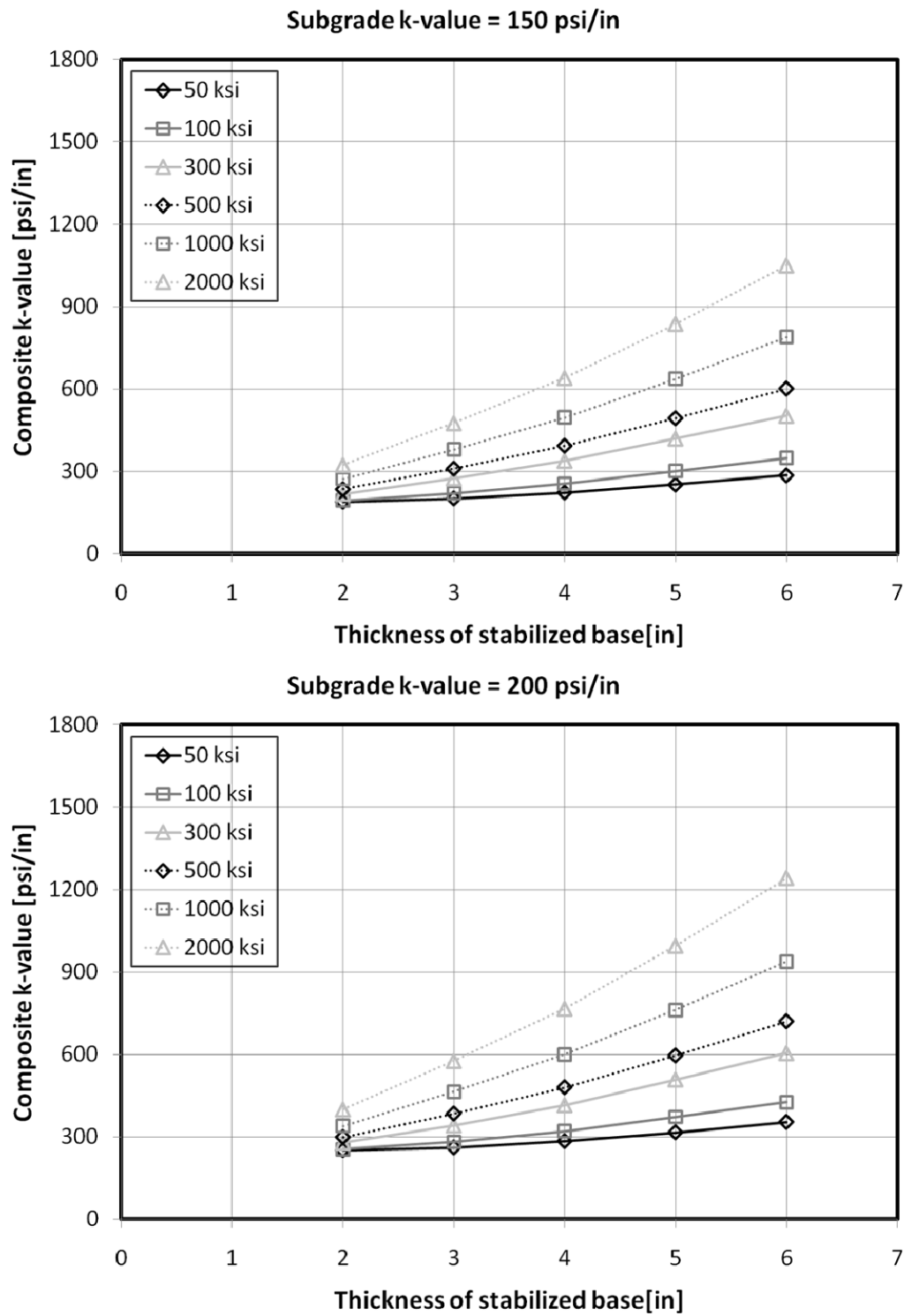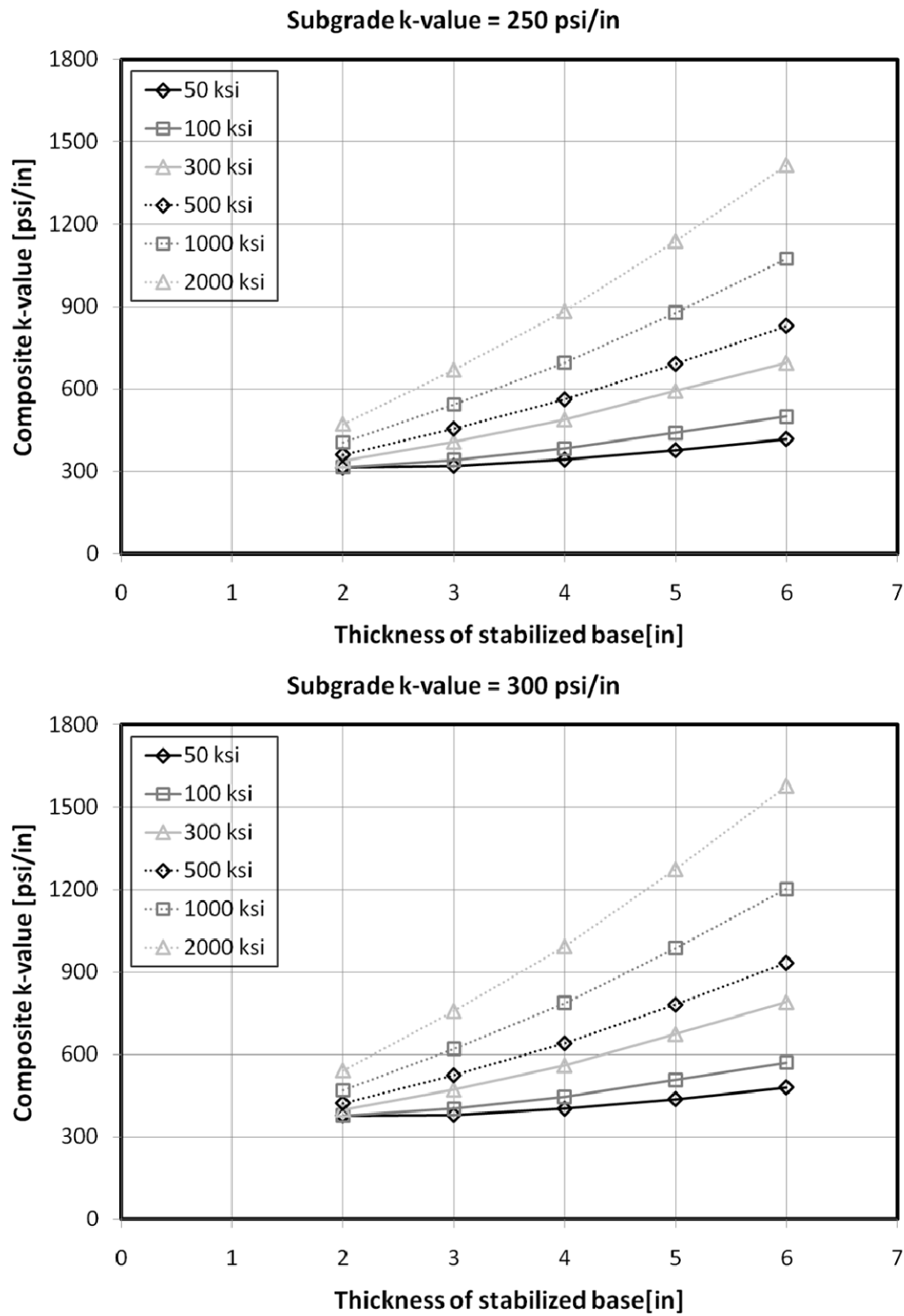
Figure A 3. Effects of thickness of stabilized base on composite *k*-value (3)
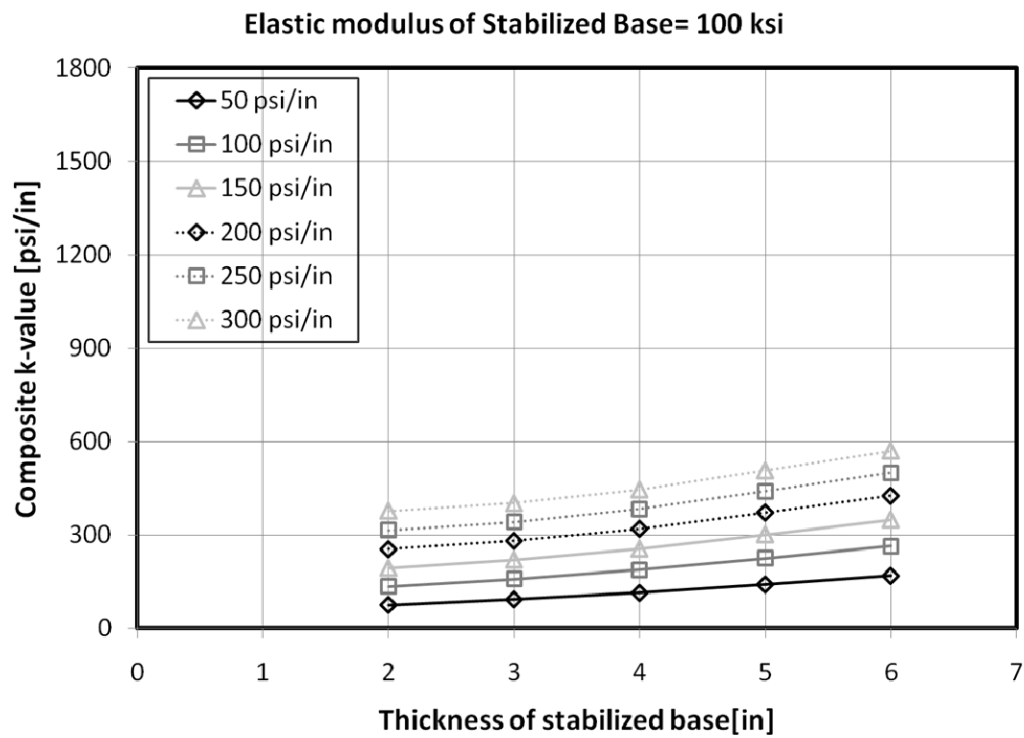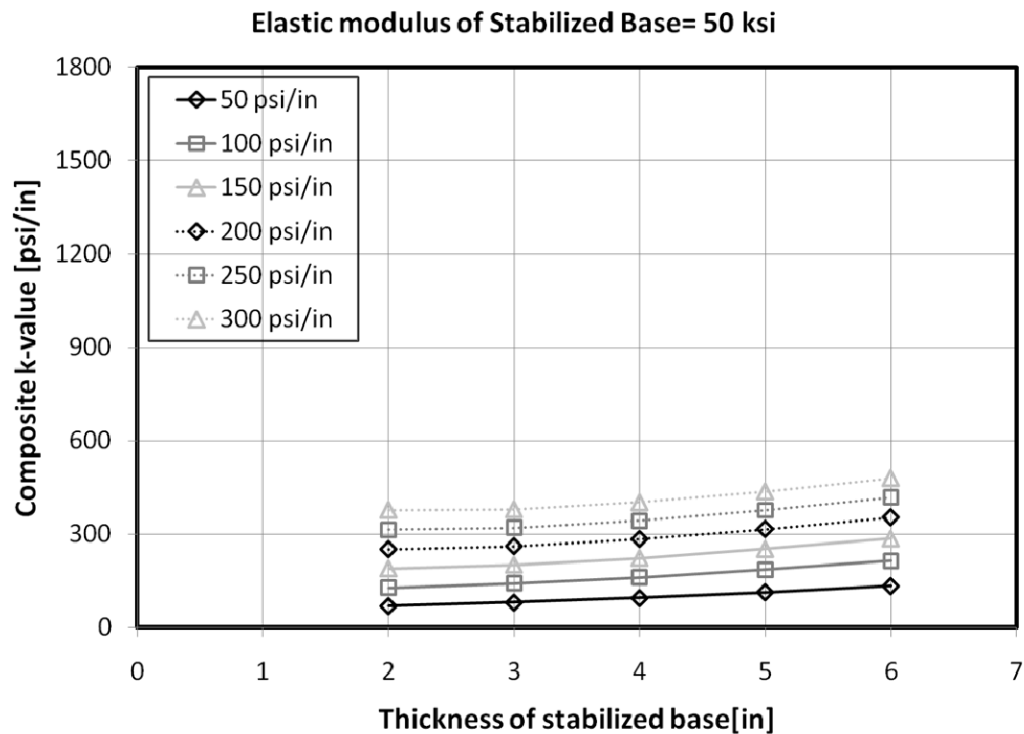
Figure A 4. Effects of thickness of stabilized base on composite *k*-value (4)
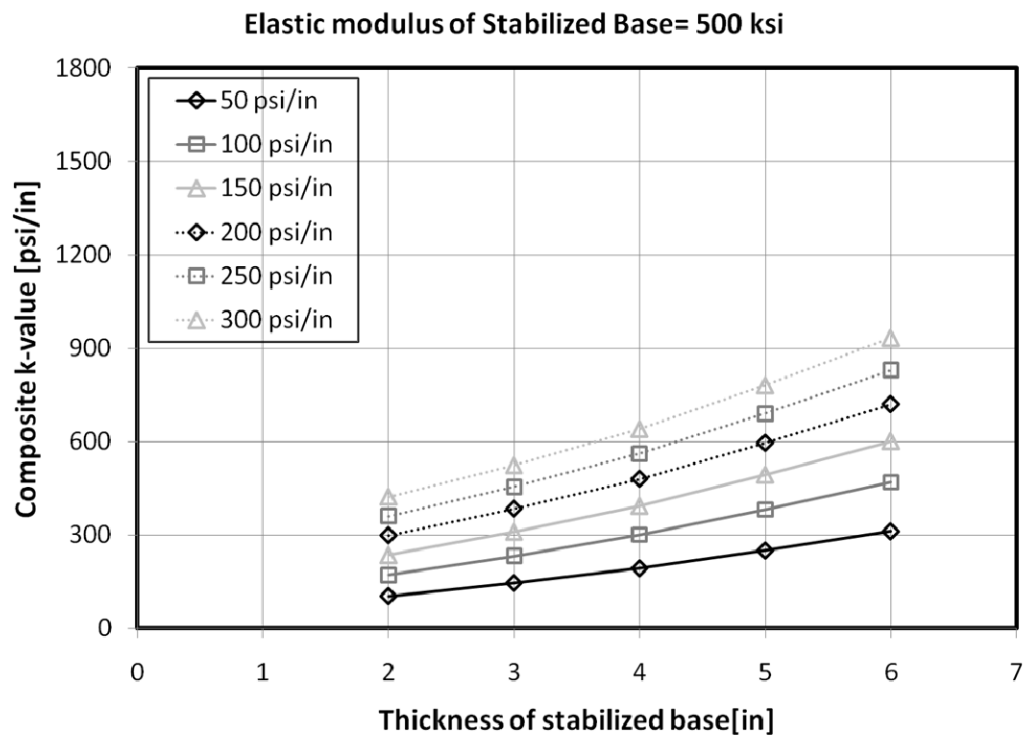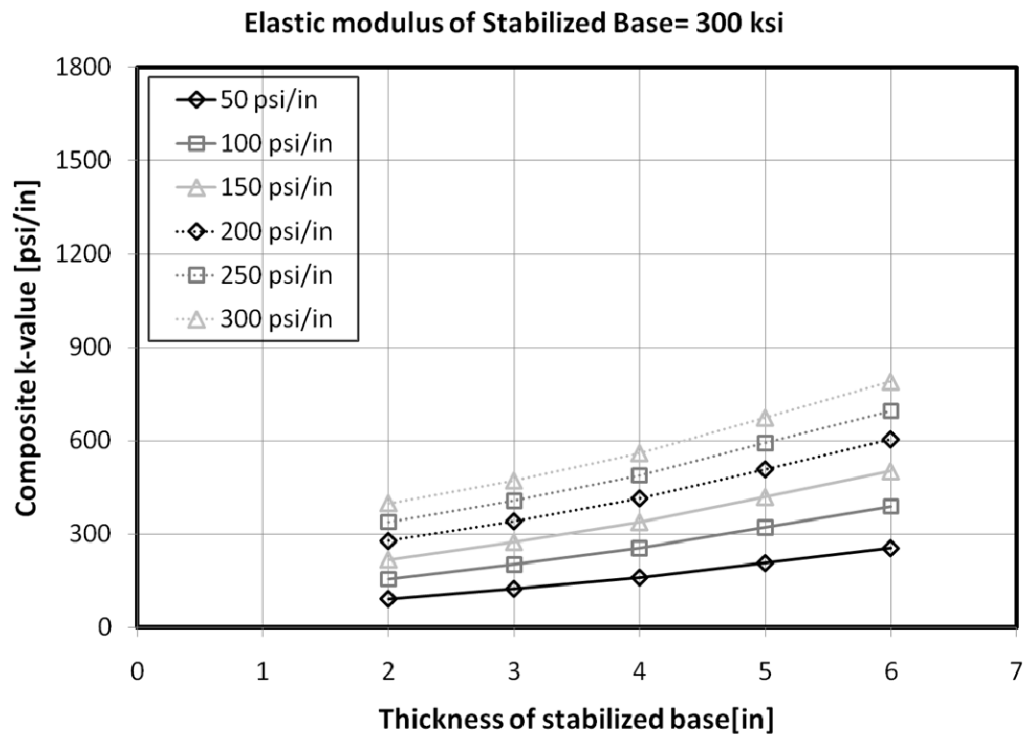
Figure A 5. Effects of thickness of stabilized base on composite *k*-value (5)
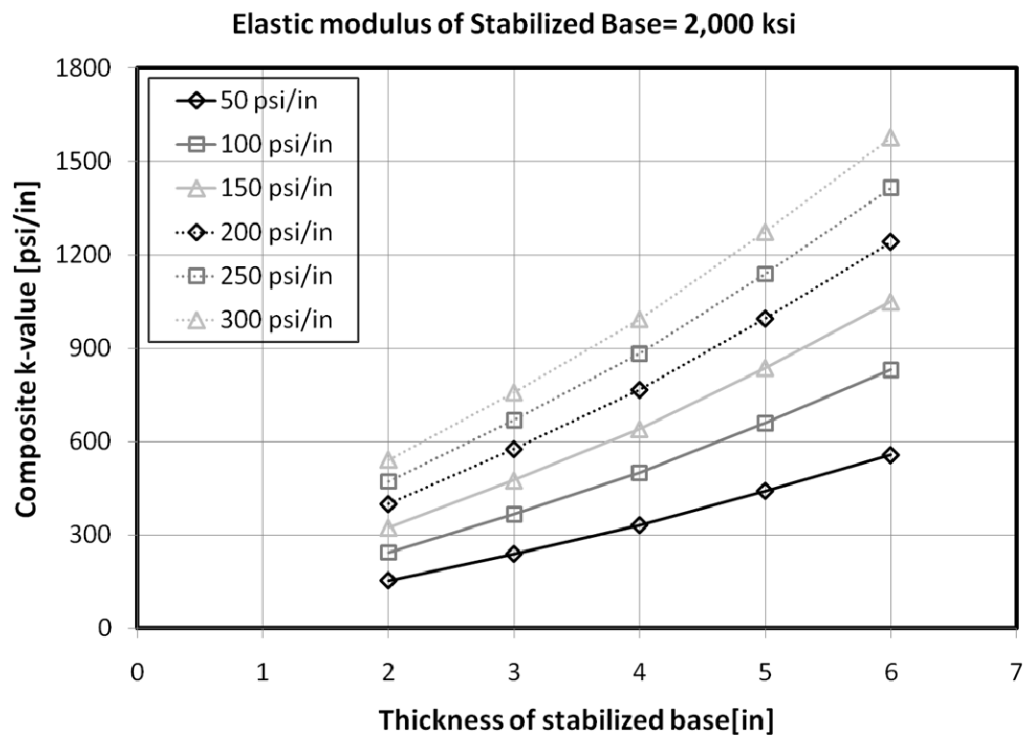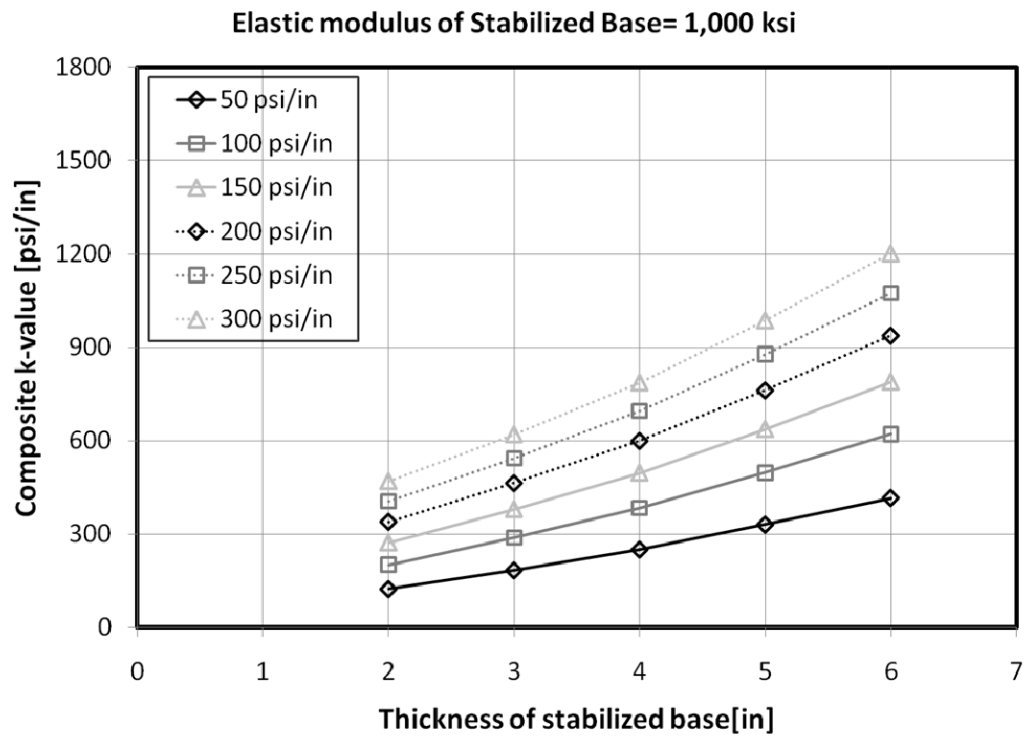
Figure A 6. Effects of thickness of stabilized base on composite *k*-value (6)

Effects of Modulus of Elasticity of Base Material on Composite k-value
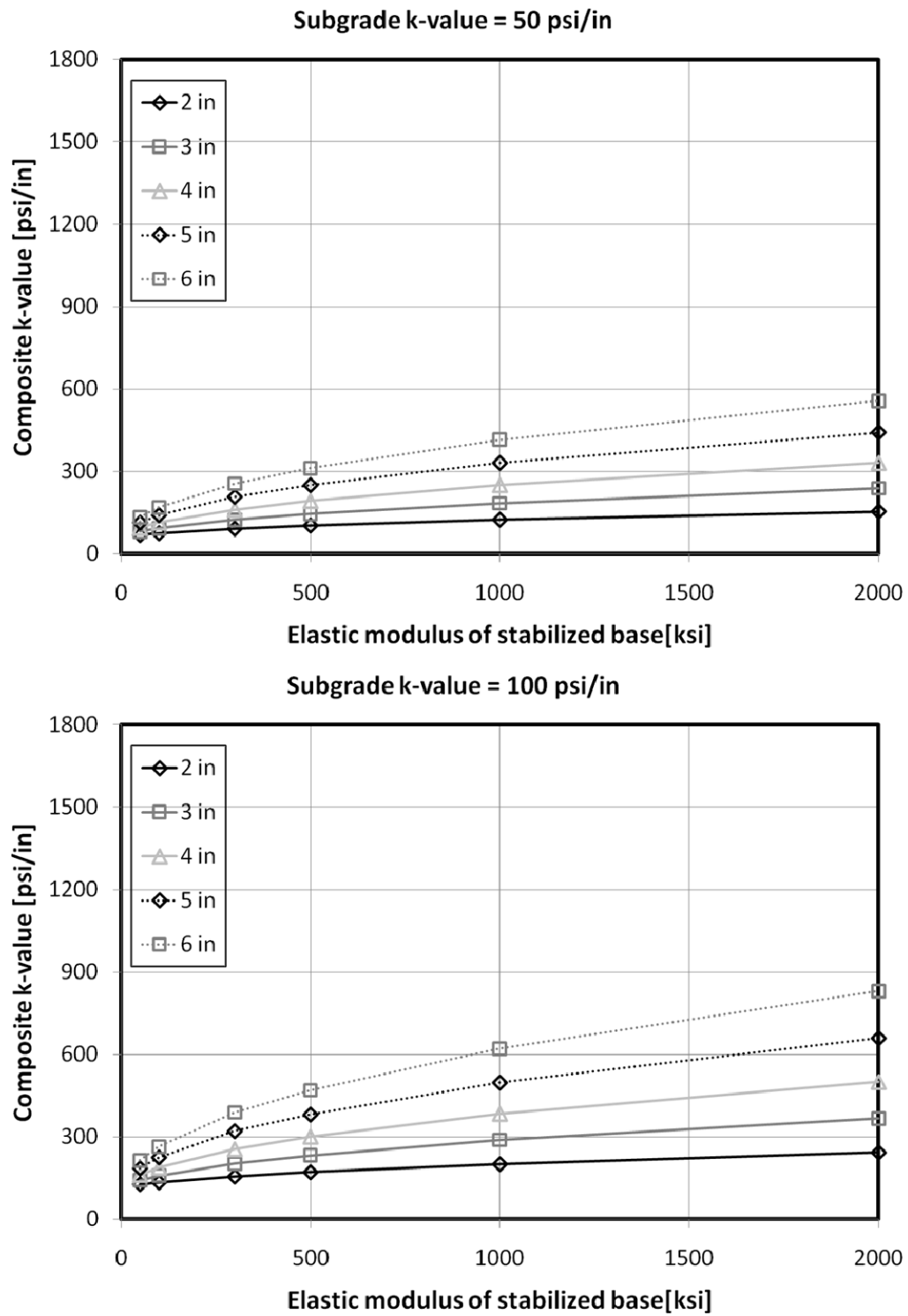
Figure A 7. Effects of elastic modulus of base on composite *k*-value (1)
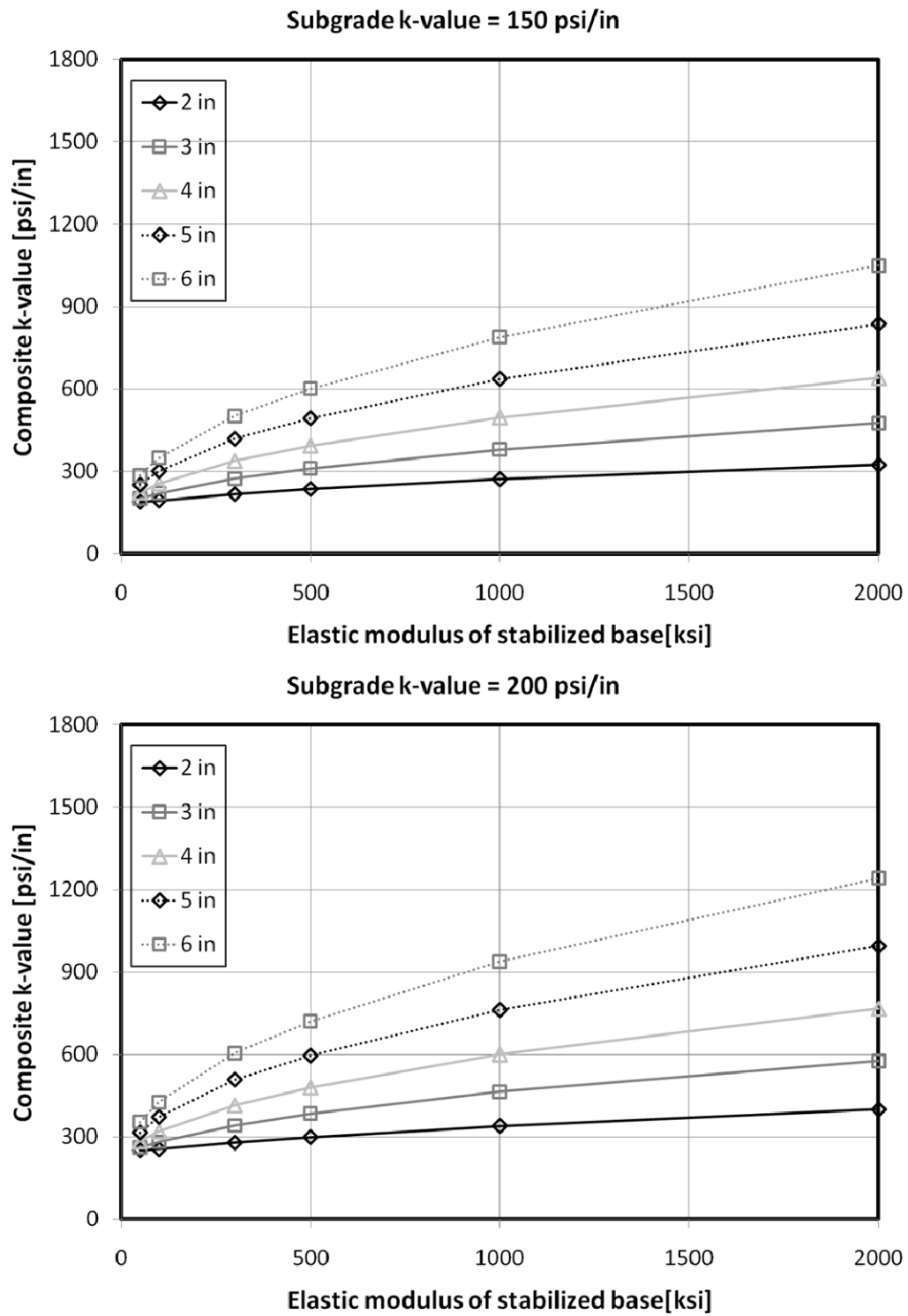
Figure A 8. Effects of elastic modulus of base on composite *k*-value (2)
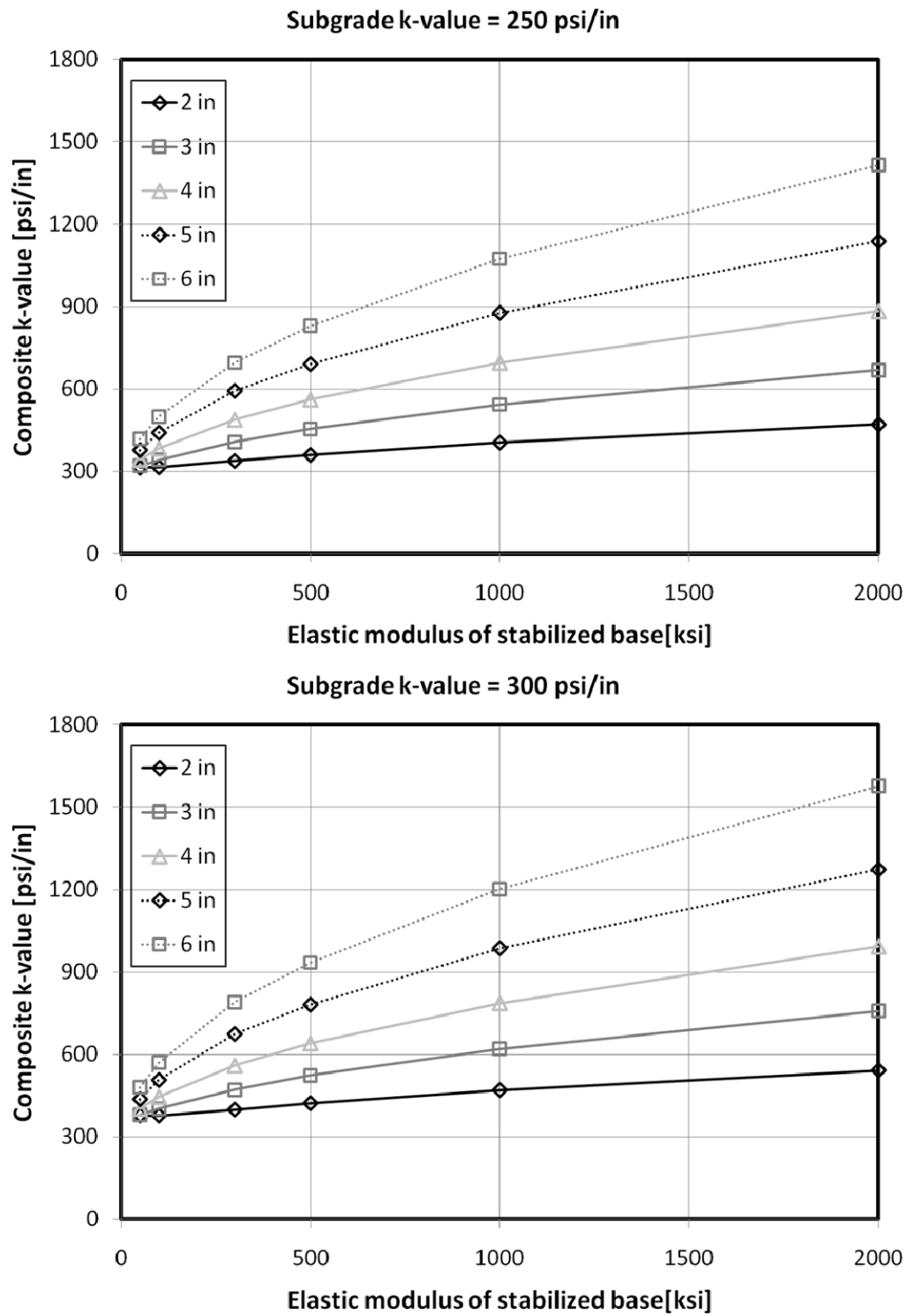
Figure A 9. Effects of elastic modulus of base on composite *k*-value (3)

Thickness of Stabilized Base= 2 in

Thickness of Stabilized Base= 3 in
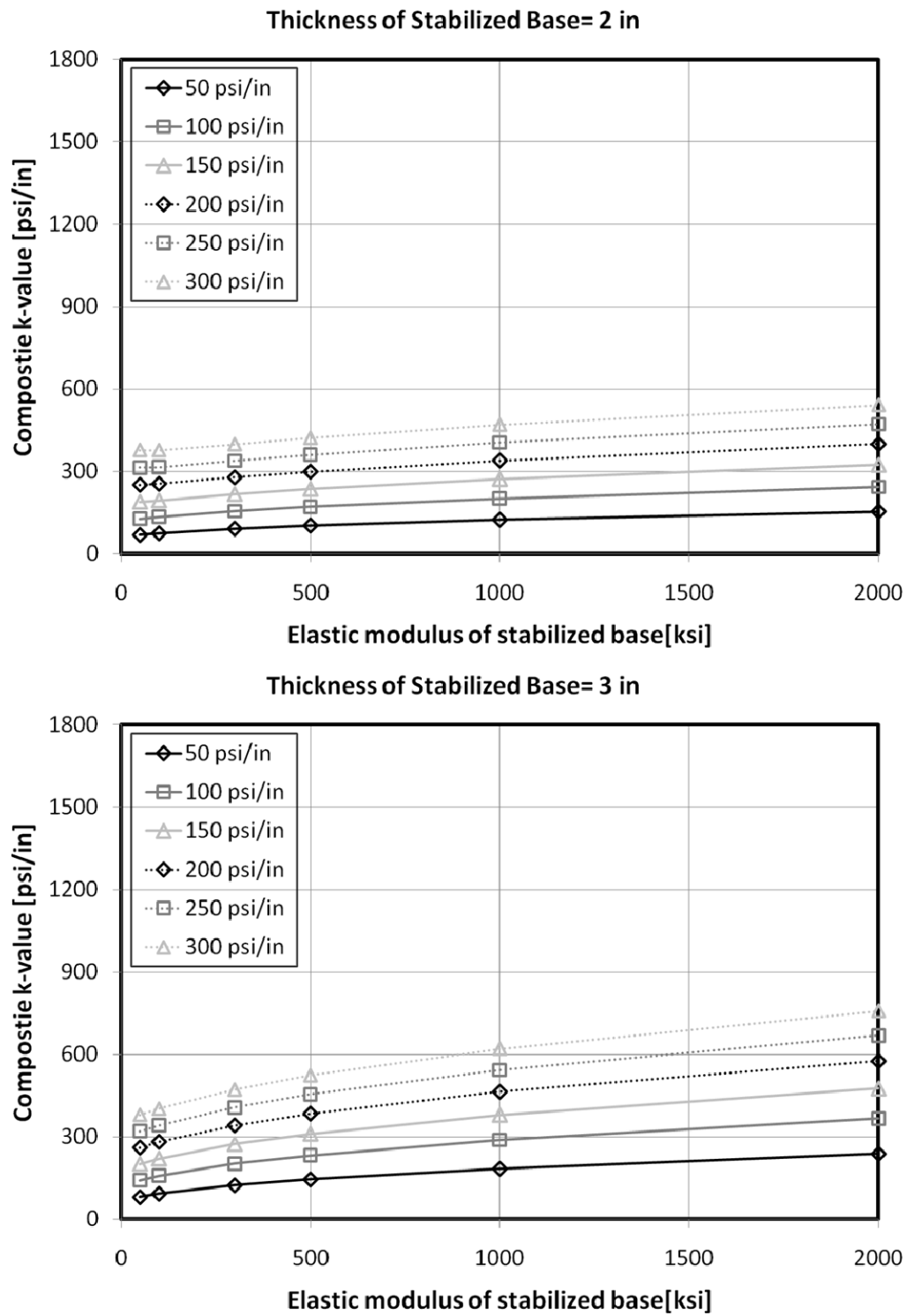
Figure A 10. Effects of elastic modulus of base on composite *k*-value (4)
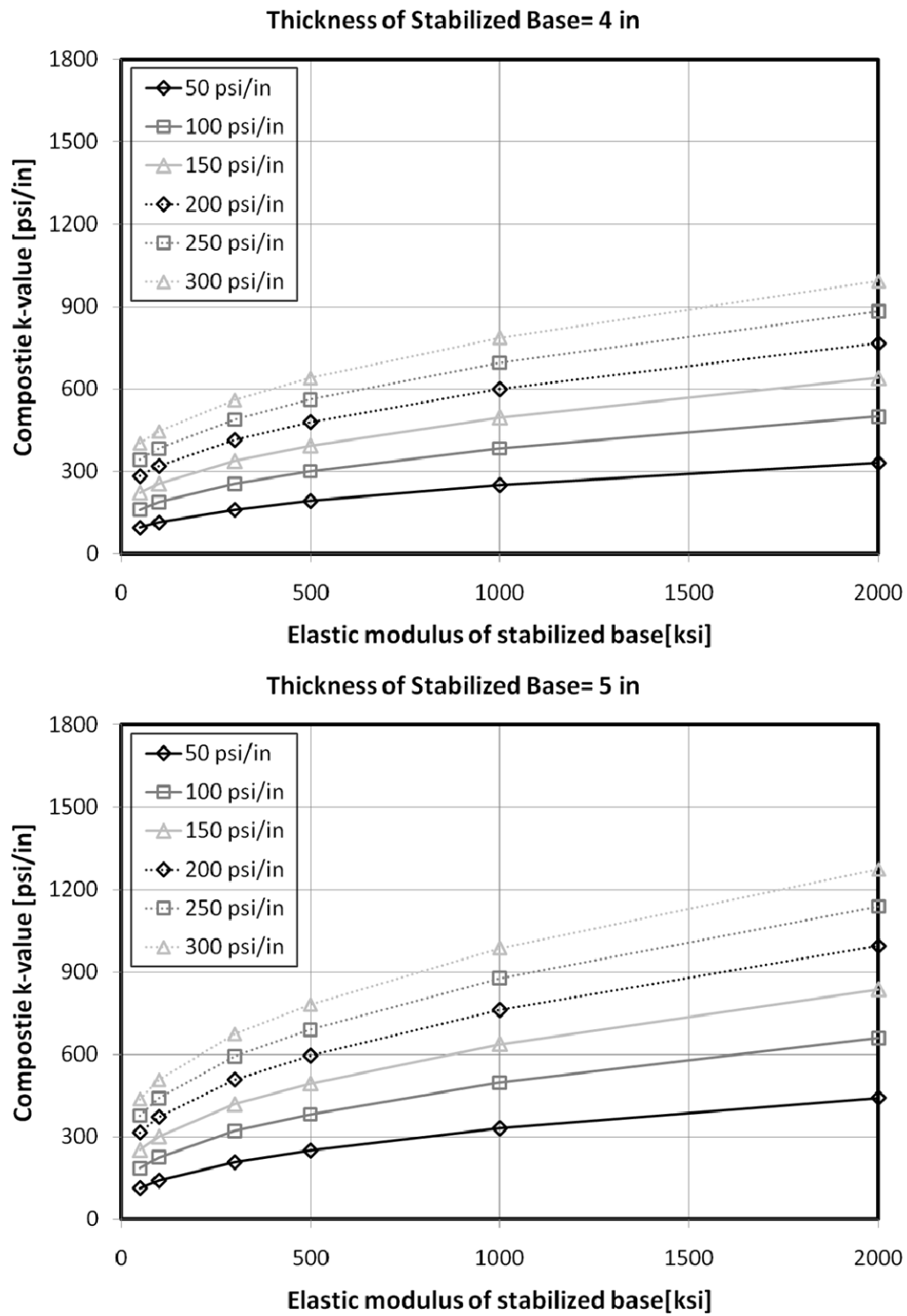
Figure A 11. Effects of elastic modulus of base on composite _k_-value (5)
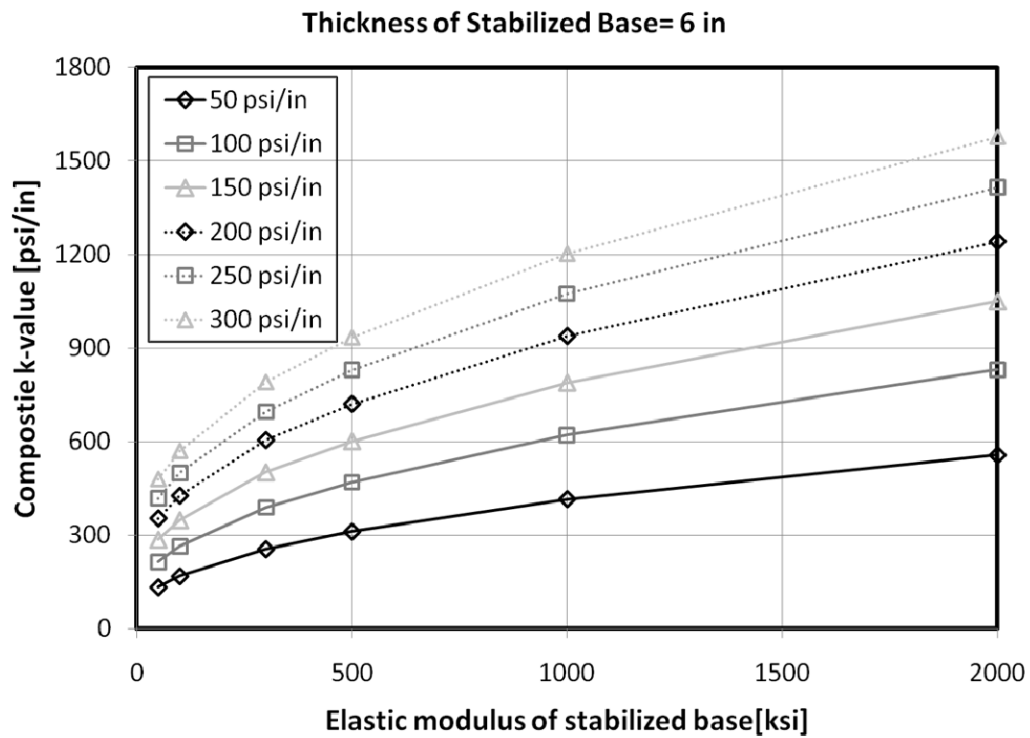
Figure A 12. Effects of elastic modulus of base on composite *k*-value (6)

➢ *Effects of k-value of Subgrade Layer on Composite k-value*
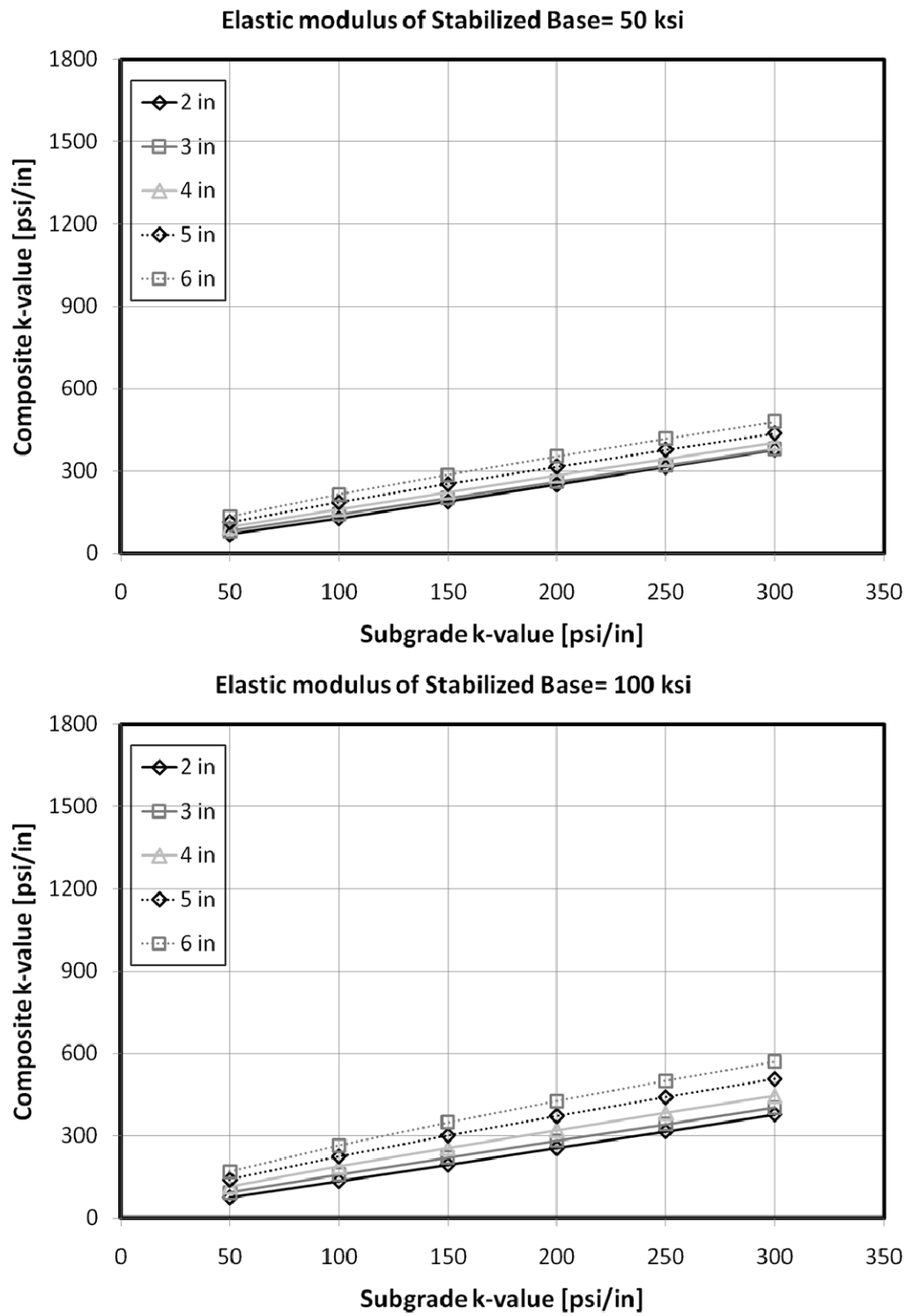
Figure A 13. Effects of *k*-value of subgrade layer on composite *k*-value (1)
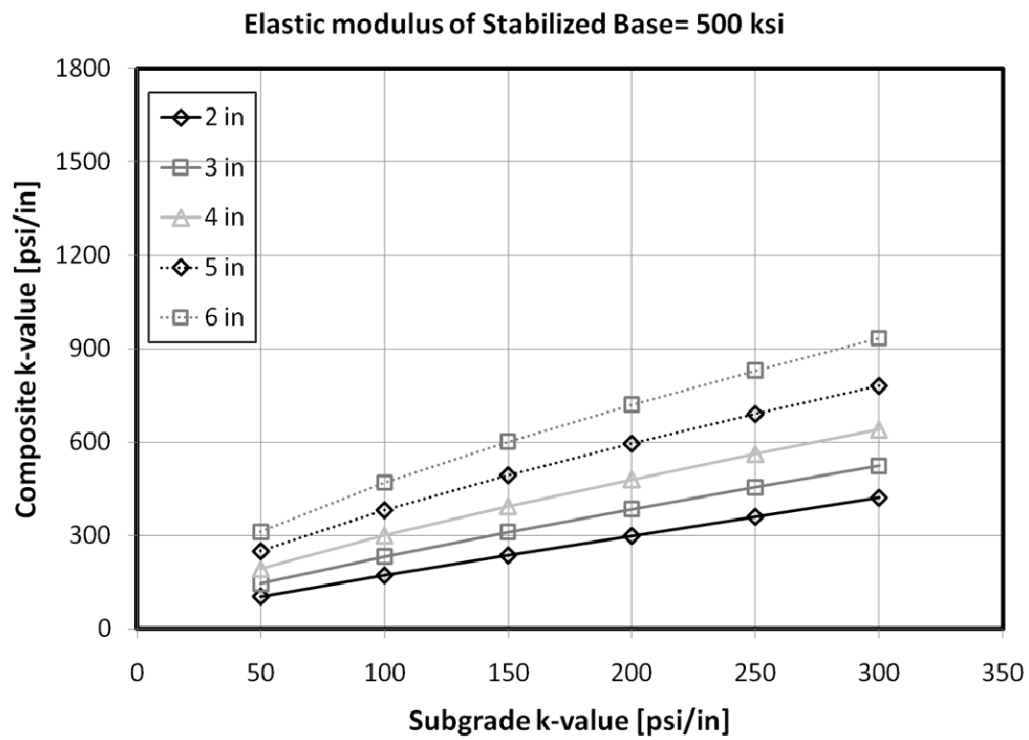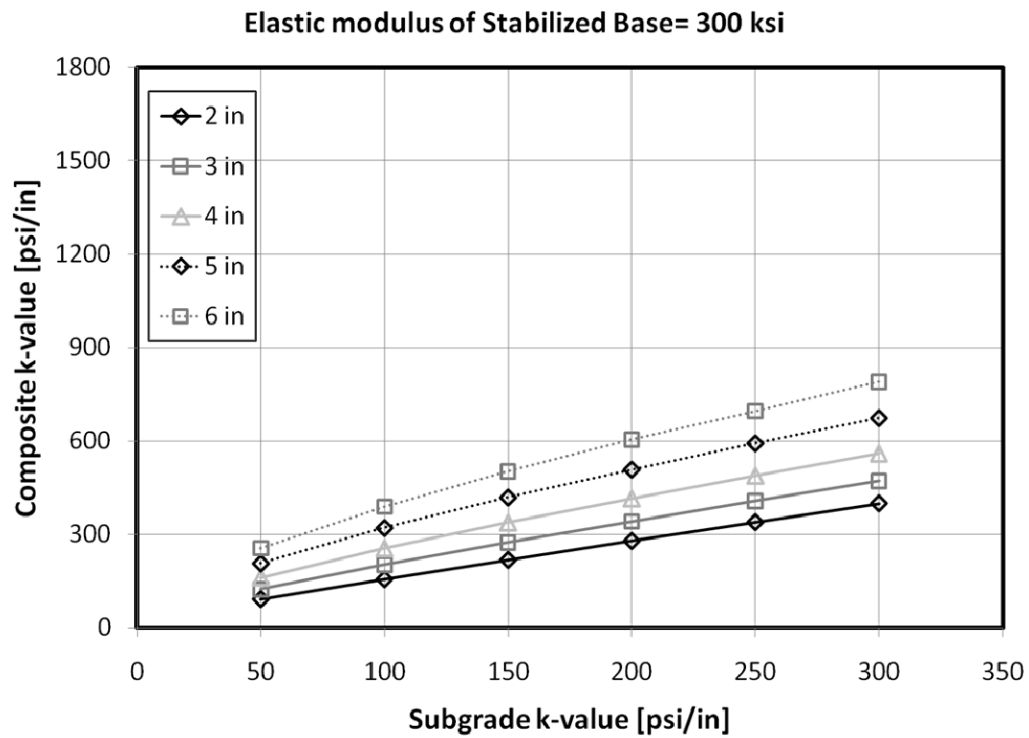
Figure A 14. Effects of *k*-value of subgrade layer on composite *k*-value (2)
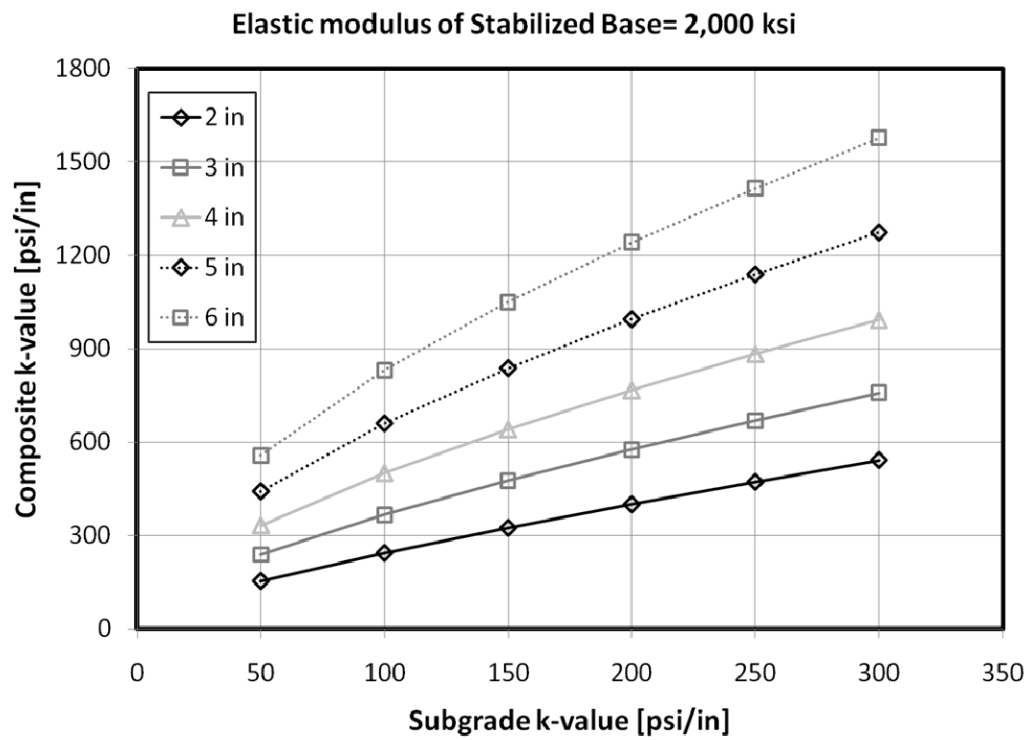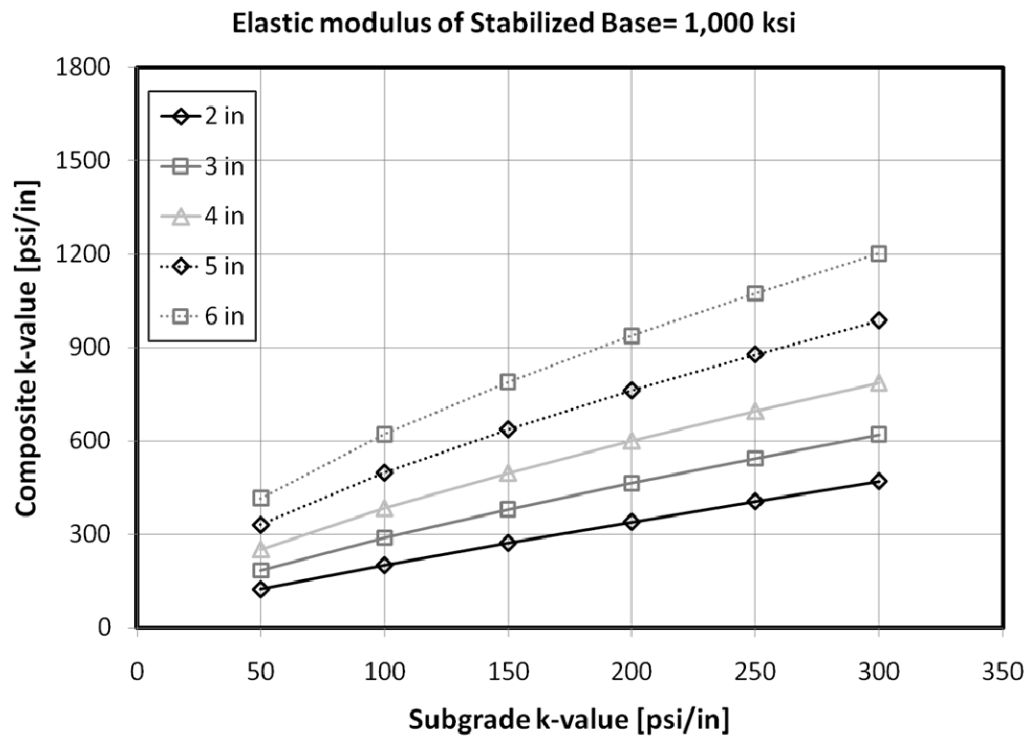
Figure A 15. Effects of *k*-value of subgrade layer on composite *k*-value (3)
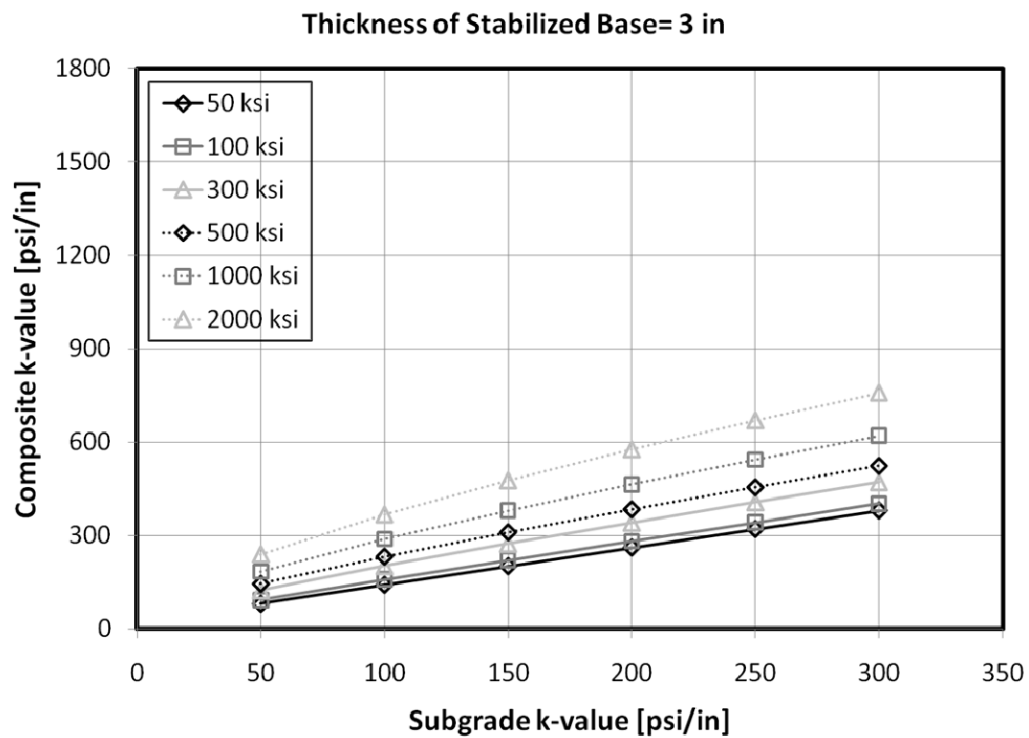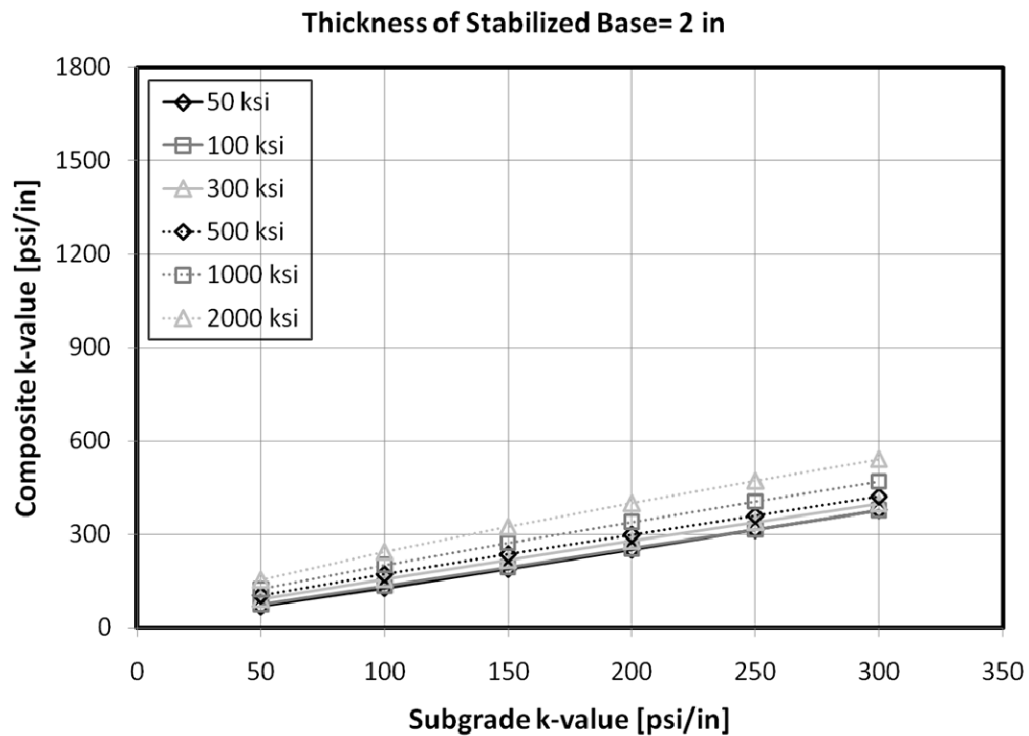
Figure A 16. Effects of *k*-value of subgrade layer on composite *k*-value (4)
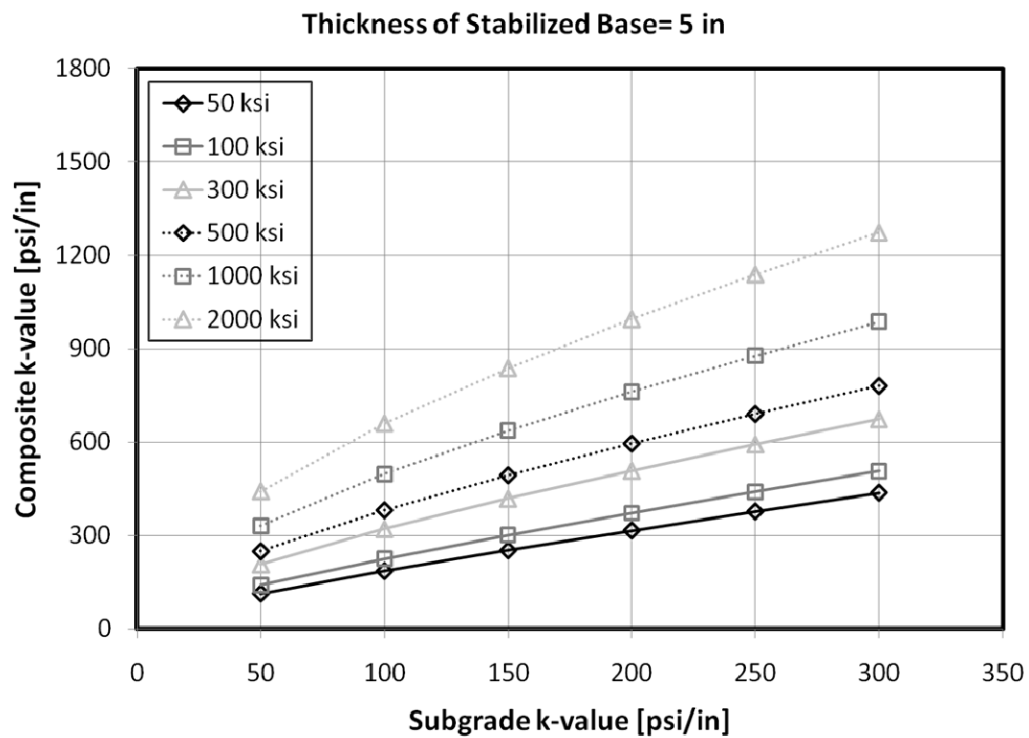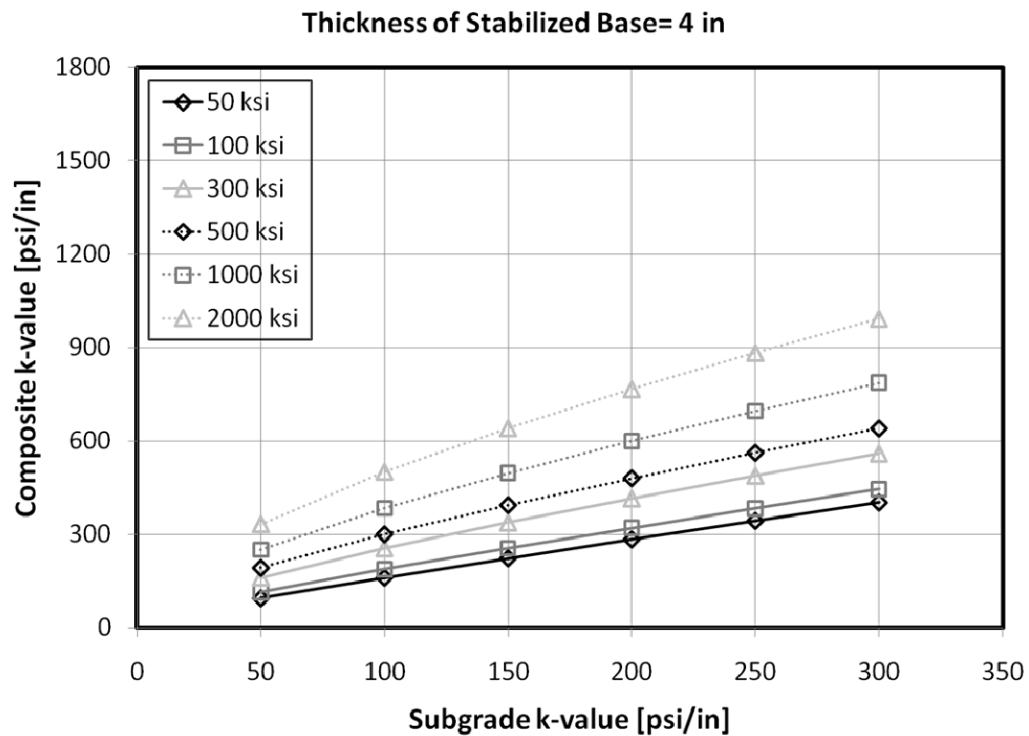
Figure A 17. Effects of *k*-value of subgrade layer on composite *k*-value (5)
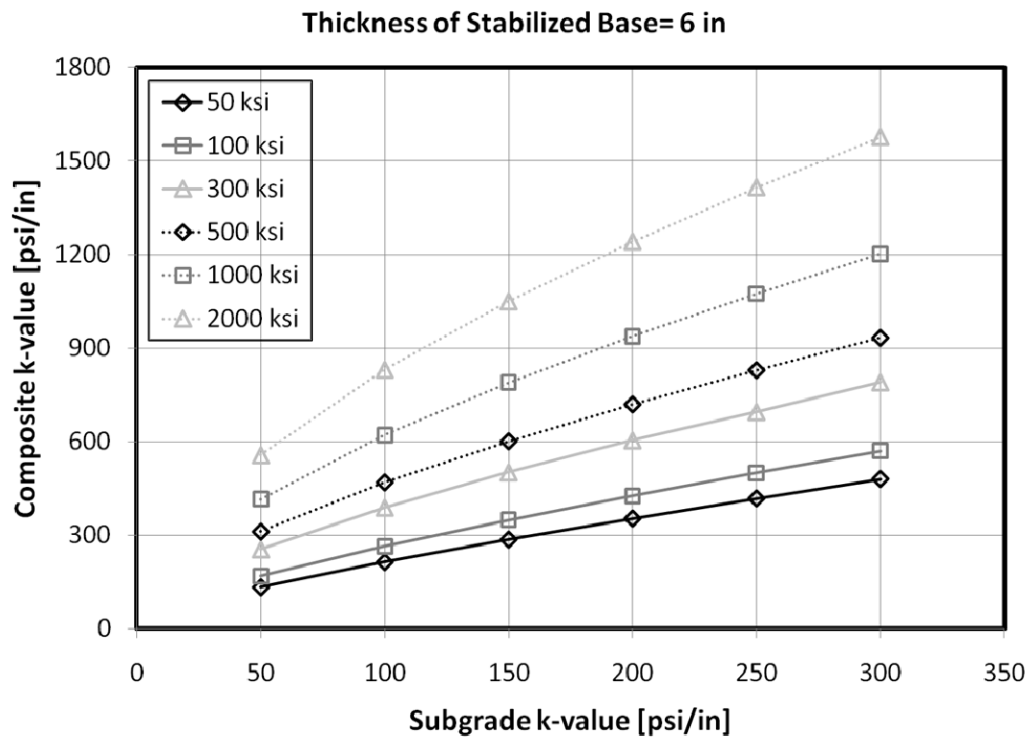
Figure A 18. Effects of *k*-value of subgrade layer on composite *k*-value (6)

APPENDIX B

Effects of Support Layer Properties on Maximum Critical Stress
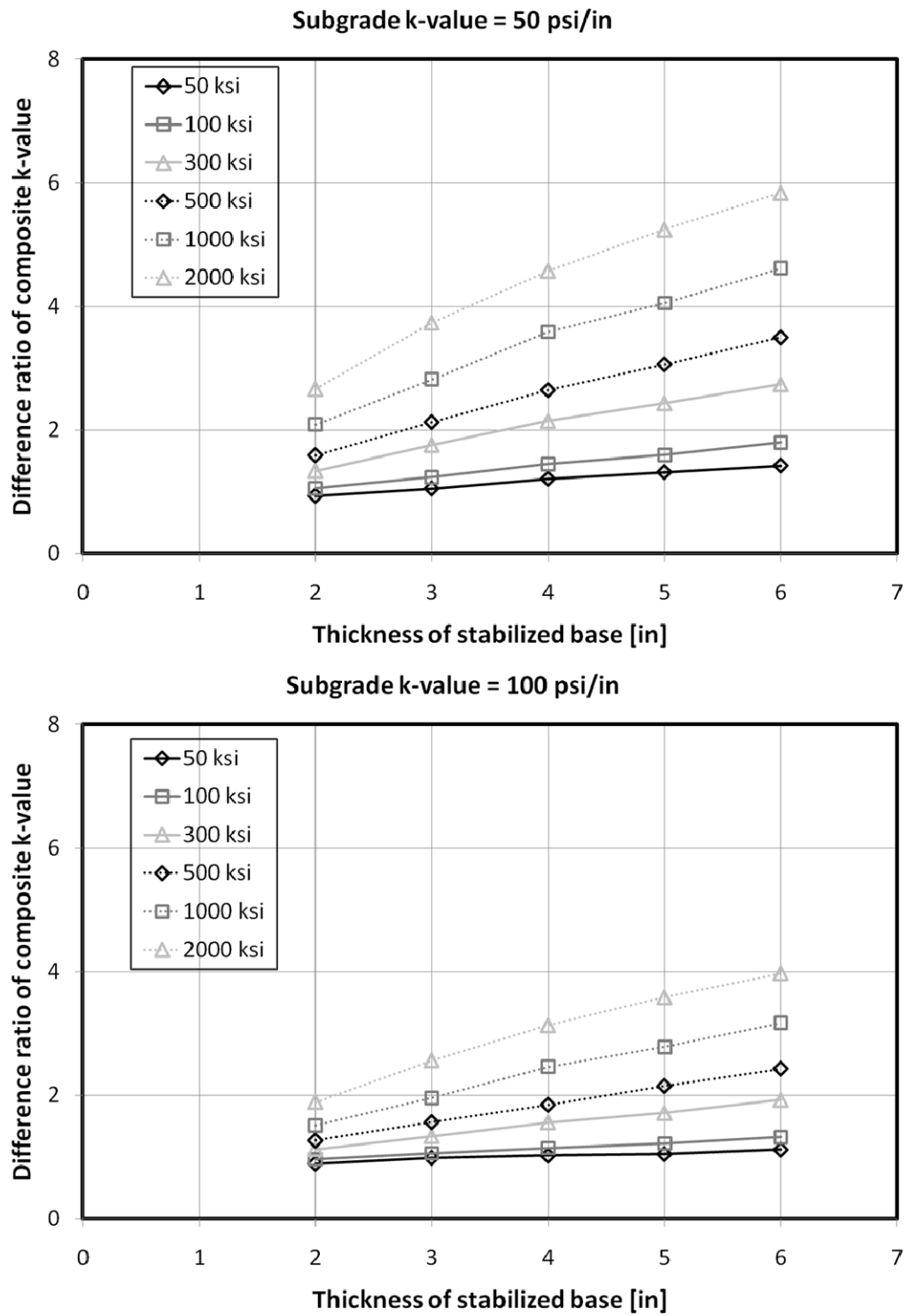**under Temperature and Wheel Loadings**
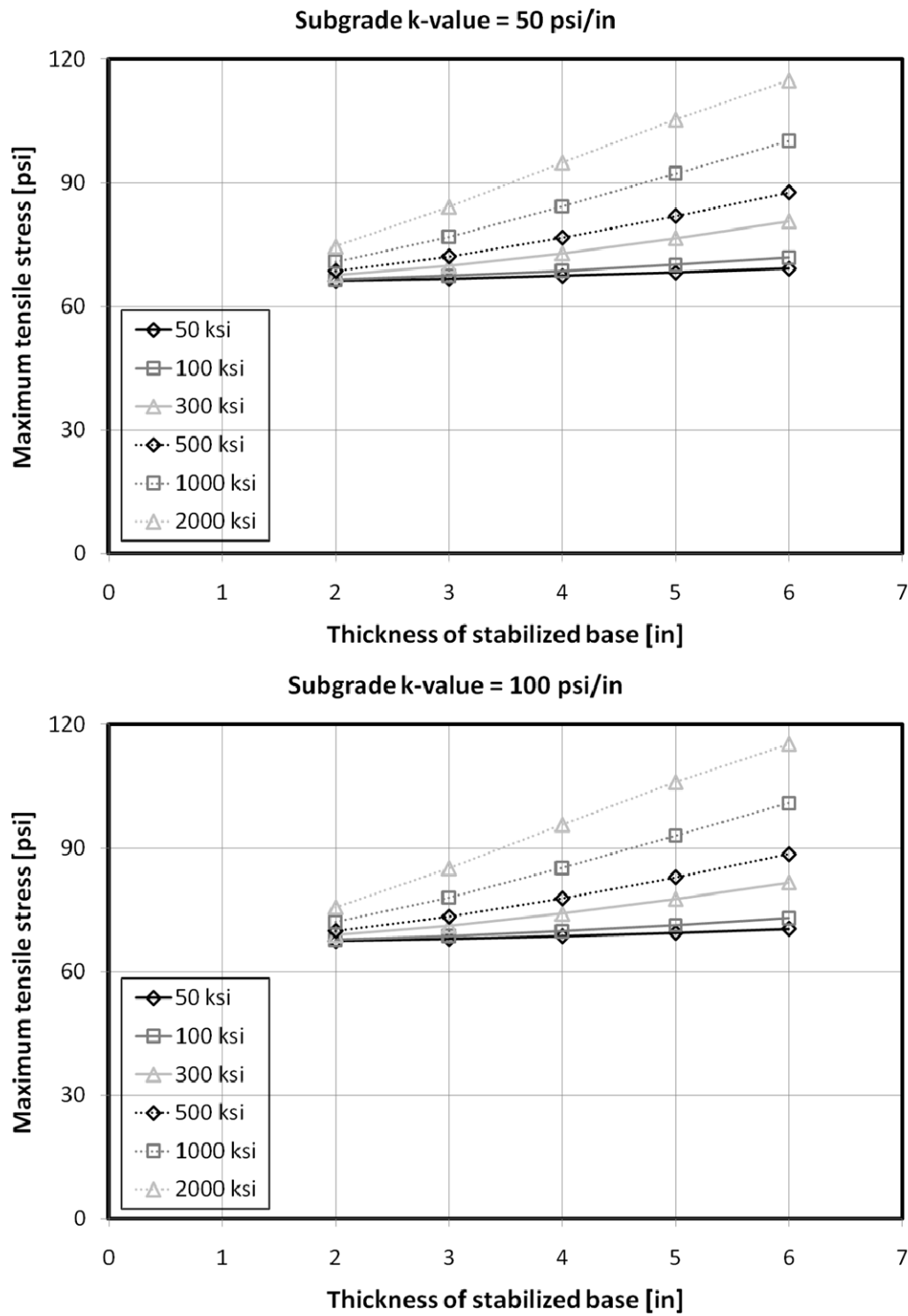
Figure B 1. Effects of thickness of stabilized base under temperature loading (1)
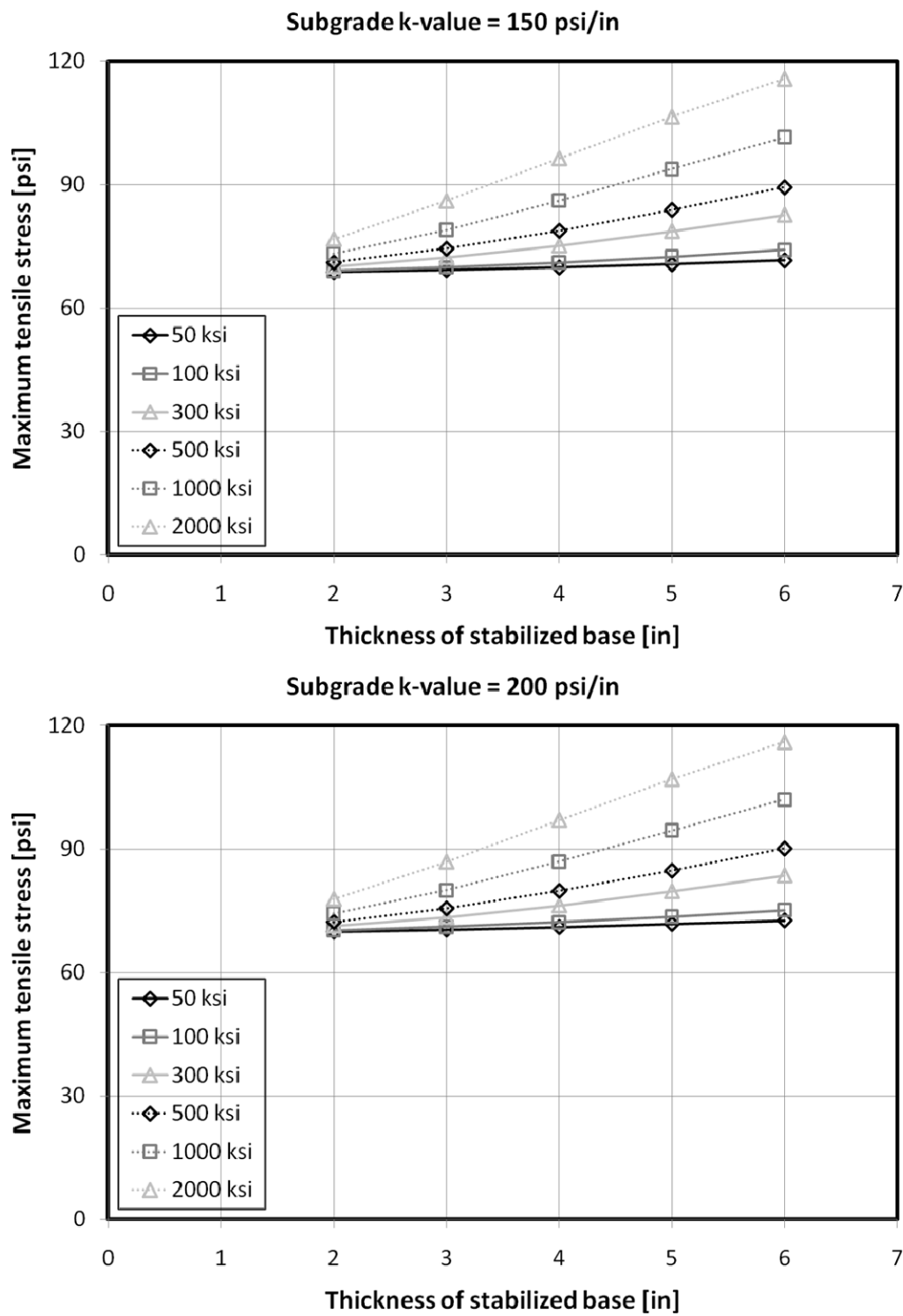
Figure B 2. Effects of thickness of stabilized base under temperature loading (2)

234
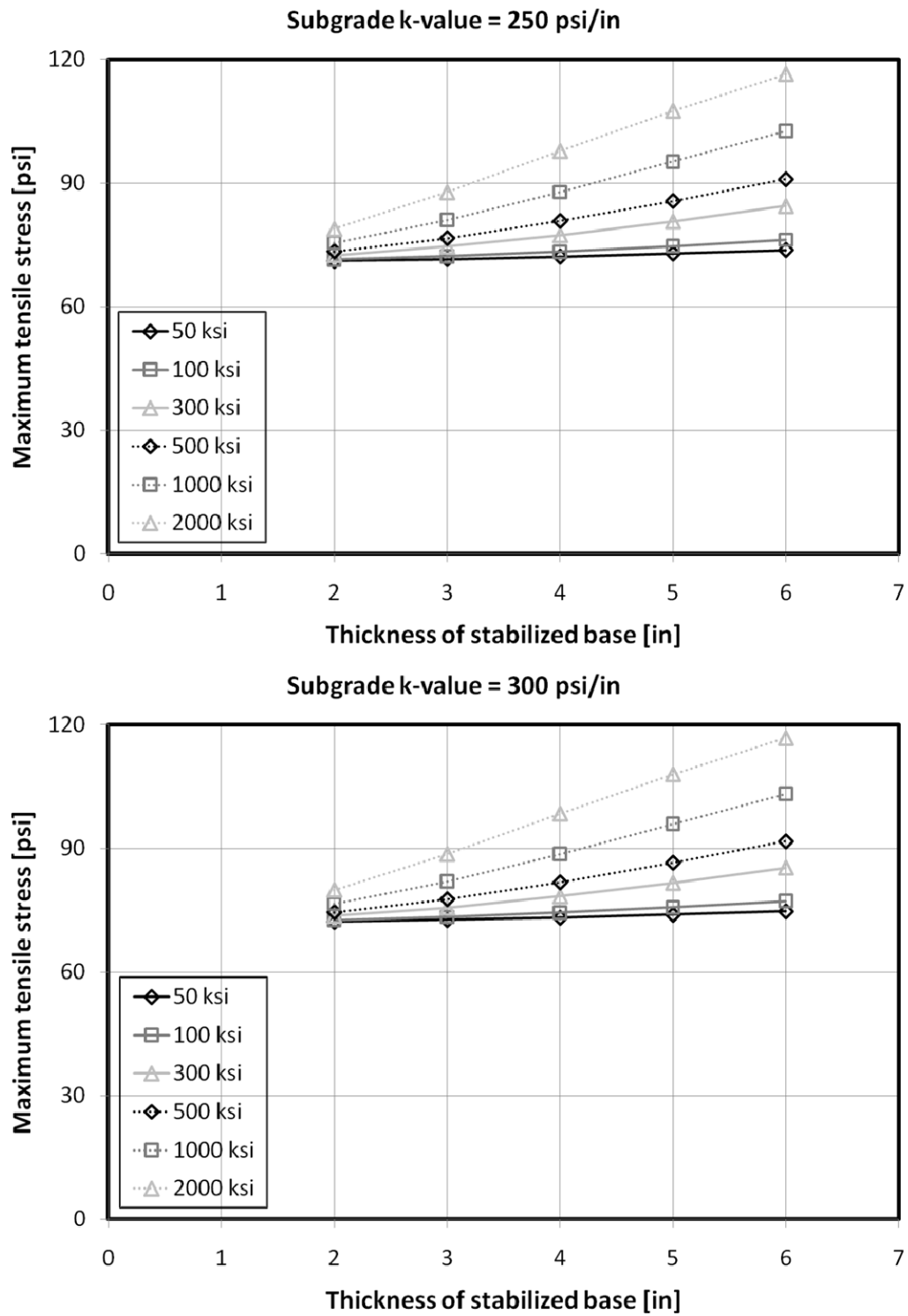
Figure B 3. Effects of thickness of stabilized base under temperature loading (3)
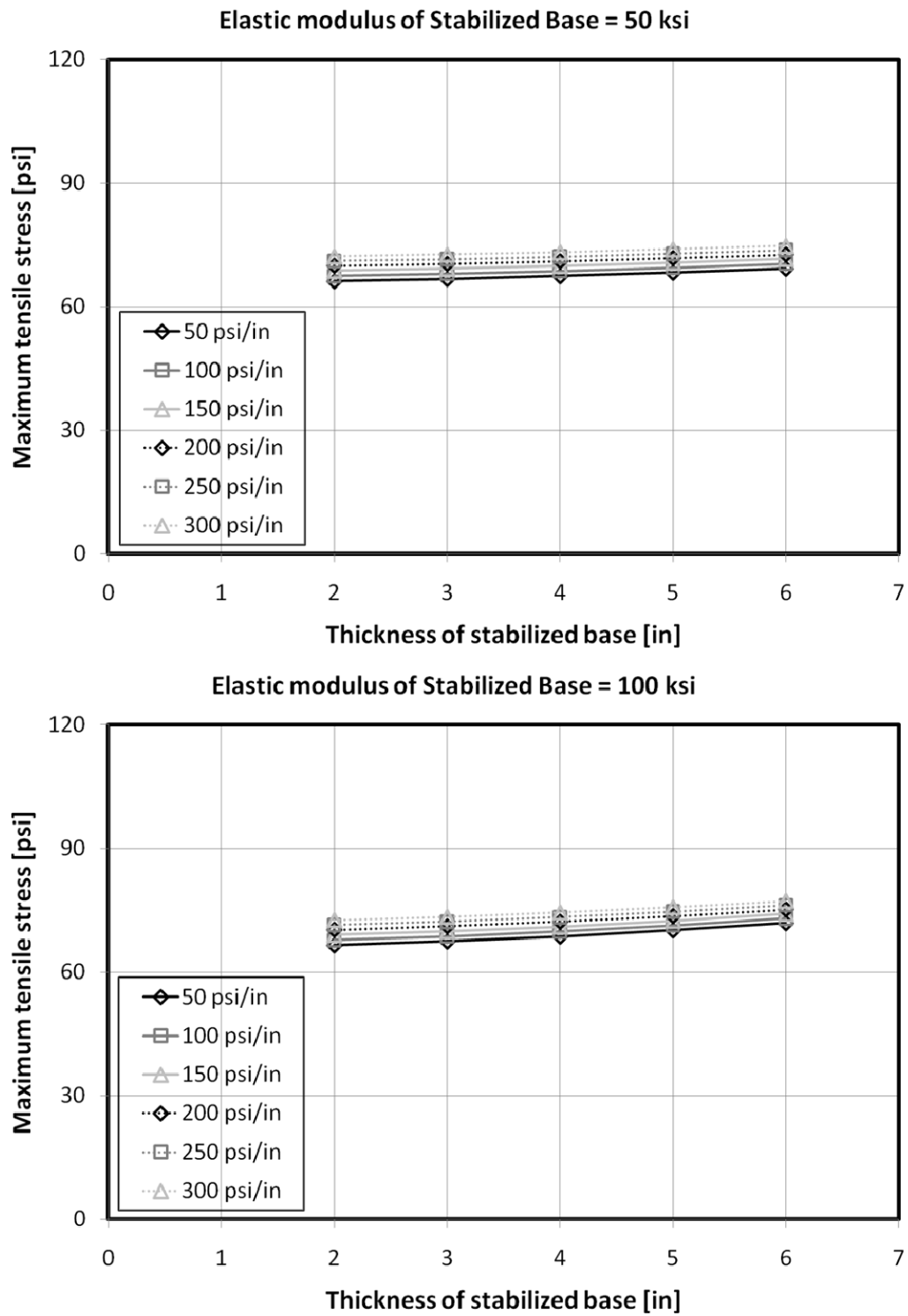
Figure B 4. Effects of thickness of stabilized base under temperature loading (4)
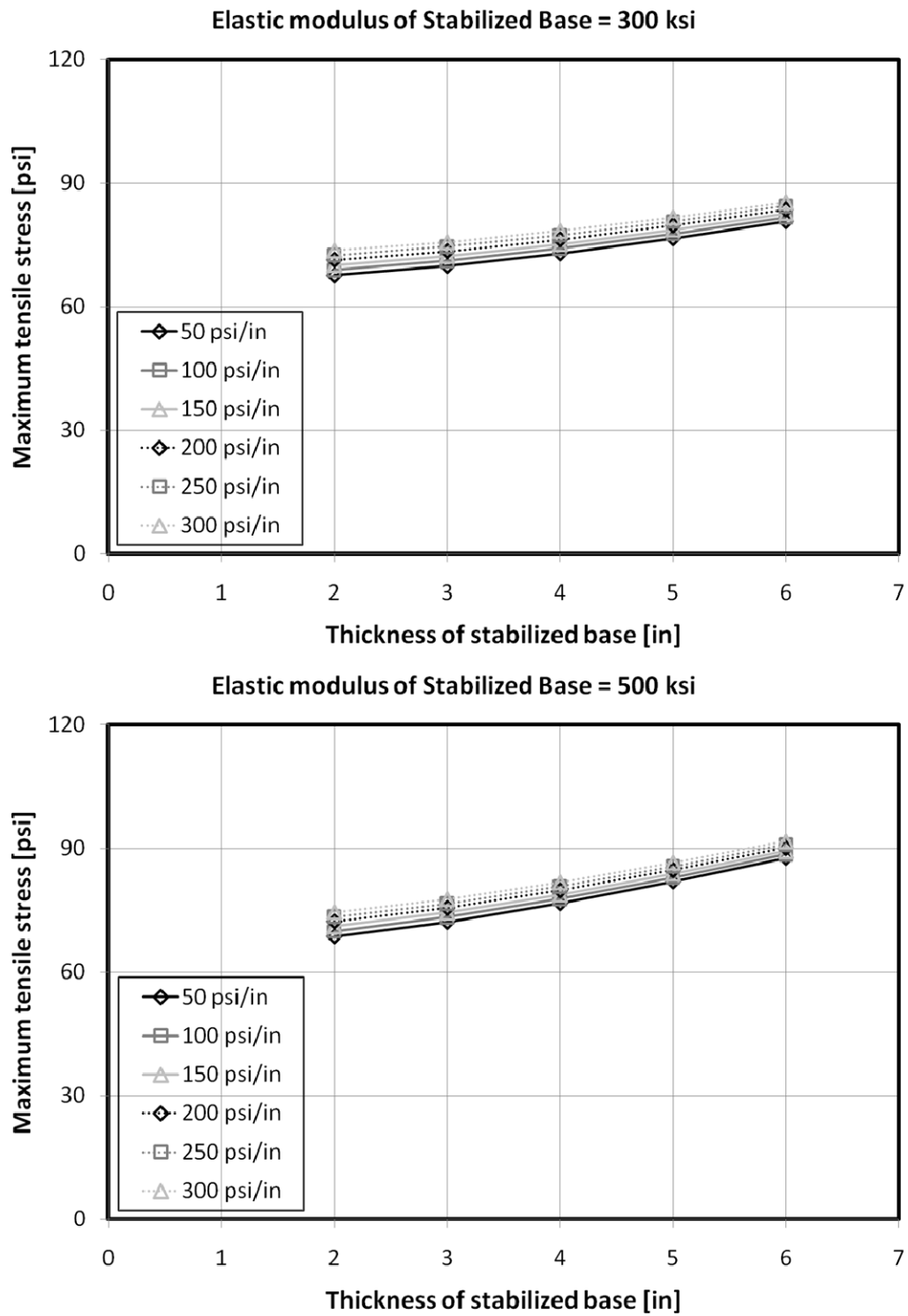
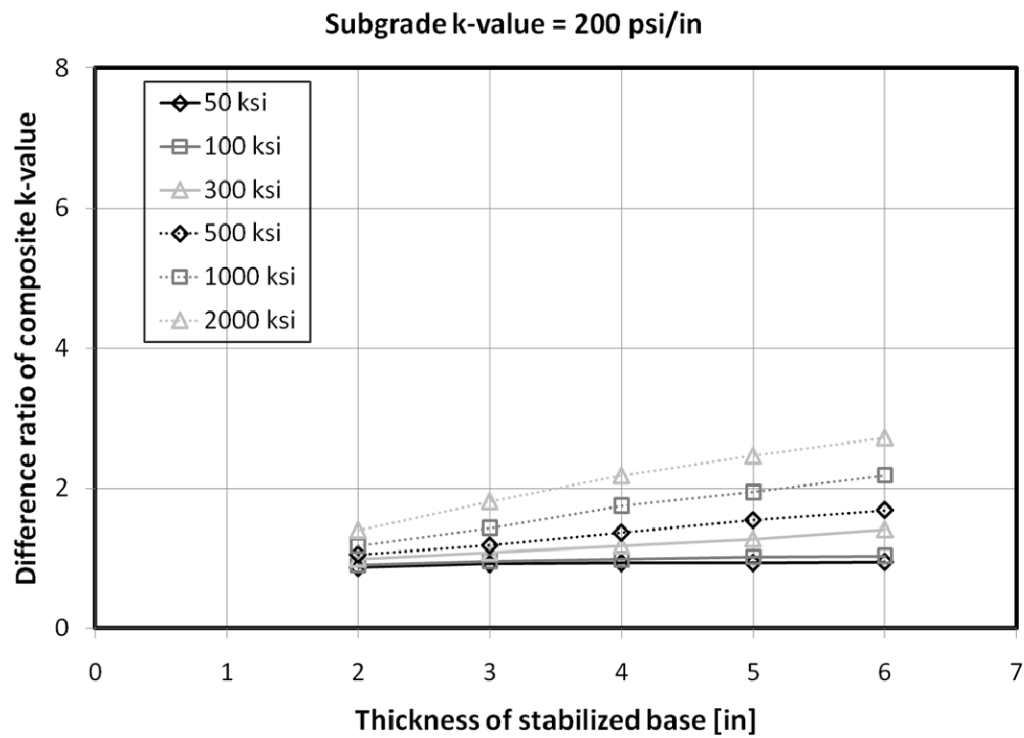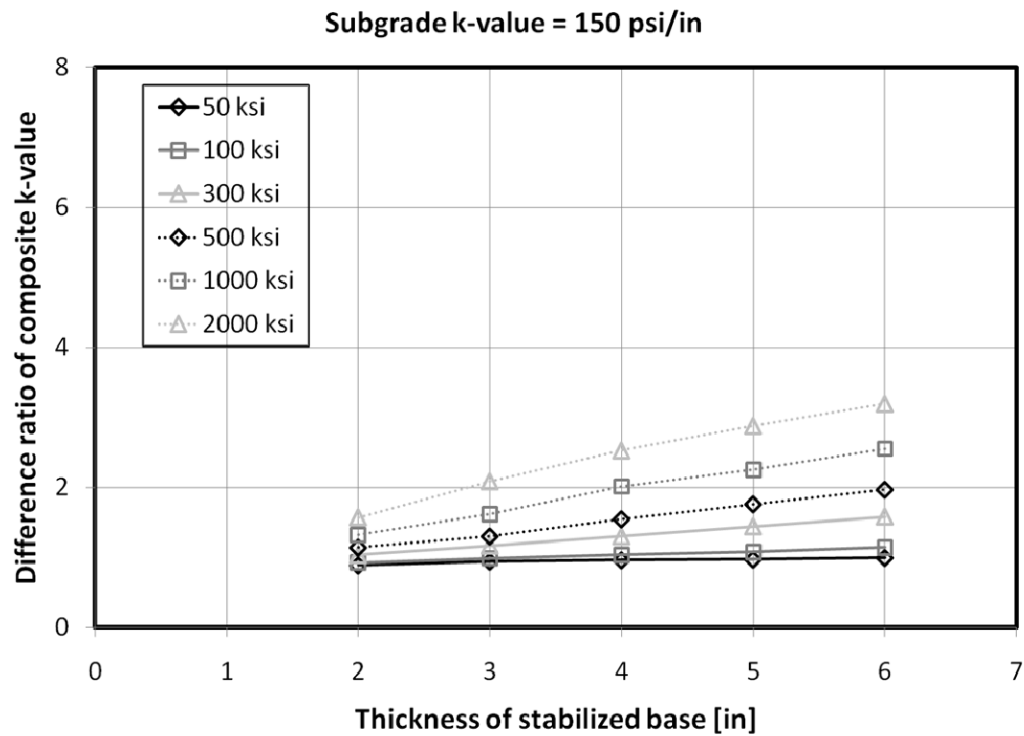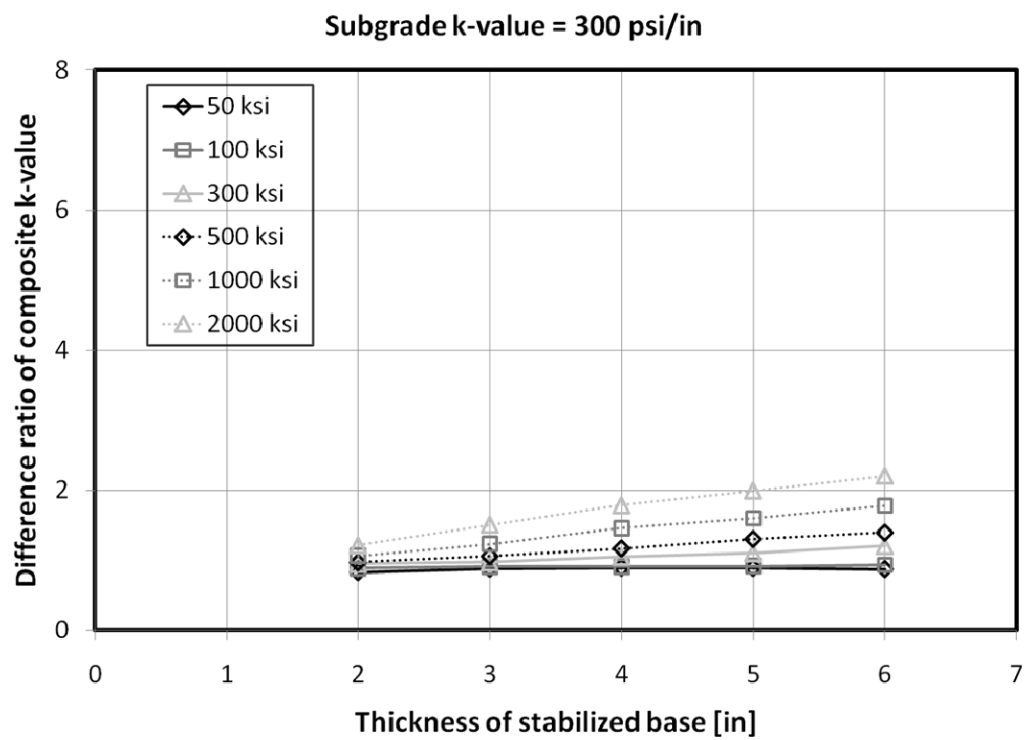**Figure B 5. Effects of thickness of stabilized base under temperature loading (5)**
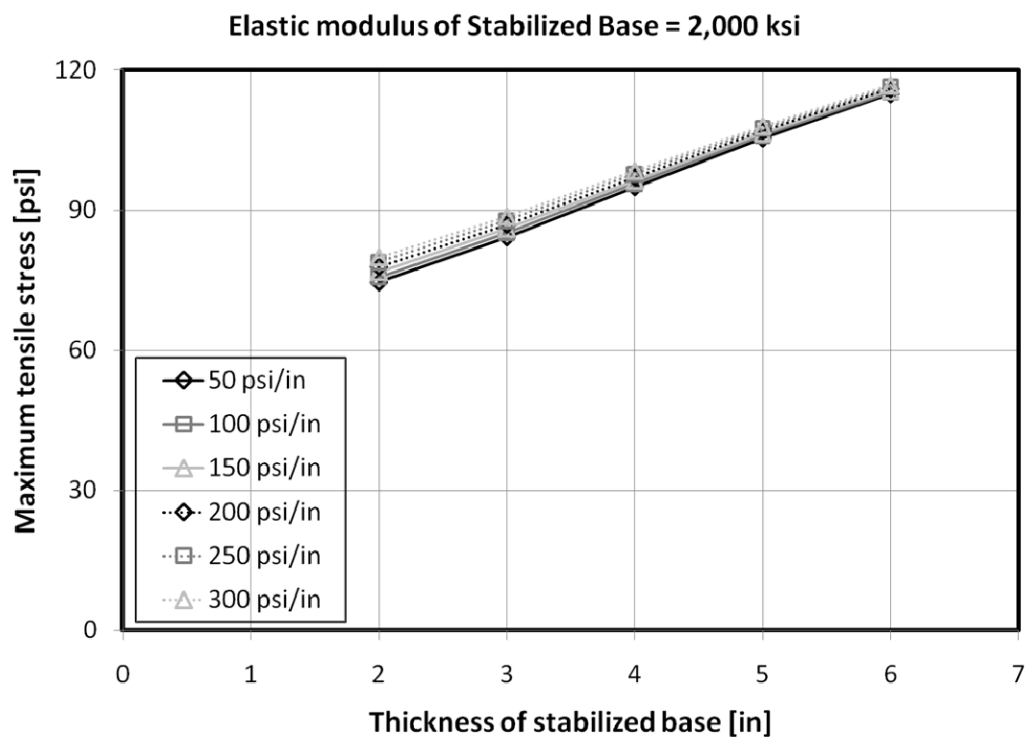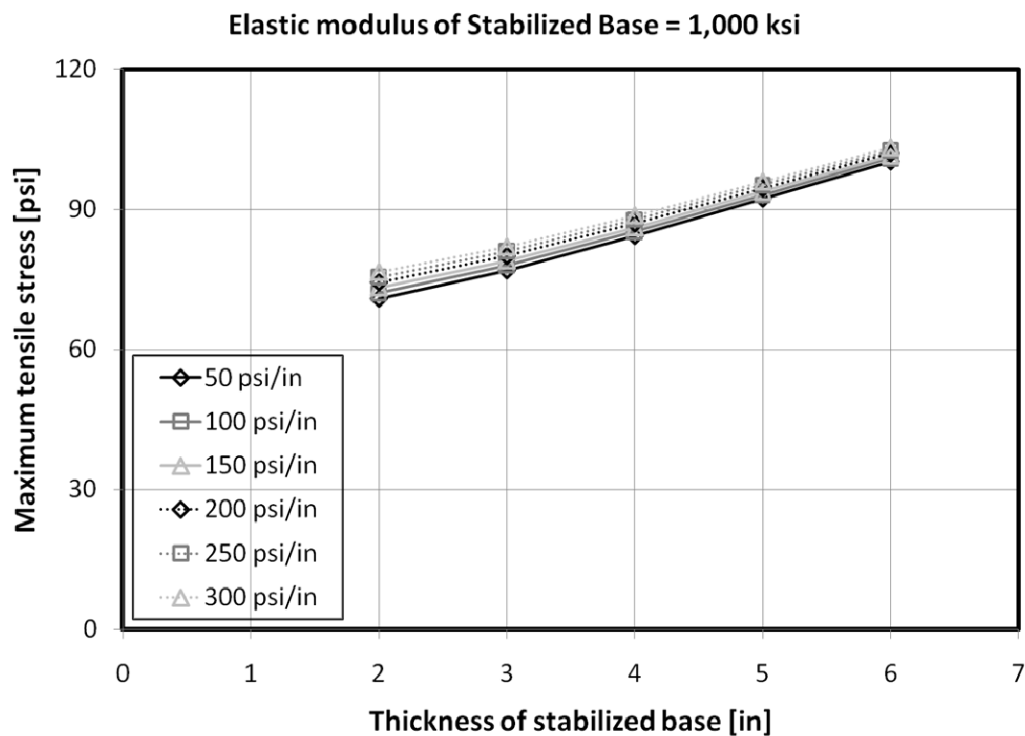
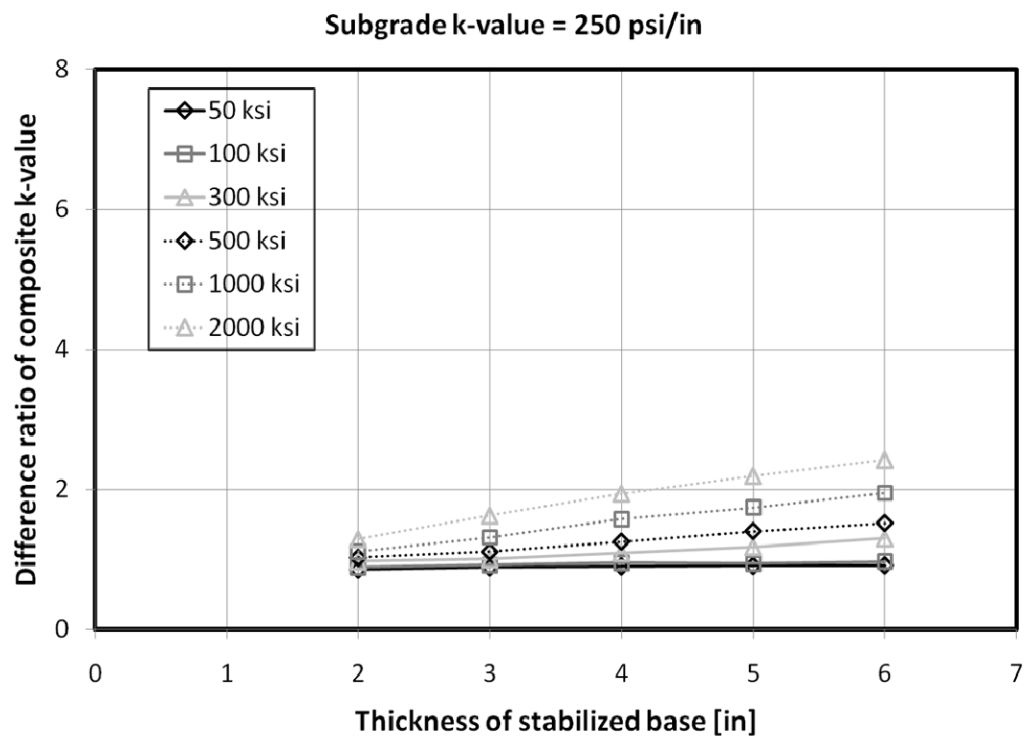**Figure B 6. Effects of thickness of stabilized base under temperature loading (6)**
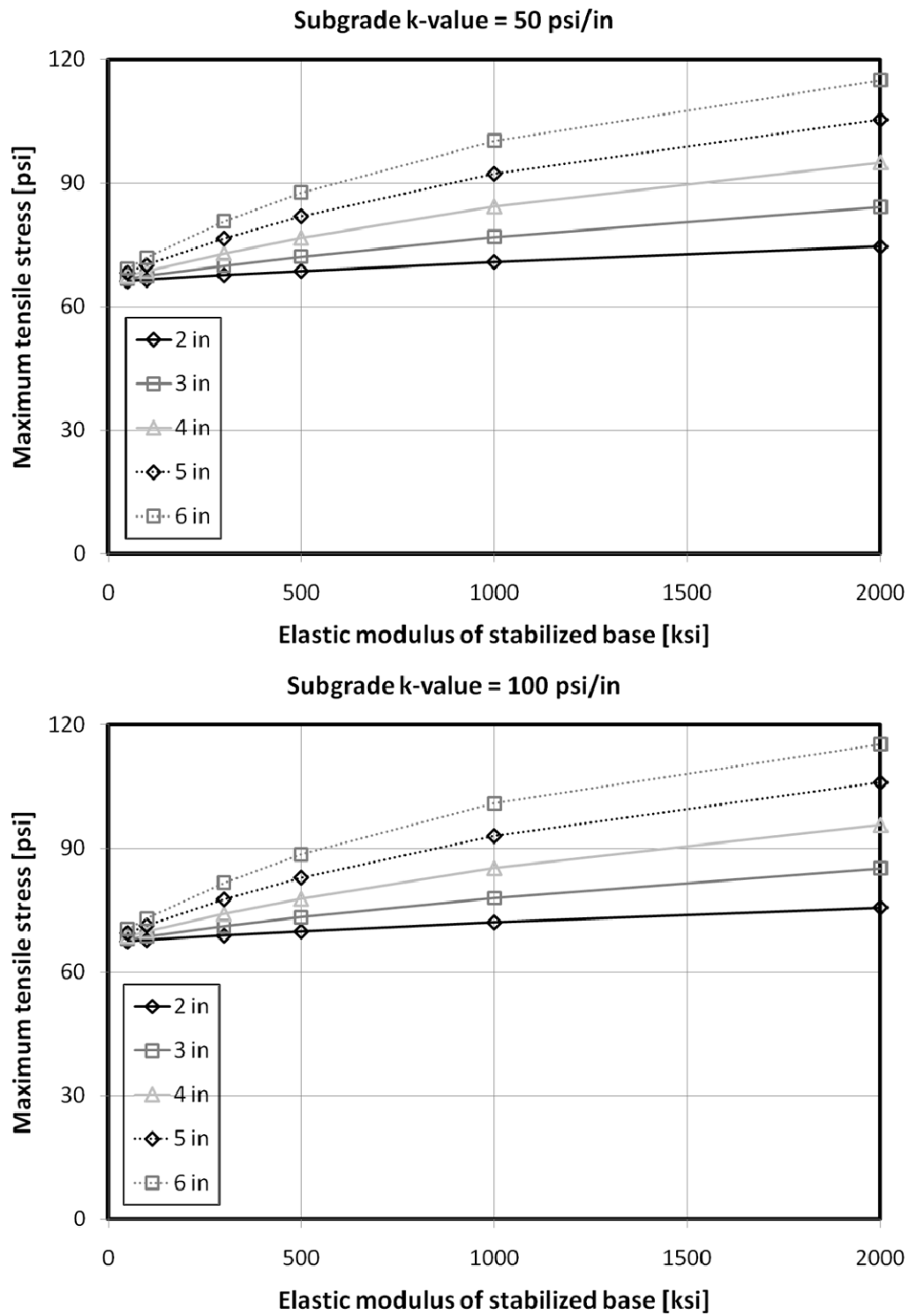
Figure B 7. Effects of elastic modulus of base under temperature loading (1)
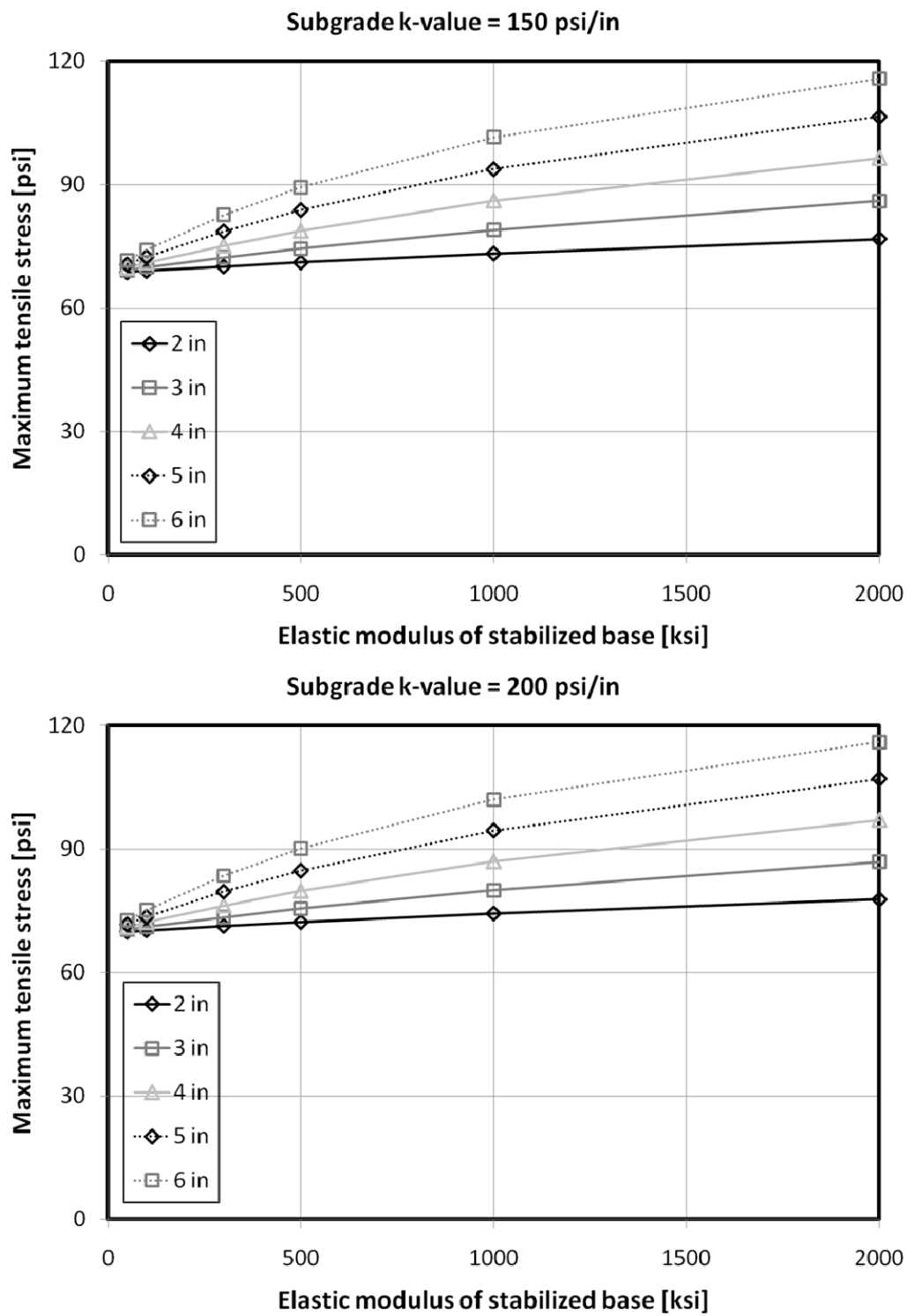
Figure B 8. Effects of elastic modulus of base under temperature loading (2)
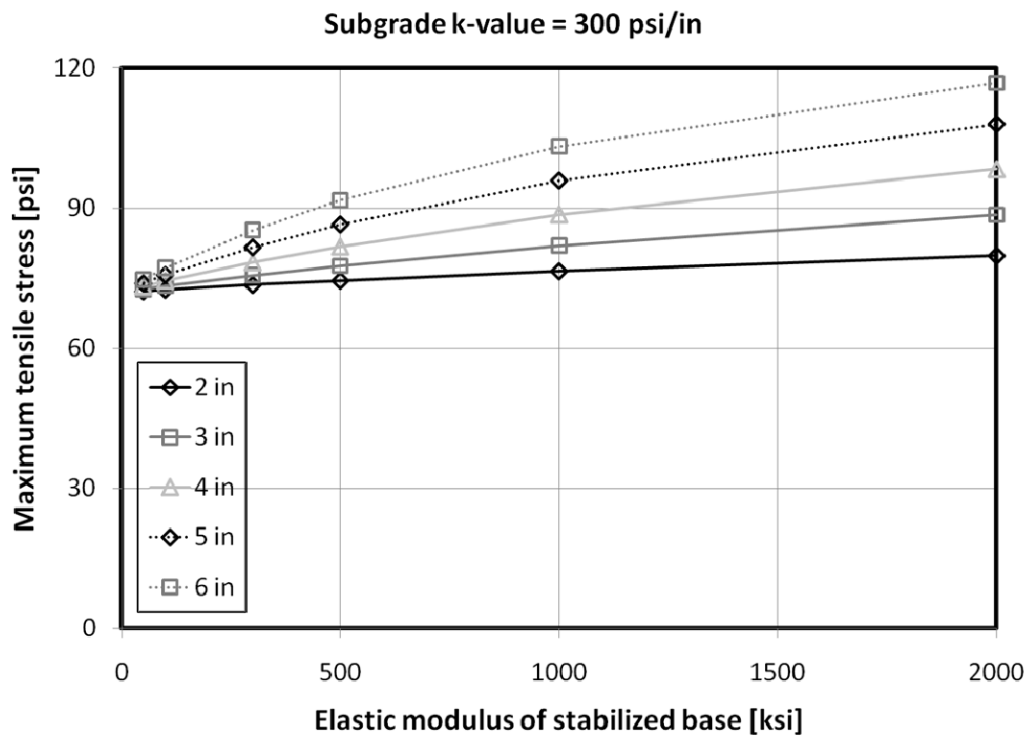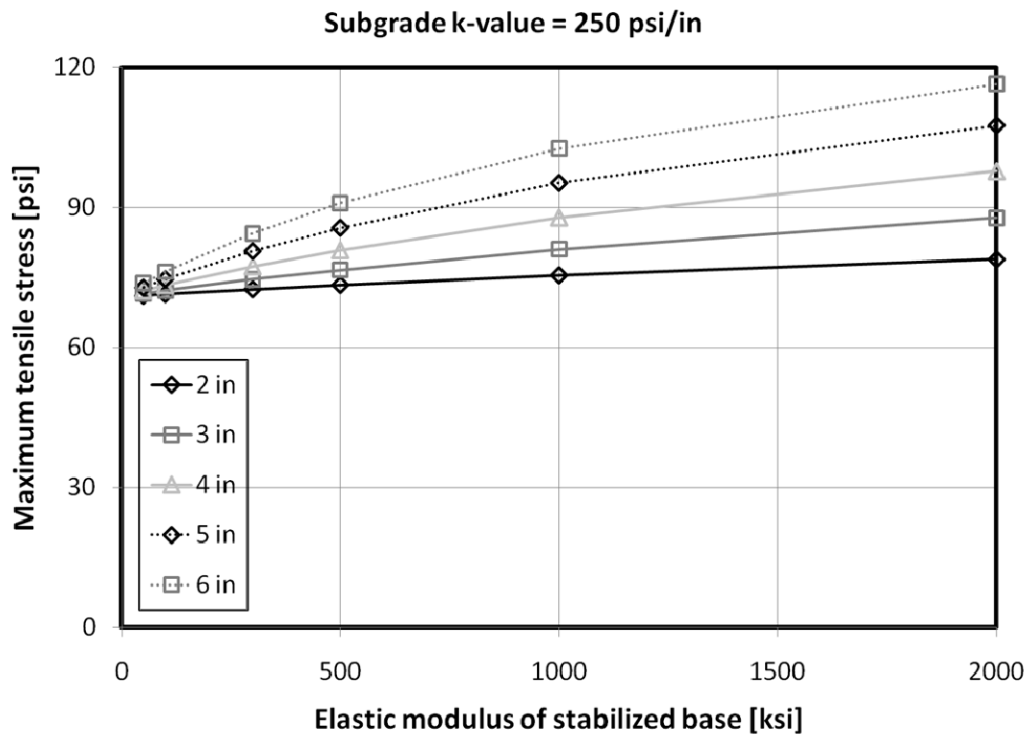
Figure B 9. Effects of elastic modulus of base under temperature loading (3)
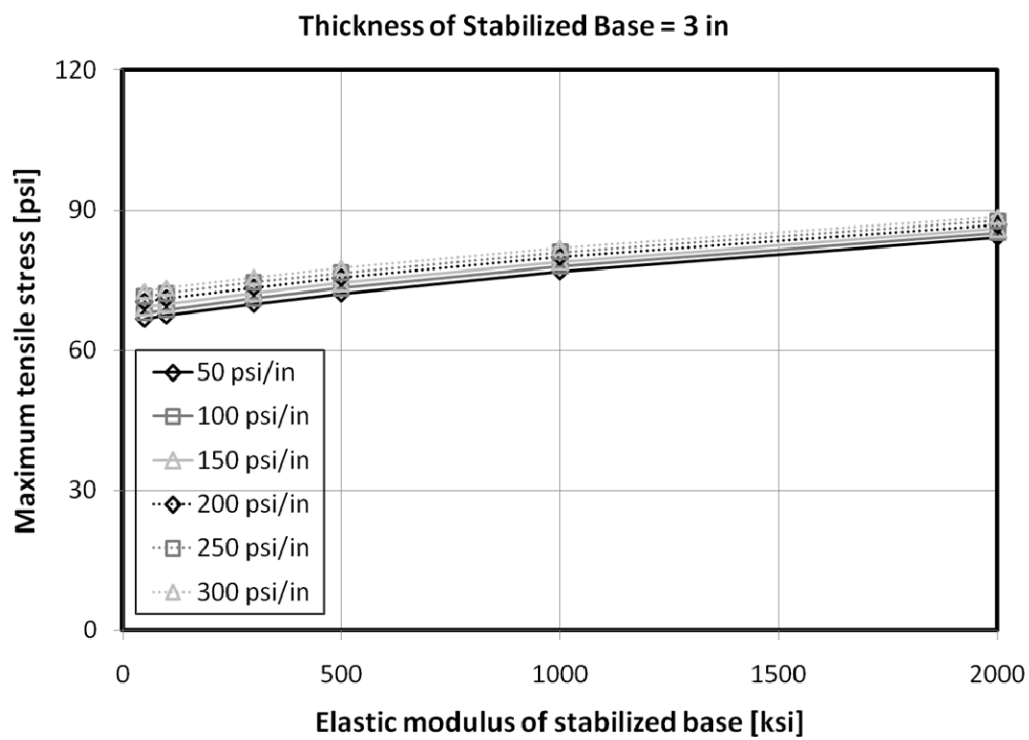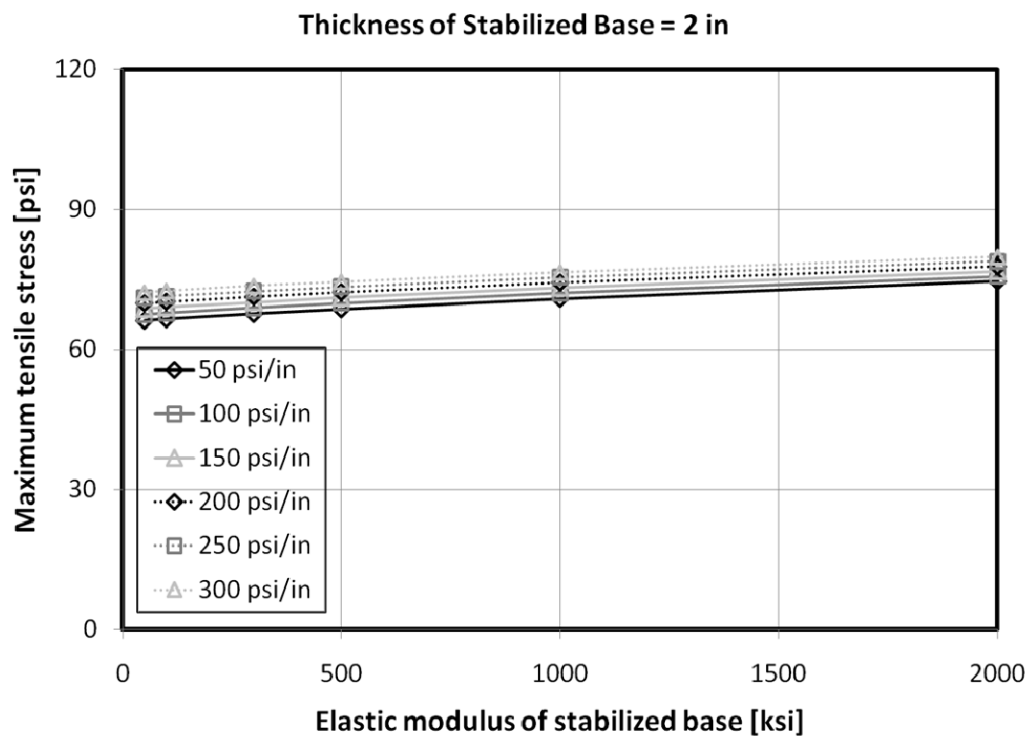
Figure B 10. Effects of elastic modulus of base under temperature loading (4)
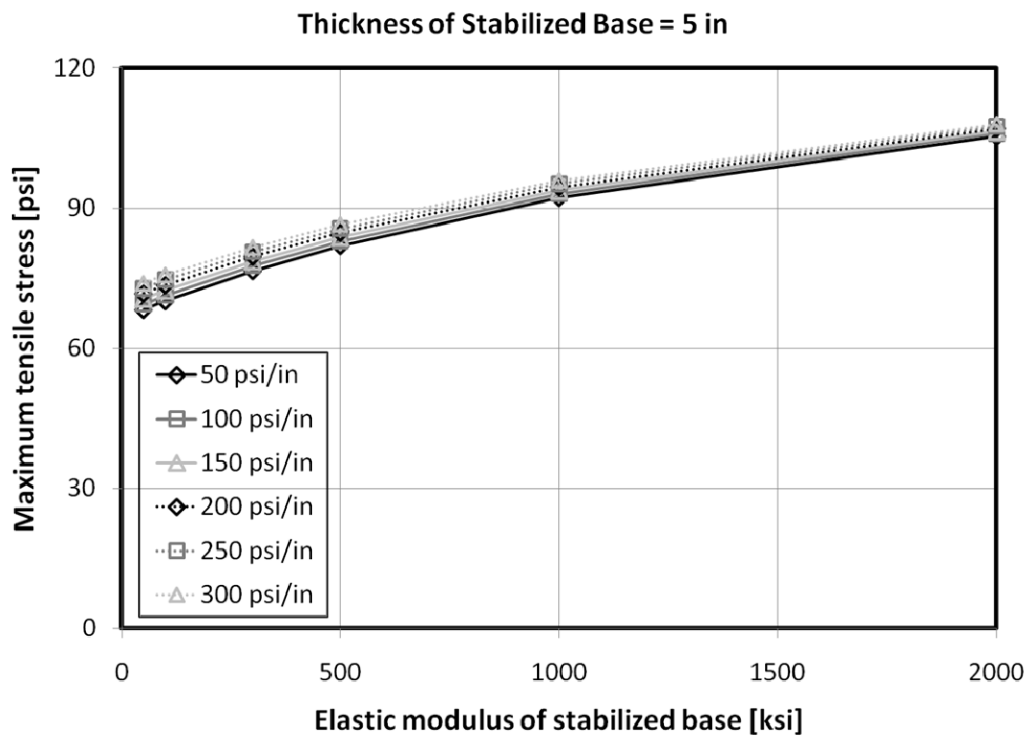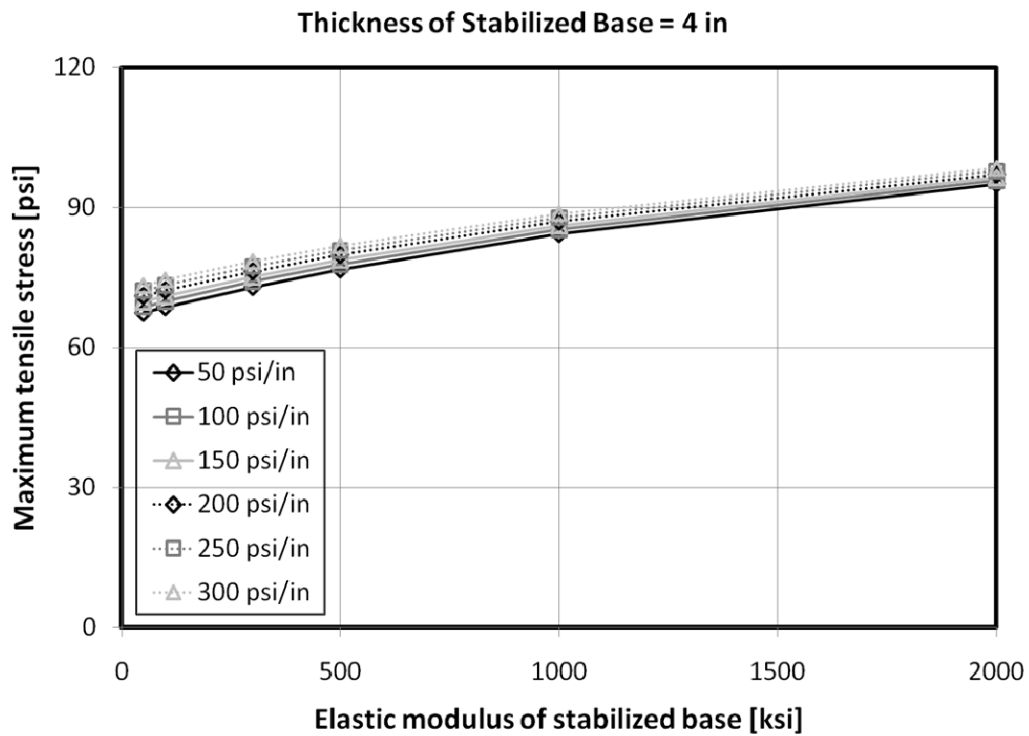
Figure B 11. Effects of elastic modulus of base under temperature loading (5)
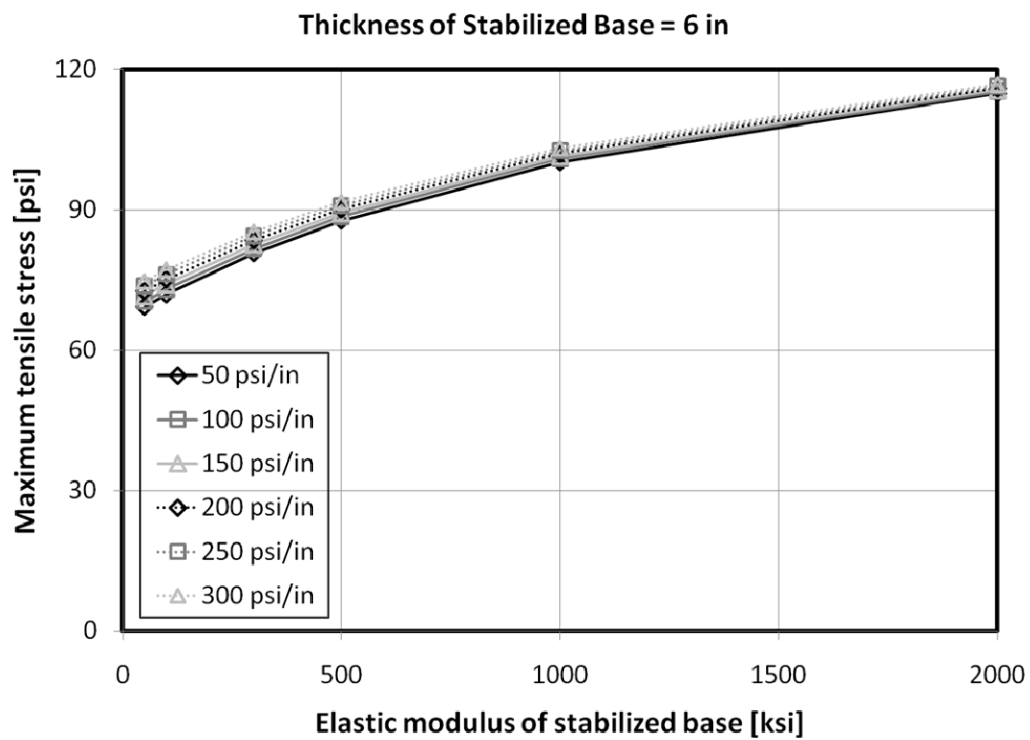
Figure B 12. Effects of elastic modulus of base under temperature loading (6)
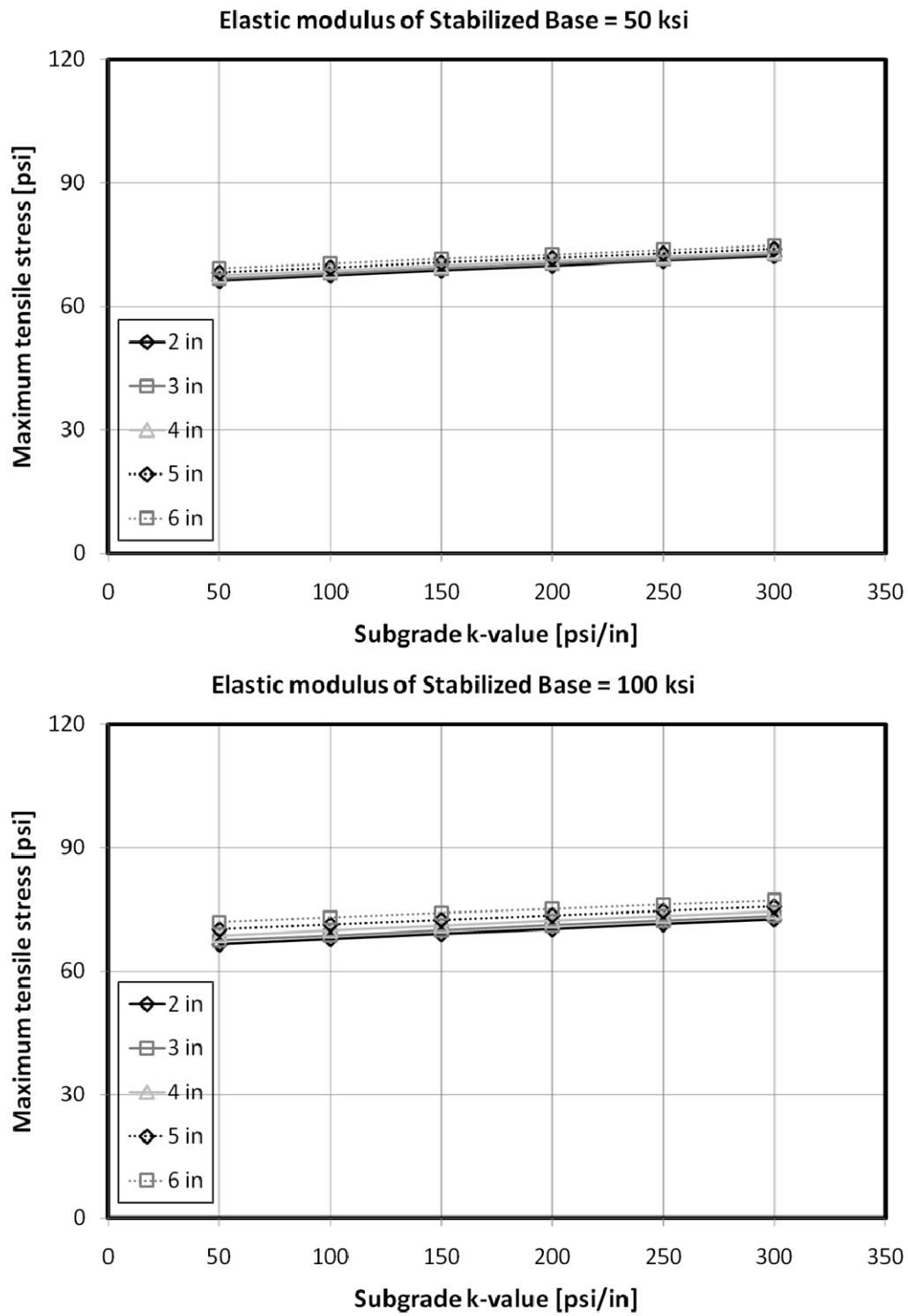
Figure B 13. Effects of *k*-value of subgrade layer under temperature loading (1)
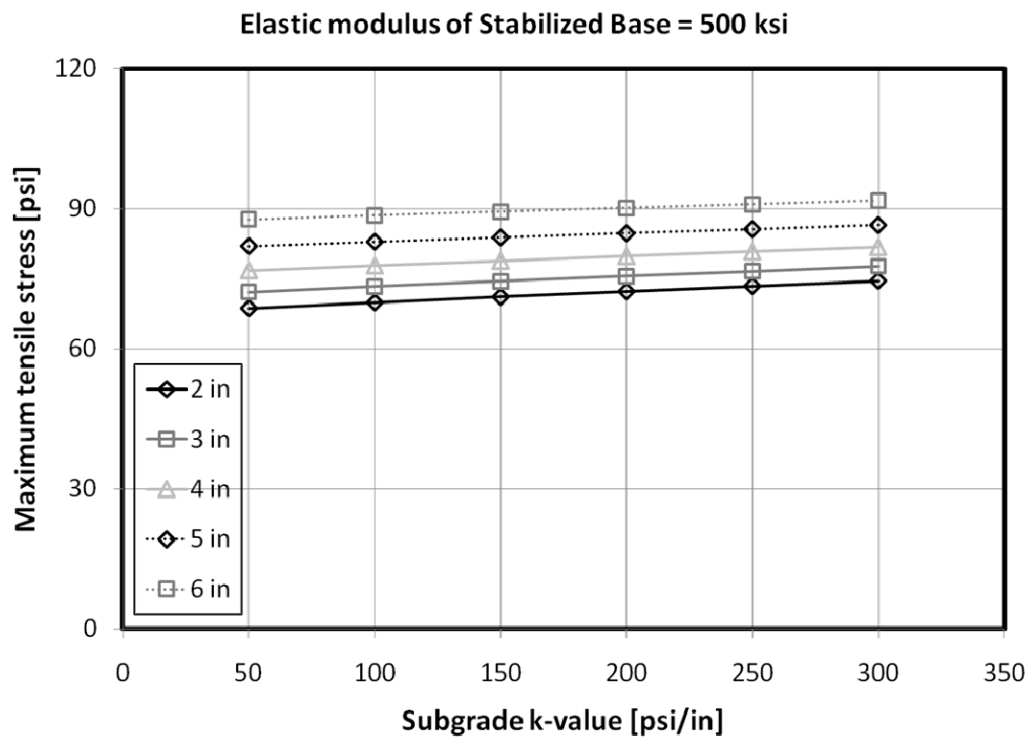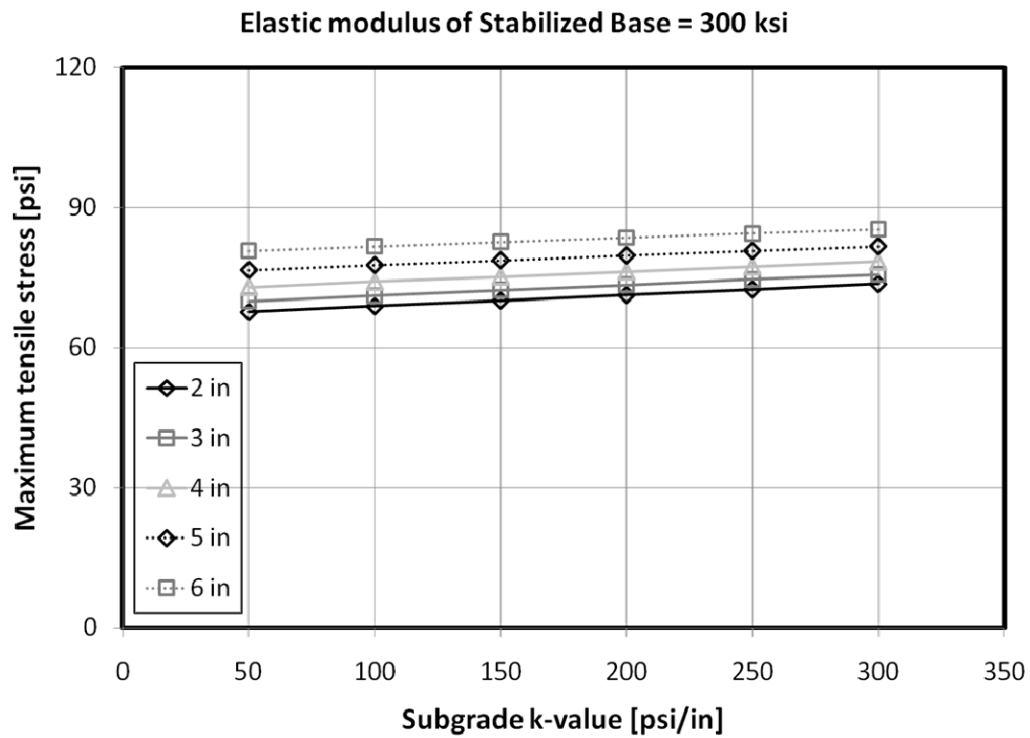
Figure B 14. Effects of *k*-value of subgrade layer under temperature loading (2)
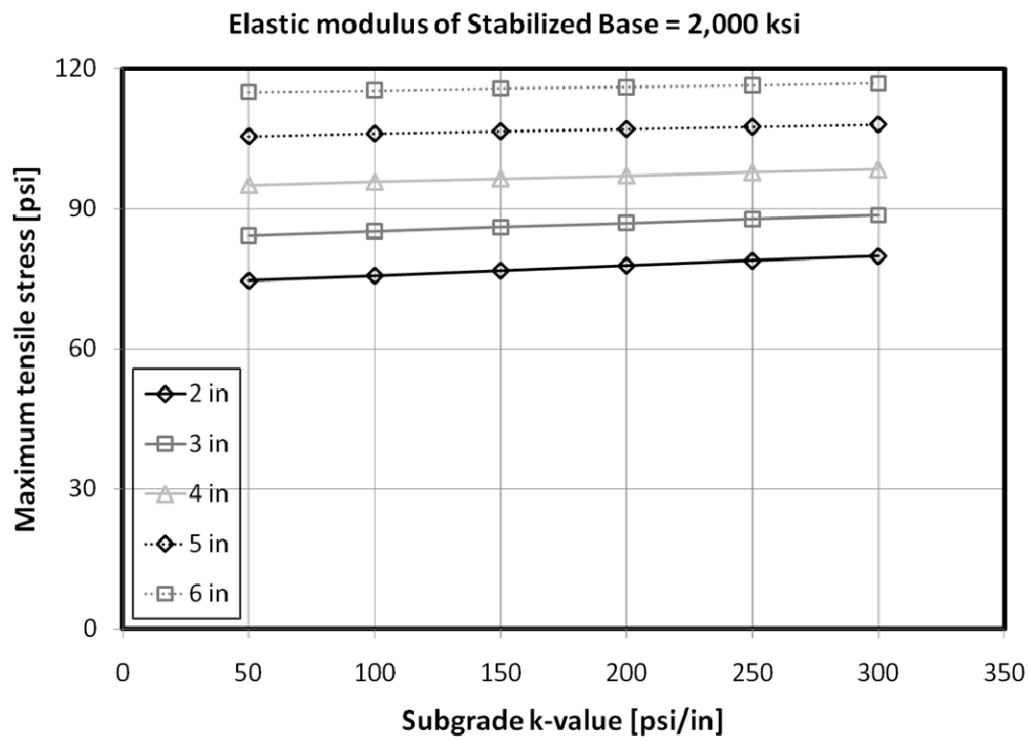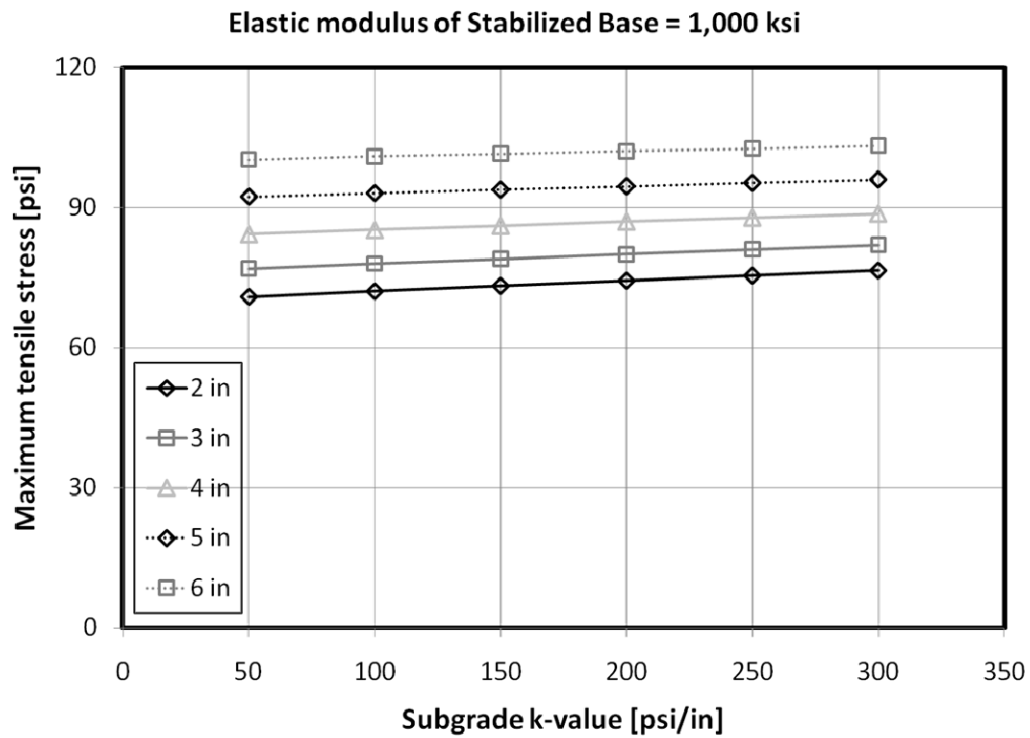
Figure B 15. Effects of *k*-value of subgrade layer under temperature loading (3)
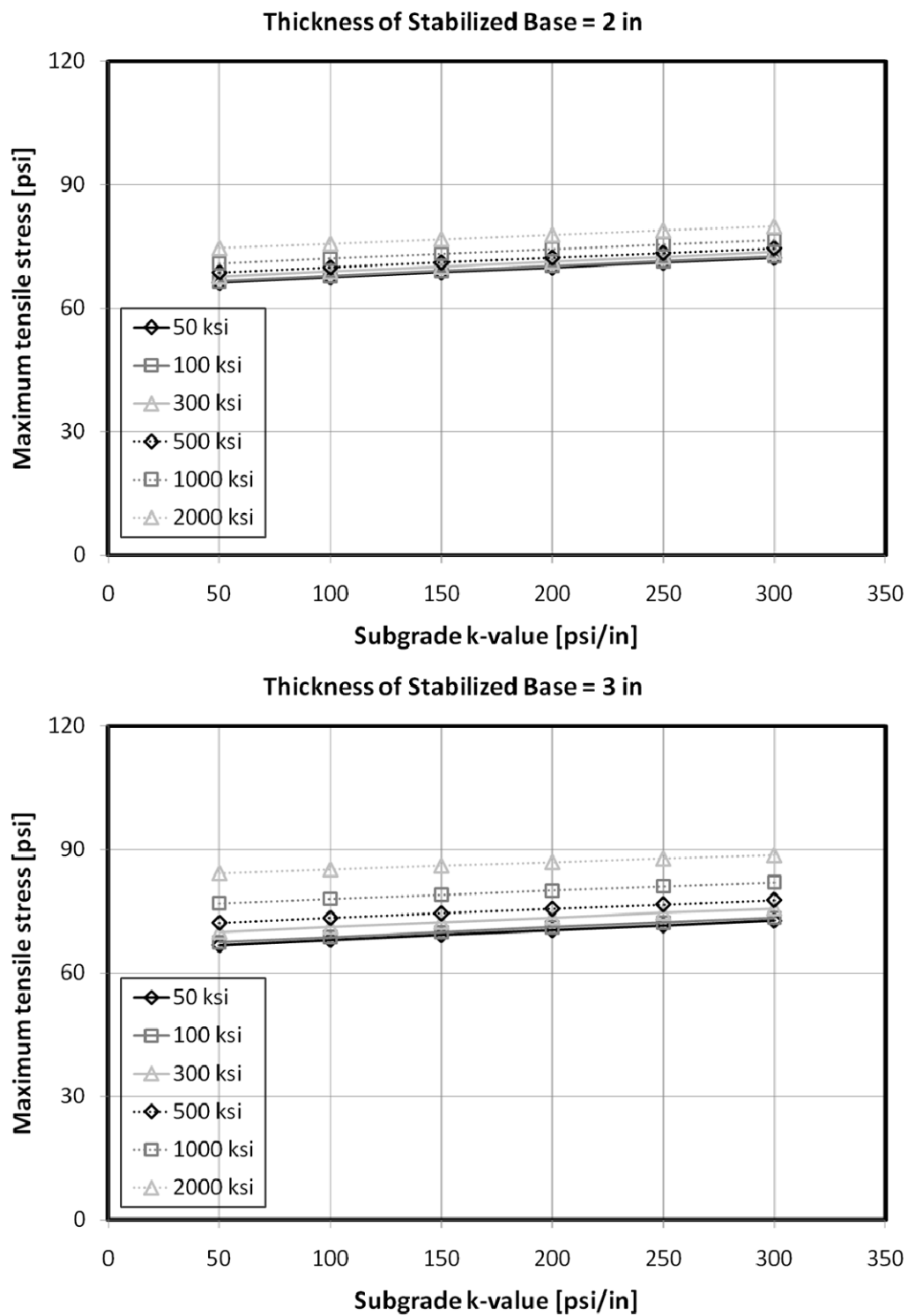
Figure B 16. Effects of *k*-value of subgrade layer under temperature loading (4)
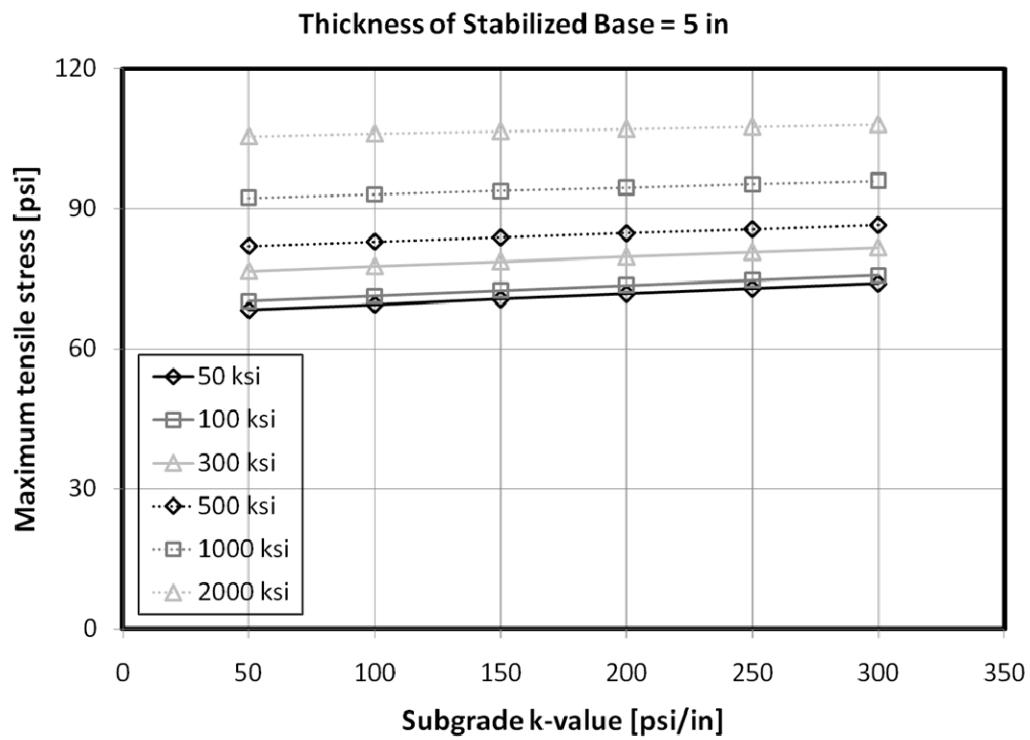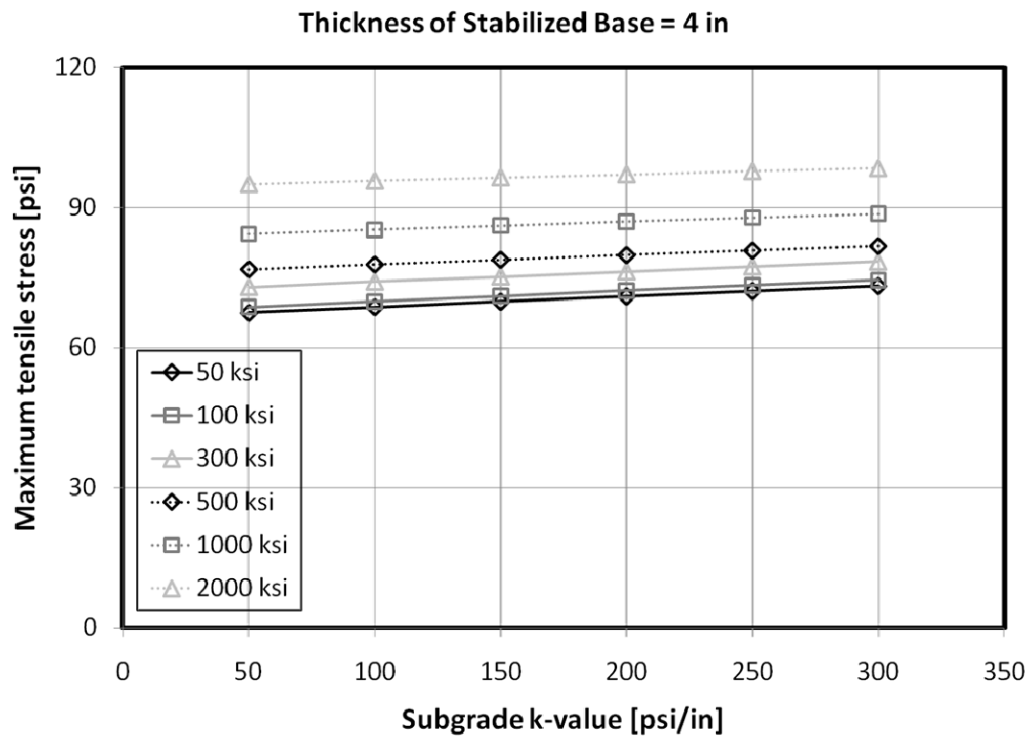
Figure B 17. Effects of *k*-value of subgrade layer under temperature loading (5)
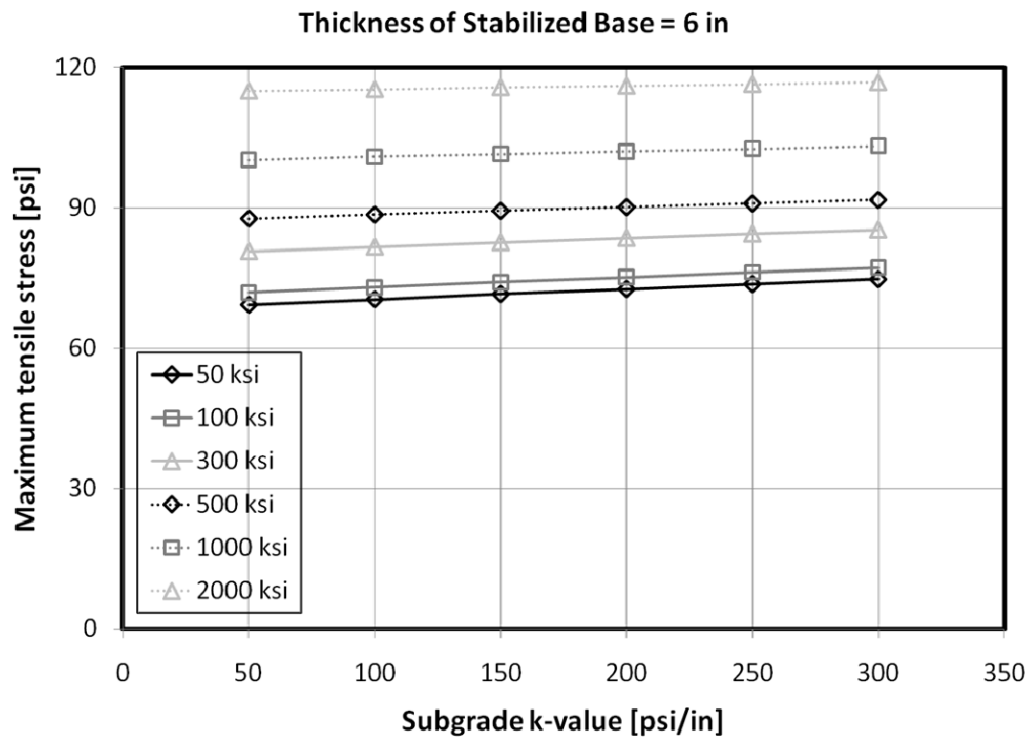
Figure B 18. Effects of *k*-value of subgrade layer under temperature loading (6)

➢ *Effects of Thickness of Stabilized Base Layer Under Wheel Loading*
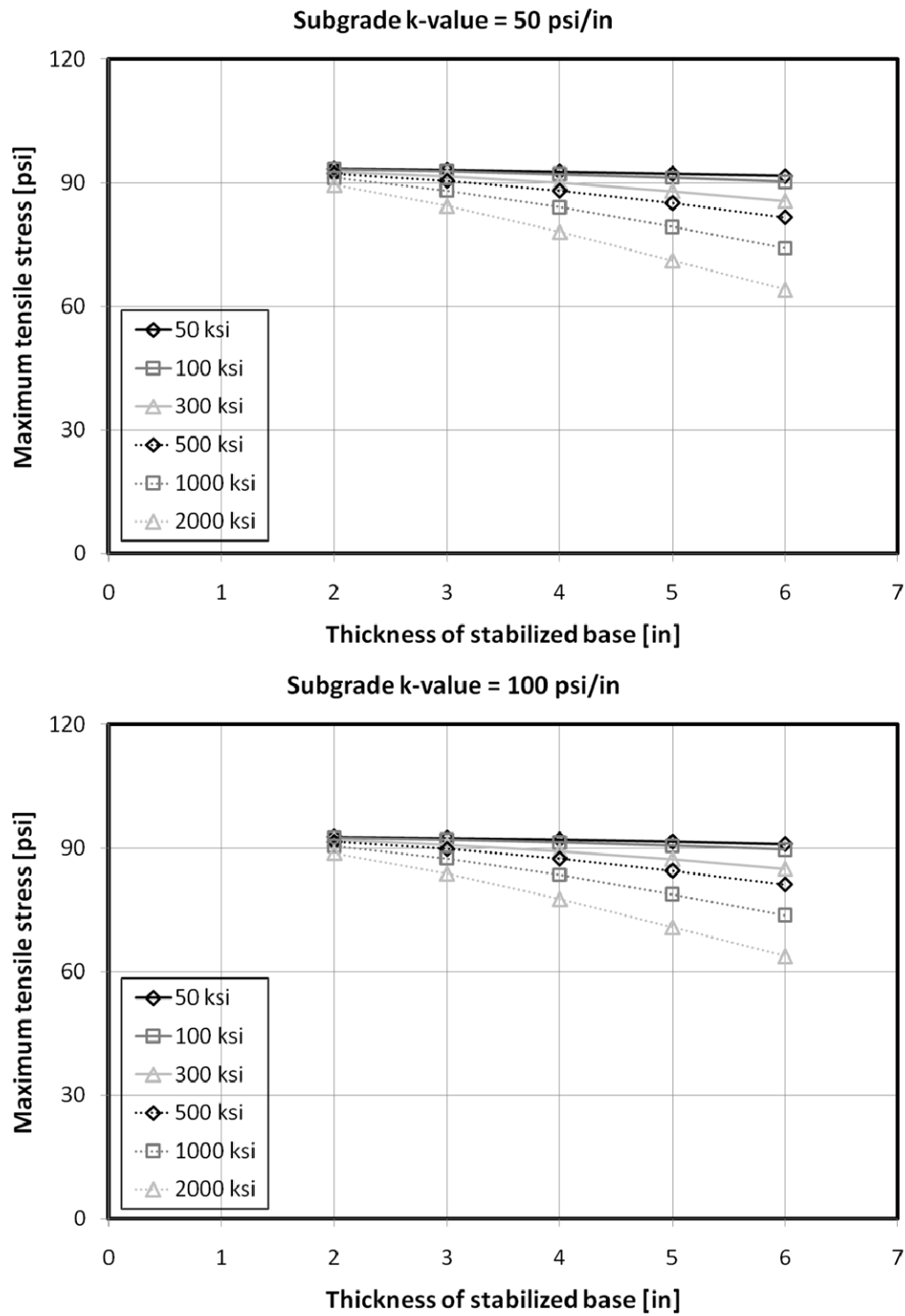
Figure B 19. Effects of thickness of stabilized base under wheel loading (1)
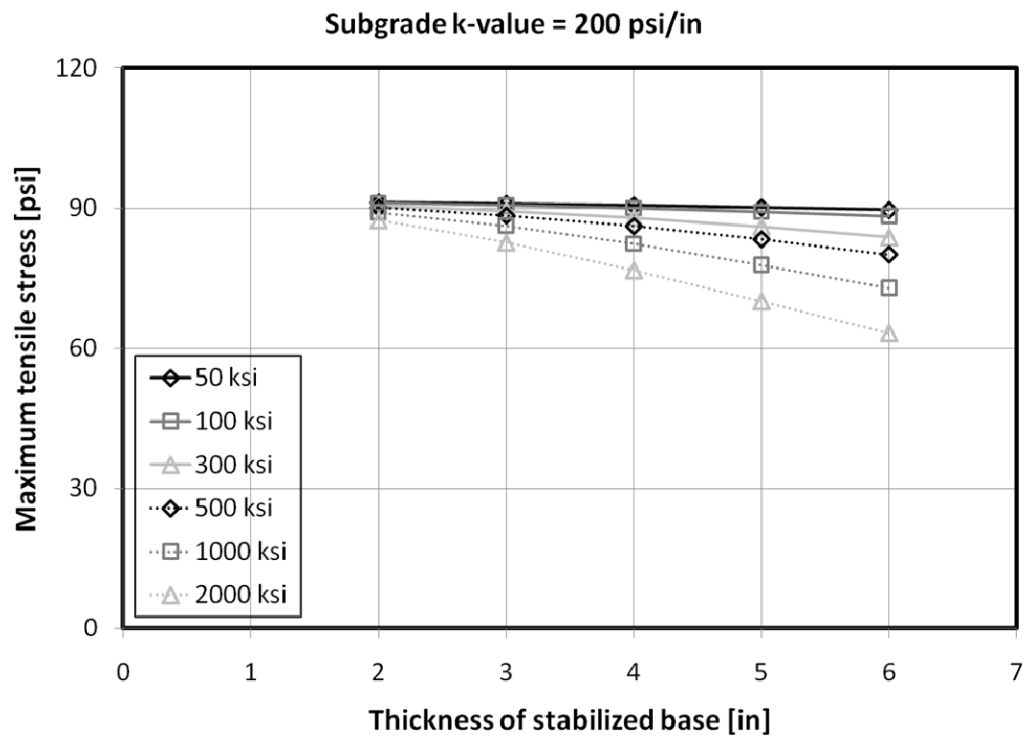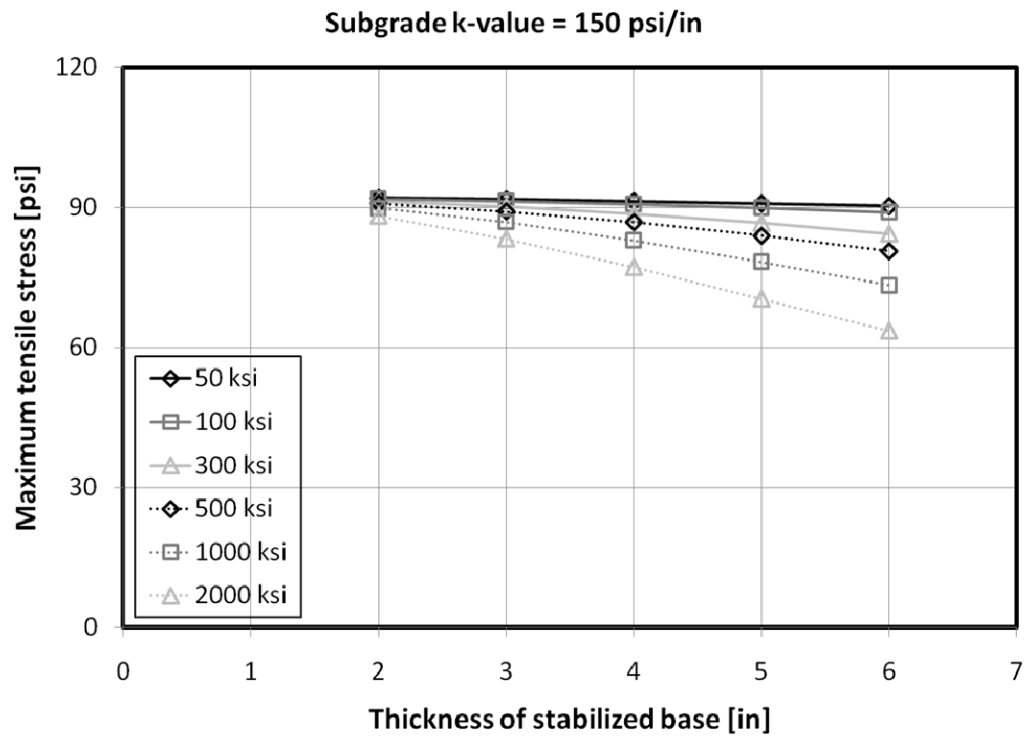
Figure B 20. Effects of thickness of stabilized base under wheel loading (2)
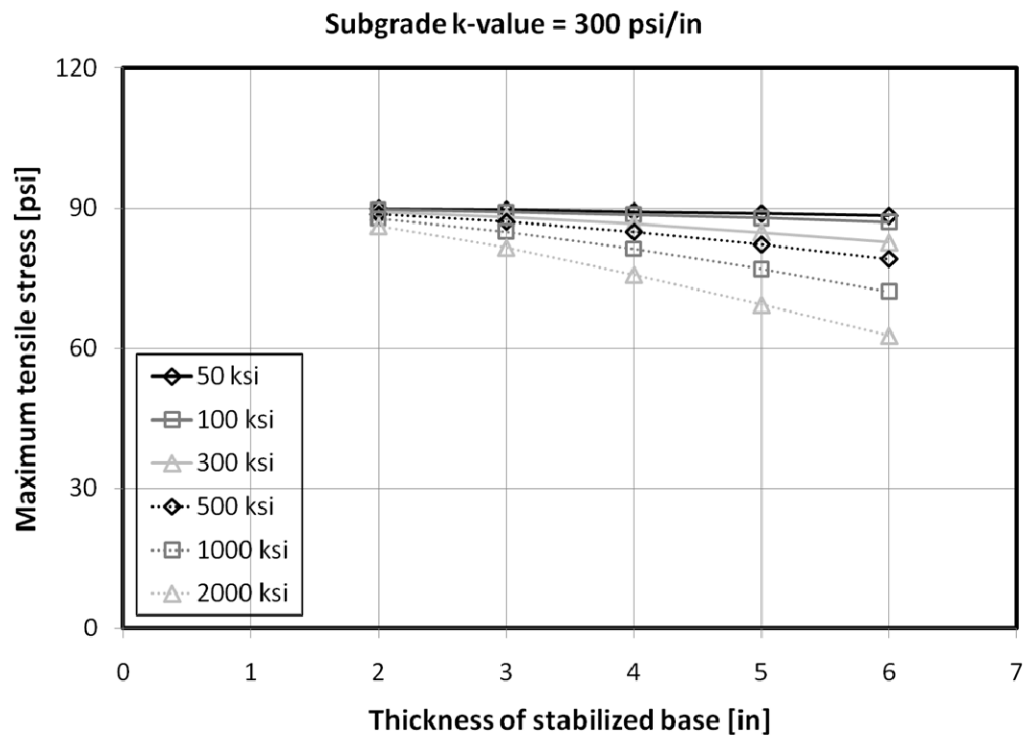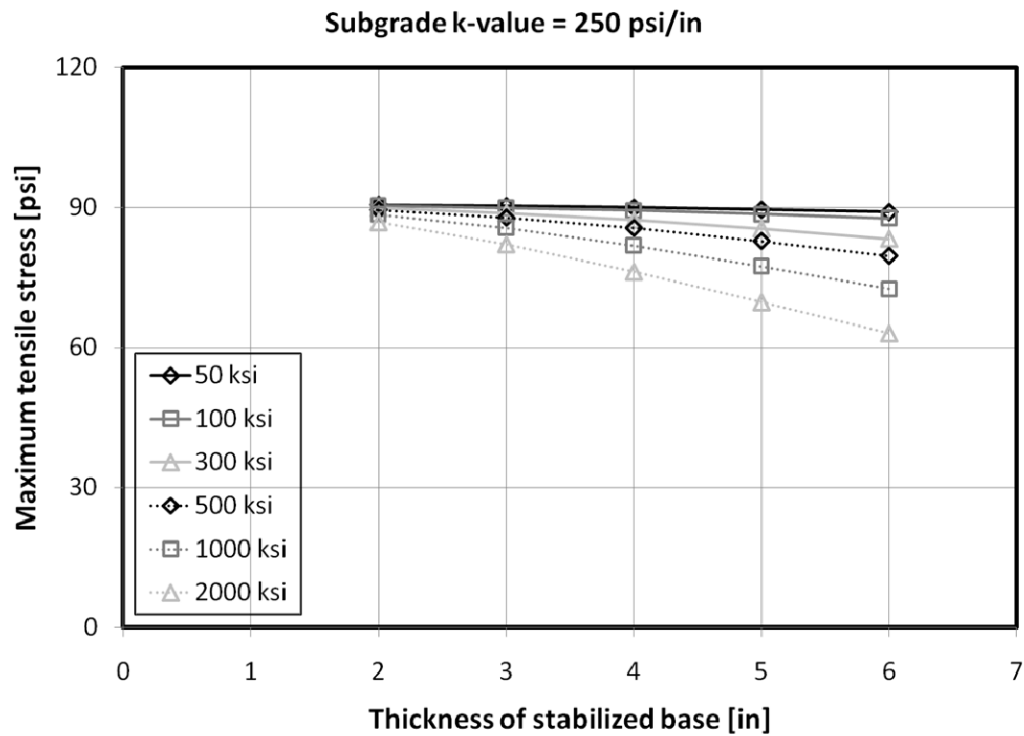
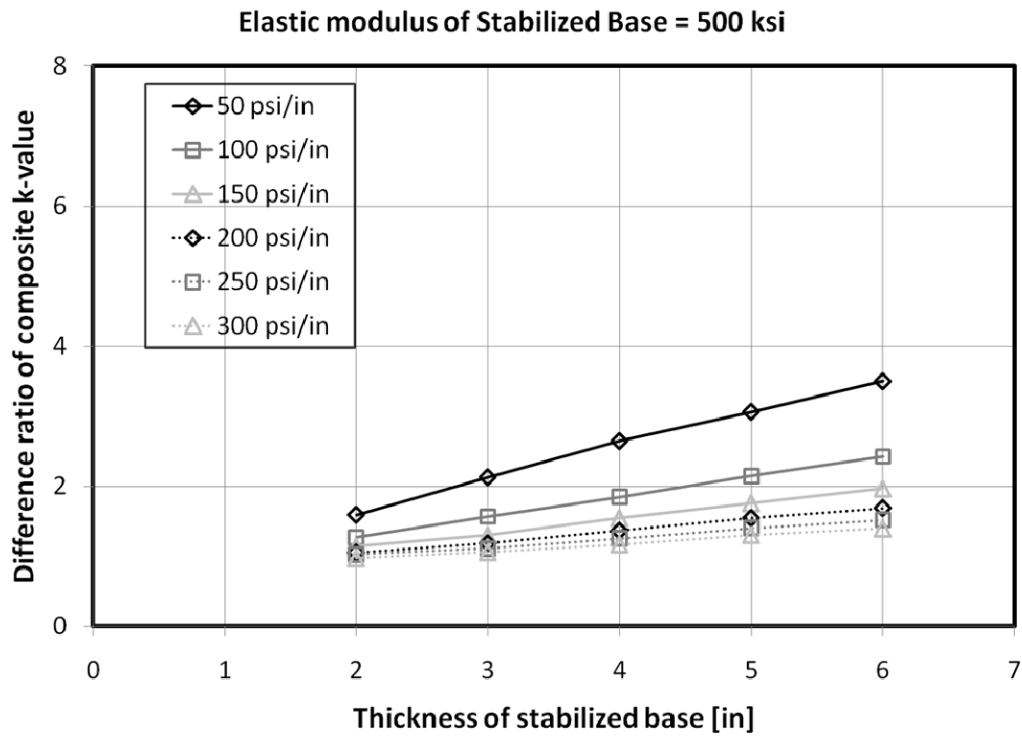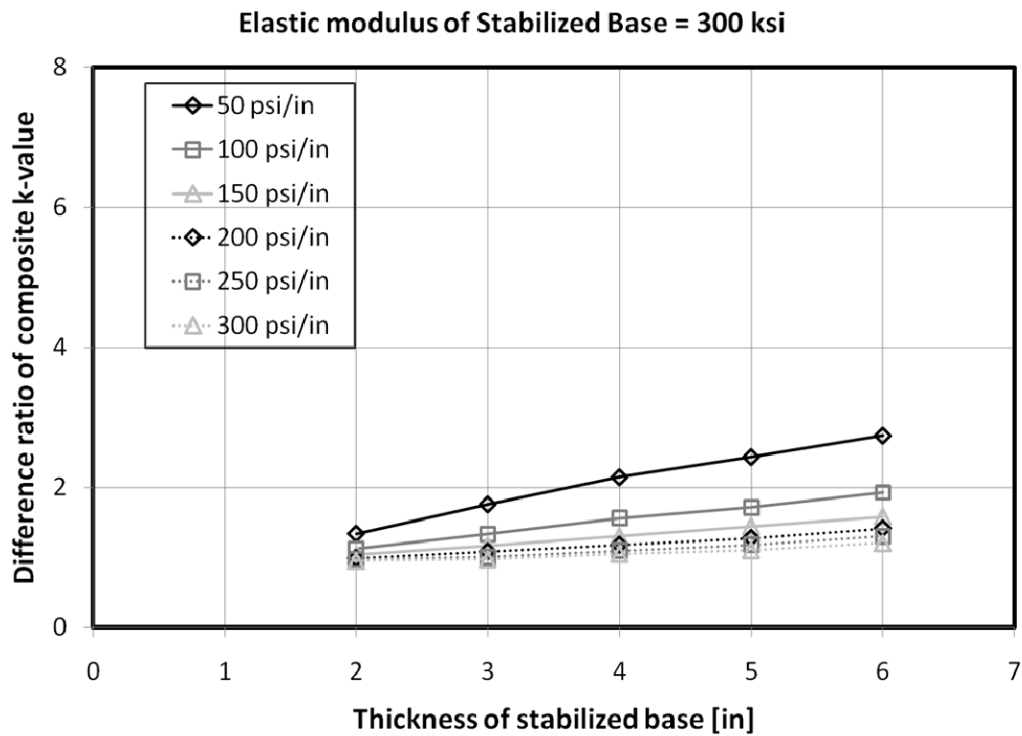**Figure B 21. Effects of thickness of stabilized base under wheel loading (3)**
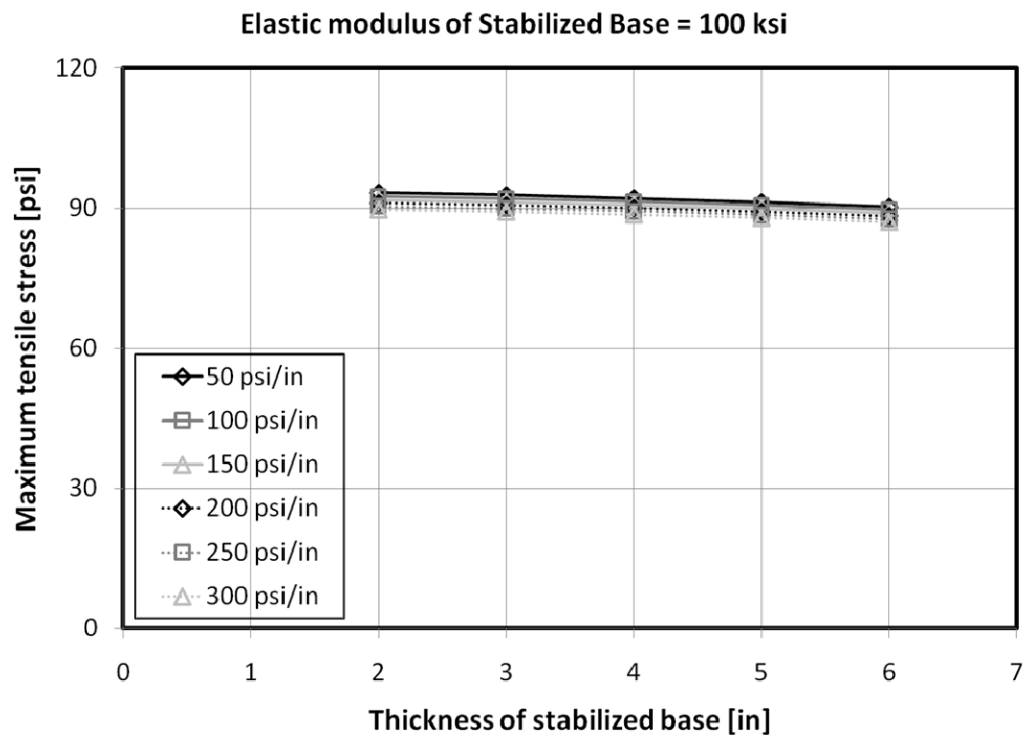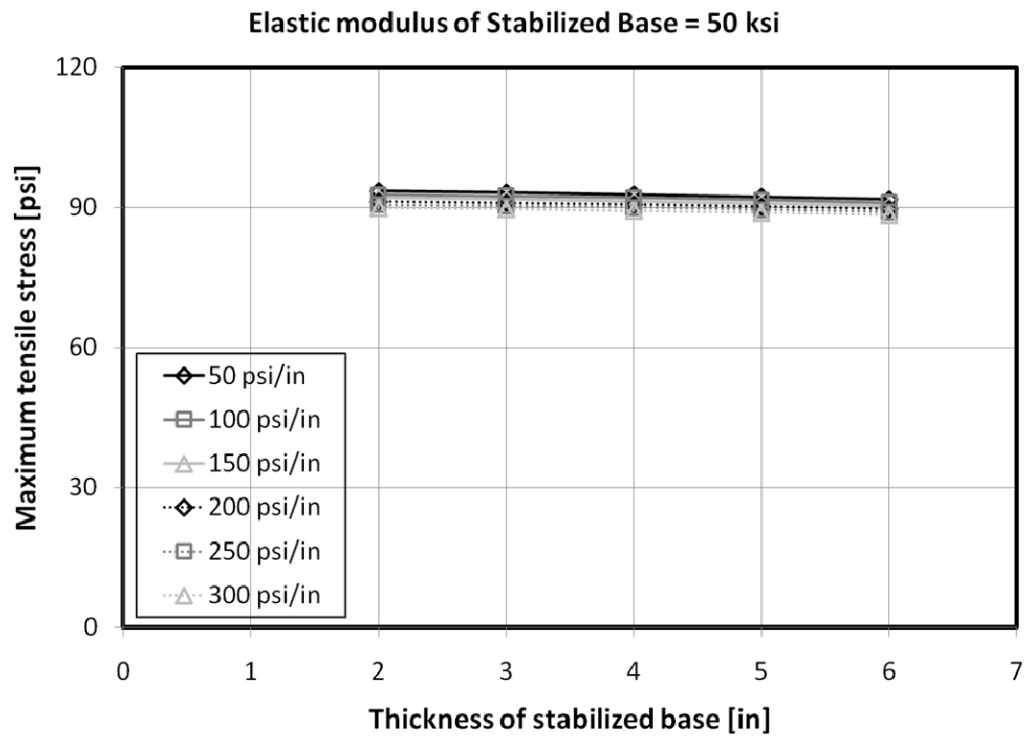
Figure B 22. Effects of thickness of stabilized base under wheel loading (4)
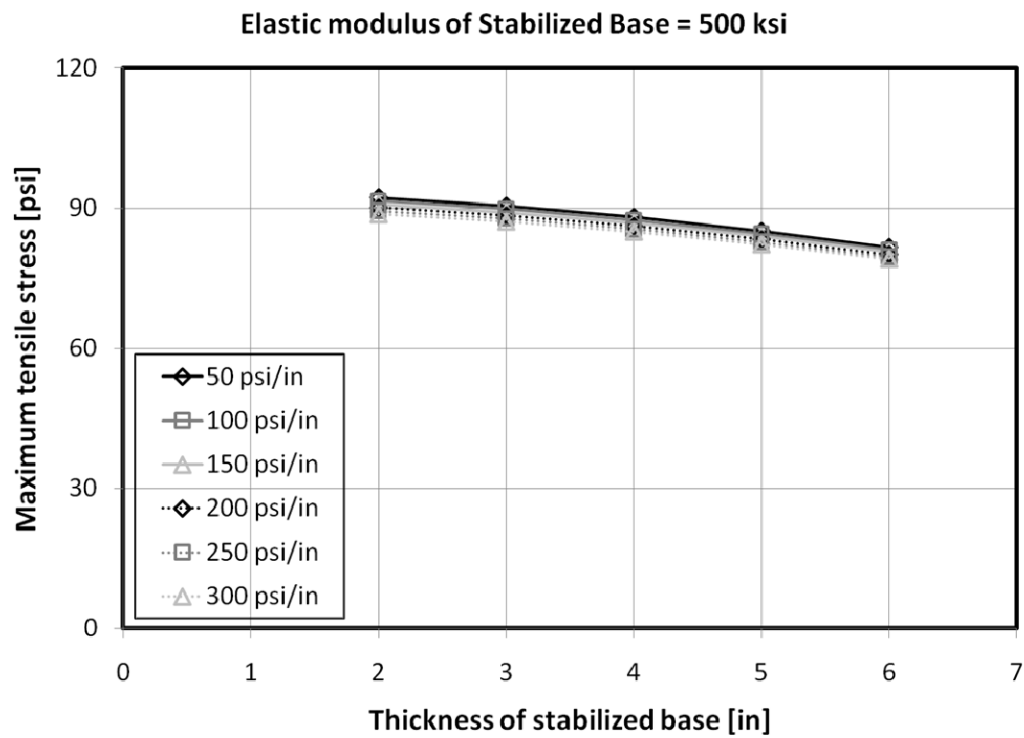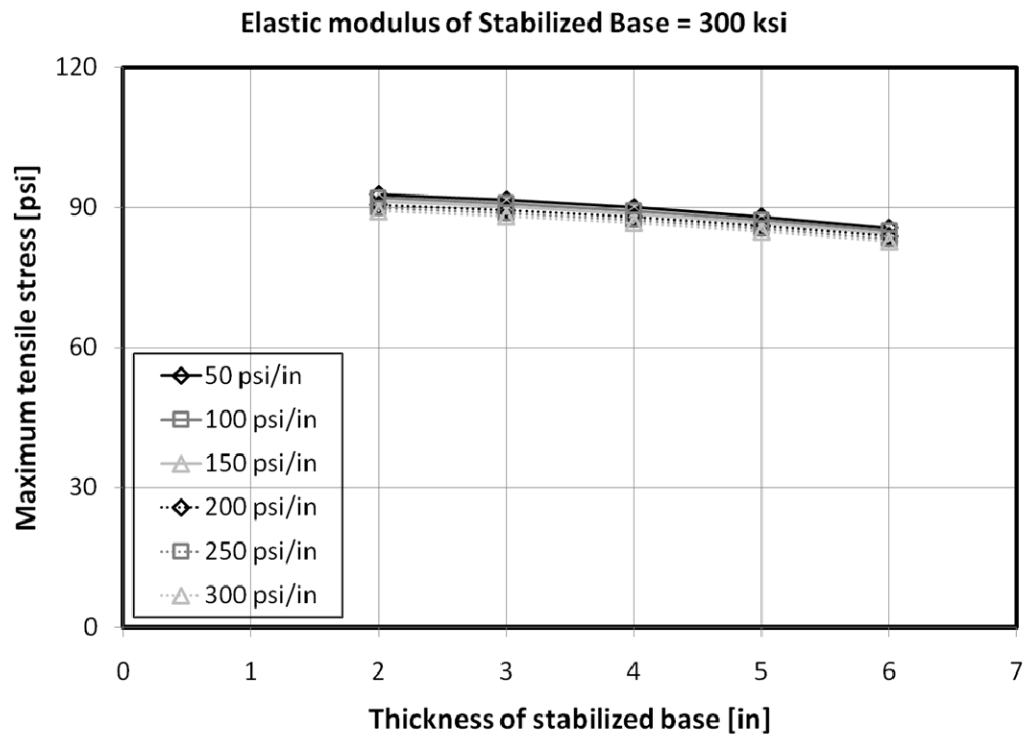
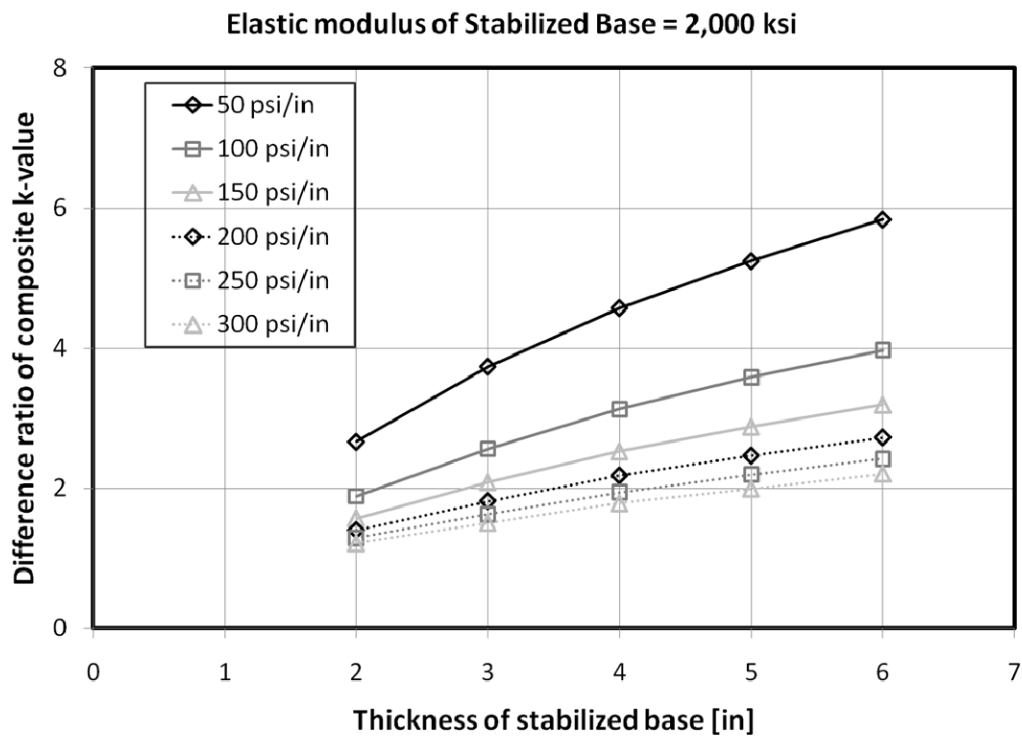**Figure B 23. Effects of thickness of stabilized base under wheel loading (5)**
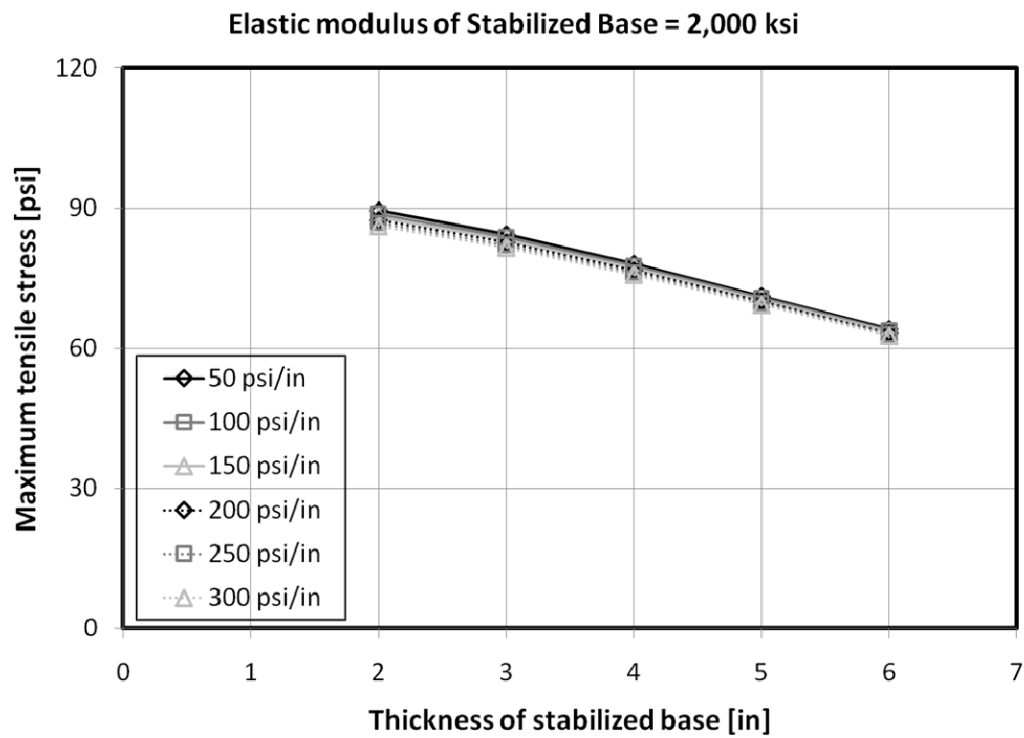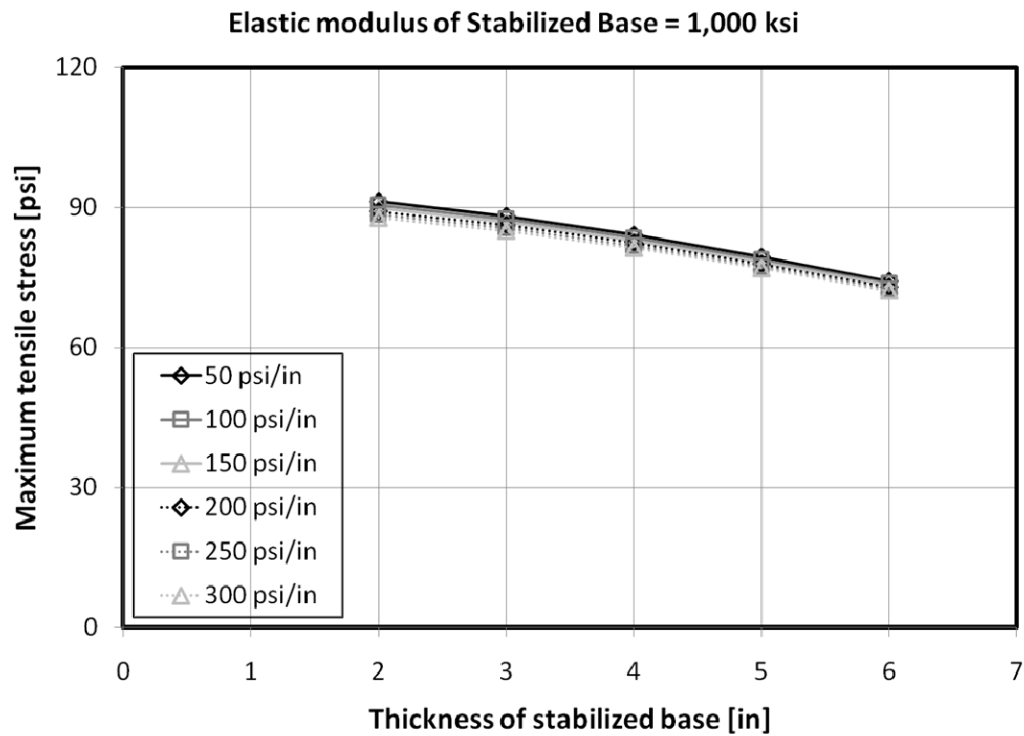
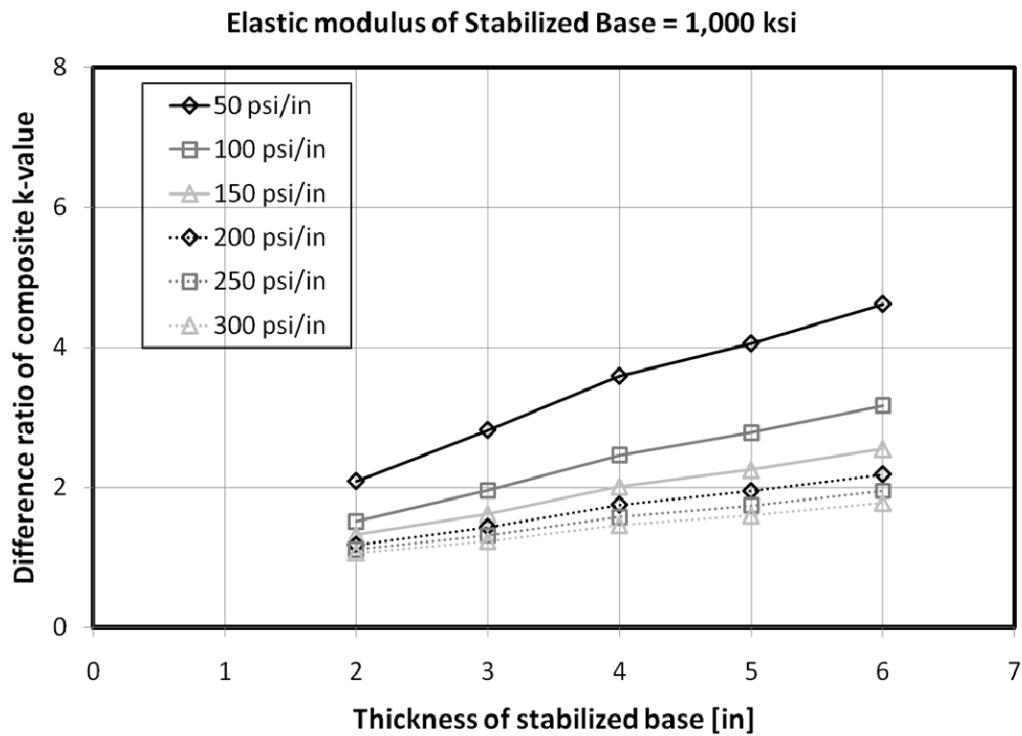**Figure B 24. Effects of thickness of stabilized base under wheel loading (6)**

➢ *Effects of Modulus of Elasticity of Base Material Under Wheel Loading*
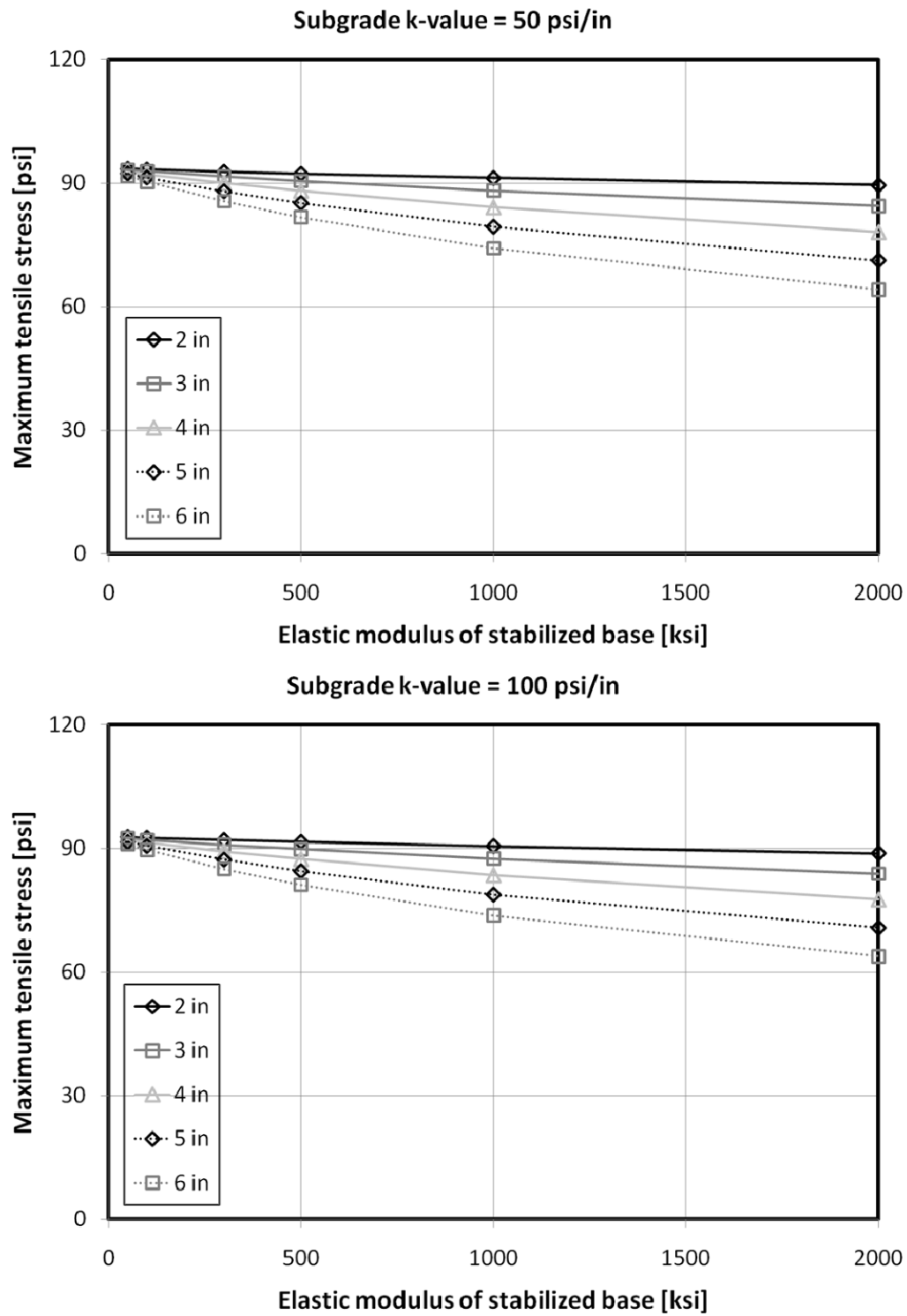
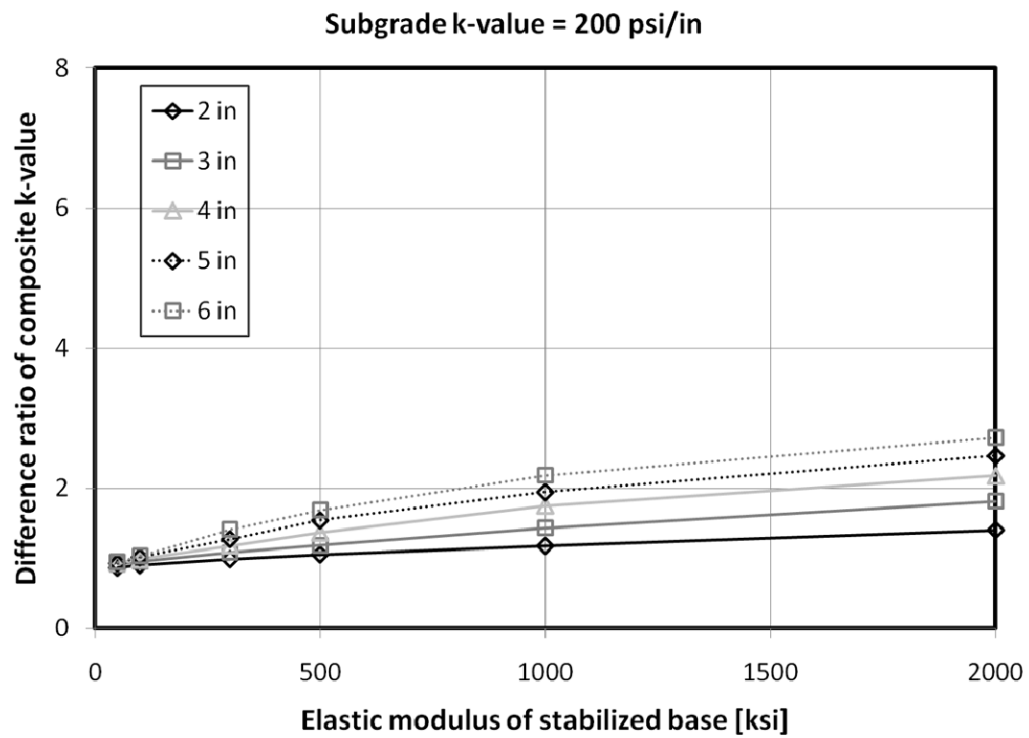**Figure B 25. Effects of elastic modulus of base under wheel loading (1)**
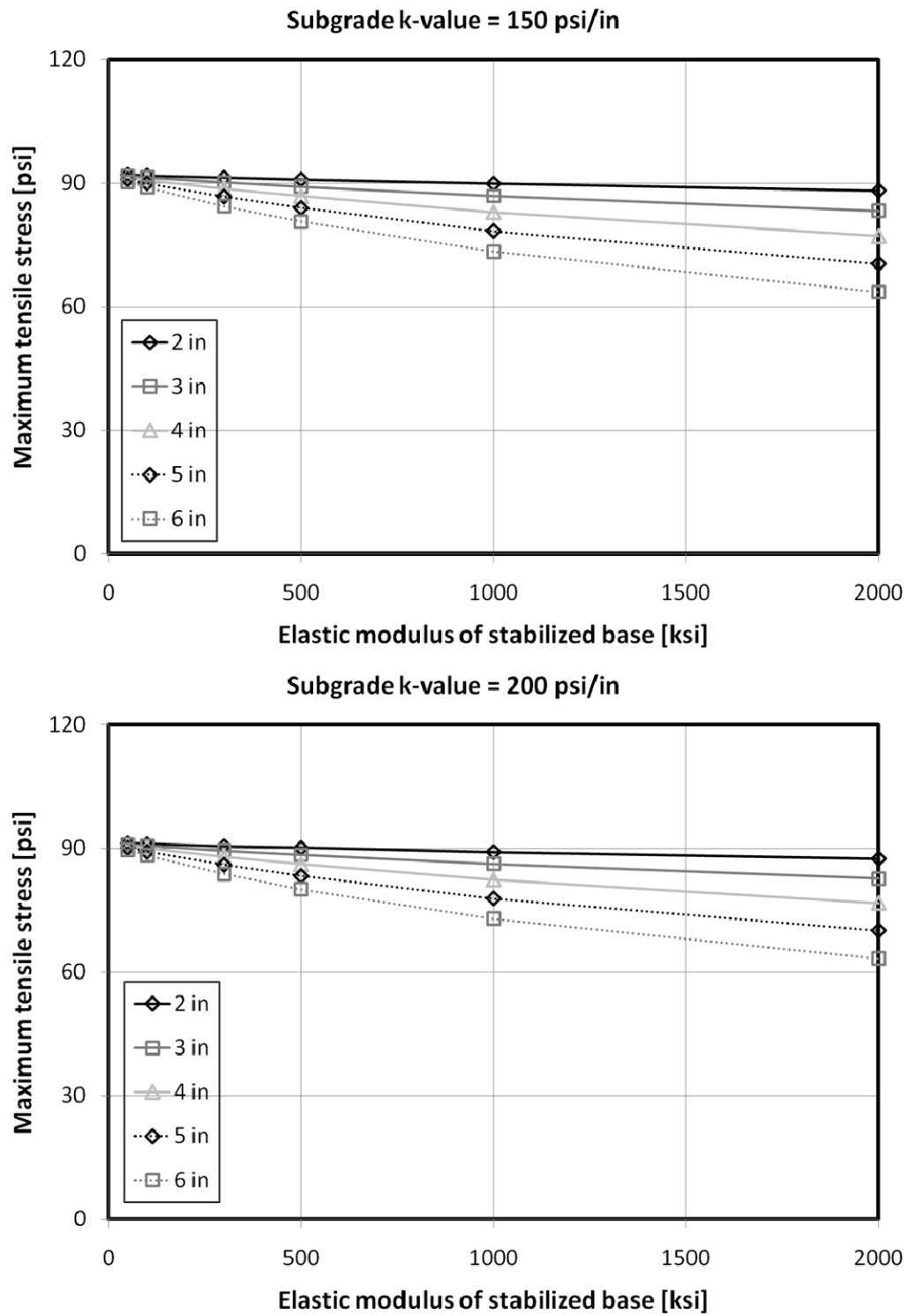
Figure B 26. Effects of elastic modulus of base under wheel loading (2)
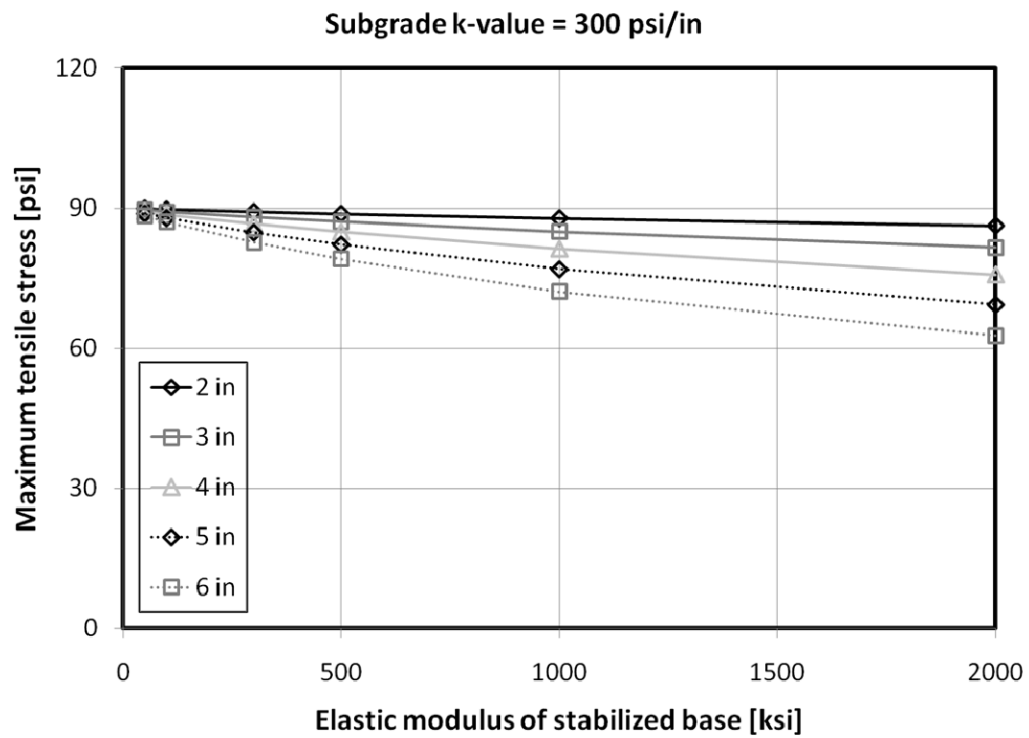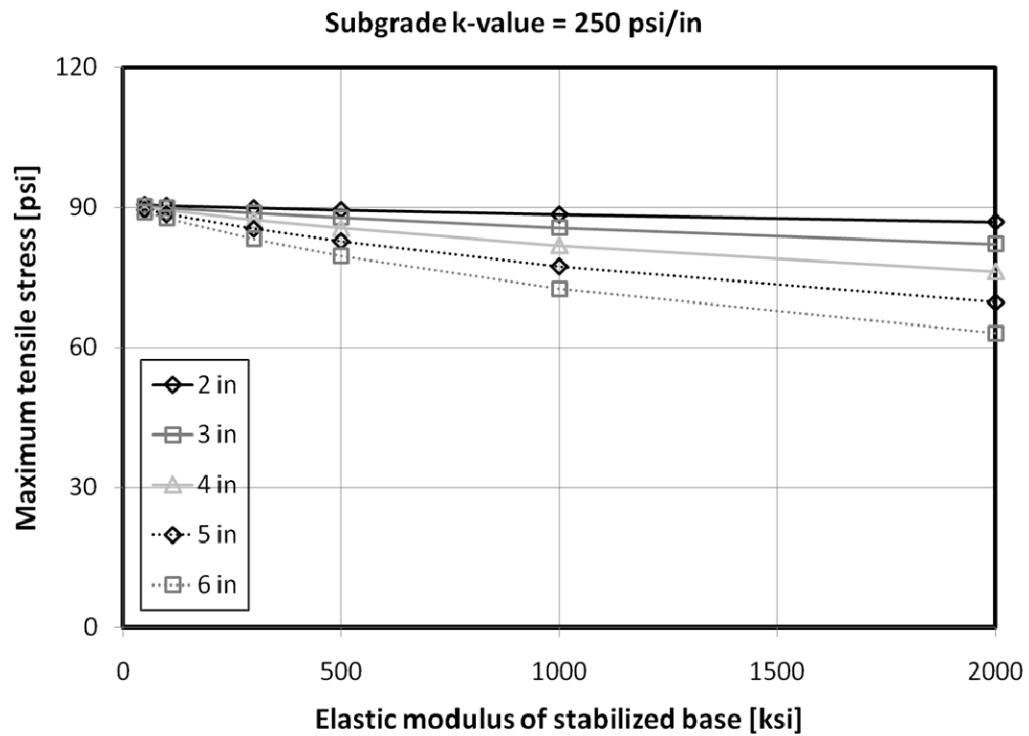
Figure B 27. Effects of elastic modulus of base under wheel loading (3)

Thickness of Stabilized Base = 2 in


Thickness of Stabilized Base = 3 in
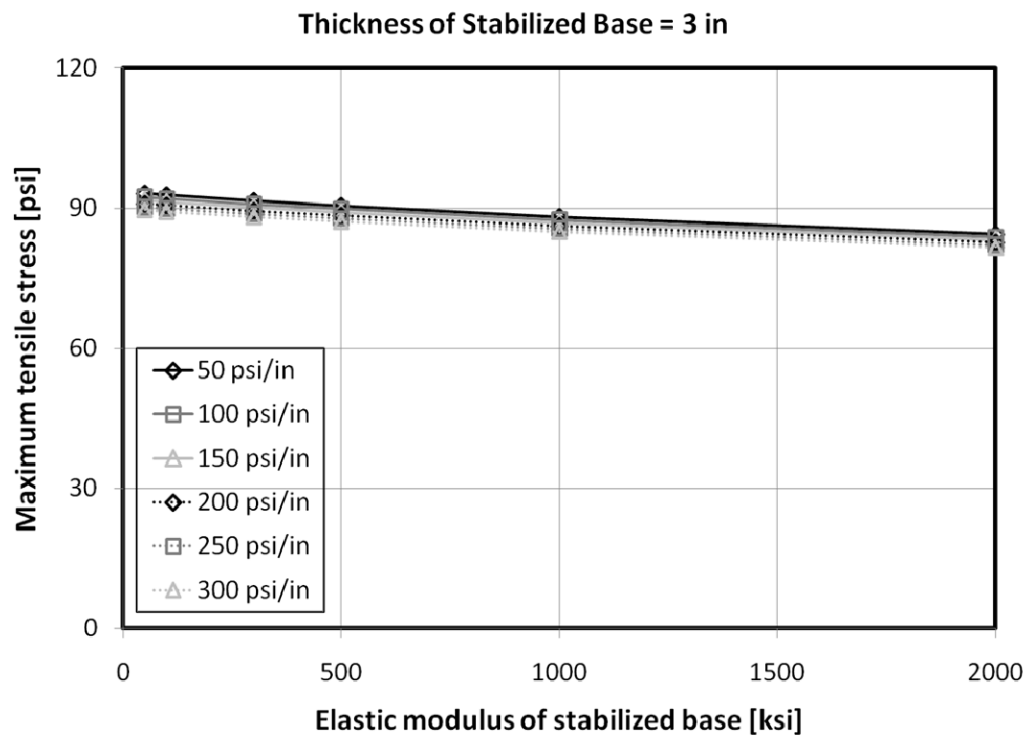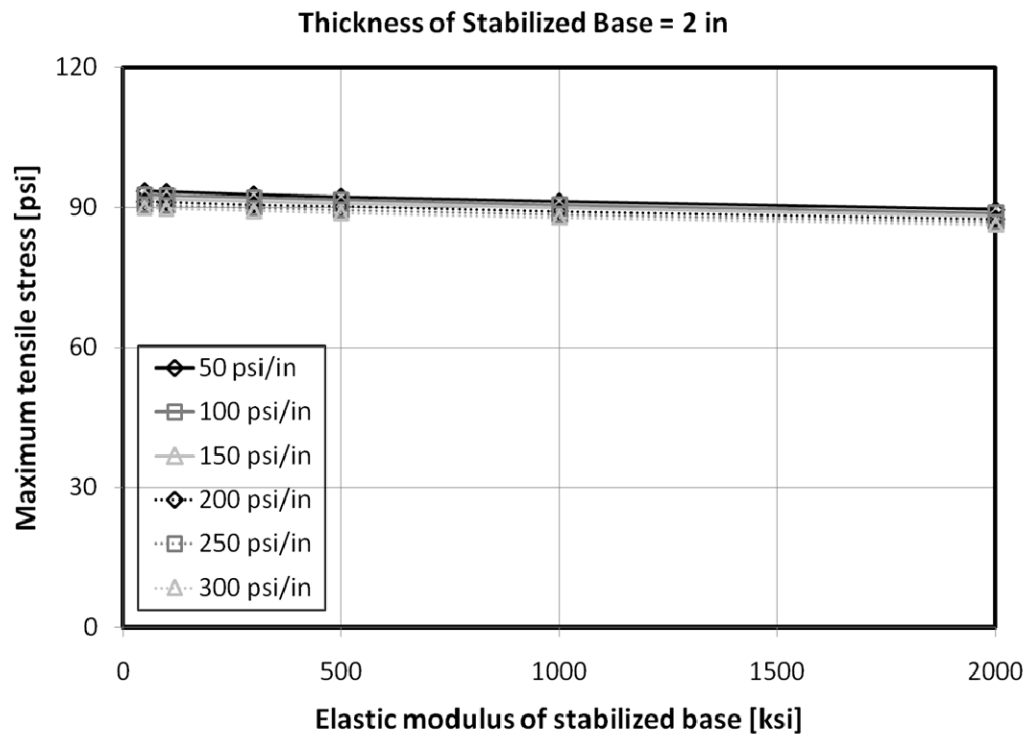
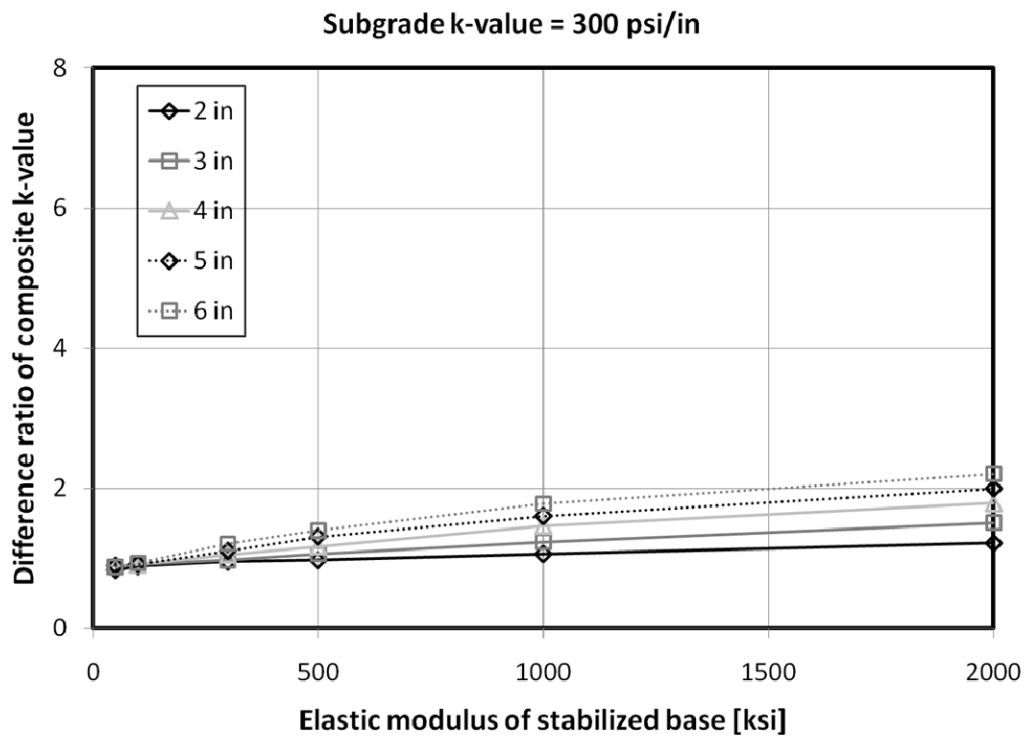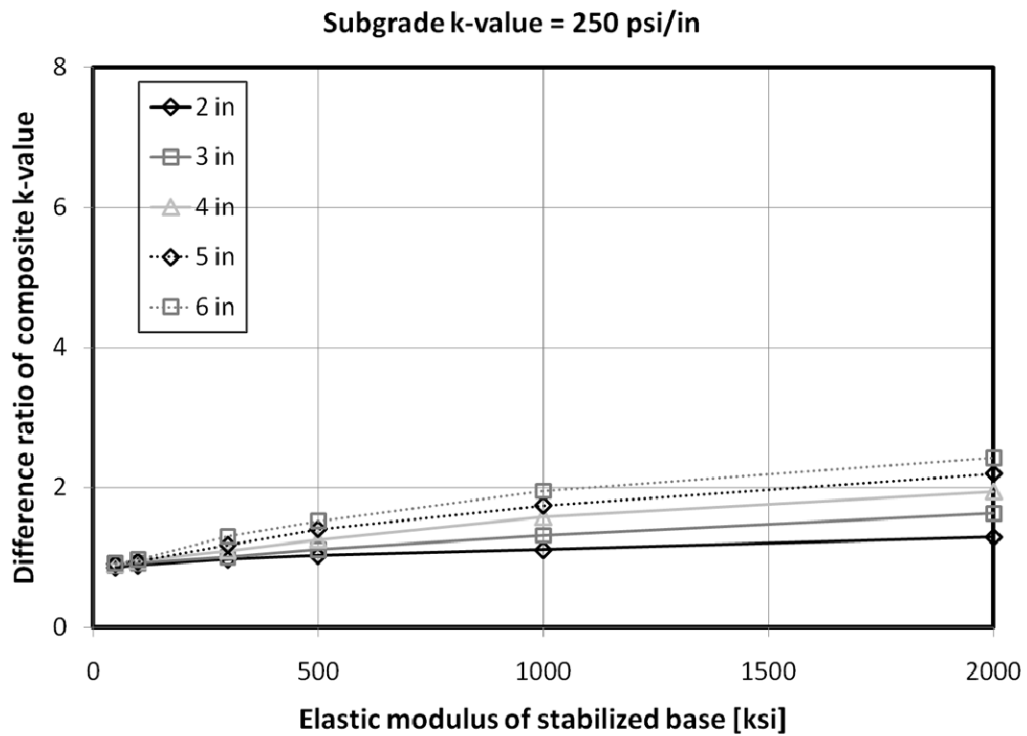**Figure B 28. Effects of elastic modulus of base under wheel loading (4)**
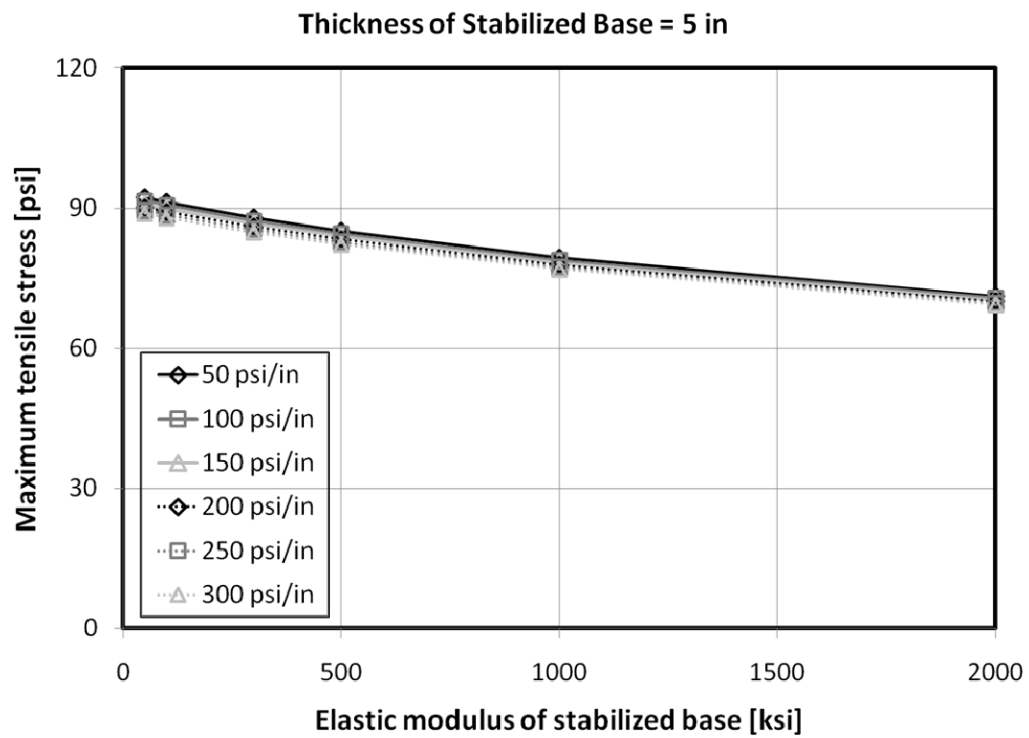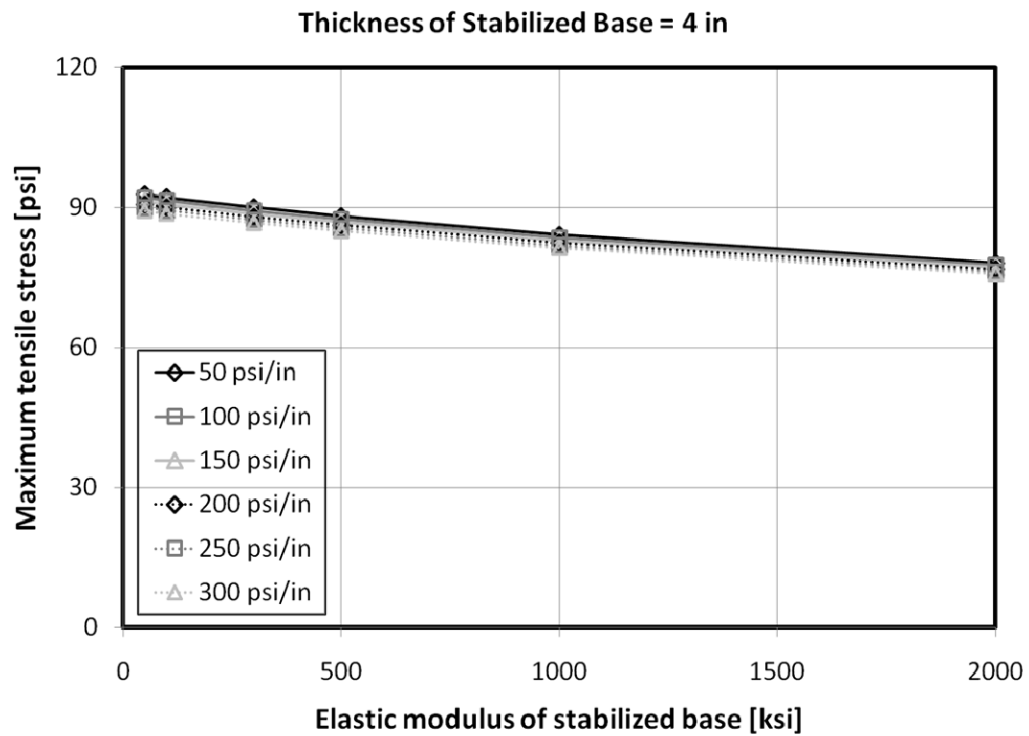
Figure B 29. Effects of elastic modulus of base under wheel loading (5)
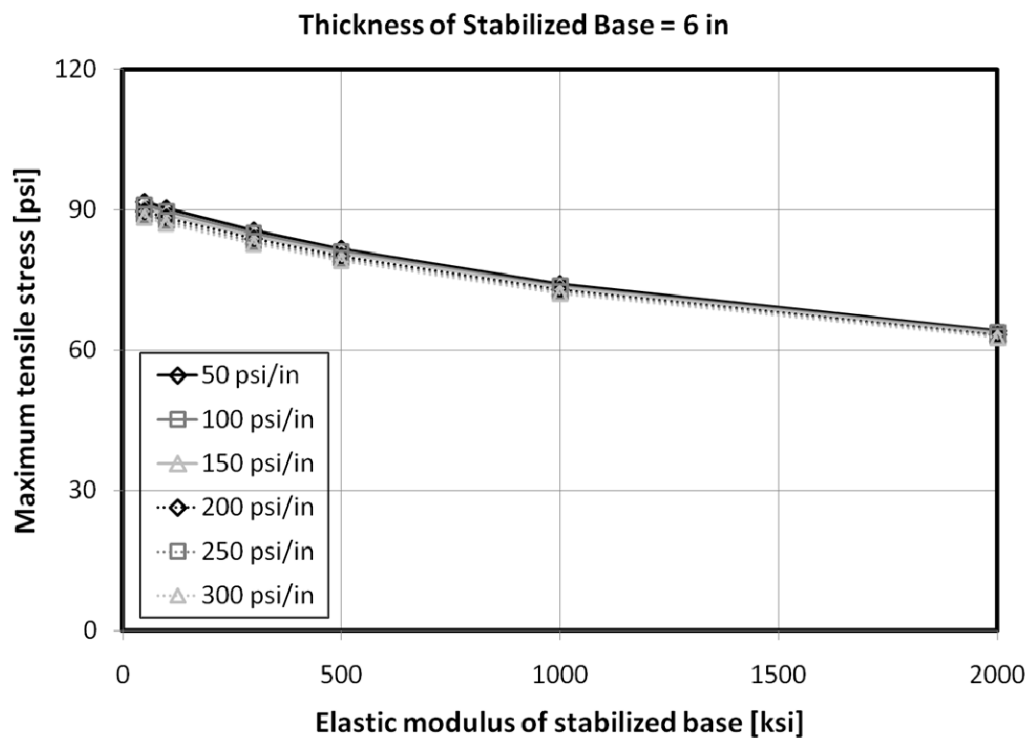
Figure B 30. Effects of elastic modulus of base under wheel loading (6)

➢ *Effects of k-value of Subgrade Layer Under Wheel Loading*
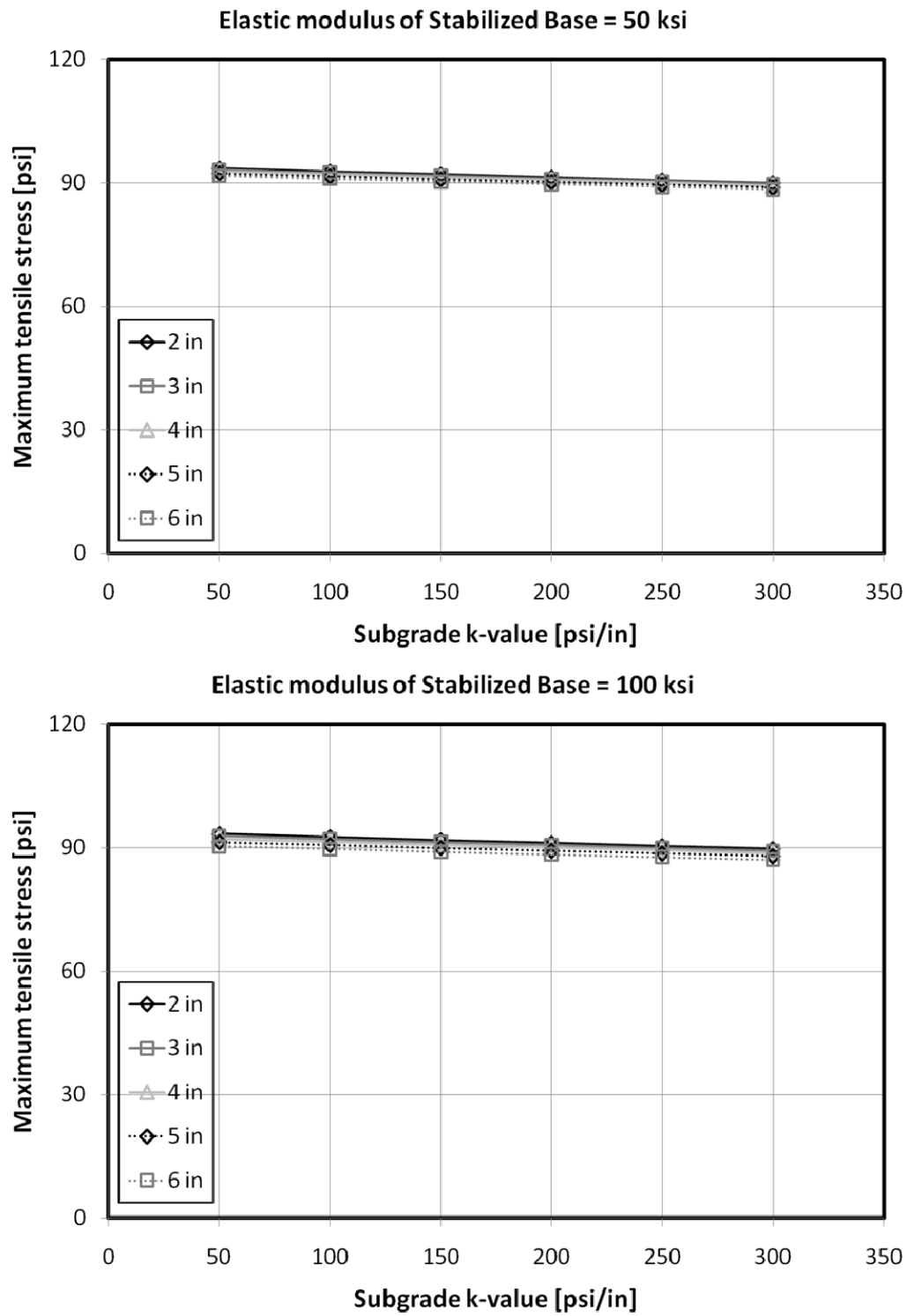
Figure B 31. Effects of *k*-value of subgrade layer under wheel loading (1)

Elastic modulus of Stabilized Base = 300 ksi

Elastic modulus of Stabilized Base = 500 ksi
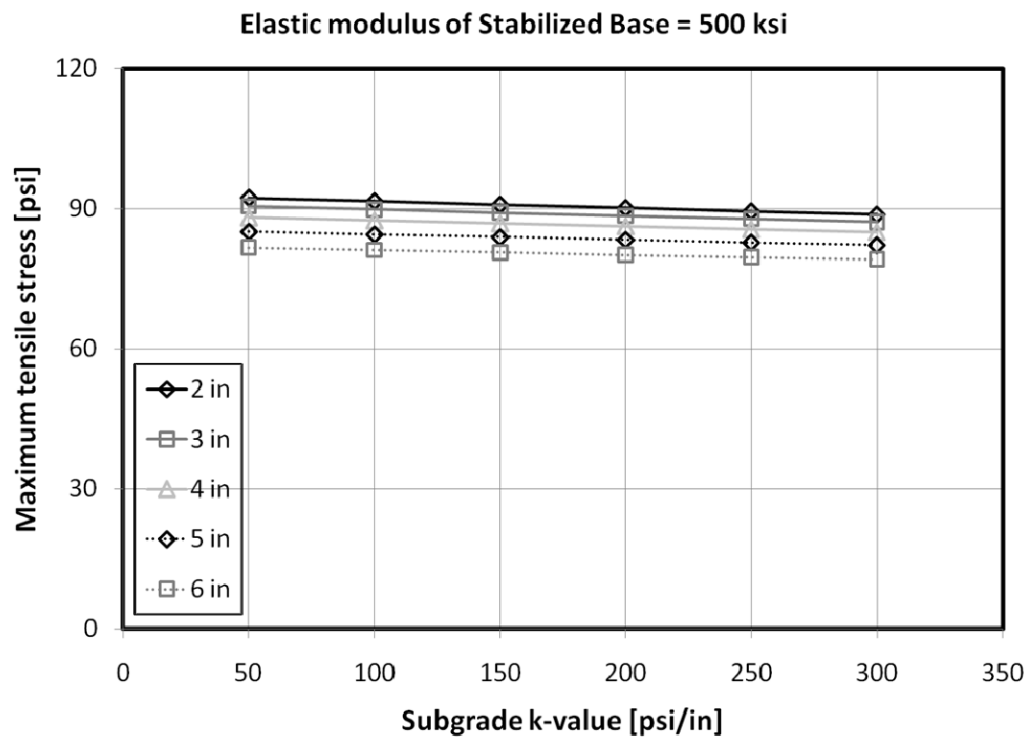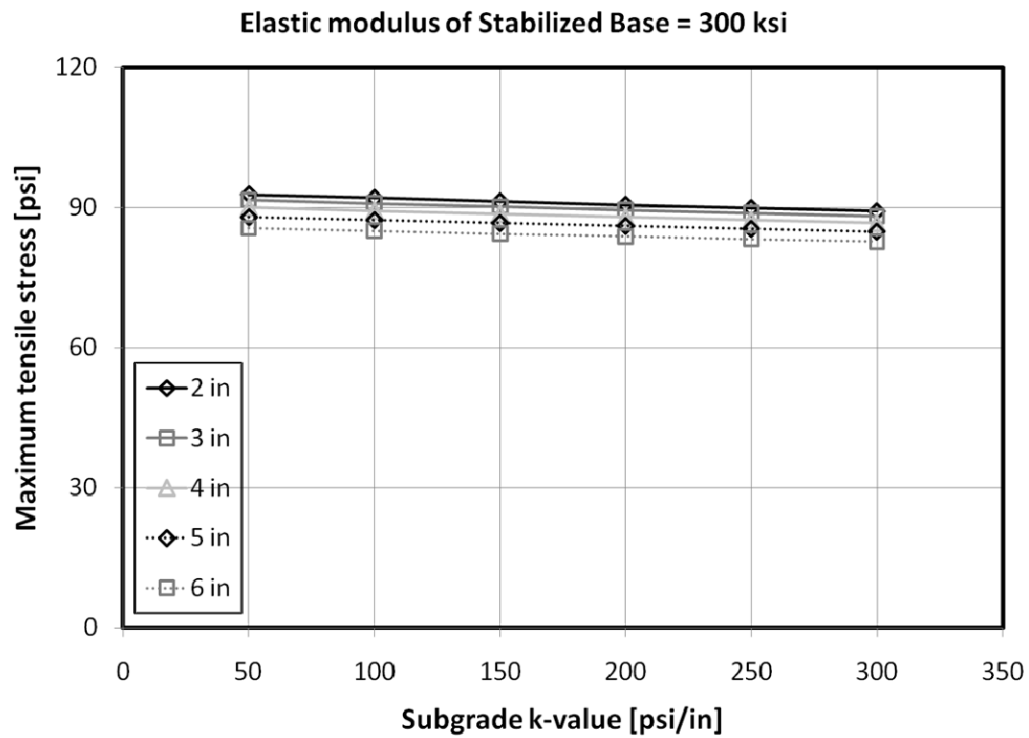
Figure B 32. Effects of *k*-value of subgrade layer under wheel loading (2)
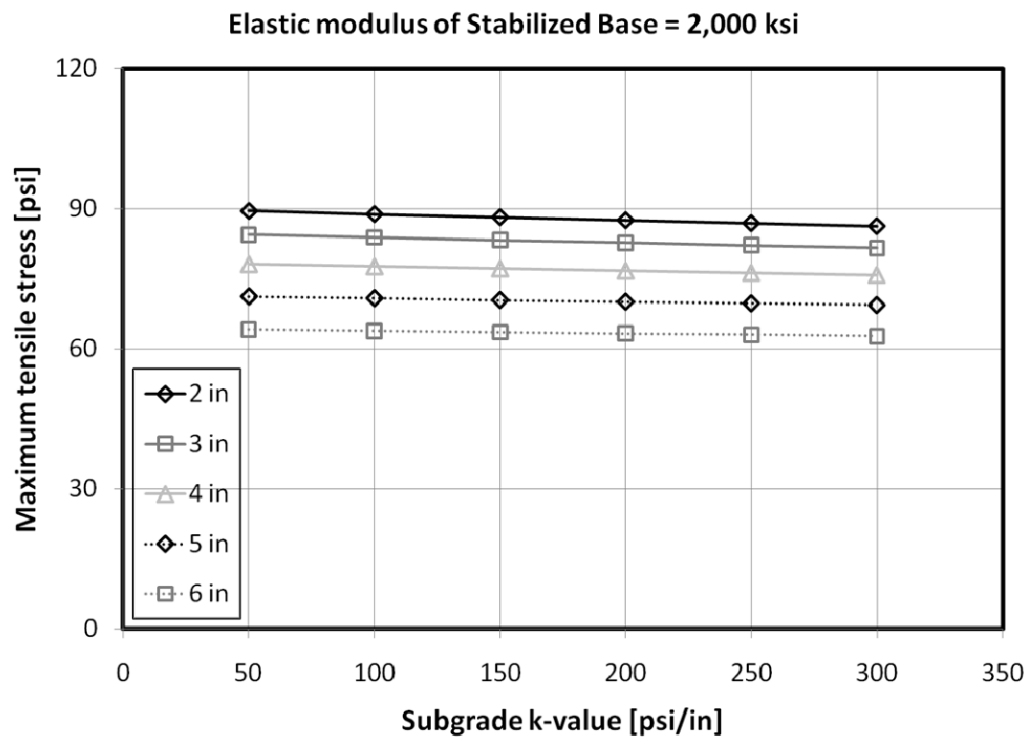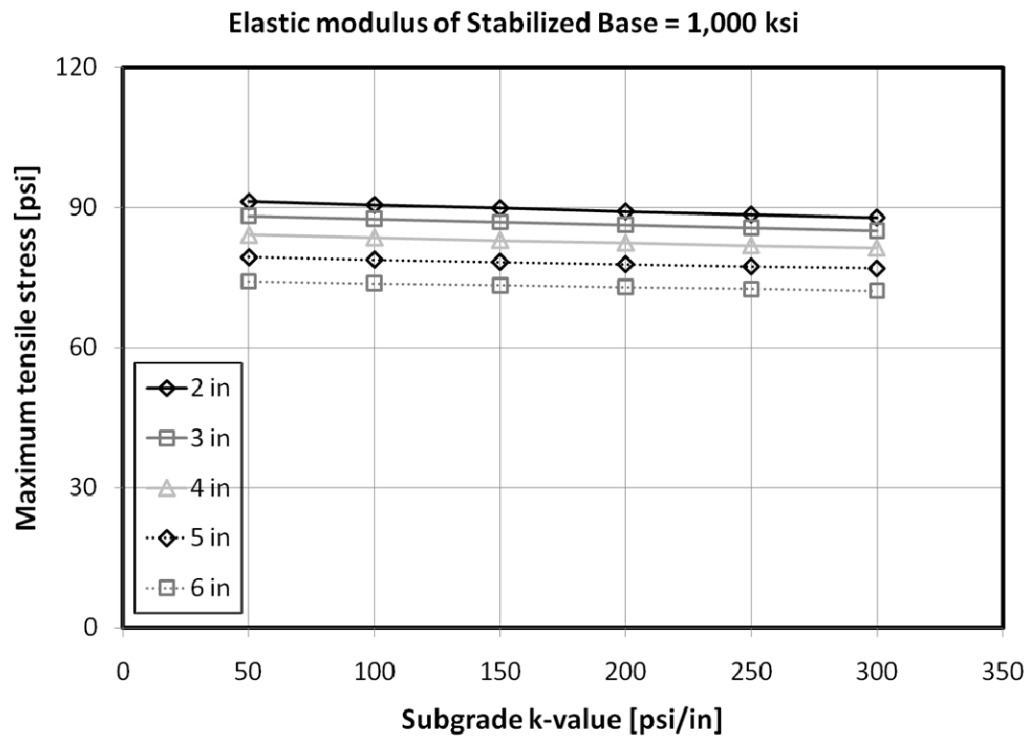
Figure B 33. Effects of *k*-value of subgrade layer under wheel loading (3)

Thickness of Stabilized Base = 2 in

Thickness of Stabilized Base = 3 in
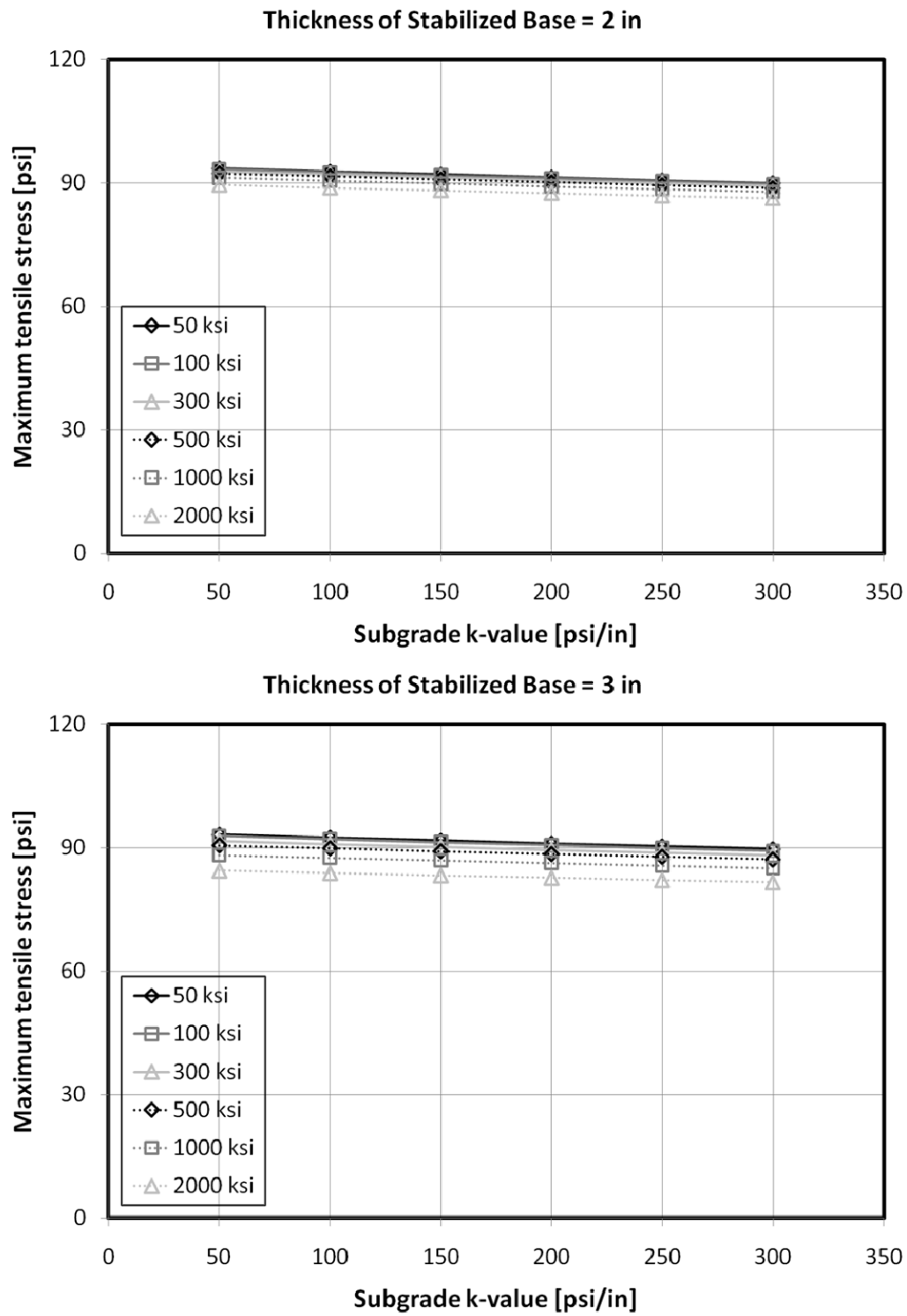
Figure B 34. Effects of *k*-value of subgrade layer under wheel loading (4)

266

Thickness of Stabilized Base = 4 in

Thickness of Stabilized Base = 5 in
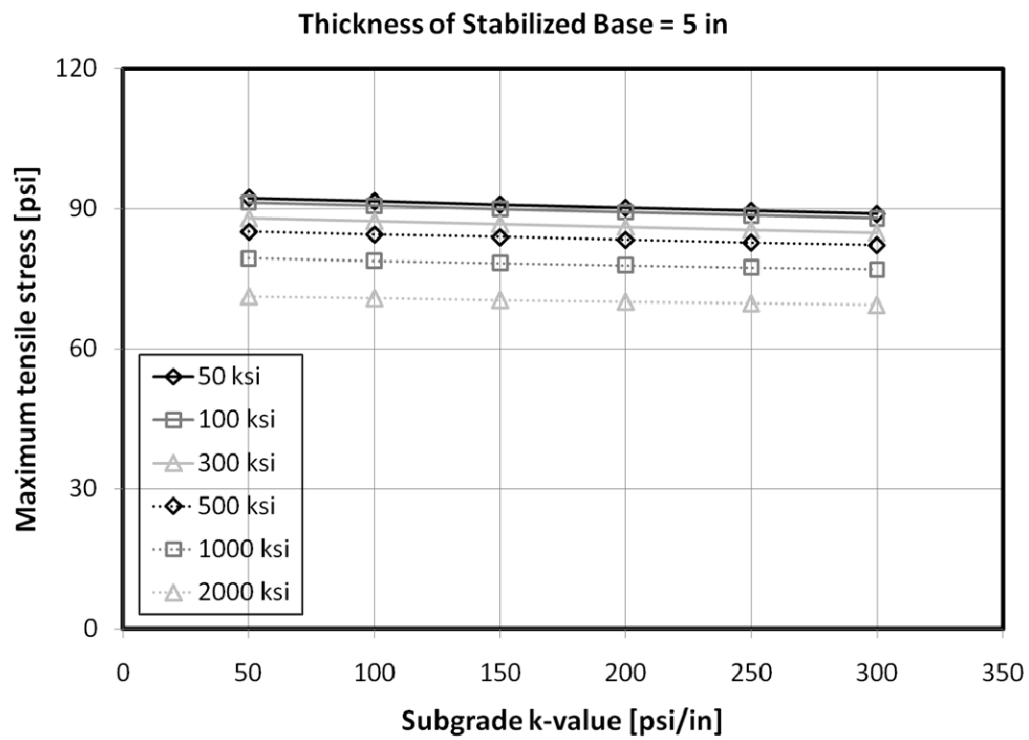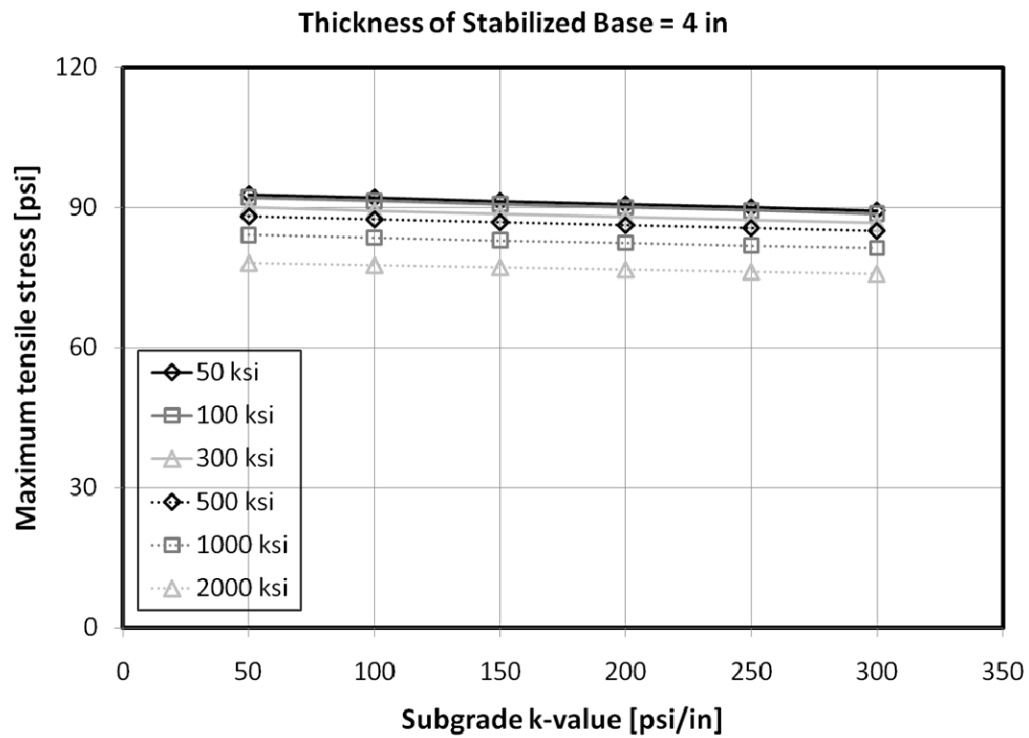
Figure B 35. Effects of *k*-value of subgrade layer under wheel loading (5)
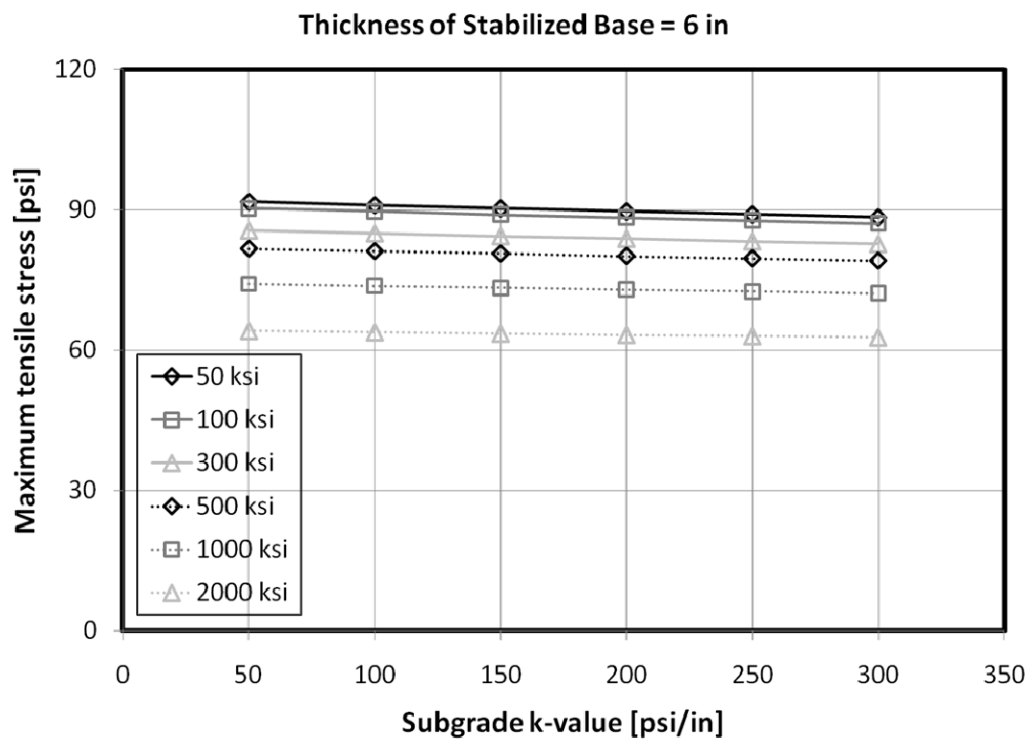
Figure B 36. Effects of *k*-value of subgrade layer under wheel loading (6)

APPENDIX C

Effects of Support Layer Properties on Difference Ratio of Composite *k*-value

Between Directly Computed Composite *k*-value

using Elastic and *k*-value Composite Support Model and

Back-found Composite *k*-value using Simple Support Model

under Temperature and Wheel Loadings

➢ *Effects of Thickness of Stabilized Base Layer Under Temperature Loading*

Figure C 1. Effects of thickness of stabilized base under temperature loading (1)

Figure C 2. Effects of thickness of stabilized base under temperature loading (2)

Figure C 3. Effects of thickness of stabilized base under temperature loading (3)
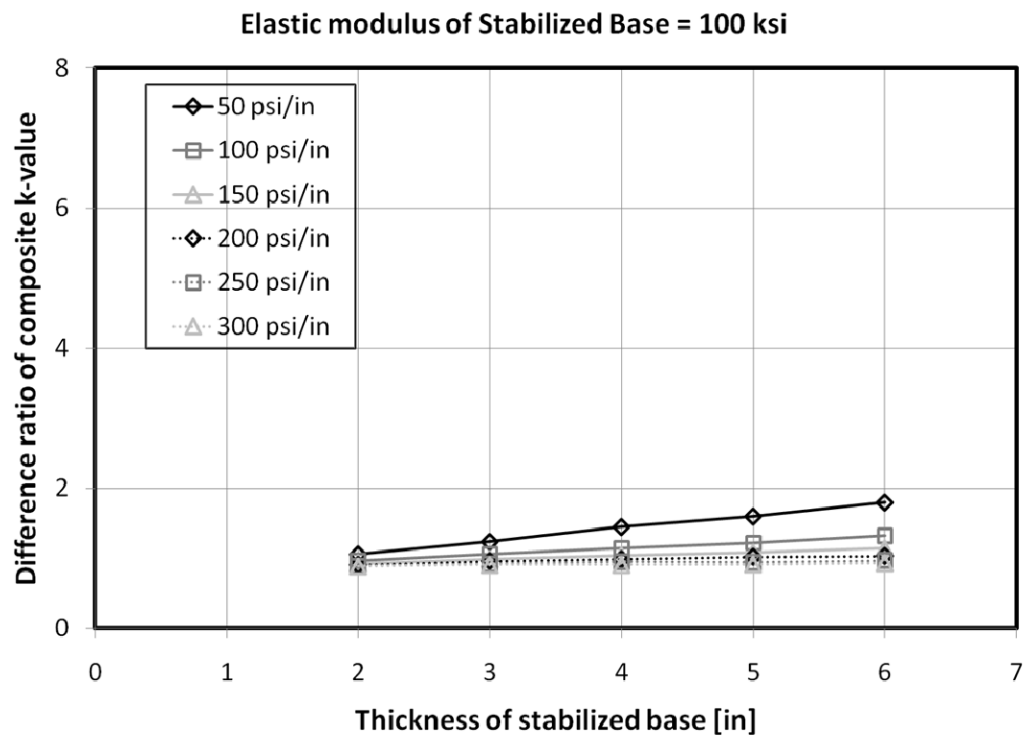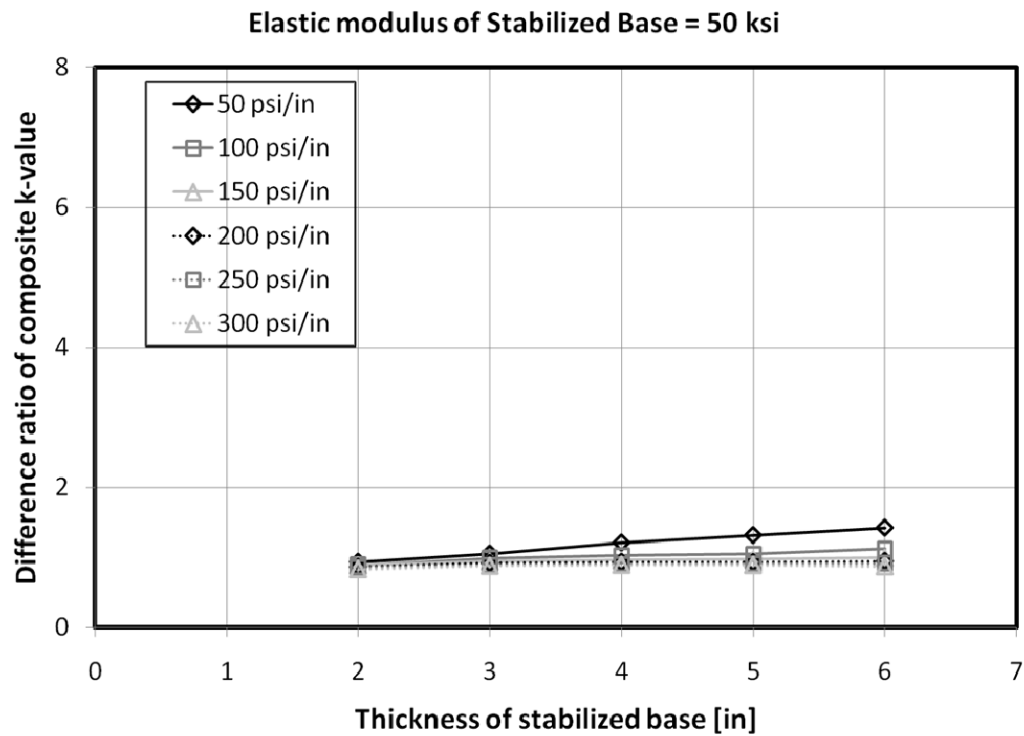
Figure C 4. Effects of thickness of stabilized base under temperature loading (4)

Figure C 5. Effects of thickness of stabilized base under temperature loading (5)

Figure C 6. Effects of thickness of stabilized base under temperature loading (6)

➢ *Effects of Modulus of Elasticity of Base Material Under Temperature Loading*
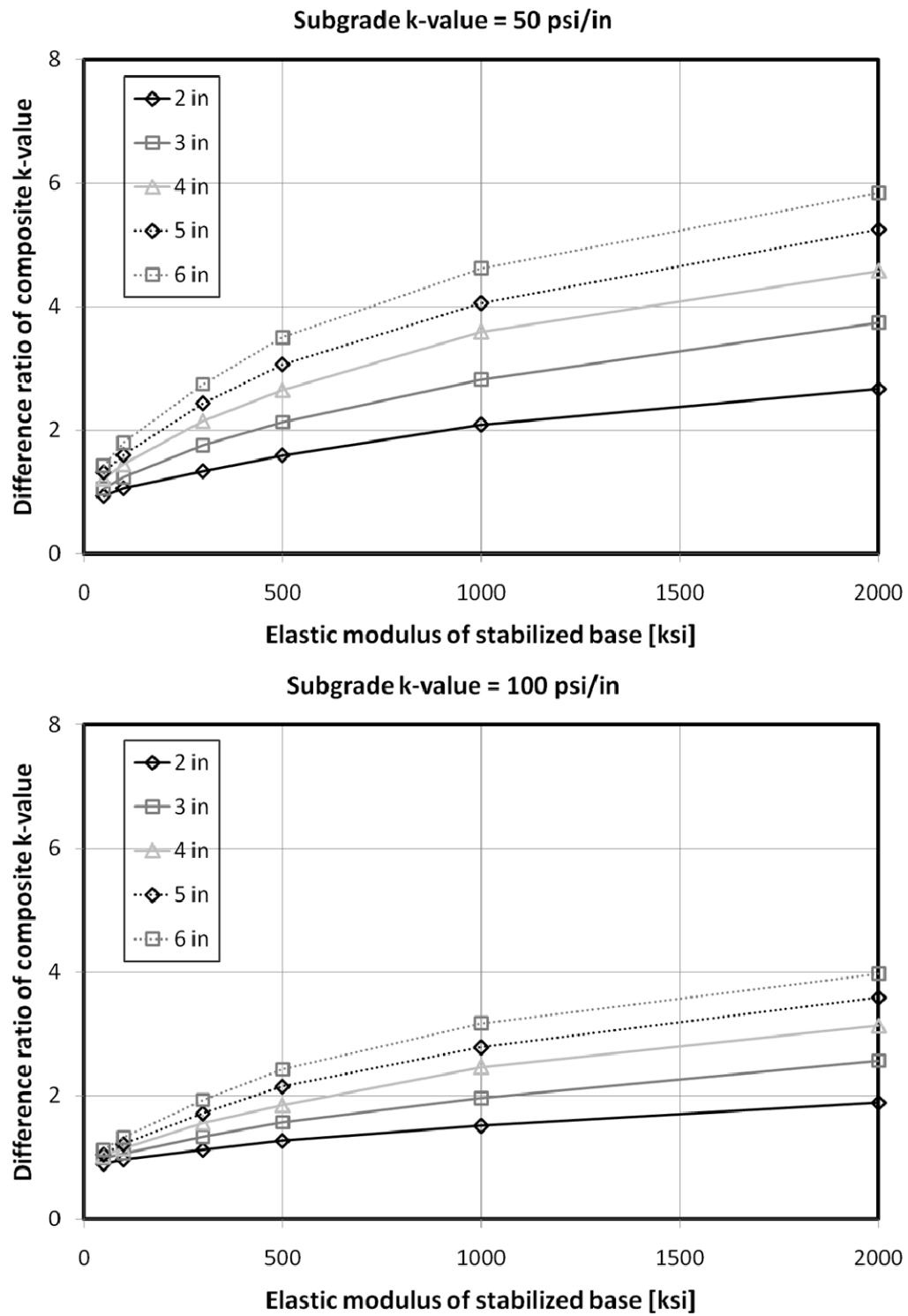
Figure C 7. Effects of elastic modulus of base under temperature loading (1)
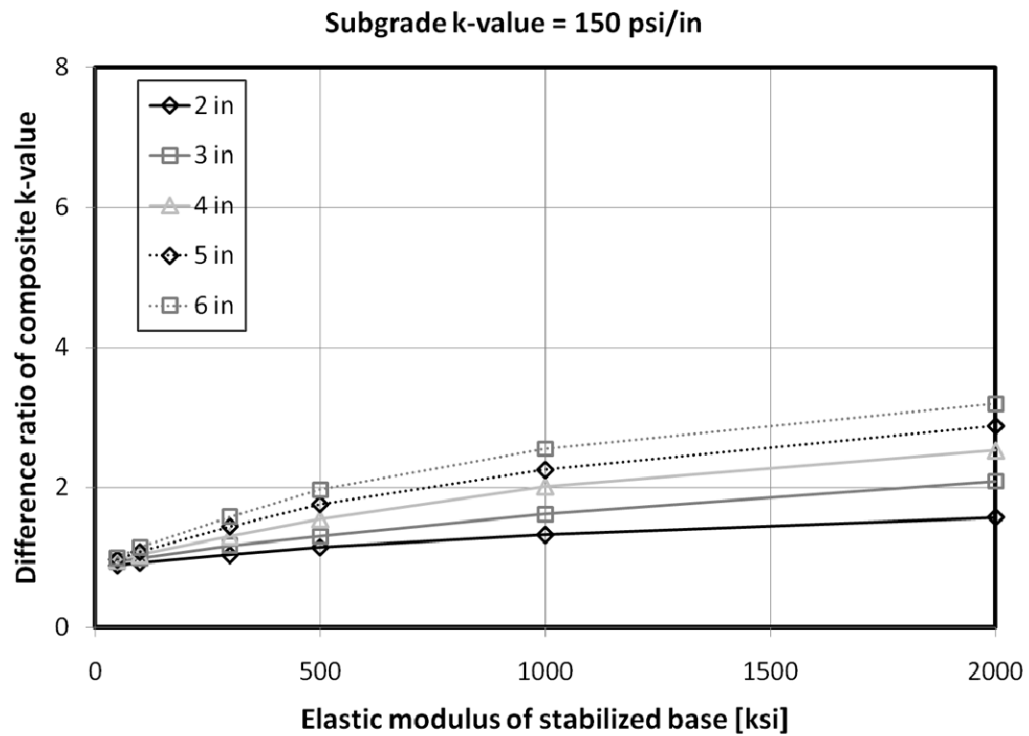
Figure C 8. Effects of elastic modulus of base under temperature loading (2)

Figure C 9. Effects of elastic modulus of base under temperature loading (3)
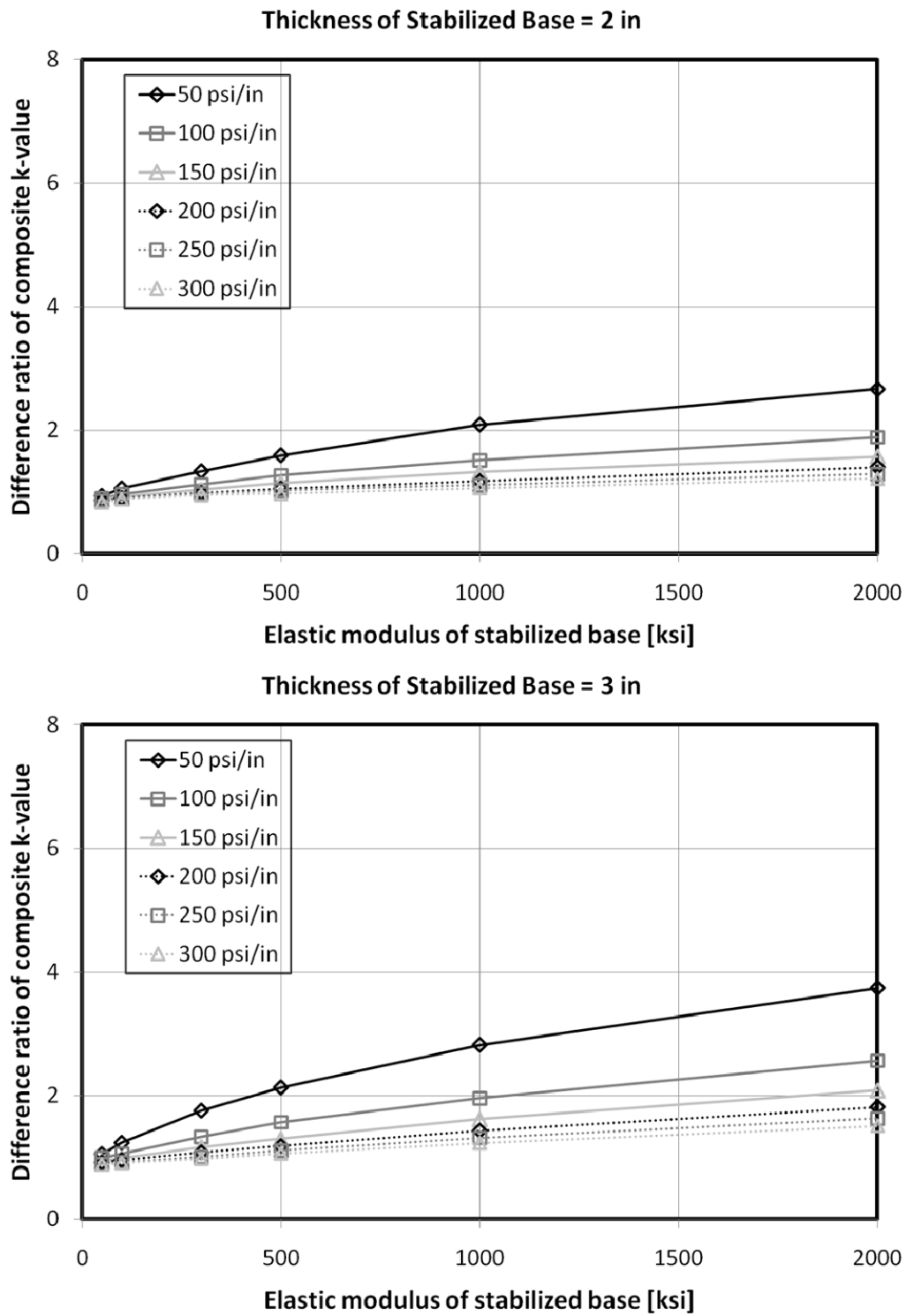
Figure C 10. Effects of elastic modulus of base under temperature loading (4)
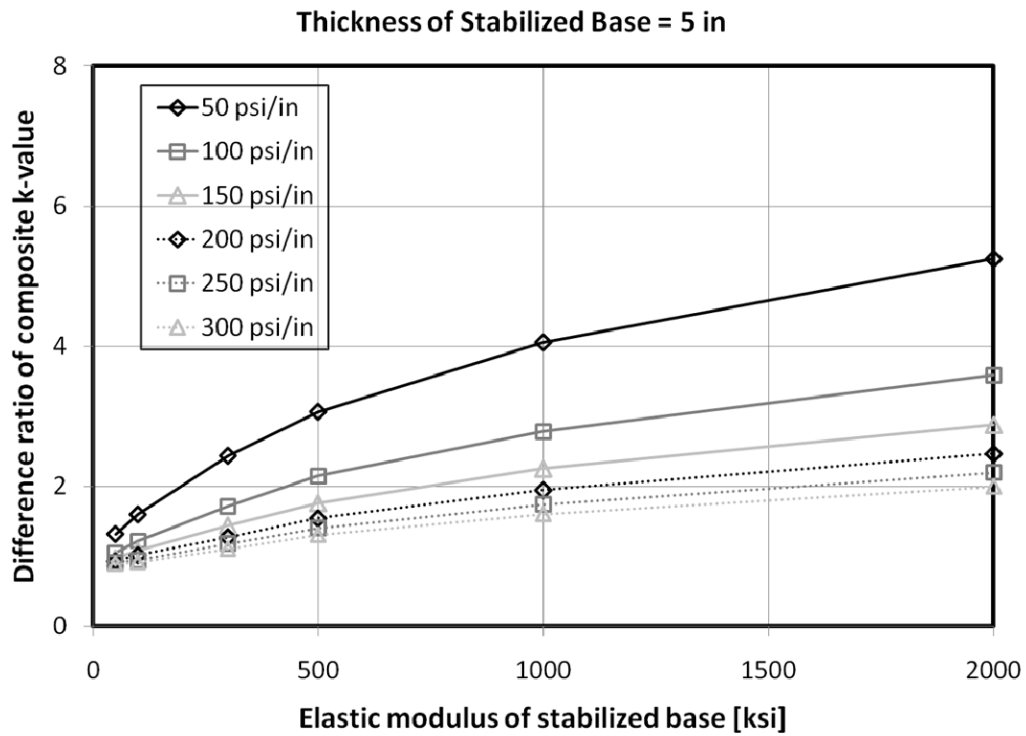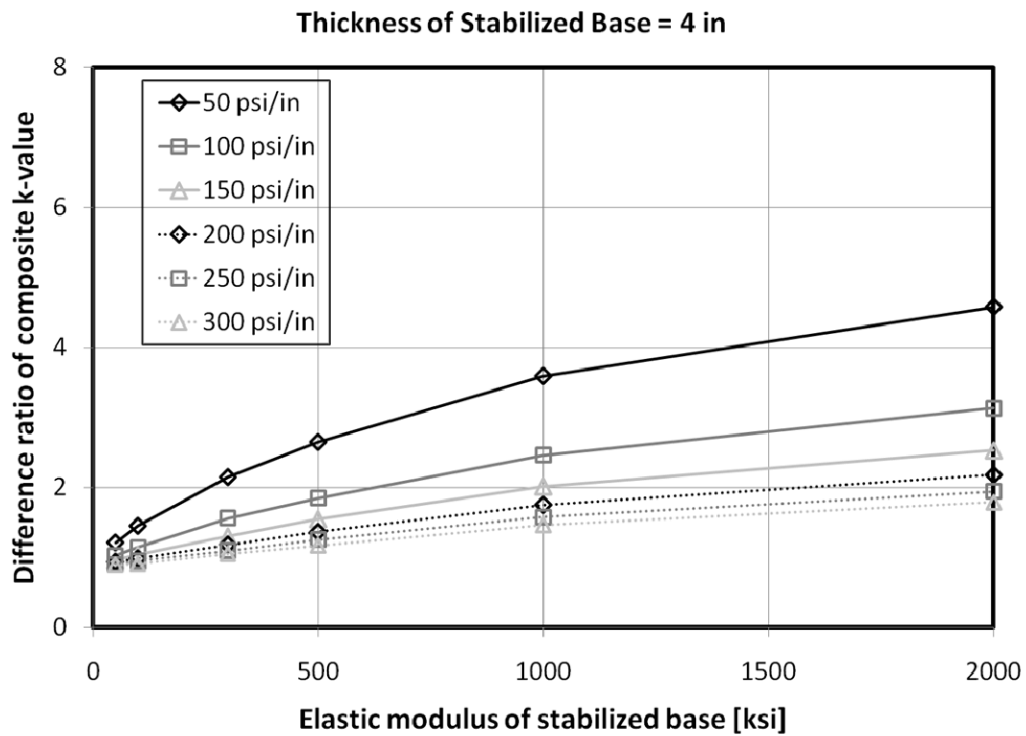
Figure C 11. Effects of elastic modulus of base under temperature loading (5)
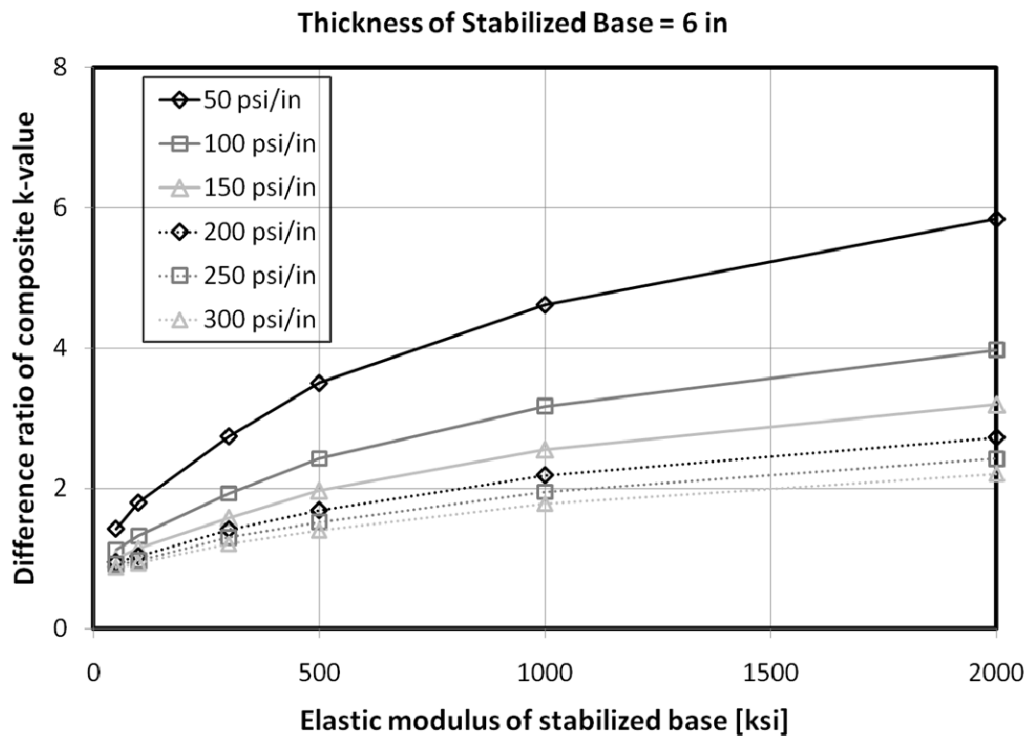
Figure C 12. Effects of elastic modulus of base under temperature loading (6)

➤ *Effects of k-value of Subgrade Layer Under Temperature Loading*

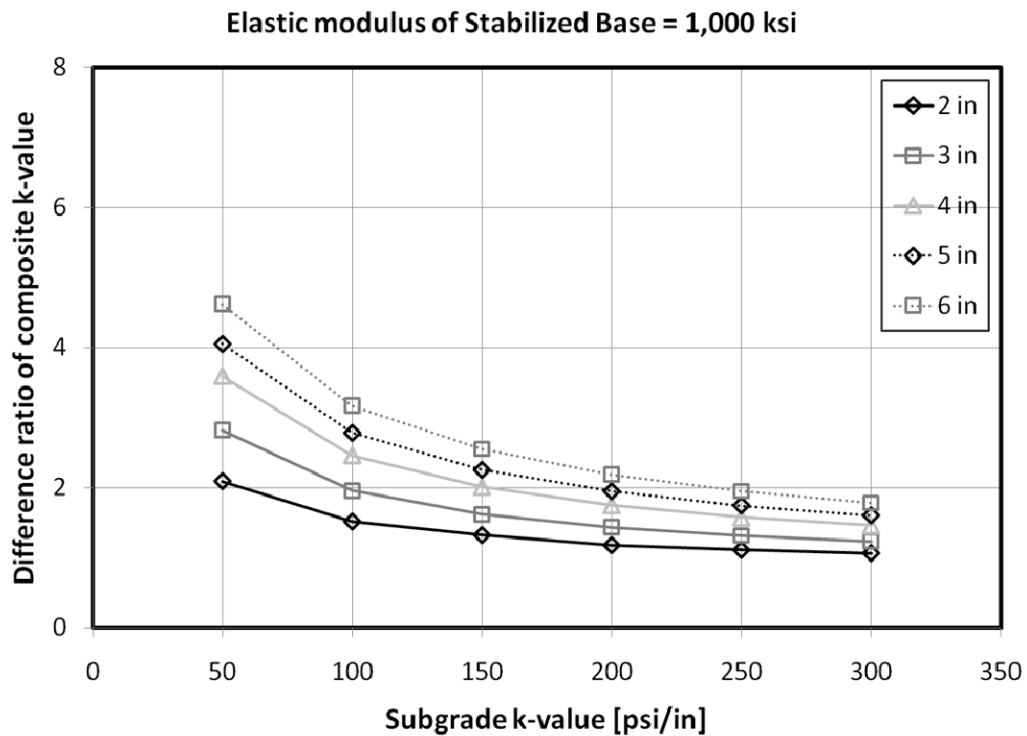**Elastic modulus of Stabilized Base = 50 ksi**

Elastic modulus of Stabilized Base = 100 ksi
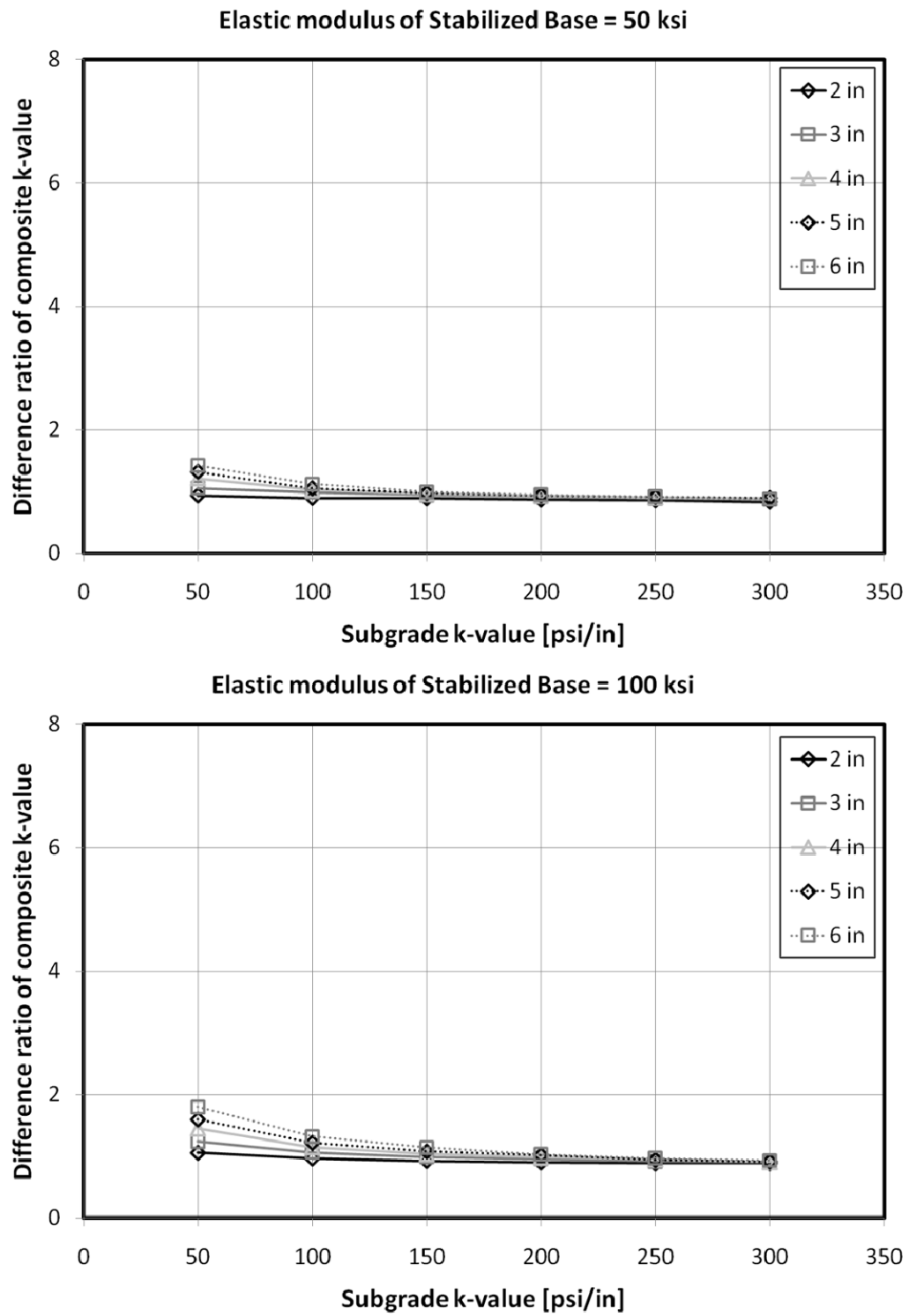
Figure C 13. Effects of *k*-value of subgrade layer under temperature loading (1)

Elastic modulus of Stabilized Base = 300 ksi

Elastic modulus of Stabilized Base = 500 ksi
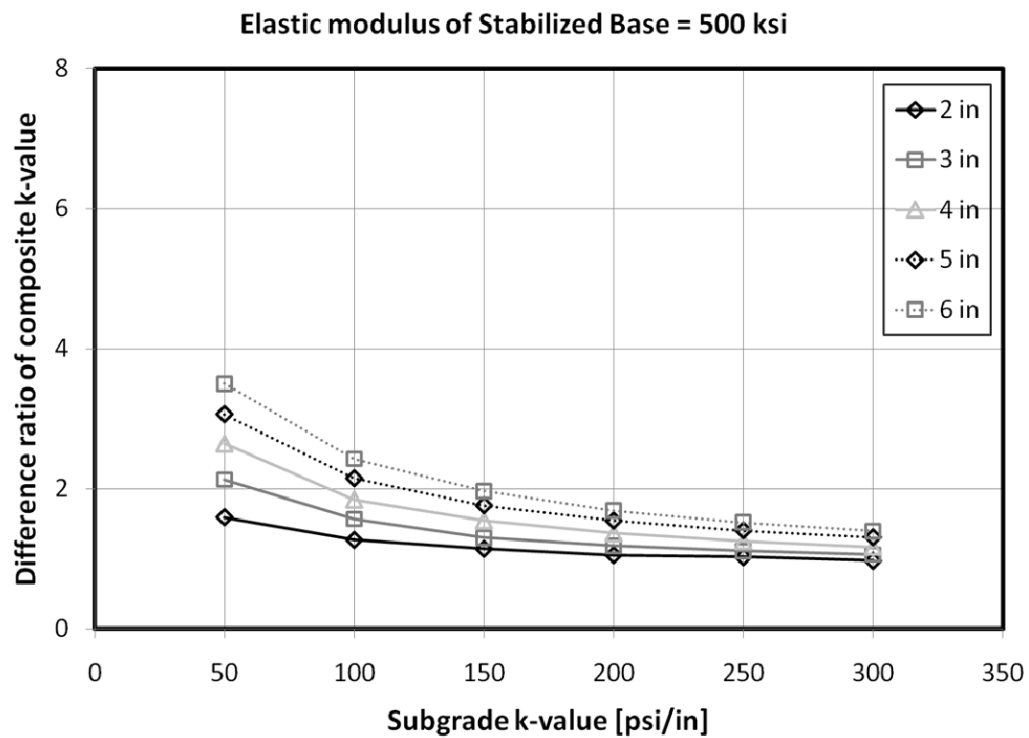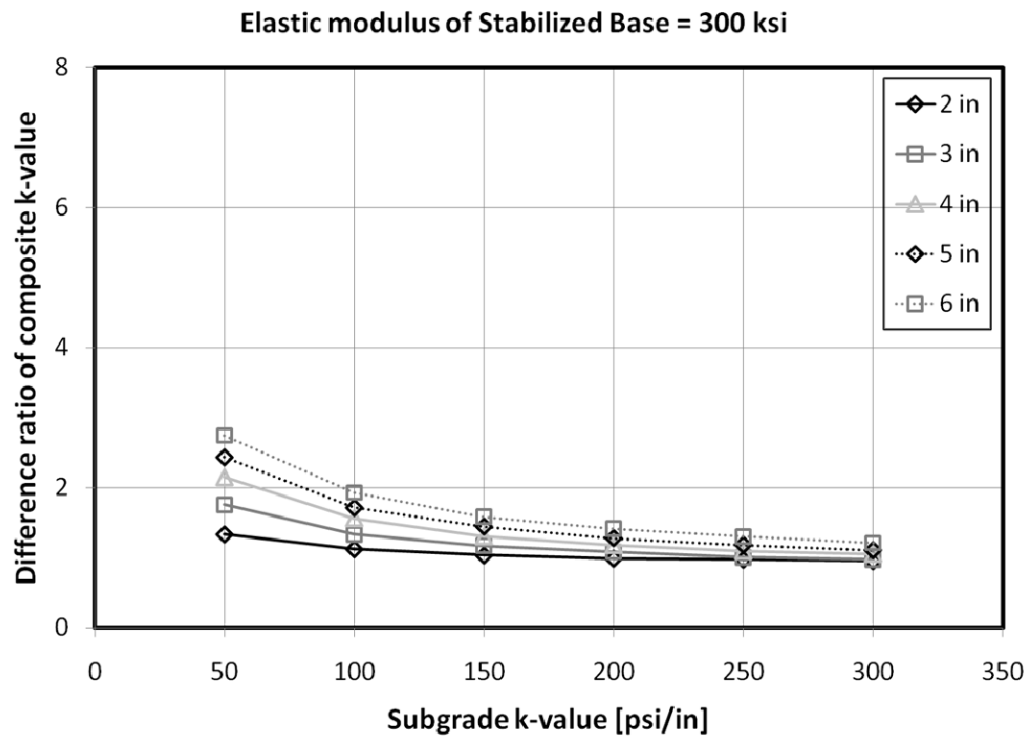
Figure C 14. Effects of *k*-value of subgrade layer under temperature loading (2)

283
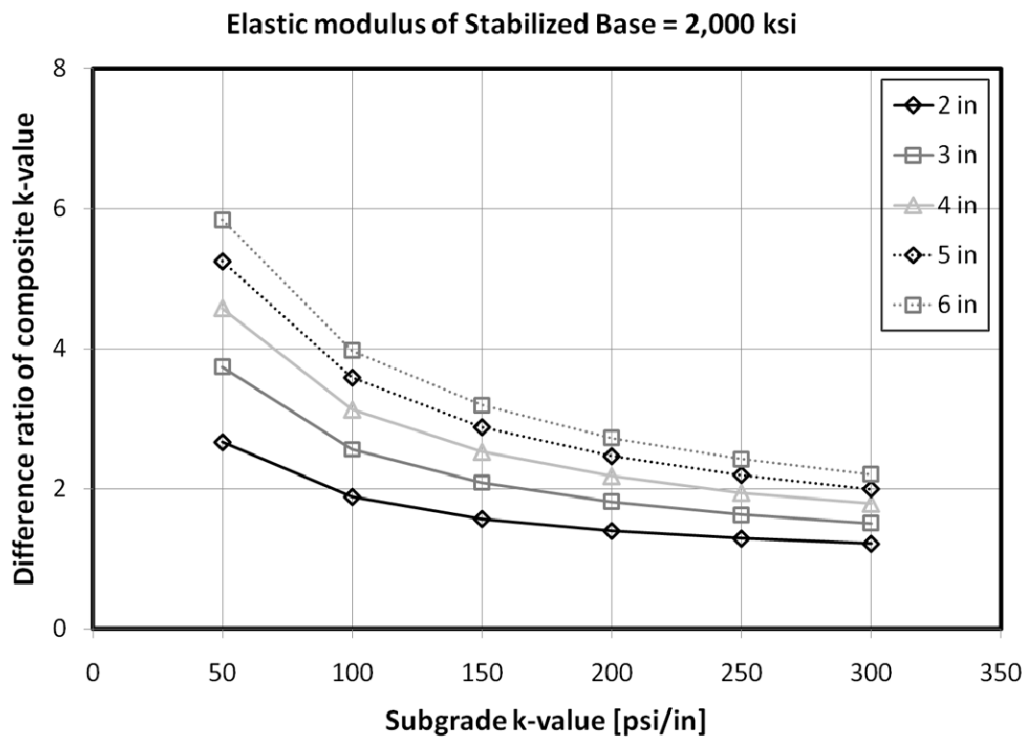
Figure C 15. Effects of *k*-value of subgrade layer under temperature loading (3)
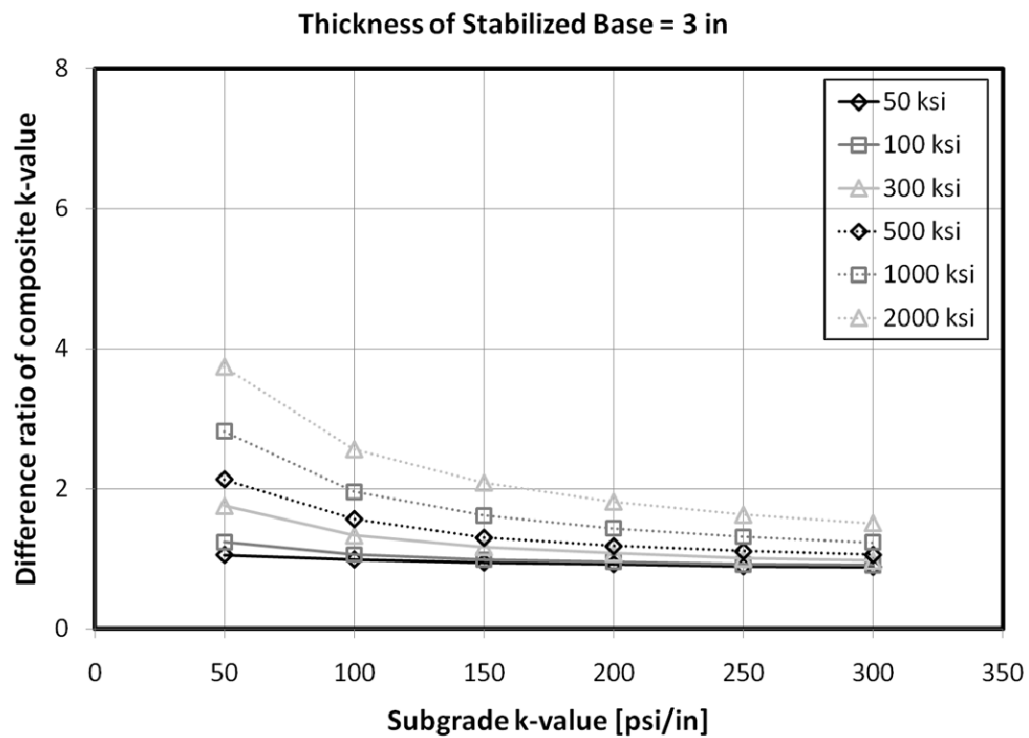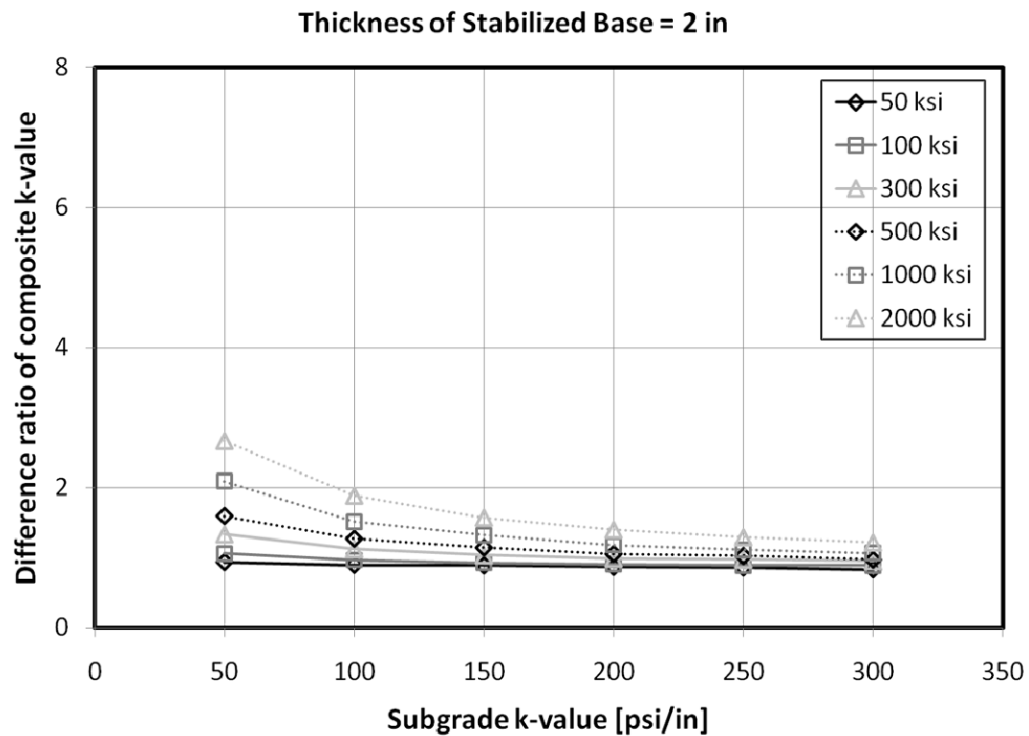
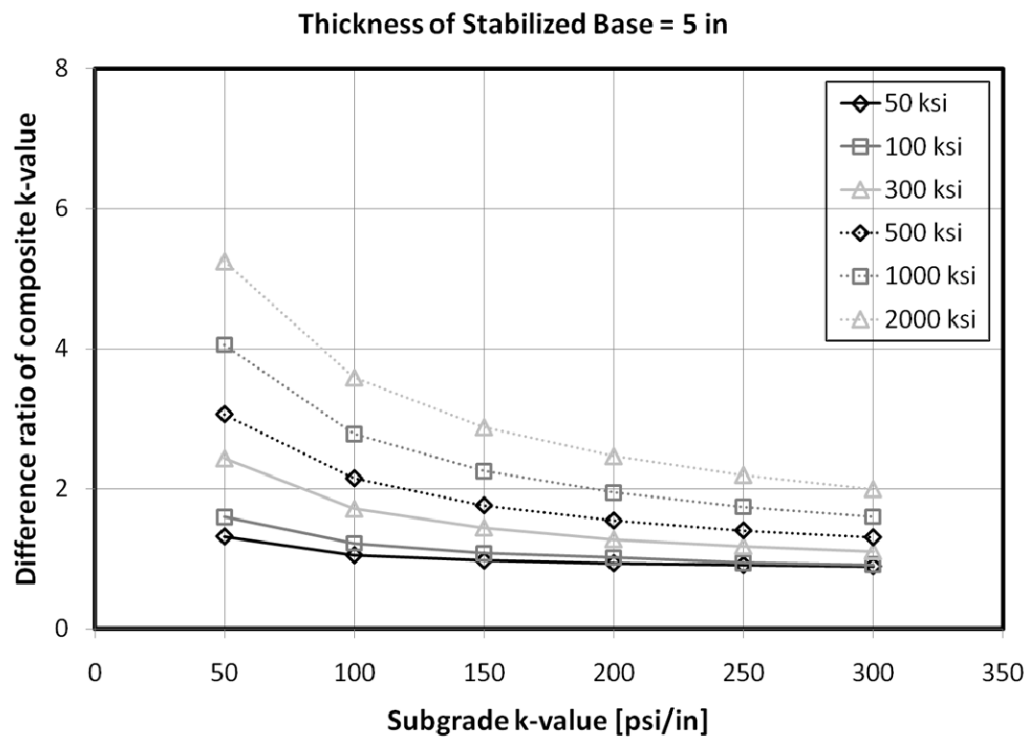**Figure C 16. Effects of *k*-value of subgrade layer under temperature loading (4)**
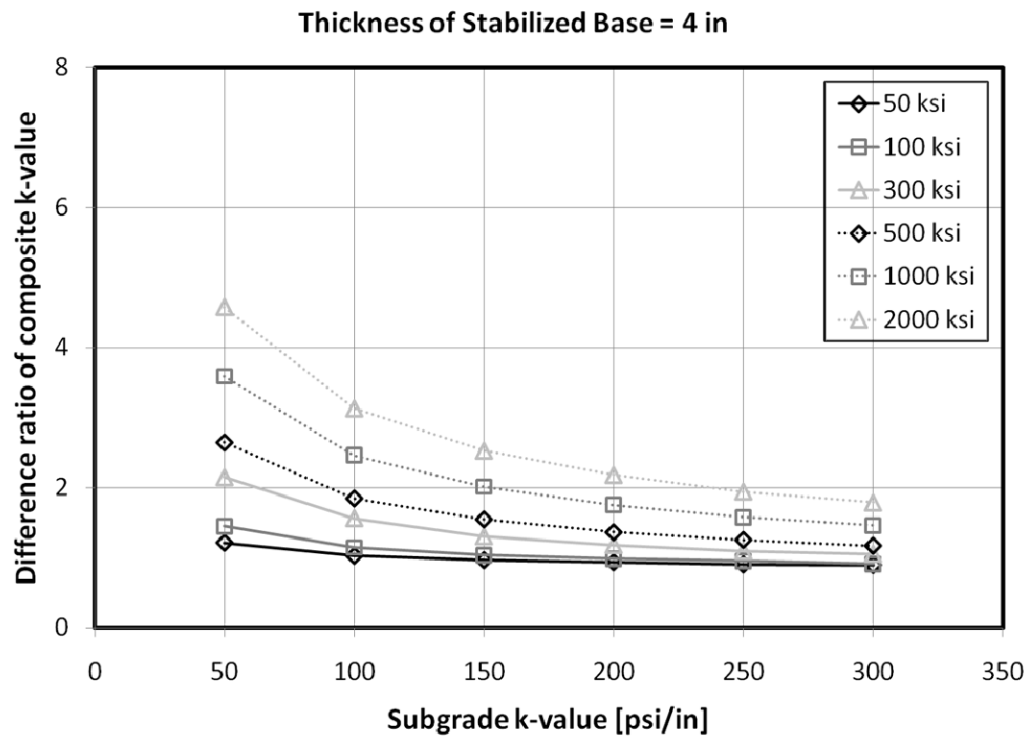
Figure C 17. Effects of *k*-value of subgrade layer under temperature loading (5)
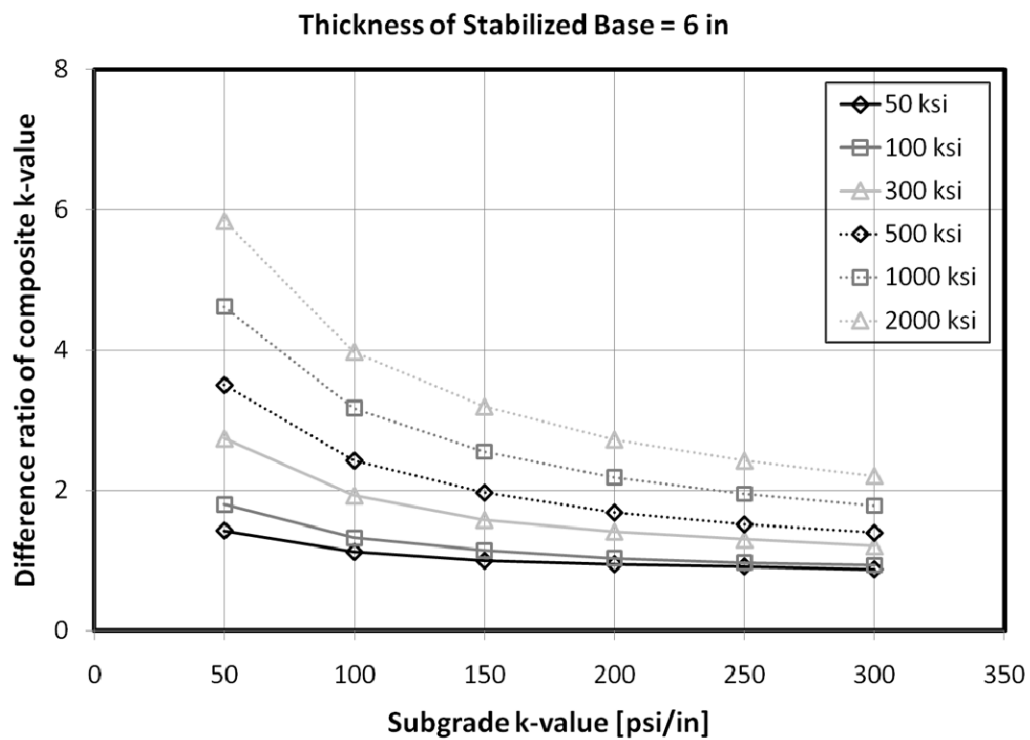
Figure C 18. Effects of *k*-value of subgrade layer under temperature loading (6)

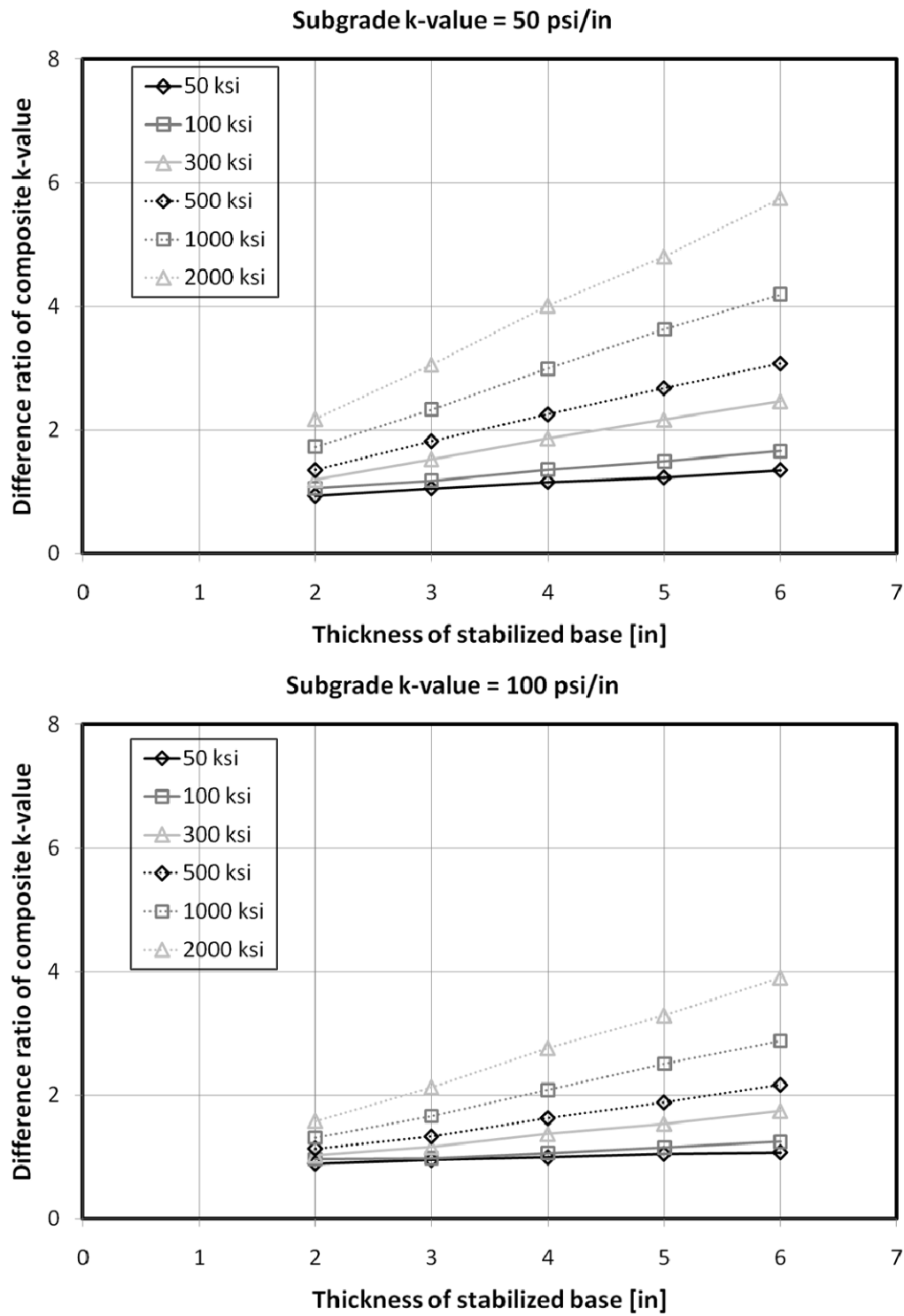➤ *Effects of Thickness of Stabilized Base Layer Under Wheel Loading*

Figure C 19. Effects of thickness of stabilized base under wheel loading (1)

Figure C 20. Effects of thickness of stabilized base under wheel loading (2)
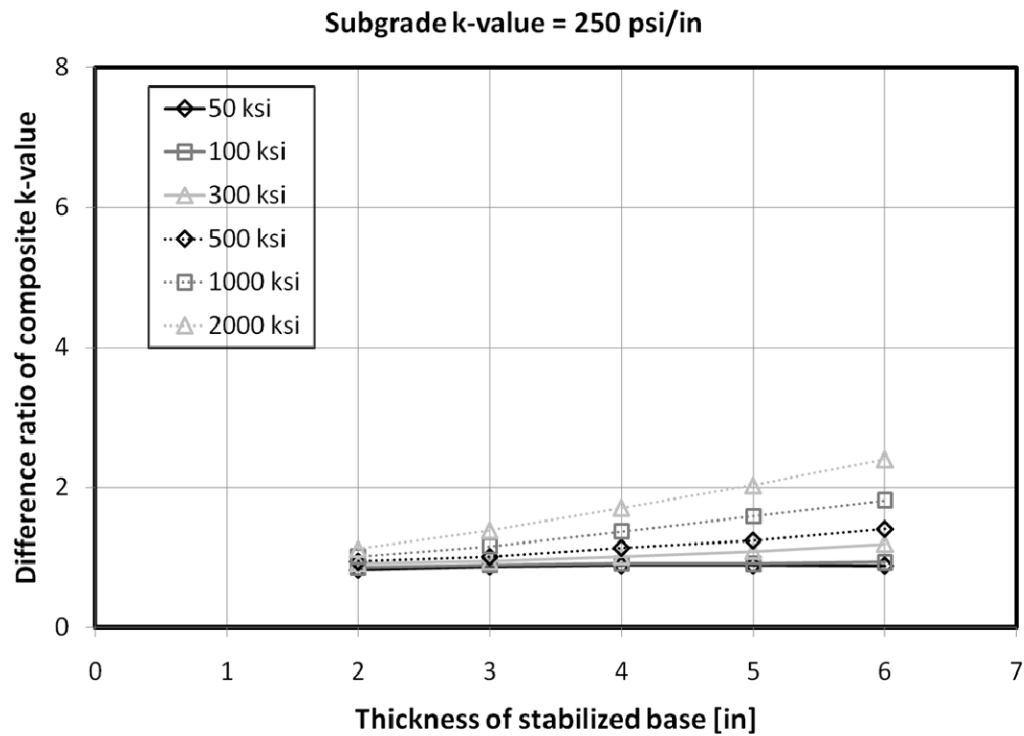
Figure C 21. Effects of thickness of stabilized base under wheel loading (3)
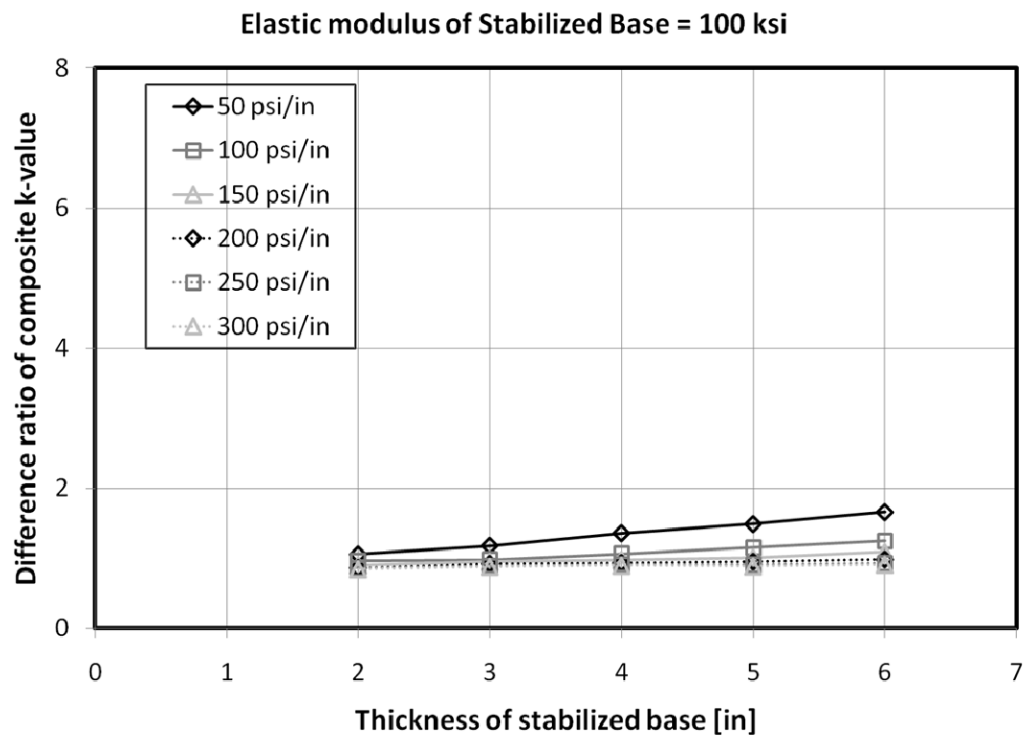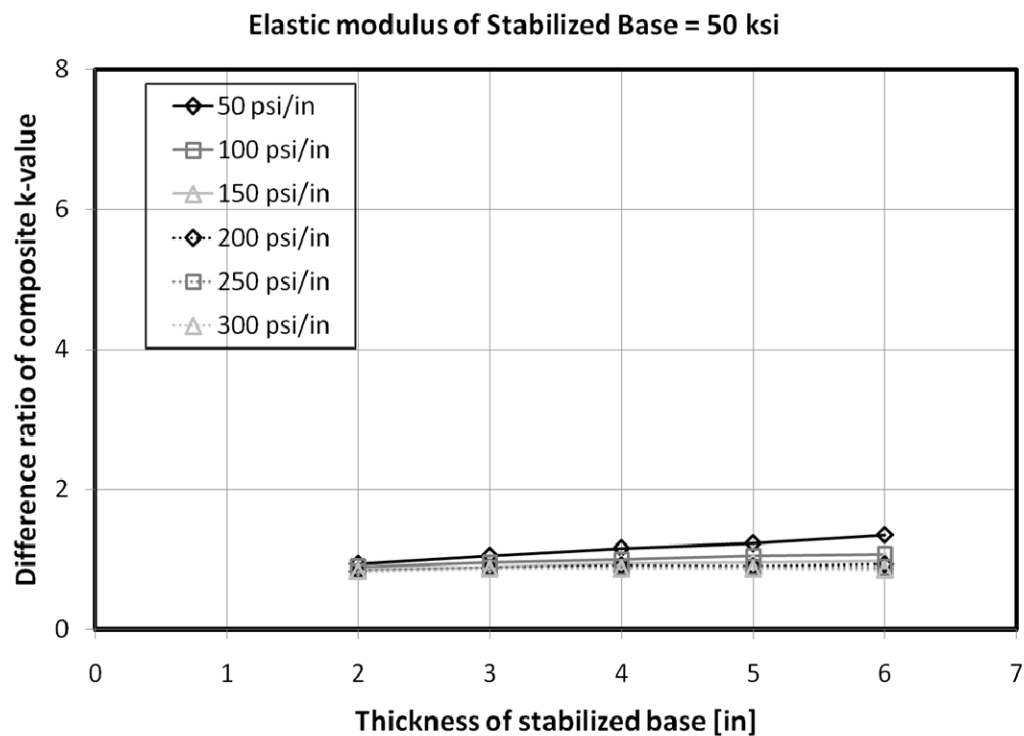
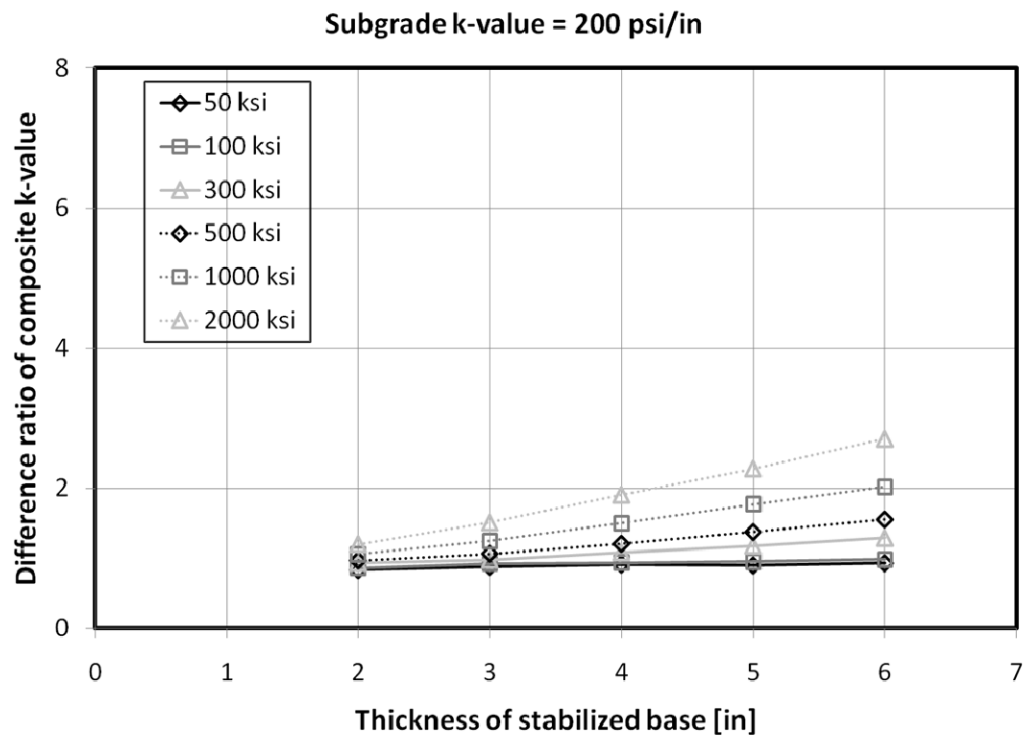**Figure C 22. Effects of thickness of stabilized base under wheel loading (4)**
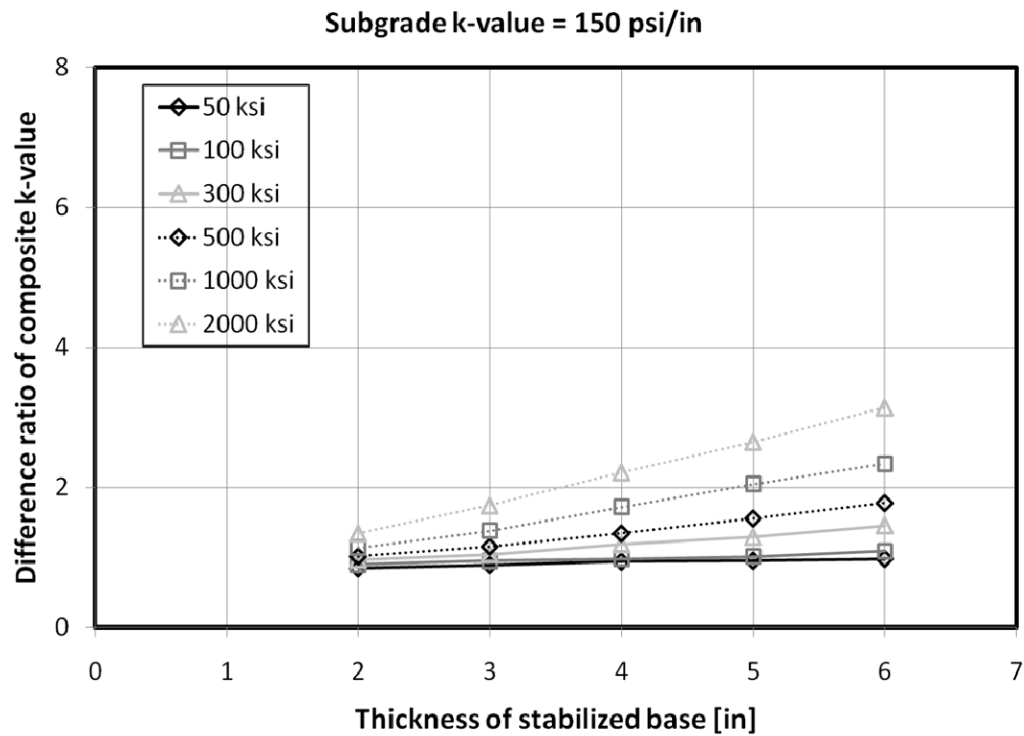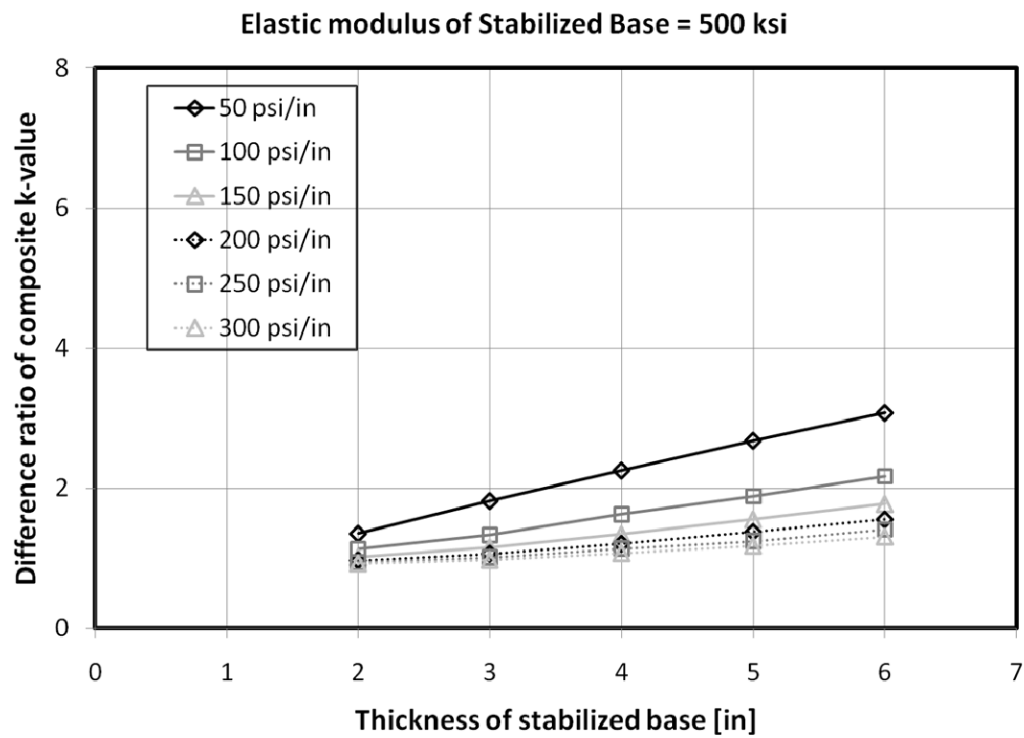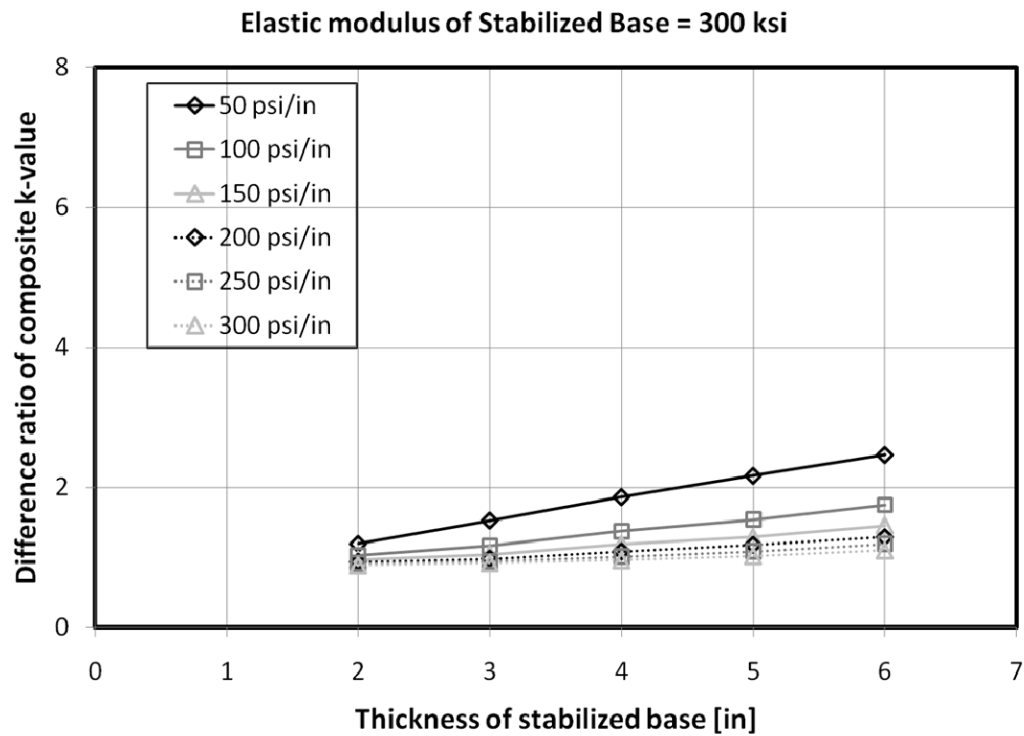
Figure C 23. Effects of thickness of stabilized base under wheel loading (5)
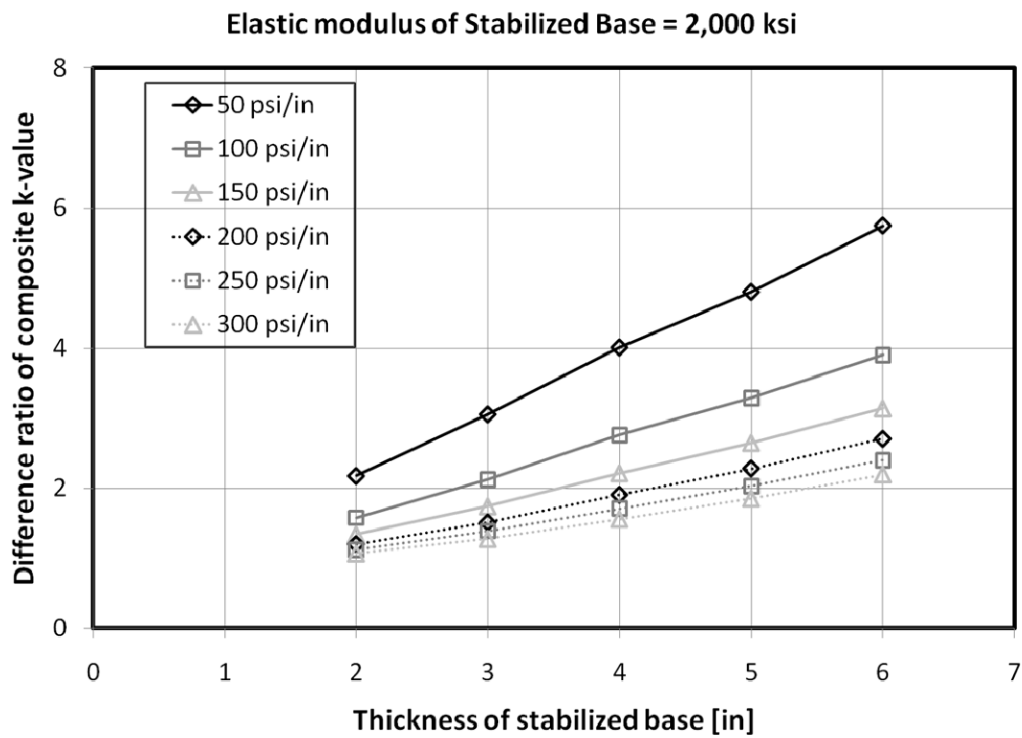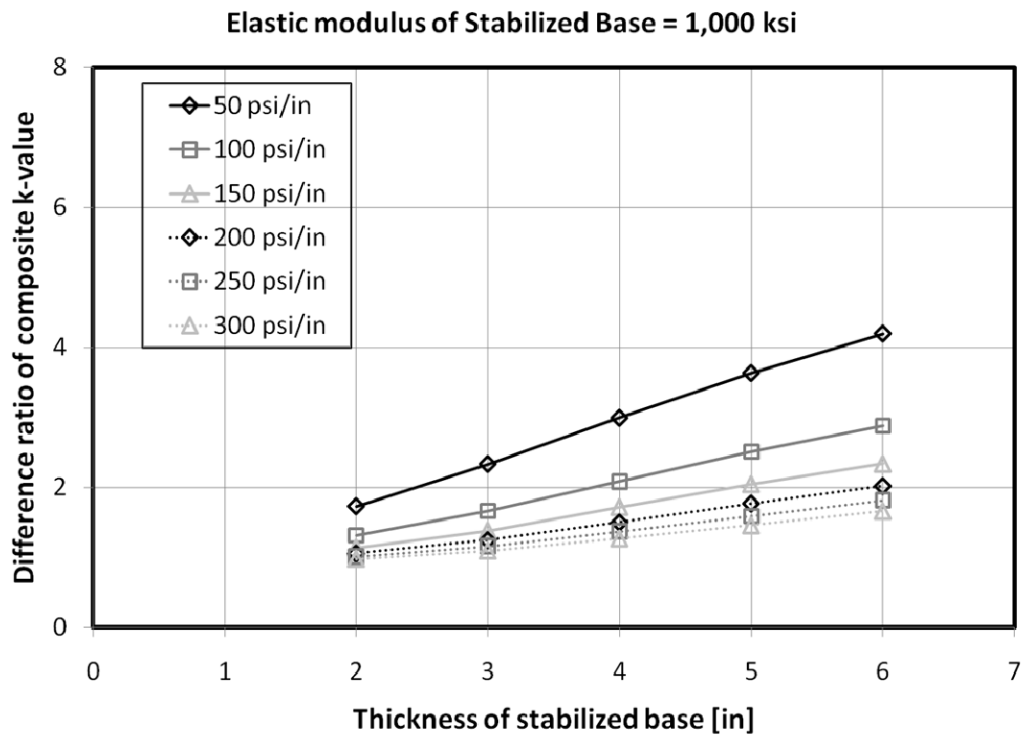
Figure C 24. Effects of thickness of stabilized base under wheel loading (6)
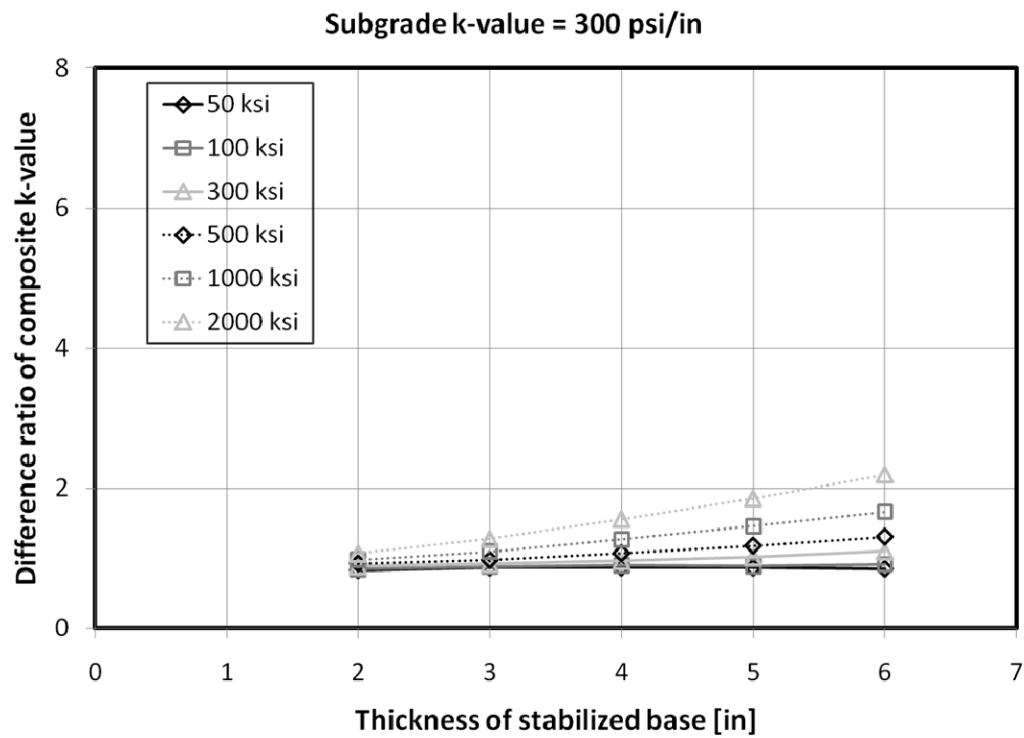
➢ *Effects of Modulus of Elasticity of Base Material Under Wheel Loading*
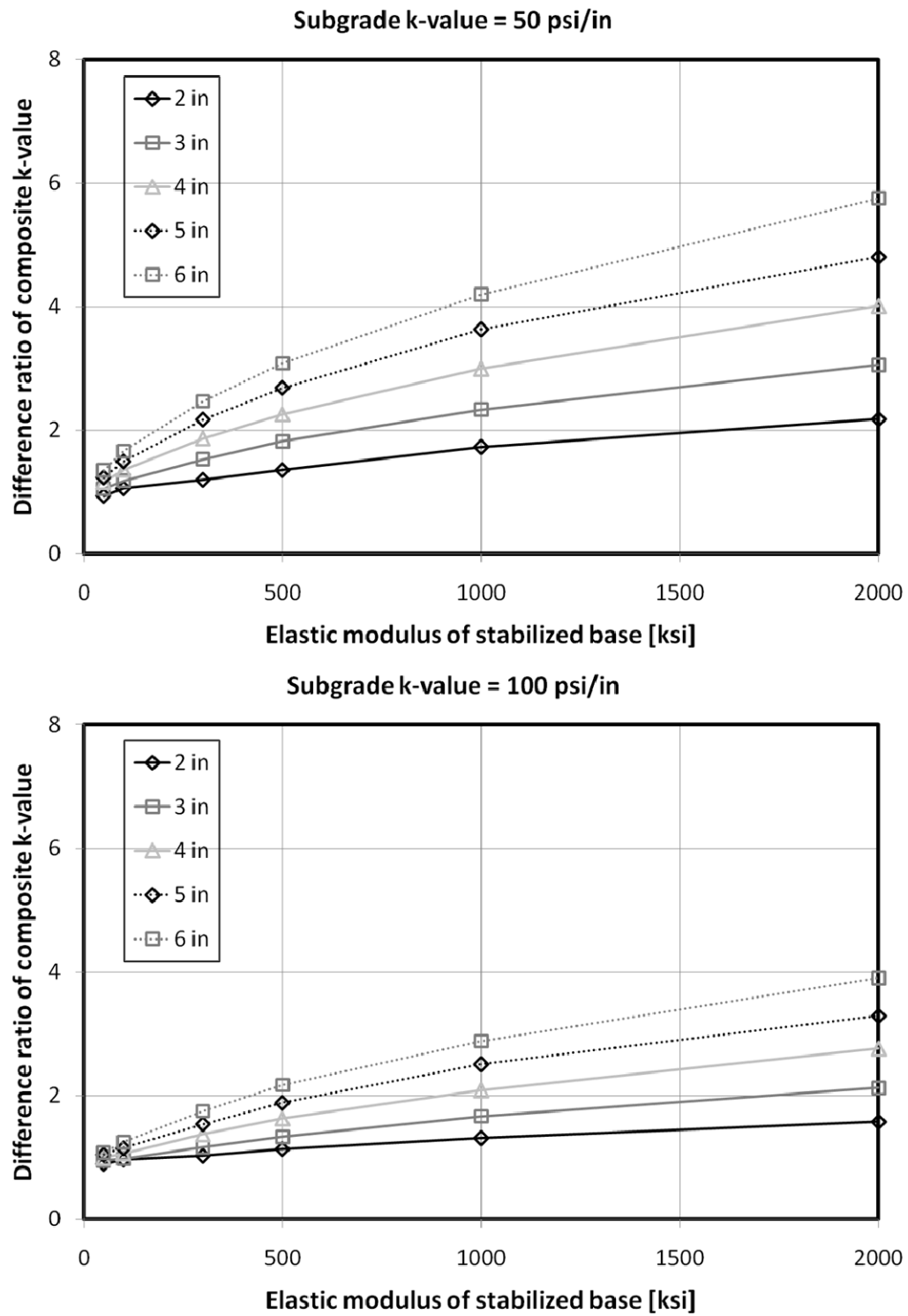
Figure C 25. Effects of elastic modulus of base under wheel loading (1)
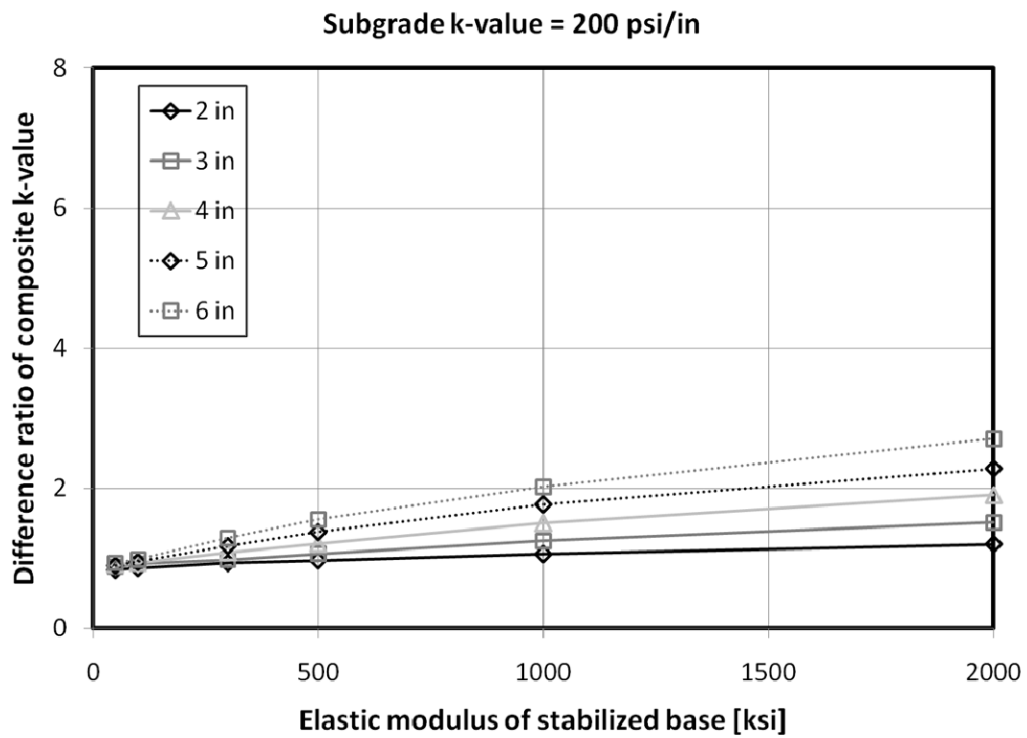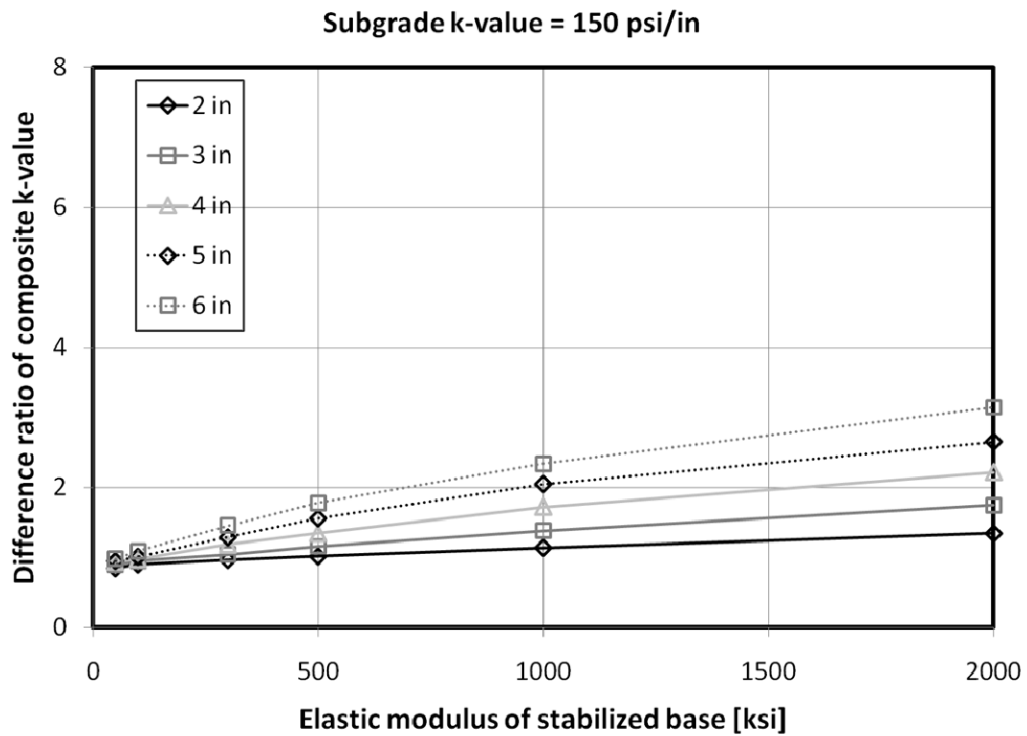
Figure C 26. Effects of elastic modulus of base under wheel loading (2)
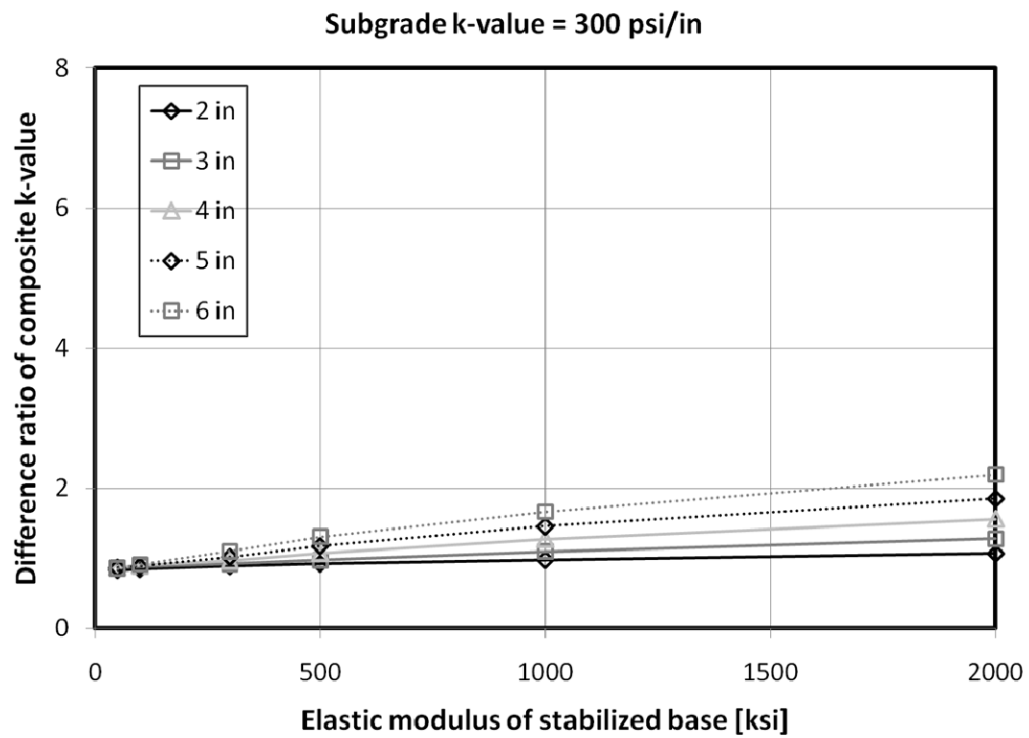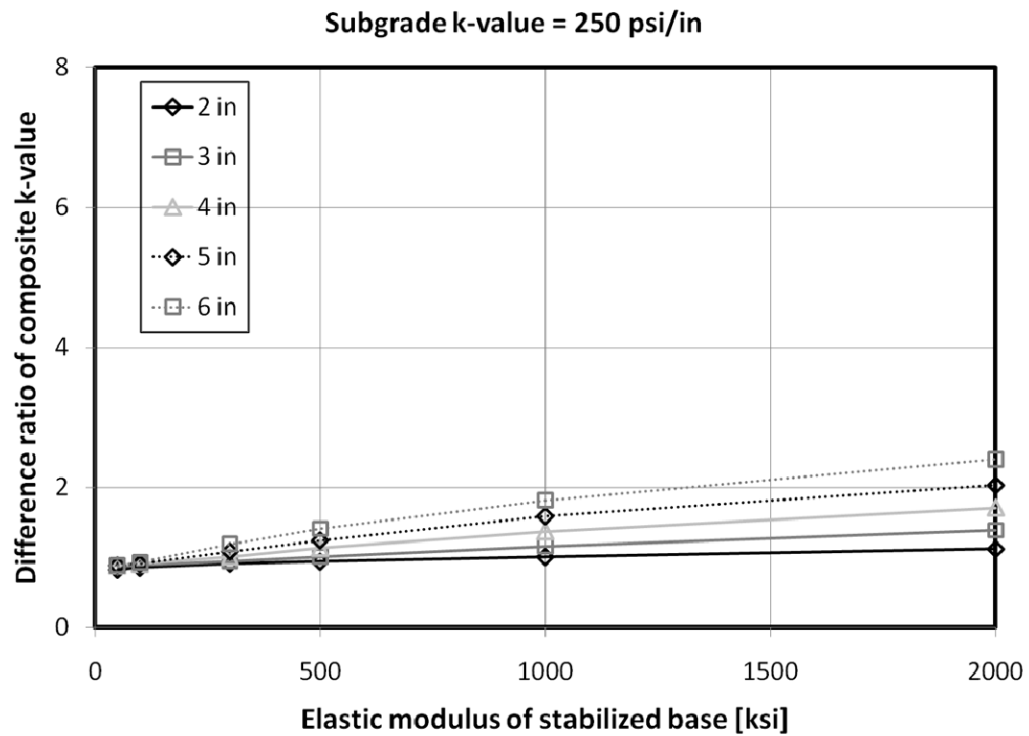
Figure C 27. Effects of elastic modulus of base under wheel loading (3)
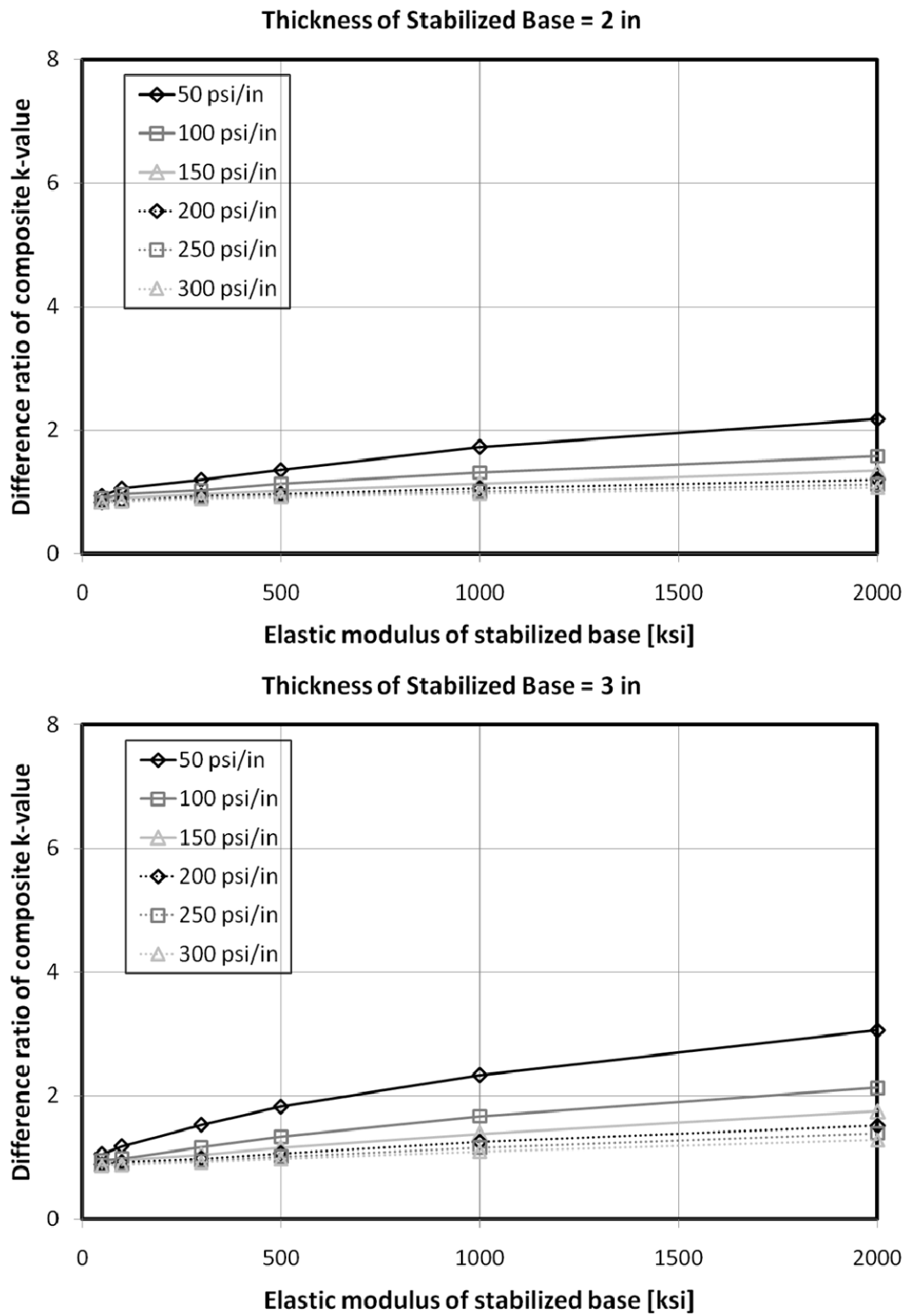
Figure C 28. Effects of elastic modulus of base under wheel loading (4)
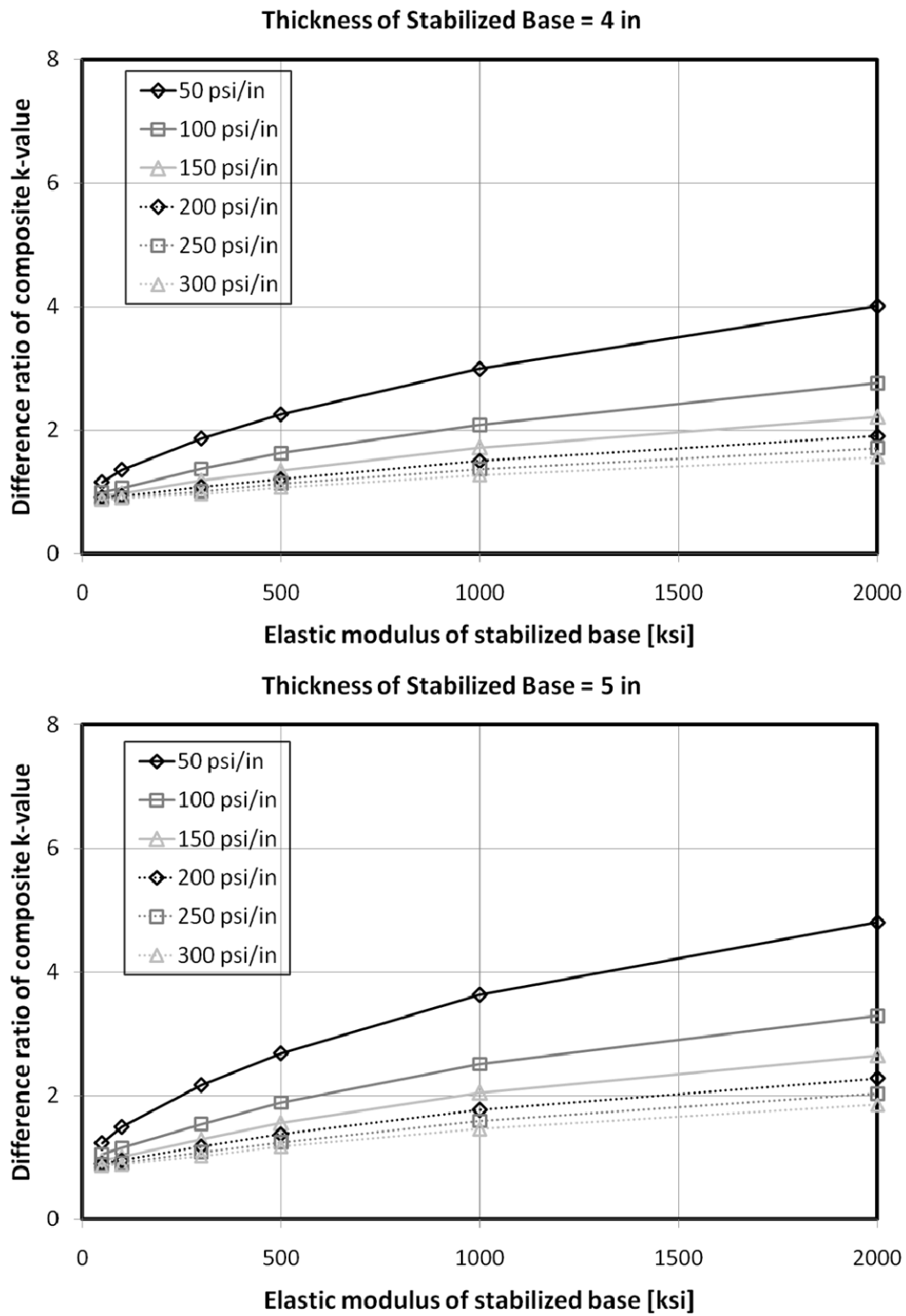
Figure C 29. Effects of elastic modulus of base under wheel loading (5)
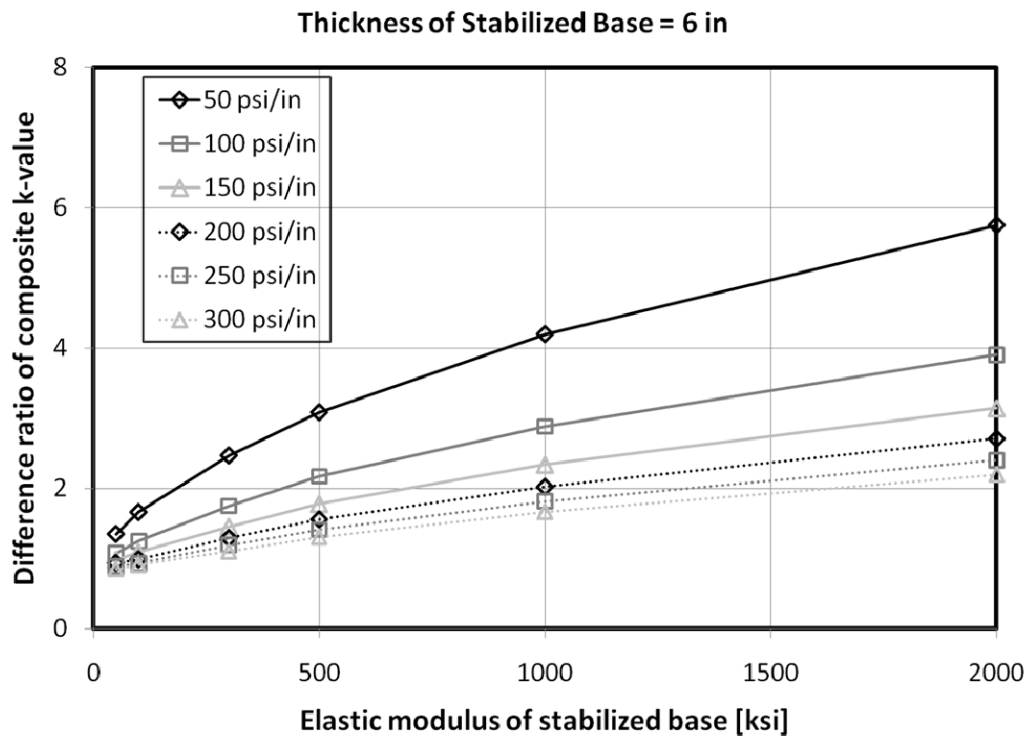
Figure C 30. Effects of elastic modulus of base under wheel loading (6)

➢ *Effects of k-value of Subgrade Layer Under Wheel Loading*

Figure C 31. Effects of *k*-value of subgrade layer under wheel loading (1)
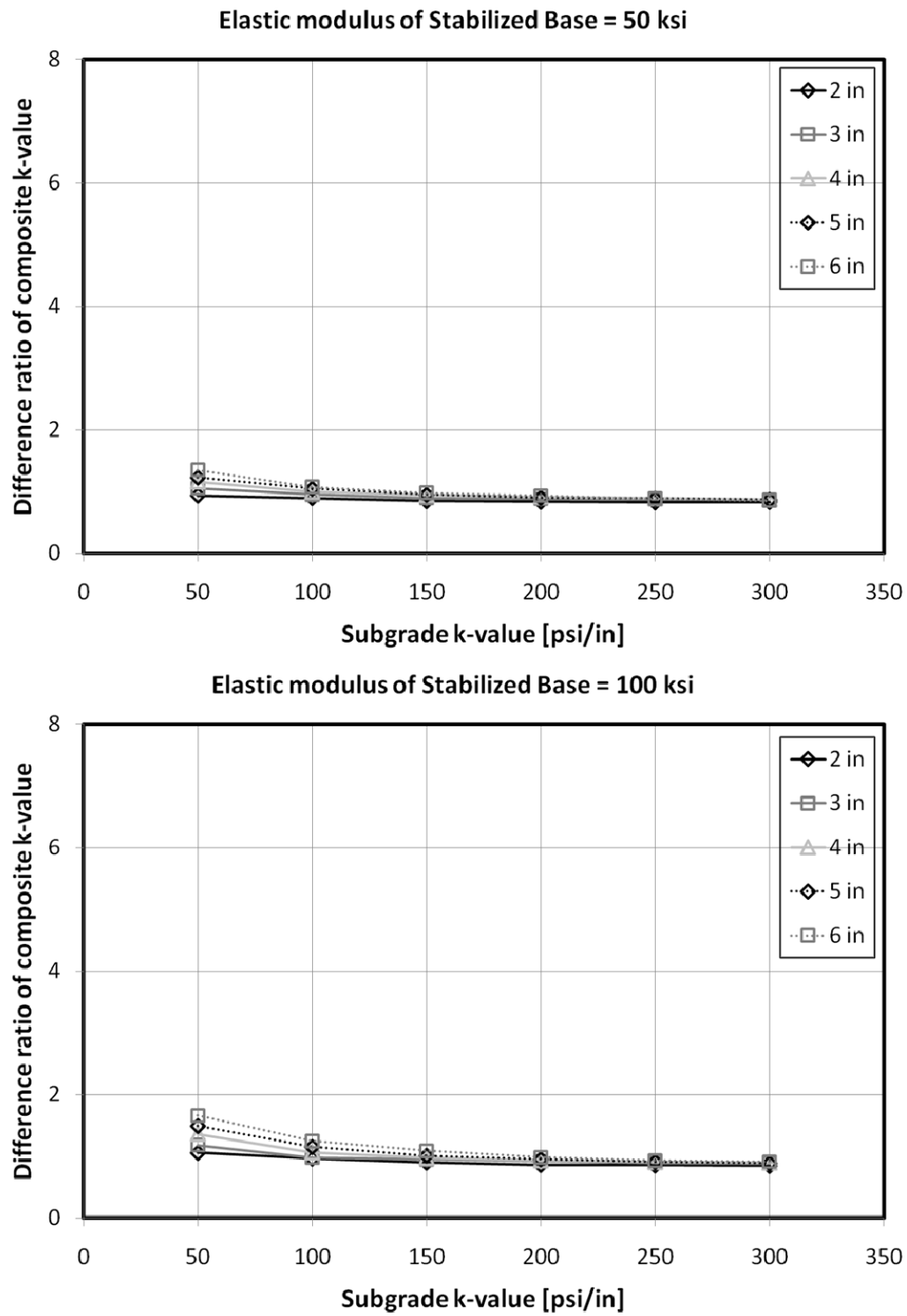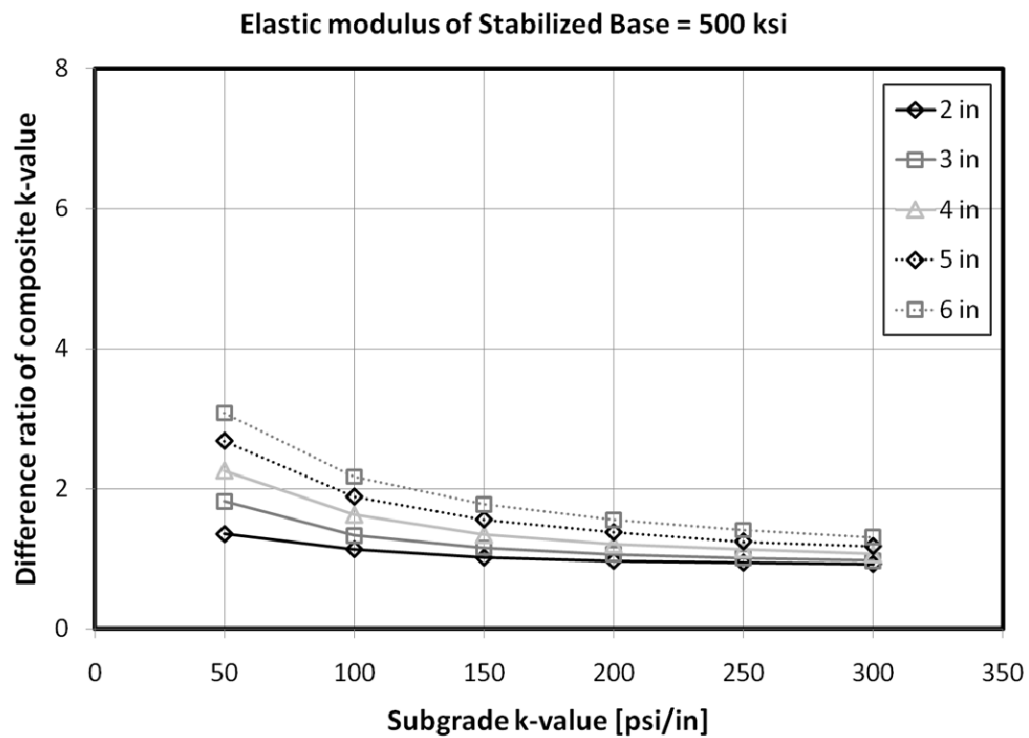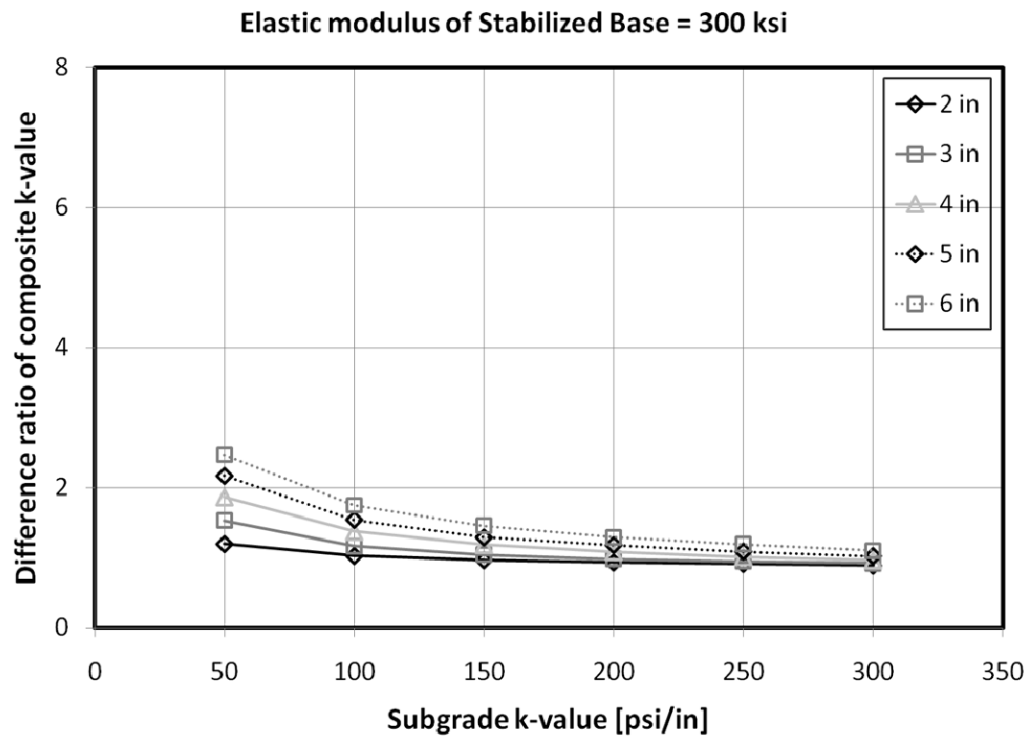
Figure C 32. Effects of *k*-value of subgrade layer under wheel loading (2)
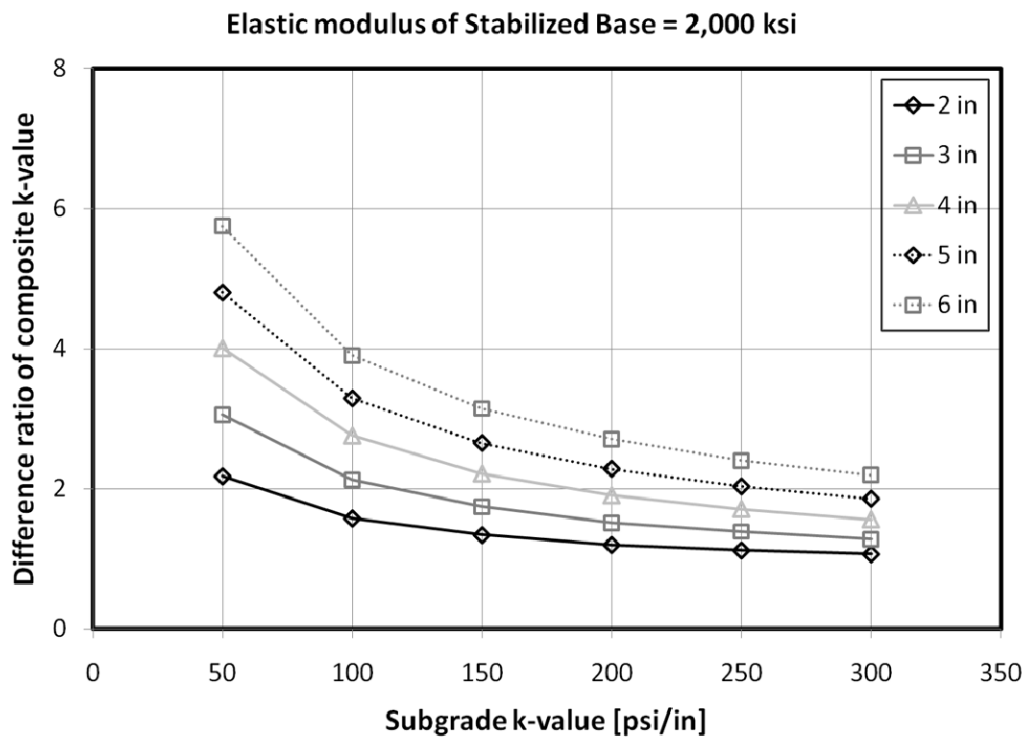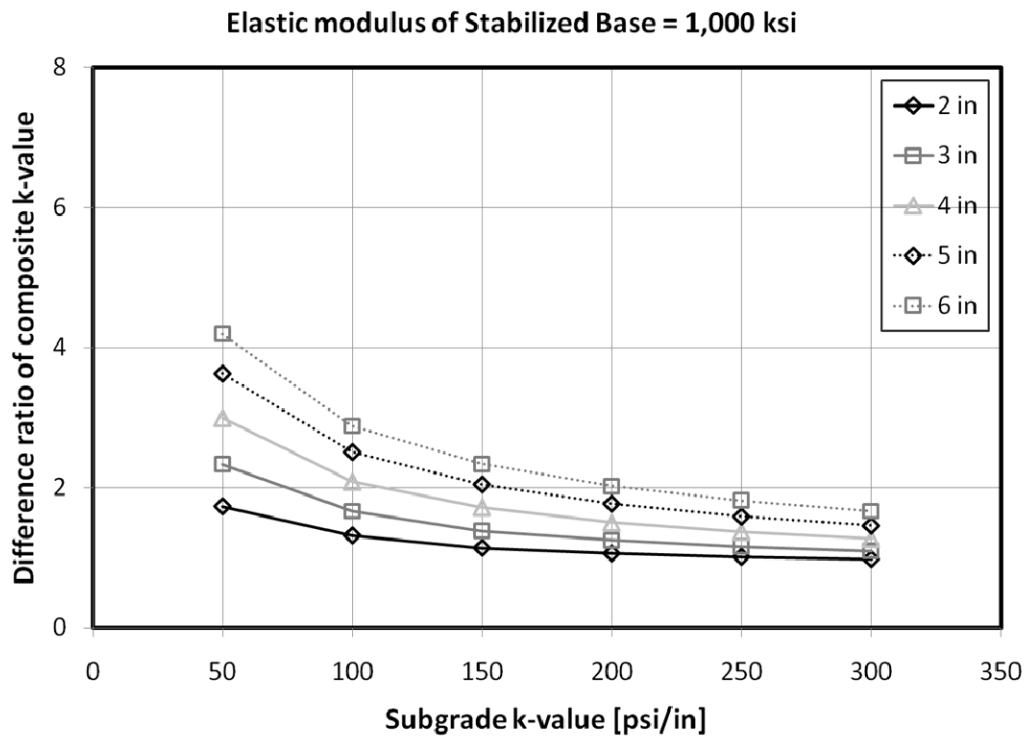
Figure C 33. Effects of *k*-value of subgrade layer under wheel loading (3)
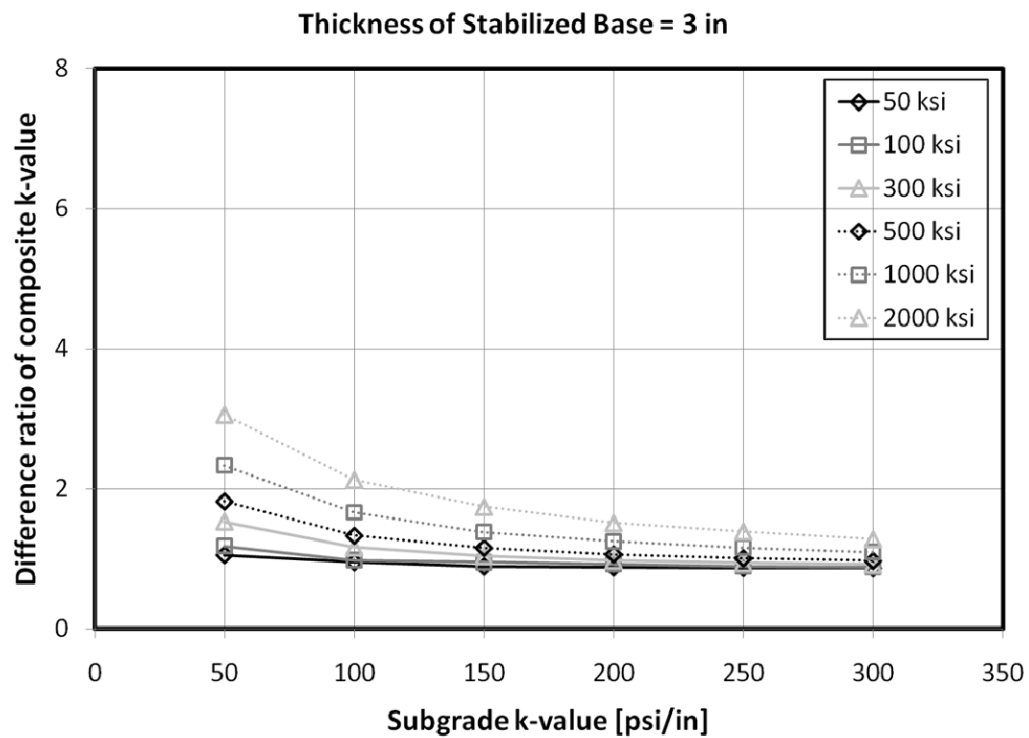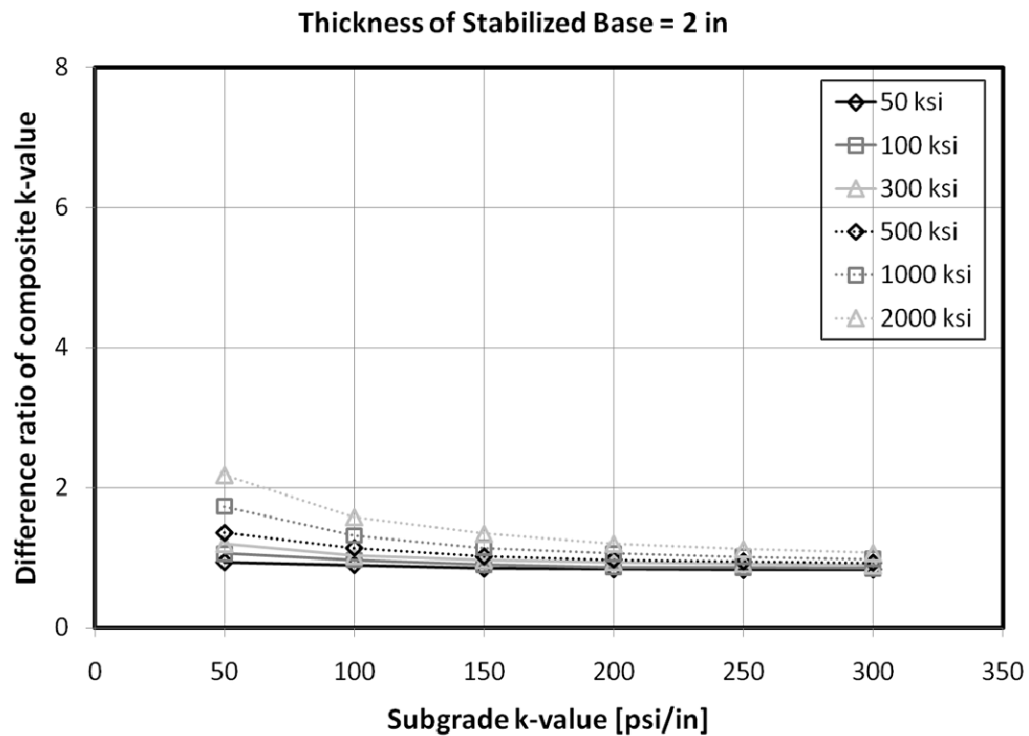
Figure C 34. Effects of *k*-value of subgrade layer under wheel loading (4)
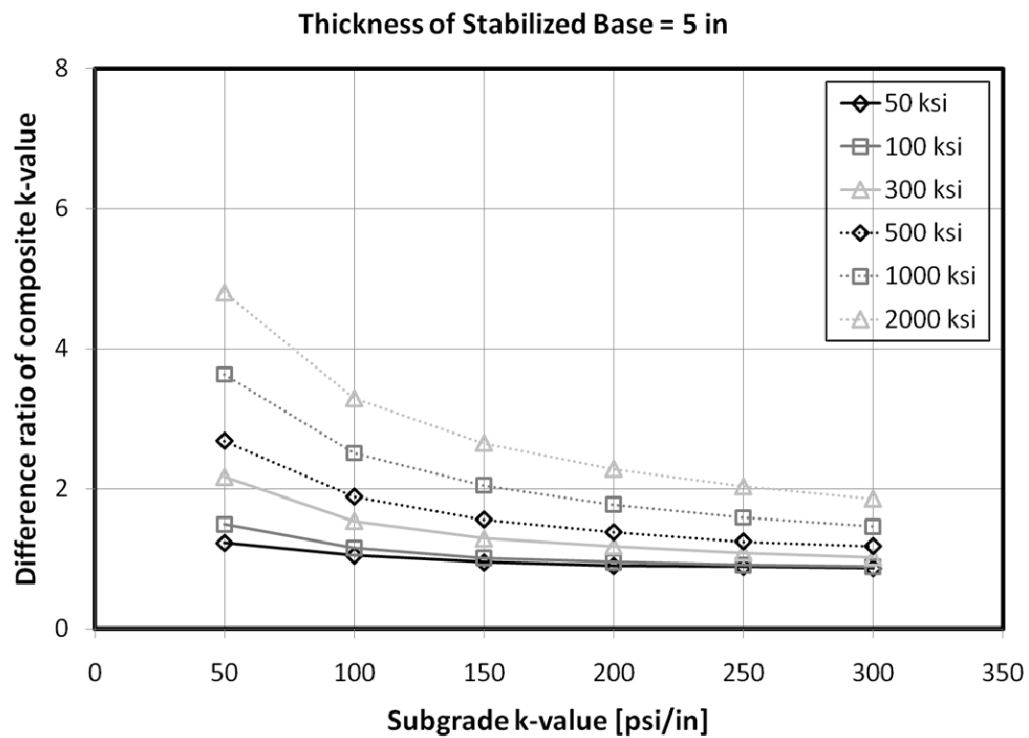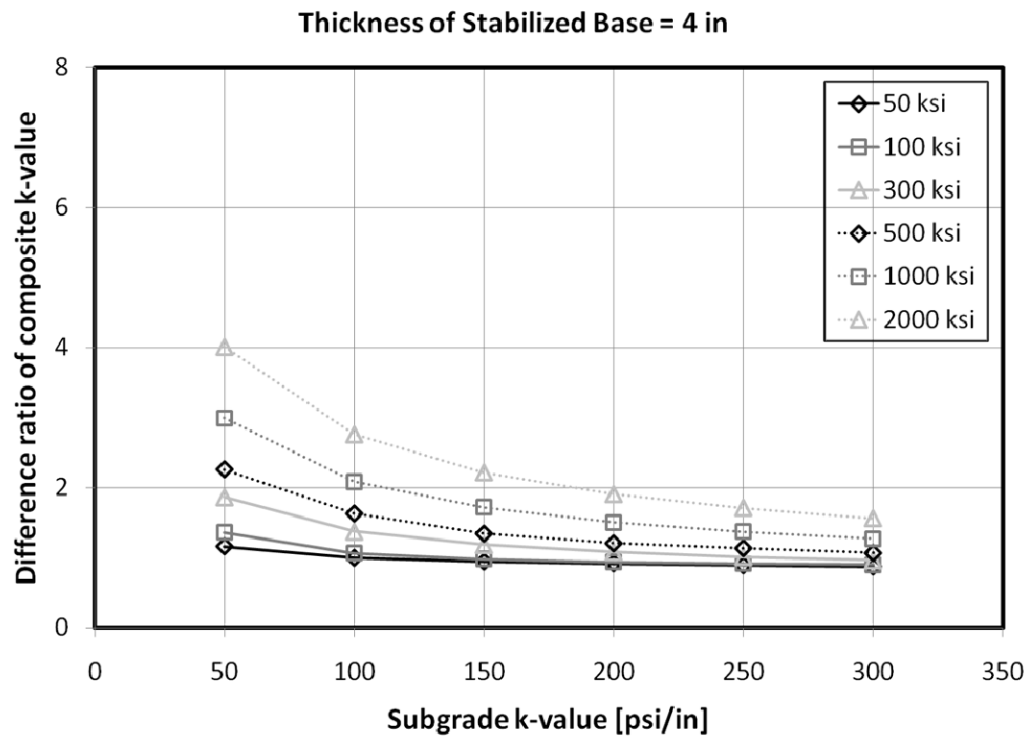
Figure C 35. Effects of *k*-value of subgrade layer under wheel loading (5)
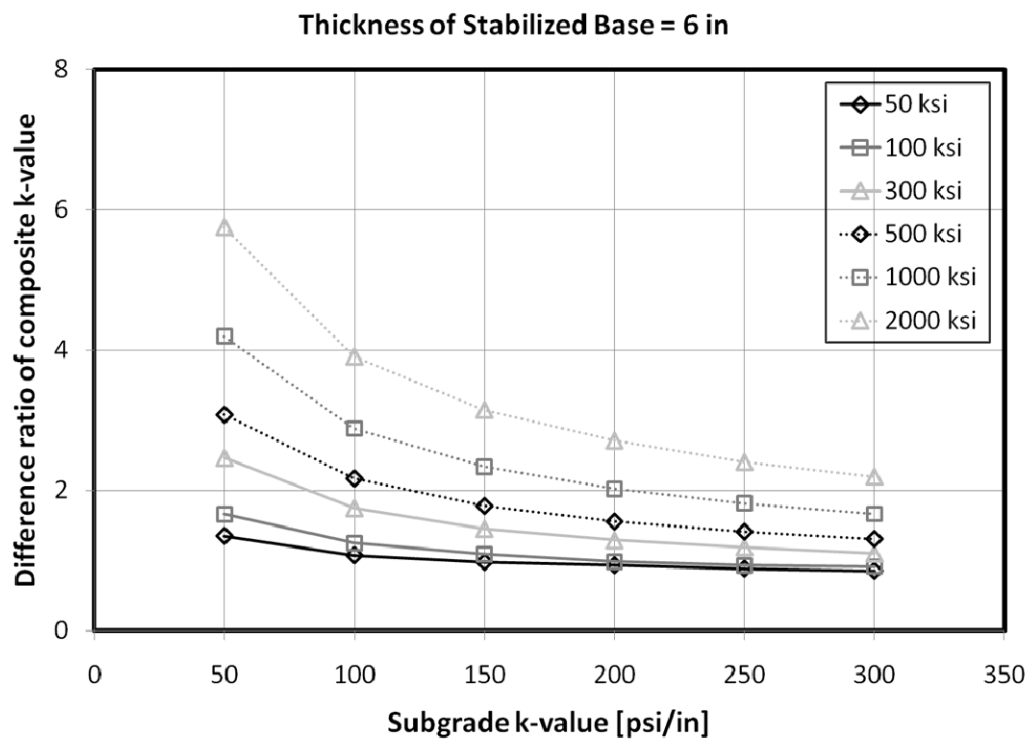
Figure C 36. Effects of *k*-value of subgrade layer under wheel loading (6)

APPENDIX D

ABAQUS Input Sample

```
*HEADING
CRCP: 2D-CRCP,
************************************************************
**SLAB LENGTH = 6FT.
**SLAB THICKNESS = 12IN.
**LONGITUDINAL STEEL = 5IN. DEPTH
**LONGITUDINAL STEEL BAR SIZE = #6
************************************************************
*PREPRINT, ECHO=NO, HISTORY=NO, MODEL=NO
*RESTART, WRITE, FREQ=1
************************************************************
**Discretize concrete slab using 2D PLANE STRAIN elements
************************************************************
********************************
**SLAB
********************************
*NODE
1,0.,0.
73,36.,0.
2401,0.,12.
2473,36.,12.
*NGEN,NSET=SLAB_BOT
1,73,1
*NGEN,NSET=SLAB_TOP
2401,2473,1
*NFILL,NSET=SLAB
SLAB_BOT,SLAB_TOP,24,100
*ELEMENT,TYPE=CPE4R,ELSET=SLAB
1,1,2,102,101
*ELGEN,ELSET=SLAB
1,72,1,1,24,100,100
********************************
*SOLID SECTION, ELSET=SLAB, MATERIAL=CONCRETE
6.
*MATERIAL, NAME=CONCRETE
*ELASTIC
3.0E6, 0.15
*DENSITY
0.0867
*EXPANSION
0.000006
****************************************************************
**Discretize stabilized base using 2D PLANE STRAIN elements
****************************************************************
***************************
**4 IN STABILIZED BASE
***************************
*NODE
3001,0.,0.
3073,36.,0.
3801,0.,-4.
3873,36.,-4.
*NGEN,NSET=SUBBASE_TOP
```

```
3001,3073,1
*NGEN,NSET=SUBBASE_BOT
3801,3873,1
*NFILL,NSET=SUBBASE
SUBBASE_TOP,SUBBASE_BOT,8,100
*ELEMENT,TYPE=CPE4R,ELSET=SUBBASE
3001,3101,3102,3002,3001
*ELGEN,ELSET=SUBBASE
3001,72,1,1,8,100,100
*******************************************
*SOLID SECTION, ELSET=SUBBASE, MATERIAL=STABILIZED
6.
*MATERIAL, NAME=STABILIZED
*ELASTIC
300000.,0.3
*DENSITY
0.0867
*EXPANSION
0.000006
****************************************************************
**DISCRETIZE LONGITUDINAL STEEL USING BEAM ELEMENTS
****************************************************************
*NODE
5001,0.,6.
5073,36.,6.
*NGEN,NSET=L_STEEL
5001,5073,1
*******************************************
*ELEMENT, TYPE=B21, ELSET=L_STEEL
5001,5001,5002
*ELGEN,ELSET=L_STEEL
5001,72,1,1
*******************************************
*BEAM SECTION, ELSET=L_STEEL, MATERIAL=L_STEEL, SECTION=CIRC
0.375
*MATERIAL, NAME=L_STEEL
*ELASTIC
2.9E7, 0.29
*DENSITY
0.28
*EXPANSION
0.000005
*******************************************************************
**CONNECTION LONGITUDINAL STEEL AND CONCRETE
*******************************************************************
*********************************
**BOND SLIP
*********************************
*ELEMENT, TYPE=SPRING2, ELSET=BSP
6002,1202,5002
*ELGEN, ELSET=BSP
6002,71,1,1
*SPRING, ELSET=BSP, NONLINEAR
```

```
1,1
0.,-0.008
-317.925,-0.004
-906.675,-0.002
-824.25,-0.001
0.,0.
824.25,0.001
906.675,0.002
317.925,0.004
0.,0.008
*ELEMENT, TYPE=SPRING2,ELSET=BSP_END
6001,1201,5001
6073,1273,5073
*SPRING, ELSET=BSP_END, NONLINEAR
1,1
0.,-0.008
-158.9625,-0.004
-453.3375,-0.002
-412.125,-0.001
0.,0.
412.125,0.001
453.3375,0.002
158.9625,0.004
0.,0.008
*********************************
**VERTICAL BONDING
*********************************
*ELEMENT, TYPE=SPRING2, ELSET=BSP_VER
6102,1202,5002
*ELGEN, ELSET=BSP_VER
6102,71,1,1
*SPRING, ELSET=BSP_VER
2,2
25000000000.
*ELEMENT, TYPE=SPRING2,ELSET=BSP_VER_END
6101,1201,5001
6173,1273,5073
*SPRING, ELSET=BSP_VER_END
2,2
12500000000.
******************************************************
**SLAB AND STABILIZED BASE
******************************************************
*************************************
**LONGITUDINAL FRICTION
*************************************
*ELEMENT, TYPE=SPRING2, ELSET=SUBBASE_FRIC
7002,2,3002
*ELGEN, ELSET=SUBBASE_FRIC
7002,71,1,1
*SPRING, ELSET=SUBBASE_FRIC
1,1
450.
```

309

```
*ELEMENT, TYPE=SPRING2, ELSET=SUBBASE_FRIC_END
7001,1,3001
7073,73,3073
*SPRING, ELSET=SUBBASE_FRIC_END
1,1
225.
***********************************
**VERTICAL COMPATIBILITY
***********************************
*ELEMENT, TYPE=SPRING2, ELSET=SUBBASE_VER
7102,2,3002
*ELGEN, ELSET=SUBBASE_VER
7102,71,1,1
*SPRING, ELSET=SUBBASE_VER
2,2
1000000000.
*ELEMENT, TYPE=SPRING2, ELSET=SUBBASE_VER_END
7101,1,3001
7173,73,3073
*SPRING, ELSET=SUBBASE_VER_END
2,2
500000000.
************************************************************
**BASE AND SUBGRADE COMPATIBILITY
************************************************************
**************************
**LONGITUDINAL FRICTION
**************************
*ELEMENT, TYPE=SPRING1, ELSET=UFRIC
8002,3802
*ELGEN, ELSET=UFRIC
8002,71,1,1
*SPRING, ELSET=UFRIC
1
66.
*ELEMENT, TYPE=SPRING1,ELSET=UFRIC_END
8001,3801
8073,3873
*SPRING, ELSET=UFRIC_END
1
33.
************************************************************
**MODULUS OF SUBGRADE REACTION (K-VALUE)
************************************************************
*ELEMENT, TYPE=SPRING1, ELSET=UFRIC_VER
8102,3802
*ELGEN, ELSET=UFRIC_VER
8102,71,1,1
*SPRING, ELSET=UFRIC_VER, NONLINEAR
2
-450.,-1.
0.,0.
*ELEMENT, TYPE=SPRING1,ELSET=UFRIC_VER_END
```

```
8101,3801
8173,3873
*SPRING, ELSET=UFRIC_VER_END, NONLINEAR
2
-225.,-1.
0.,0.
************************************************************
**CRACK BEHAVIOR MODELING USING TENSIONLESS SPRING
************************************************************
*ELEMENT, TYPE=SPRING1, ELSET=CRACK
10001,73
*ELGEN,ELSET=CRACK
10001,25,100,1
*SPRING,ELSET=CRACK, NONLINEAR
1
0.,0.005
100000000000.,1.
************************************************************
**BOUNDARY CONDITIONS
************************************************************
*NGEN, NSET=SLAB_BC
1,2401,100
*NGEN, NSET=SUBBASE_BC
3001,3801,100
3073,3873,100
*NSET, NSET=L_STEEL_BC
5001,5073
*BOUNDARY
SLAB_BC,1
SUBBASE_BC,1
L_STEEL_BC,1
L_STEEL_BC,6
************************************************************
*INITIAL CONDITIONS, TYPE=TEMPERATURE
SLAB, 95.0
L_STEEL, 95.0
************************************************************
**TEMPERATURE NODE SET
************************************************************
*NSET, NSET=TOP1,GEN
2401,2473,1
*NSET, NSET=TOP2,GEN
2301,2373,1
*NSET, NSET=TOP3,GEN
2201,2273,1
*NSET, NSET=TOP4,GEN
2101,2173,1
*NSET, NSET=TOP5,GEN
2001,2073,1
*NSET, NSET=TOP6,GEN
1901,1973,1
*NSET, NSET=TOP7,GEN
1801,1873,1
```

```
*NSET, NSET=TOP8,GEN
1701,1773,1
*NSET, NSET=TOP9,GEN
1601,1673,1
*NSET, NSET=TOP10,GEN
1501,1573,1
*NSET, NSET=TOP11,GEN
1401,1473,1
*NSET, NSET=TOP12,GEN
1301,1373,1
*NSET, NSET=MID,GEN
1201,1273,1
*NSET, NSET=BIT12,GEN
1101,1173,1
*NSET, NSET=BOT11,GEN
1001,1073,1
*NSET, NSET=BOT10,GEN
901,973,1
*NSET, NSET=BOT9,GEN
801,873,1
*NSET, NSET=BOT8,GEN
701,773,1
*NSET, NSET=BOT7,GEN
601,673,1
*NSET, NSET=BOT6,GEN
501,573,1
*NSET, NSET=BOT5,GEN
401,473,1
*NSET, NSET=BOT4,GEN
301,373,1
*NSET, NSET=BOT3,GEN
201,273,1
*NSET, NSET=BOT2,GEN
101,173,1
*NSET, NSET=BOT1,GEN
1,73,1
**************************************
**LOADING SET
**************************************
*ELSET,ELSET=LOAD, GEN
2367,2372,1
**************************************
**GRAVITY LOAD
**************************************
*STEP, NAME=STEP-1, NLGEOM=YES
*STATIC
0.1,0.1
*DLOAD
SLAB, GRAV, 9.8, 0.,-1.,0.
SUBBASE, GRAV, 9.8, 0.,-1.,0.
L_STEEL, GRAV, 9.8, 0.,-1.,0.
*OUTPUT, FIELD, VARIABLE=PRESELECT, FREQUENCY=1
*OUTPUT, HISTORY, VARIABLE=PRESELECT, FREQUENCY=1
```

```
*END STEP
**********************************
**TEMPERATURE LOAD
**********************************
*STEP,NAME=STEP-2,NLGEOM=YES
*STATIC
0.1,0.1
*TEMPERATURE
top1,      85.00
top2,      85.82
top3,      86.60
top4,      87.34
top5,      88.06
top6,      88.73
top7,      89.38
top8,      89.98
top9,      90.56
top10,     91.09
top11,     91.60
top12,     92.07
mid,       92.50
bot12,     92.90
bot11,     93.26
bot10,     93.59
bot9,      93.89
bot8,      94.15
bot7,      94.38
bot6,      94.57
bot5,      94.72
bot4,      94.84
bot3,      94.93
bot2,      94.98
bot1,      95.00
*END STEP
***************************************
**VEHICLE WHEEL LOAD
***************************************
*STEP,NAME=STEP-3,NLGEOM=YES
*STATIC
0.1,0.1
*DLOAD
LOAD,P3,34.45
************************************************************
**OUTPUT
************************************************************
*ELSET, ELSET=SLAB_CENTER, GEN
1,2301,100
*EL PRINT, ELSET=SLAB_CENTER
S11
************************************************************
*OUTPUT, FIELD, VARIABLE=PRESELECT, FREQUENCY=1
*OUTPUT, HISTORY, VARIABLE=PRESELECT, FREQUENCY=1
*END STEP
```

BIBLIOGRAPHY

AASHTO, "AASHTO Guide for Design of Pavement Structures, Volume 2", American Association of State Highway and Transportation Officials, Washington D. C., 1986.

AASHTO, "AASHTO Guide for Design of Pavement Structures", American Association of State Highway and Transportation Officials, Washington D. C., 1993.

ACPA, "Subgrades and Subbases for Concrete Pavements", American Concrete Pavement Association, 2007.

ASTM D 1196, "Standard Test Method for Nonrepetitive Static Plate Load Tests of Soils and Flexible Pavement Components, for Use in Evaluation and Design of Airport and Highway Pavements," American Society for Testing and Materials, Pennsylvania, 2004.

Biot, M. A., "Bending of an Infinite Beam on an Elastic Foundation," Osterreich. Bauzeitung, No. 25, 1932.

Bradbury, R.D., "Reinforced Concrete Pavements", Wire Reinforcement Institute, Washington, D.C., 1938.

Burmister, D. M., Palmer, L.A., Barber, E. S., Casagrande, A., and Middlebrooks, T. A., "The Theory of Stress and Displacement in Layered Systems and Applications to the Design of Airport Runways," Highway Research Board Proceedings, Vol. 23, pp. 126-148, 1943.

Cho, B.H., "Behavior of Continuously Reinforced Concrete Pavement under Environmental and Vehicle Loads", Master Thesis, Kyung Hee University, 2007.

Choubane, B., and Tia, M., "Analysis and verification of thermal gradient effects on concrete pavement", J. Transp. Eng., 121(1), pp. 75–81, 1995.

Choubane, B., and Tia, M., "Nonlinear temperature gradient effect on maximum warping stresses in rigid pavements", Transportation Research Record 1370, Transportation Research Board, Washington, D.C., pp. 11–19, 1992.

Coonse, J., "Estimating California Bearing Ratio of COHESIVE piedmont Residual Soil using the Scala Dynamic Cone Penetrometor", Master's thesis, North Carolina State University, Raleigh, N.C., 1999.

Crovetti, J. A., "Evaluation of Jointed Concrete Pavement Systems Incorporating Open-Graded Permeable Base," Ph.D. thesis, University of Illinois at Urbana-Champaign, 1994.

CRSI, "CRCP in Louisiana – Then and Now", Concrete Reinforcing Steel Institute, Case History Report No. 62, 2004

CRSI, "CRCP: The Illinois Experience", Concrete Reinforcing Steel Institute, Case History Report No. 55, 2001.

CRSI, "CRCP: Virginia is for Innovation", Concrete Reinforcing Steel Institute, Case History Report No. 64, 2005.

CRSI, "Paving the Prairie States: CRCP's Success in North and South Dakota", Concrete Reinforcing Steel Institute, Case History Report No. 58, 2002.

Daloglu, T., and Vallabhan, C. V., "Values of k for Slab on Winkler Foundation," ASCE, Journal of Geotechnical and Geoenvironmental Engineering, Volume 126, Issue 5, pp. 463-471, May 2000.

Darter, M.I. and Barenberg, E.J., "Design of Zero-Maintenance Plain Jointed Concrete Pavement, Volume 2 – Design Manual", University of Illinois at Urbana-Champaign, Report No. FHWA-RD-77-112, 1977.

Darter, M.I., "Design of Zero-Maintenance Plain Jointed Concrete Pavement, Volume 1 – Development of Design Procedures", University of Illinois at Urbana-Champaign, Report No. FHWA-RD-77-112, 1977.

Davids, W.G., Turkiyyah, G.M., and Mahoney, J.P., "EVERFE: Rigid Pavement Three-Dimensional Finite Element Analysis Tool", Transportation Research Record, Vol. 1629, pp. 41 – 49, 1998.

Ese, Dag, Myre, Jostein, Nos, Per Magne, and Vaernes, Einar., "the Use of Dynamic Cone Penetrometer (DCP) for road strengthening design in Norway", Proc., Int. Conf. on Bearing Capacity of Rd. and Airfield. pp3-22, 1994.

Friberg, B.F., "Frictional Resistance Under Concrete pavements and Restraint Stresses in Long Reinforced Slabs", Proceedings, Highway Research Board, Vol. 33, 1934.

Gabr, M. A., Hopkins, K., Coonse, J. and Hearne, T., "DCP Criteria for Performance Evaluation of Pavement Layers", Journal of Performance of Constructed Facilities, Nov.2000, pp141-148, 2000.

Goldbeck, A.T., "Friction Tests of Concrete on Various Subbases", Public Roads, United States Department of Agriculture, July 1924.

Ha, S. and Won, M., "Develop Mechanistic/Empirical Design for CRCP", Project No. 0-5832, PMC meeting, Texas Tech University, Texas Department of Transportation, Feb 06, 2009.

Harik, I.E., Jianping, P., Southgate, H., and Allen, D., "Temperature effects on Rigid Pavements", Journal of Transportation Engineering, ASCE, Vol. 120, No. 1, pp. 127 – 143, 1994.

Harison, A., "Correlation between California Bearing Ratio and Dynamic Cone Penetrometer Strength Measurement of Soils", Proc. Instn Civ. Engrg, Part2, pp.832-844, 1987.

Heckel, L., Open-Graded Drainage Layers: Performance Problems under Continuously Reinforced Concrete Pavements in Illinois, 6th International Conference on Concrete Pavement Design and Materials for High Performance, Purdue, 1997.

Heukelom, W., and Klomp, A.J.G. (1962), "Dynamic testing as a means of controlling pavement during and after construction," Proceedings of the 1st international conference on the structural design of asphalt pavement, University of Michigan, Ann Arbor, MI.

Hiller, J. E. and Roesler, J. R., "Simplified Nonlinear Temperature Curling Analysis for Jointed Concrete Pavements", Journal of Transportation Engineering, ASCE, July 2010.

Hoffman, M. S. and M. R. Thompson, "Mechanistic Interpretation of Nondestructive Pavement Testing Deflections," Transportation Engineering Series No. 32, Illinois Cooperative Highway and Transportation Research Series No. 190, University of Illinois at Urbana-Champaign, 1981.

Hogg, A. H. A., "Equilibrium of a Thin Plate, Symmetrically Loaded, Resting on an Elastic Foundation of Infinite Depth." Philosophical Mag., Vol. 25, pp. 576-582, 1938.

Huang, Y.H., "Pavement Analysis and Design", Prentice Hall, 1993.

Ioannides, A. M., and Khazanovich, L., "Nonlinear temperature effects on multilayered concrete pavements", J. Transp. Eng., 124(2), pp. 128–136, 1998.

Ioannides, A. M., and Salsilli-Murua, R., "Temperature curling in rigid pavement: An

application of dimensional analysis", Transportation Research Record 1227, Transportation Research Board, Washington, D.C., pp. 1–11, 1999.

Jung, Y., Zollinger D.G., Won, M., and Wimsatt, A.J., "Subbase and Subgrade Performance Investigation for Concrete Pavement", Texas Transportation Institute, Texas A&M University, Texas Department of Transportation, May 2009.

K. T. Hall, "Performance, Evaluation, and Rehabilitation of Asphalt-Overlaid Concrete Pavements." Ph.D. Thesis, University of Illinois at Urbana-Champaign, 1991.

Khazanovich, L., Yu, H.T., Rao, S., Galasova, K., Shats, E., and Jones R., "ISLAB2000 – Finite Element Analysis Program for Rigid and Composite Pavements", User's Guide, ERES Consultants, Champaign, IL, 2000.

Kim, S., Won, M., and McCullough, B.F., "CRCP-10 Computer Program User's Guide", Center for Transportation Research, University of Texas at Austin, Texas Department of Transportation, August 2001.

Kim, S.-M., Won, M.C., and McCullough, B.F., "Development of a Finite Element Program for Continuously Reinforced Concrete Pavements", Research Report 1758-S, Center for Transportation Research, University of Texas at Austin, 1997.

Kim, S.-M., Won, M.C., and McCullough, B.F., "Effect of Transverse Reinforcement on CRC Pavement Response to Thermal Loads", Proceedings of the 2nd International Symposium on 3D Finite Element for Pavement Analysis, Design, and Research, Charleston, West Virginia, pp. 43-64, 2000b.

Kim, S.-M., Won, M.C., and McCullough, B.F., "Mechanistic Modeling of Continuously Reinforced Concrete Pavement", ACI Structural Journal, Vol. 100, No. 5, American Concrete Institute, pp. 674-682, 2003.

Kim, S.-M., Won, M.C., and McCullough, B.F., "Numerical Modeling of Continuously Reinforced Concrete Pavement Subjected to Environmental Loads", Transportation Research Record, No. 1629, Transportation Research Board, National Research Council, pp. 76-89, 1998.

Kim, S.-M., Won, M.C., and McCullough, B.F., "Three-dimensional Analysis of Continuously Reinforced Concrete Pavements", Transportation Research Record, No. 1730, Transportation Research Board, National Research Council, pp. 43-52, 2000a.

Kleyn, E.G., "the Use of the Dynamic Cone Penetrometer (DCP)", Transvaal Roads, Department, Report No. L2/74, Pretoria.1975.

LaCourseiere, S.A., Darter, M.I., and Smiley, S.A., "Structural Distress mechanisms in Continuously Reinforced Concrete Pavement," Transportation Engineering Series No.20, University of Illinois at Urbana-Champaign, 1978.

Lee, Y. H., and Darter, M. I., "Mechanistic design models of loading and curling in concrete pavements." Proc., Airport Pavement Innovations — Theory to Practice, ASCE, Reston VA., 1993.

Livneh, M, Ishai, I. and Livneh, N. A., "Effect of Vertical Confinement on Dynamic Cone Penetrometer Strength Values in Pavement and Subgrade Evaluations", Transportation Research Record 1473, pp.1-8, 1994.

Losberg, A., "Design Methods for Structurally Reinforced Concrete Pavements," Trans., Chalmers Univ. of Tech., No. 250, Gothenburg, 1961.

Luo, X., Salgado, R. and Altschaeffl, A., "Dynamic Cone Penetration Test to Access the Mechanical Properties of Subgrade Soil", Indiana Department of Transportation, Report No. FHWA/IN/JTRP-98/13, 1998.

Masad, E., Taha, R., and Muhunthan, B., "Finite element analysis of temperature effects on plain-jointed concrete pavements", J. Transp. Eng., 122(5), pp. 388–398, 1996.

Middlebrooks, T.A. and Bertram, G.E., "Soil Tests for Design of Runway Pavements", Proceedings, Highway Research Board, 1942.

Mirambell, E., "Temperature and stress distributions in plain concrete pavements under thermal and mechanical loads." Proc., 2nd Int.Workshop on the Design and Rehabilitation of Concrete Pavements, Siguenza, Spain, pp. 121–135, 1990.

Mohamed, A.R., and Hansen, W., "Effect of Nonlinear Temperature Gradient on Curling Stress in Concrete Pavements", Transportation Research Record 1568, Transportation Research Board, pp. 65 – 71, 1997.

Nam, J., "Early-Age Behavior of CRCP and Its Implications for Long-Term Performance", Ph.D. Dissertation, University of Texas at Austin, 2005.

NCHRP 1-37A, "Guide for the Mechanistic-Empirical Design of New and Rehabilitated Pavement Structures", Final Report, National Cooperative Highway Research Program, Transportation Research Board, National Research Council, March 2004.

Panak, John J. and Matlock, Hudson, "A Discrete-Element Method of Analysis for Orthogonal Slab and Grid Bridge Floor Systems", Center for Highway Research, University of Texas at Austin, 1972.

Phillippe, R.R, "Field Bearing Tests Applied to Pavement Design", Symposium on Load Tests of Bearing Capacity of Soils, American Society for Testing and materials, Special Technical Publication No. 79, 1947.

Pickett, G., and Ray, G.K., "Influence Charts for Concrete Pavements," American Society of Civil Engineers Transactions, Paper No. 2425, Vol. 116, pp. 49 – 73, 1951.

Rasmussen, Robert O., Rogers, Richard, and Ferragut, Theodore R., "Continuously Reinforced Concrete Pavement Design and Construction Guidelines", Federal Highway Administration and Concrete Reinforcing Steel Institute, May 2009.

Salgado, R. and Yoon, S., "Dynamic Cone Penetration Test (DCPT) for Subgrade Assessment", Purdue University, Indiana Department of Transportation, FHWA/IN/JTRP-2002/30, February 2003.

Scala, A.J., "Simple Methods of Flexible Pavement Design Using Cone Penetrometers", Proceeding of 2nd Australian-New Zealand Conference of Soil Mechanics and Foundation Engineering, pp. 73, 1956.

Selezneva, O., Darter, M., Zollinger, D., and Shoukry, S., "Characterization of Transverse Cracking Spatial Variability Using LTPP Data for CRCP Design", Transportation Research Board 82nd Annual Meeting, Washington, D.C., January 2003.

SRA International, Inc., "FAA Finite Element Design Procedure for Rigid Pavements", U.S. Department of Transportation, Federal Aviation Administration, Washington, DC, August 2007.

Stott, J.P., "Tests on Materials for Use as Sliding layers Under Concrete Road Slabs", Road Research Laboratory, DSIR, 1961.

Suh, C., Kim, D., and Won, M., "Development of the Thickness Design for Concrete Pavement Overlays Over Existing Asphalt Pavement Structures", Report No. 0-5482-2, Texas Department of Transportation, February 2008.

Suh, Y.C., Hankins, K., and McCullough, B.F., "Early-Age Behavior of Continuously Reinforced Concrete Pavement and Calibration of the Failure Prediction Model in the CRCP-7 Program," Research Report 1244-3, Center for Transportation Research, The University of Texas at Austin, March 1992.

Teller, L. W. and Sutherland, E. C., "The Structural Design of Concrete Pavements, Part 5, An Experimental Study of the Westergaard Analysis of Stress Conditions in Concrete Pavements of Uniform Thickness," Public Roads, Vol. 23, No. 8, 1943.

Tex-104-E, "Determining Liquid Limits of Soils", Texas Department of Transportation, August 1999.

Tex-105-E, "Determining Plastic Limits of Soils", Texas Department of Transportation, August 1999.

Tex-106-E, "Calculating The Plasticity Index of Soils", Texas Department of Transportation, August 1999.

Tex-107-E, "Determining The Bar Linear Shrinkage of Soils", Texas Department of Transportation, August 1999.

Tex-110-E, "Particle Size Analysis of Soils", Texas Department of Transportation, August 1999.

Tex-125-E, "Determining Modulus of Sub-grade Reaction (k-Value)" Texas Department of Transportation, 1999.

Tex-142-E, "Laboratory Classification of Soils for Engineering Purposes", Texas Department of Transportation, August 1999.

Tex-145-E, "Determining Sulfate Content of Soils - Colorimetric Method", Texas Department of Transportation, February 2005.

Tex-146-E, "Conductivity Test for Field Detection of Sulfate in Soil", Texas Department of Transportation, February 2005.

Texas Department of Transportation, "Average Low Bid Unit Price", Webpage : http://www.txdot.gov/insdtdot/orgchart/cmd/cserve/bidprice/s_0201.htm, Nov 19, 2010.

Texas Department of Transportation, "Guidelines for Modification and Stabilization of Soils and Base for Use in Pavement Structures", Texas Department of Transportation, September 2005.

Texas Department of Transportation, "Pavement Design Guide", Texas Department of Transportation, November 2008.

The Transtec Group, Inc., "CRCP in Texas: Five Decades of Experience," Concrete Reinforcing Steel Institute, 2004.

Thompson, M. R., Dempsey, B. J., Hill, H., and Vogel, J., "Characterizing Temperature Effects for Pavement Analysis and Design", Transportation Research Record 1121,

Transportation Research Board, pp. 14 - 22, 1987.

Timms, A.G., "Evaluating Subbase Friction Reducing Mediums for Rigid Pavements", Highway Research Record 60, Highway Research Board, Washington, D. C., 1963.

US TECH, "Report on the 1992 U.S. Tour of European Concrete Highways", Federal Highway Administration, U.S. Department of Transportation, Washington D.C., 1992.

Vesic, A., "Bending of Beams Resting on Isotropic Elastic Solid," Proceedings ASCE, Journal of Engineering Mechanics Division, Vol. 87, EM2, pp. 35-51, 1961.

Vesic, A., Saxena, S., Analysis of Structural Behavior of AASHO Road Test Rigid Pavements," Highway Research Board, NCHRP Report 97, 1970

Washington Asphalt Pavement Association, "WAPA Asphalt Pavement Guide", Webpage : http://www.asphaltwa.com/wapa_web/index.htm

Wesevich, J.W., McCullough, B.F., and Burns, N.H., "Stabilized Subbase Friction Study for Concrete Pavements", Center for Transportation Research, University of Texas at Austin, 1987.

Westergaard, H. M., "Analysis of Stresses in Concrete Roads Caused by Variations of Temperature", Public Roads, Vol. 8, No. 3, pp. 54~60, 1927b.

Westergaard, H. M., "Stresses in Concrete Pavement Computed by Theoretical Analysis", Public Loads, Vol. 7, No. 2, pp. 25~35, 1926.

Westergaard, H. M., "Theory of Concrete Pavement Design," Proceedings, Highway Research Board, Part Ⅰ, pp. 175-181, 1927a.

Westergaard, H. M., "Theory of Stresses in Road Slabs," Proceedings, Fourth Annual Meeting of the Highway Research Board, 1925.

White, D.J., Harrington, D., Ceylan, H., and Rupnow, T., "Fly Ash Soil Stabilization for Non-Uniform Subgrade Soils, Volume II: Influence of Subgrade Non-Uniformity of PCC Pavement Performance", Center for Transportation Research and Education, Iowa State University, April 2005.

White, D.J., Vennapusa, P., and Jahren, C.T., "Determination of the Optimum Base Characteristics for Pavements", Center for Transportation Research and Education, Iowa State University, Iowa Department of Transportation, May 2004.

Wimsatt, A.J., McCullough, B.F., and Burns, N.H., "Methods of Analyzing and Factors Influencing Frictional Effects of Subbases", Center for Transportation Research, University of Texas at Austin, 1987.

Yoder, E.J. and Witczak, M.W., Principles of Pavement Design, John Wiley and Sons, Inc., 1975.

Yu, H.T., Khazanovich, L., Rao, S., Darter, M.I., Quintus, H.V., Guidelines for Subsurface Drainage Based on Performance, National Cooperative Highway Research Program Final Report 1-34, Transportation Research Board, National Research Council, 1999.

Zollinger, D. G., and Barenberg, E. J., "Field Investigation of Punchout Distress in Continuously Reinforced Concrete Pavement in Illinois", Transportation Research Record, No. 1286, Transportation Research Board, 1990, pp. 1-13.

Zollinger, D., "Investigation of Punchout Distress of Continuously Reinforced Concrete Pavement," Ph.D. Dissertation, University of Illinois at Urbana-Champaign, 1989.

Zollinger, D., and Barenberg, E.J., "Continuously Reinforced Pavement: Punchouts and Other Distresses and Implications for Design," Project IHR-518, Illinois Cooperative Highway Research Program, 1990.

VITA

Byoung Hooi Cho was born in Seoul, South Korea on July 2nd, 1979, as the second son of Myung Won Cho and Gye Ok Jang. After completing his work at Kwang Nam High School in Seoul, he entered the department of landscape architecture in Kyung Hee University, South Korea in 1998. After completing 3 semesters, he served in the Korean Army for 26 months. He transferred his major to civil engineering after returned to school in 2002, and he received the degree of Bachelor of Science in February 2005 with Cum Laude honors. He entered the Graduate School of Kyung Hee University, South Korea in September 2005. Upon receiving the degree of Master of Science in civil engineering in 2007, he entered the Graduate School of the University of Texas at Austin to pursue a doctoral degree in civil engineering.

Permanent Address: 308-701 Sambo APT., Inchang-Dong, Guri-Si, Gyeonggi-Do, South Korea 471-734

Permanent E-mail: cbh1979@gmail.com

This Dissertation was typed by Byoung Hooi Cho.